ANALYTICAL AND EXPERIMENTAL STUDIES OF AN OPTIMUM HELIUM LIQUEFACTION CYCLE.

by

MOSES MINTA

B. Sc.(Hons), University of Science and Technology Kumasi, Ghana.
(1977)
S.M., Mechanical Engineering, Massachusetts Institute of Technology
(1981)

Submitted to the Department of Mechanical
Engineering in partial fulfillment of the
Requirement for the Degreee of

DOCTOR OF SCIENCE

at the
MASSACHUSETTS INSTITUTE OF TECHNOLOGY
February 1984

© Massachusetts Institute Of Technology 1984

Signature of Author_____
Department of Mechanical Engineering
February 14,1984

Certified by_____
Joseph L. Smith, Jr.
Thesis Supervisor

Accepted by_____
Warren M. Rohsenow
Chairman, Department Committee on Graduate Students

MASSACHUSETTS INSTITUTE
OF TECHNOLOGY

JUL 17 1984 Archives

LIBRARIES

ANALYTICAL AND EXPERIMENTAL STUDIES OF AN OPTIMUM HELIUM LIQUEFACTION CYCLE.

by

MOSES MINTA

Submitted to the Department of Mechanical Engineering
on February 14,1984 in partial fulfillment of the
requirements for the Degree of Doctor of Science

ABSTRACT

A typical helium liquefaction cycle consists of a compression stage, a precooling stage, and an expansion stage. Continuum models for the precooling stage are presented and involve heat exchangers with continuously distributed expansion stages. The models with reversible heat exchange facilitate investigating the effect of the non-ideal behaviour of helium at low temperatures on the cycle performance, decoupled from other loss mechanisms. An optimum cycle configuration is synthesized from the resulting performance curves by direct discretization.

A new optimization technique for helium liquefaction cycles is also introduced. The method is based on a continuum model for the precooling stage. Variational calculus techniques are used to minimize the generated entropy subject to two constraints derived from the first law of thermodynamics: continuity of mass flow rate and a fixed heat exchange area. The utility of the method is demonstrated. Unlike conventional schemes the cycle configuration is an output of the design algorithm. Other results are used to initialize the design parameters for a final parametric optimization.

Experimental work to demonstrate the feasibility of implementing the optimum cycle is also reported. This involved the design, fabrication, and testing of a supercritical expander with a programmable hydraulic-pneumatic control logic. The performance of the device is reported.

Thesis Supervisor: Dr. Joseph L. Smith, Jr.
Title: Professor of Mechanical Engineering.

ACKNOWLEDGEMENTS

I wish to thank the members of my thesis committee, Professors Maher A. El-Masri, Yukikazu Iwasa and Joseph L. Smith, Jr., for their suggestions and guidance of this work. I am particularly grateful to Prof. Smith who has singlehandedly supervised my graduate work at MIT. His support and guidance has been invaluable and his dedication to work and attention to detail has been inspiring. His energy and enthusiasm has been fascinating and he has never ceased to amaze me with his insight, foresight and ingenuity. It has been a real joy working with him.

The staff members of the Cryogenic Engineering Laboratory – George Robinson, Karl Benner, Warren Shea, Mike Demaree, Bill Finley, Bob Gertsen, Ray and Rachel – have been very helpful at various phases of the work. Karl Benner was particularly helpful in the fabrication and assembly processes (and in "splitting" pizzas for lunch).

An impressive atmosphere of camarade has always existed among students in the laboratory which I will always cherish. Larry liberally shared his expertise in instrumentation. Carl's incessant questions and company greatly lightened the drudgery of the deep night sessions. Tony, Bill, Al and Jim were most helpful on the several occasions that I had to mount and dismount the vacuum jacket. Hank and Kate's regular invitations provided timely escape for relaxation. Joe, Ken, Maury, John Schwoer and other students who have gone through the laboratory all added other dimensions to life at MIT which helped brighten the years spent here. Phillip, Gilberto and Marie have also been good company. Jill arrived early enough to pick up the typographical errors and to give me her quiz.

Jim and Josefina's friendship I have come to value greatly especially when the heat was on to get the thesis typed. I have also come to enjoy the friendship of several people outside the laboratory which has greatly lightened my days at MIT including Sam, Gerald, Mobil, Ademola and Bill. Anna at the Plasma Fusion Center and Pondy at the Artificial Intelligence Laboratory have been very helpful in the use of the word

processor, Tex, on ITS and Oz respectively. I'm very grateful to them.

The financial support from the Cryogenic Engineering Laboratory during this work is greatly appreciated. The numerical integration was done using the MACSYMA algebraic manipulation system at the Laboratory for Computer Science.

Above all I am grateful to God who rules and overules in our lives for His continual provision. Finally, I wish to acknowledge the sacrifices of the people closest to me by dedicating this thesis to my Family:

Anna, my mother

Anna, my daughter

Vicky, my wife

Akwasi, my brother.

TABLE OF CONTENTS

Abstract 2

Acknowledgements 3

Table of Contents 5

List of Tables 8

List of Figures 9

List of Symbols 12

Chapter 1 **Introduction** 16

1.1 Introduction 16

1.2 History of cryogenic refrigeration 17

1.3 Applications of cryogenic processes 24

1.4 Research objective 29

1.4.1 Cryogenic refrigeration at the MIT Cryogenic Engineering Lab 29

1.4.2 Problem statement 30

Chapter 2 **Thermodynamic Principles of Refrigeration Cycles** 33

2.1 Introduction 33

2.2.1 Entropy flow analysis 34

2.2.2 Generated entropy as performance index 37

2.3 General requirement for refrigeration 39

2.4 Mechanical refrigeration cycles 41

Chapter 3 **An Optimum Configuration for Helium Liquefaction Cycles** 57

3.1 Introduction 57

3.2 Cold end irreversibility 59

3.3 Model I: Continuously distributed full-flow expanders 60

3.3.1 Refrigeration mode 60

3.3.2 Liquefaction mode 66

3.4 Model II: Continuously distributed full-pressure ratio expanders 67
3.4.1 Refrigeration mode 71
3.4.2 Liquefaction mode 76
3.5 Cold end configuration 77
3.6 Summary 81

Chapter 4 **An Entropy Flow Optimization Algorithm for Helium Liquefaction Cycles** 84
4.1 Introduction 84
4.2 Description of model 85
4.2.1 Ideal gas model: refrigeration mode 88
4.2.2 Ideal gas model: liquefaction mode 91
4.2.3 Real gas model: refrigeration mode 99
4.2.4 Real gas model: liquefaction mode 108
4.2.5 Alternative expander arrangement 109
4.3 Discussion of results 113
4.4 Design algorithm 114
4.5 Cost analysis 117
4.6 Conclusion 121

Chapter 5 **Experiments** 123
5.1 Introduction 123
5.1.1 SVC program 123
5.1.2 Turbine versus reciprocating expanders 125
5.2 Expander design 127
5.2.1 Historical evolution of reciprocating expanders 127
5.2.2 General description of expanders 130
5.2.3 Expander sizing 152
5.3 Experimental procedure 156
5.4 Instrumentation 157
5.4.1 Required measurements 158

5.4.2 Pneumatic circuit diagnostics 162
5.5 Summary of results 177
5.5.1 Refrigeration capacity 177
5.5.2 Wet expander tests 178
5.5.3 Single phase expander tests 179
5.6 Conclusion 180

Chapter 6 **Conclusion** 181
6.1 Summary 181
6.2 Suggestion for further work 184

Appendices . . . . . .
A Generated entropy as performance index 186
B Reversible precooling models 190
B1 Full-pressure ratio expanders 190
B2 Full-flow expanders 194
C Finite heat exchange temperature difference model 200
C1 Ideal gas model: refrigeration mode 200
C2 Ideal gas model: liquefaction mode 211
C3 Real gas model: refrigeration mode 220
C4 Real gas model: liquefaction mode 227
C5 Alternative expander arrangement 234
D Computer codes 244
D1 Parametric optimization 244
D2 Numerical integration 257
E1 Instrumentation 268
E2 Analysis of results 279
References 284
Biographical sketch 292

LIST OF TABLES

1.1 Critical point parameters for some cryogenic fluids 19

3.1 Turning point temperatures for refrigeration mode 66

3.2 State point parameters for cold end configuration 78

4.0 State point parameters for optimized 3-expander SVC cycle 116

5.1 Heat loss as function of displacer length 155

5.2 Typical time distribution of cycle processes 174

5.3 Typical results for refrigeration capacity 178

5.4 Results for single phase expander test 180

E2.1 Static heat leak test results 281

E2.2 Estimates of conduction/radiation loss 283

LIST OF FIGURES

1.1 Typical P-V Curve for a Pure Substance 18

1.2 Schematic of the Linde-Hampson System for Air Liquefaction 22

1.3 Collin's Cryostat 25

2.1 Refrigeration System Composed of a Series of Refrigerators 38

2.4.1 Reversed Carnot Cycle 42

2.4.2 Reversible Refrigeration Cycles: (a) Ericcson; (b) Stirling 43

2.4.3 Vapour Compression Cycle 44

2.4.4 J-T Cycle (a) Schematic (b) T-S Diagram 46

2.4.5 Schematic of Ejector Cycle 47

2.4.6 Cascade Cycle for Helium Liquefaction 48

2.4.7 Schematic of an Ideal Gas Cycle 50

2.4.8 Schematic of the Claude Cycle 52

2.4.9 Stirling Cycle 54

2.4.10 Gifford-McMahon Cycle 54

2.4.11 VM Cycle 56

2.4.12 Solvay Cycle 56

3.1 Reversible Continuum Model (a) Mass Crossflow; (b) Variable High Pressure . 61

3.2 Typical Performance Curve for Mass Crossflow Model: Mass Flow Rate . . . 63

3.3 Cold End Performance Curves for Mass Crossflow Model 64

3.4 Cold End Performance Curves For Mass Crossflow Model: . . . . . Fixed Pressure Ratio 65

3.5 Specific Heat Capacity Curve for Helium 68

3.6 (a) Performance Curves for Mass Crossflow Model: Liquefaction Mode 69

3.6 (b) Cold End Performance Curves for Mass Crossflow Liquefaction Model . . 70

3.7 Performance Curve for Variable Pressure Model (Constant) Low Pressure . . . 74

3.8 Typical Performance Curve for Variable Pressure Model 75

3.9 Mass Recirculation Configuration 79

3.10 Simplified Cold End Configuration (SVC) 80
3.11 2-Expander Collin's Precooler with Optimal Cold End Configuration 82
4.1 Typical Precooling Stage of a Helium Refrigeration Cycle 86
4.2 Model for Precooling Stage: Heat Exchange with Continuous Expansion . . . 87
4.3 Performance Curves for Ideal Gas Model, Refrigeration Mode . . . . . .
(a) Mass Flow Rate Versus Temperature 92
(b) Heat Exchange Area 93
(c) Generated Entropy 94
4.4 Performance Curves for Ideal Gas Model: Refrigeration Mode (Fixed r_p) . . . 95
(a) Mass Flow Rate 95
(b) Heat Exchange Area 96
(c) Generated Entropy 97
4.5 Performance Curves for Ideal Gas Model: Liquefaction Mode 100
(a) Mass Flow Rate 100
(b) Heat Exchange Area 101
(c) Generated Entropy 102
4.6 Cold End Performance Curves for Real Gas, Refrigeration Mode 104
4.7 Performance Curves for Continuous Precooling, Refrigeration Mode . . . . . .
(Heat Exchange Area) 105
4.8 Performance Curves for Continuous Precooling, Refrigeration Mode . . . . . .
(Generated Entropy) 106
4.9 Cold End Performance Curves for Real Gas Model, Refrigeration Mode . . 107
4.10 (a) Performance Curves for Mass Crossflow Model: Liquefaction Mode . . 110
4.10 (b) Cold End Performance Curves for Mass Crossflow Liquefaction Model . 111
4.11 3-Expander Saturated Vapour Compression Cycle 115
4.12 Performance Curves for Optimal 3-Expander Cycle 118
4.13 Sensitivity of Cycle Performance to Cold End Component Efficiencies . . . 119
4.14 Saving in Cost Function Versus Cold Compressor Efficiency . . . . . .
for Optimized Cycles 122

5.2.1 Displacer-Piston Rod Connection Showing Engine Seals 138
5.2.2 Cylinder Mounting 140
5.2.3 (a) Valve Block 141
5.2.3 (b) View of Valve Block 142
5.2.4 (a) Overall Layout of Piston Motion Control System 144
5.2.4 (b) Schematic of Piston Motion Control System 145
5.2.5 Hydraulic Controller 146
5.2.6 Layout of Limit Switch Arrangement 148
5.2.7 Cutoff Switch 150
5.2.8 NOT Element 150
5.2.9 Directional Valve 151
5.3 Layout of Experimental Set-up: Determination of Refrigeration Capacity . 157
5.4.1 T-S Diagram for Defining Wet Expander Efficiency 160
5.4.2 Layout of Experimental Set-up: Static Heat Test 163
5.4.3 Phase Relationship between Pressure at The Discharge Valve Actuator . . . .
and Inlet Valve Actuator 165
5.4.4 Phase Relationship between Pressure in the Expander . . . . . .
and at the Discharge Valve Actuator 166
5.4.5 Phase Relationship between Pressure in the Expander . . . . . .
and at the Inlet Valve Actuator 167
5.4.6 Phase Relationship between Pressure at the Inlet Valve Actuator . . . . . .
and Displacement (Cylinder Volume) 168
5.4.7 Phase Relationship between Pressure at the Discharge Valve Actuator . . . . .
and Displacement (Cylinder Volume) 169
5.4.8 Ideal P-V Diagram for Expander 172
5.4.9 Ideal P-V Diagram for Single Phase Expander Mode, with Blow Down . . 173
5.4.10 Ideal P-V Diagram for Single Phase Expander without Blowdown 175
5.4.11 Ideal P-V Diagram for Two-Phase Expander 176

E1.1 Typical Cold End Calibration Curve for Allen-Bradley Resistor 271
E1.2 Full Range Calibration Curve for Allen-Bradley Resistor 272
E1.4 (a) Calibration Curves for Vapor Pressure Thermometer 275
E1.4 (b) Cold End Calibration Curves for Vapor Pressure Thermometer 276

LIST OF SYMBOLS

A	Area
C_p	Specific Heat Capacity
CF	Cost Function
CHX	Cost of Heat Exchanger
CLN_2	Cost of LN_2
CPI	Consumer Price Index
F	Helmholtz Free Energy
M	Mass Flow Rate
NTU	Number of Transfer Units
ΔP	Pressure Drop
Q	Heat Transfer
T	Temperature
ΔT	Temperature Difference
r_p	Pressure Ratio
S	Entropy
U	Internal Energy
V	Volume
v	Specific Volume
W	Work Transfer
y	Ratio of Temperature Difference to Temperature

GREEK SYMBOLS

β	Dimensionless Constant $\frac{1}{\alpha} \ln r_p$
η	Efficiency also Dimensionless Temperature
Ψ	Dimensionless Mass Flow Rate Ratio $\ln \frac{m}{m_o}$
Λ	Availability Function
γ	Specific Heat Ratio $\frac{c_p}{c_v}$
α	Dimensionless Constant $\frac{c_p}{R}$
χ	Dimensionless Constant $\frac{1}{1+y}$
μ_{JT}	Joule-Thomson Coefficient

SUBSCRIPTS

c_v	Constant Volume
ex	Expander
gen	Generated
l	Low Pressure Stream
h	High Pressure Stream
liq	Liquid
n	Normalizing Constant
o	Initial Volume
1,2	State Point

PLATES

1A Exposed Engine with control mechanism 131
1B Exposed Engine with vacuum jacket in the background 132
1C Close-up of Engine 133
1D Another close-up view of the Engine 134
1E Piston motion control mechanism 135
1F Engine with vacuum jacket being mounted 136

Chapter 1

INTRODUCTION

This chapter gives a brief history of cryogenic refrigeration and states the purpose of this thesis.

1.1. Introduction

Helium is classified as a rare gas. It is also perhaps the most difficult gas to liquefy. Yet liquid helium has been the object of more experimental and theoretical research than any other fluid except, possibly, water. There are two principal reasons for this unusual attention. First, liquid helium exhibits several peculiar properties such as superfluidity[1,2] which offer challenging scientific investigation. These properties also have potential applications that can be far-reaching. Secondly, it is an indispensable refrigerant for very low temperature work, close to absolute zero temperature. This application puts a high premium on liquid helium. Consequently, there has been a fascinating historical interest in the quest to liquefy helium.[3-6] Currently efficient and reliable methods of producing the liquid is of prime interest because the world is on the verge of commercializing superconducting processes and devices.[7]

Helium was first liquefied by Kamerlingh Onnes in the physical laboratory of the University of Leiden which he had established in 1895. However, this was the culmination of a series of successes in the liquefaction of the other cryogenic fluids, in particular, and advances in cryogenic technology, in general, starting with the liquefaction of air in 1877. Therefore the history of helium liquefaction is complete only in the context of the broader history of cryogenic refrigeration. This broader history is outlined in the next section.

Cryogenics is used here to cover temperatures below 123K, consistent with its usage by the workers of the National Bureau of Standards in Colorado.[8] This seems to be

a more widely accepted definition. Moreover, it is a natural dividing line since ordinary refrigerants like Freon and hydrogen sulphide boil above this temperature whereas the 'permanent'gases - helium,hydrogen,neon,oxygen etc have normal boiling points below 123K.

1.2 History of Cryogenic Refrigeration[3] [6,10]

Any gas may be liquefied by cooling to its condensation temperature and then extracting its latent heat of vaporization. However, for the cryogenic fluids, the condensation temperatures are very low (4.2K at 1 atmosphere for helium) and suitable refrigeration at such low temperatures, traditionally, has not been available. Early attempts to liquefy the cryogens therefore involved other processes.

Robert Boyle's work with gases resulted in his famous law which stipulates that the P- V curve for ideal gases be rectangular hyperbolae. While investigating the validity of Boyle's Law, van Marum discovered, at the end of the eighteenth century, that ammonia gas may be liquefied solely by compression to about seven atmospheres without any necessity of lowering its temperature.

In Michael Faradays's work between 1823 and 1847, he found that both pressure and temperature play a part in the change from gas to liquid. He was able to liquefy several gases by heating one end of a sealed, bent glass tube to increase the pressure of the gas trapped in it and cooling the other end below room temperature. Finally between 1861 and 1869 Thomas Andrews obtained experimental pressure-volume curves for a real gas (carbon dioxide) which showed the characteristic flat portion below the critical point Fig. 1.1. His results illustrate the Pressure-Volume relationship of real gases and indicate that isothermal compression can indeed produce liquid: if the constant temperature is below the critical temperature. Consequently, early attempts to liquefy the cryogens involved compression of the gases to very high pressures.

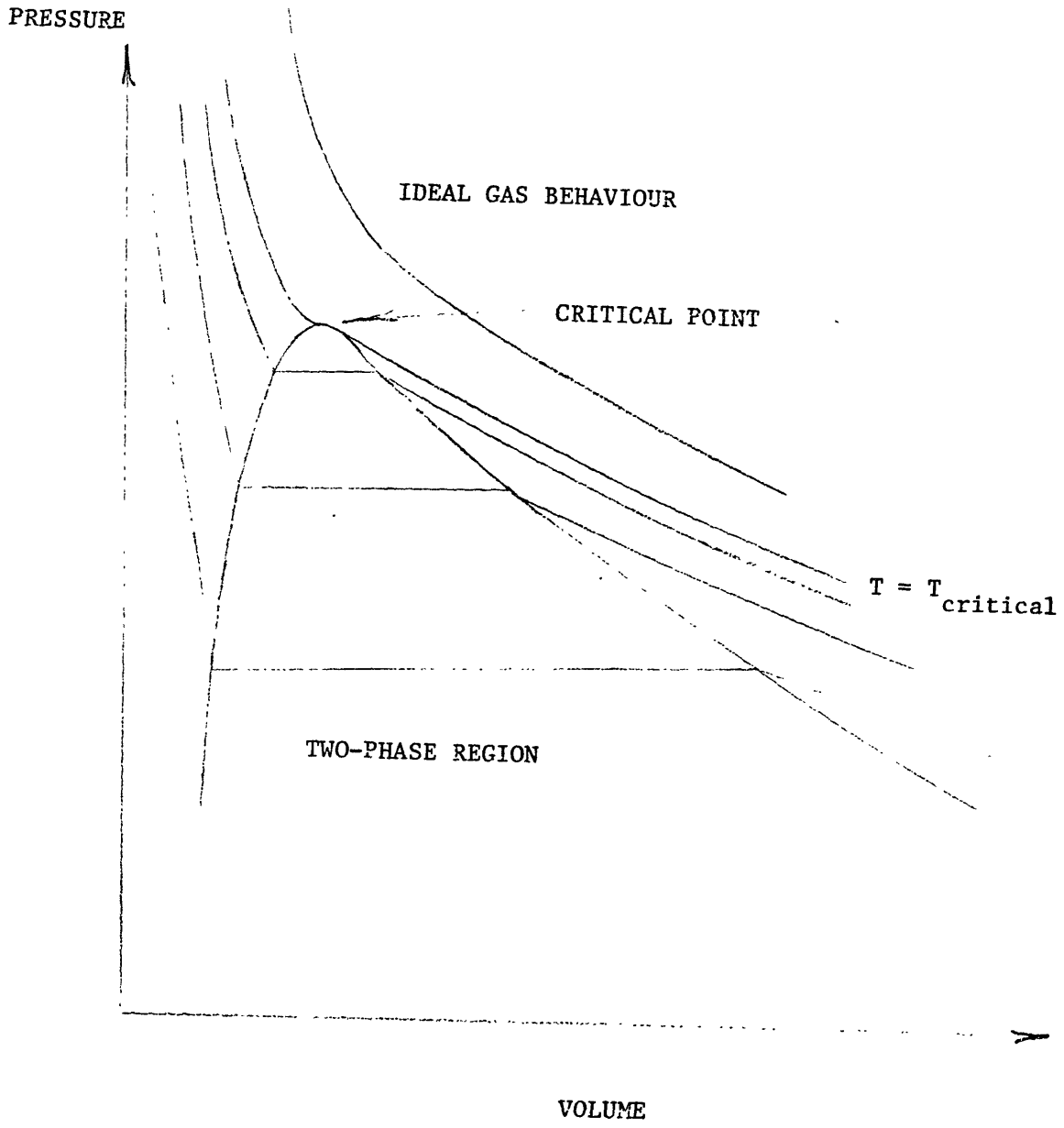


FIG. 1.1 Typical Pressure-Volume curve for a pure substance.

These attempts were unsuccessful because of the low critical point temperatures of these gases. Table 1.1 gives typical values of the critical point parameters for some cryogens.[9]

Table 1.1

Critical point parameters for some cryogenic fluids

Fluid	$T_{critical}$ (K)	$P_{critical}$ (atm)	$T_{normal\ bpt.}$ (K)
Oxygen	154.7	50.1	90.19
Nitrogen	126.1	33.49	77.395
n-Hydrogen	33.2	12.98	20.39
Helium	5.2	2.26	4.216

However, it was an effort in this direction which led Louis Cailletet, a French mining engineer to observe that expansion produces cooling when his experimental apparatus sprang a leak and the compressed gas escaped into the atmosphere. Subsequently he precooled high pressure oxygen gas in a strong-walled glass tube, released the pressure by opening a valve on the apparatus and thereby produced liquid oxygen droplets on December 2,1877.

This was the first time ever a so-called 'permanent'gas had been liquefied. Coincidentally Raoul Pictet, a Swiss physicist, also succeeded in liquefying oxygen on December 22,1877 by a completely different method now called the cascade method. This coincidence is interesting for three reasons. First, there was the initial historical confusion over who first liquefied oxygen which was justly resolved in favor of Cailletet. Secondly the different professions of the two men is representative of the two sources of contributions to cryogenic refrigeration research: Cailletet typifies the industrial world and Raoul Pictet the research scientist in an institutional laboratory. Thirdly the two processes used have been developed into the two practical liquefaction methods in use today-the method of Cailletet has been developed into well-engineered industrial cryogenic liquefaction plants; the method of Pictet has been developed into the cascade

scheme used for the laboratory liquefaction of cryogens. LNG plants also use a variation of the cascade method.

The liquid produced by Cailletet in 1877 was in the form of mist which soon evaporated. Wroblewski and Olszewski were Polish scientists investigating the physical properties of liquefied gases at the Cracow University Laboratory in the same decade. They were therefore interested in bulk quantities of liquids and introduced two techniques to achieve this for air. First they pumped on the refrigerant used for precooling the gas to further reduce the lowest temperature. Then they developed the vapor shielding concept to minimize heat leaks from ambient to the test apparatus thereby enhancing prolonged storage of the liquid. Their design consisted of a series of concentric tubes, closed at one end, surrounding the experimental test tube. The cold vapor rising from the liquid flowed through the annular spaces between the tubes intercepting some of the heat travelling toward the cold test tube. Armed with this improvement not only did they succeed in obtaining liquid oxygen in bulk quantities in April 1883, they were also successful in producing liquid nitrogen for the first time a few days later. However their attempts to liquefy hydrogen always resulted in droplets of the liquid: the heat leak to their test apparatus was still large. It thus remained for James Dewar to introduce innovations in insulation techniques and subsequently succeed in producing liquid hydrogen in bulk quantities and even go further to produce solid hydrogen.

James Dewar made three particularly significant contributions. He introduced both vacuum insulation, which drastically minimizes heat loss through convection, and the idea of changing the emissivity of radiating surfaces to reduce radiation losses. His device was a double-walled glass vessel with a silvered inner surface. These developments enabled him to liquefy hydrogen in bulk quantities in 1898. However, they were not enough to enable him to produce solid hydrogen until he further cut down on the radiation heat loss by another innovation: the radiation shielding technique. His radiation shield was a vacuum vessel filled with liquid air which surrounded the cryostat with the test apparatus. This reduced the heat leaks so substantially that he was able to

produce solid hydrogen by pumping the vapor off the liquid.

The success of Cailletet in producing liquid by expansion of a precooled high pressure gas led to pioneering efforts in the industrial application of air liquefaction in three centers. In Germany, Linde established the Linde Company for air separation and by 1897 had developed a practical cycle for liquefying air in bulk quantities. Essentially Linde precooled the high pessure gas using a set of counterflow heat exchangers (Fig. 1.2) and throttled the high pressure gas using a Joule Thompson valve. (It is surprising that although Joule and Thompson had experimented with the J-T valve process much earlier, it was Cailletet's observation that actually led to the application of the throttling process in cryogenic refrigeration). In Britain, W. Hampson independently used the same cycle (Fig.1.2) for air liquefaction and actually filed a patent for his device in England two weeks before Linde filed his in Germany. The cycle has since become known as the Linde-Hampson cycle. Meanwhile, in France, Georges Claude was developing a work-producing expansion engine to expand the high pressure gas and thus provide refrigeration by extracting work from the gas. By 1902 he had developed an air liquefaction system using an expansion engine.

The use of expansion engines in air refrigeration[10] dates back to 1849 when a Florida physician, John Gorrie published a report about his ice making device for cooling hospitals. It is even claimed that the British Engineer Richard Trevithick built several successful engines ,also for ice making, much earlier although no description of his device was ever published. Charles Siemens incorporated modifications to the Gorrie system involving heat exchangers to obtain a space cooling device in England. The credit for setting forth the essentials of the space cooling refrigerator using air expansion engines however goes to William Thompsom (Lord Kelvin). In any case it is the systematic and persistent effort of George Claude to overcome technical difficulties such as heat leaks and lubrication which led to the successful application of expansion machines in cryogenic liquefaction plants. Consequently he is often cited for introducing the use of cryogenic expansion engines. By 1907 the Claude air liquefier was producing neon as

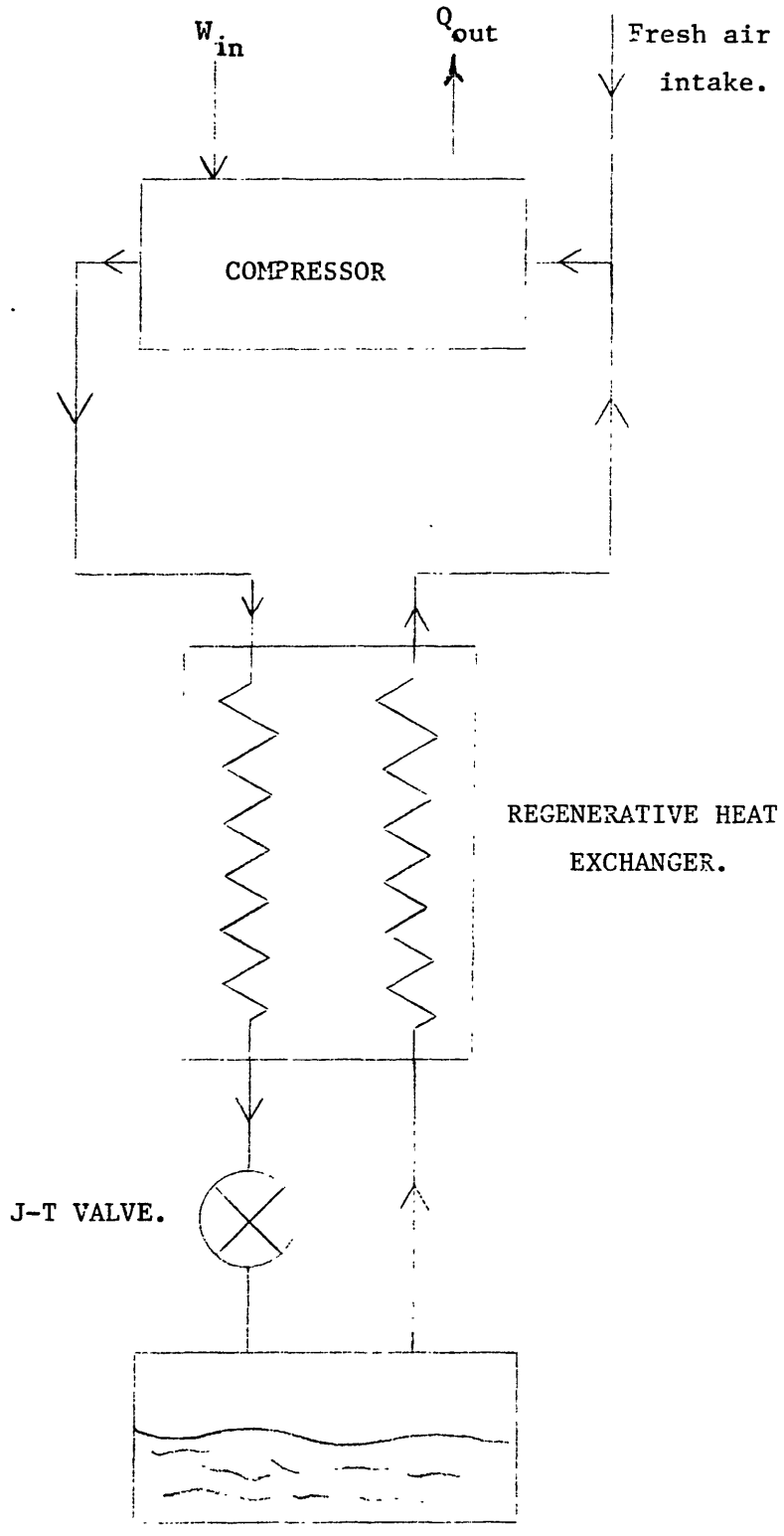


FIG. 1.2 SCHEMATIC OF THE LINDE-HAMPSON SYSTEM FOR AIR LIQUEFACTION.

a by product.

The Linde-Hampson cycle for air liquefaction as well as the Claude system had been refined by 1902. Effective insulation protocols had been established . Liquid hydrogen had been produced in large quantities and Dewar had even produced solid hydrogen. The stage was thus set for the liquefaction of helium which was seen as the gateway towards the march to absolute zero. The principal investigators actively engaged in this effort were Olszewski, James Dewar, Morris Travers and Kamerlingh Onnes. They had all tried to use Cailletet's method to liquefy helium and had failed. It was clear therefore that a Linde-Hampson type cycle was required. Kamerlingh Onnes had an advantage over the other investigators . He had methodically prepared for this onslaught by training skilled technicians. He founded a school for instrument makers and glassblowers in the Leiden laboratory. He built a large liquefaction plant for oxygen, nitrogen and air and followed it up with a hydrogen plant capable of producing four liters of liquid an hour, in 1906. Finally, by June 1908 work on building the helium liquefier had been completed and a high purity gas obtained. On July 10, 1908 he liquefied helium. This indeed was the climax of developments in the preceding thirty years. However, the success is also a tribute to his skill and careful planning especially considering the human resources involved in the operation and the complexity of the cascade machinery for helium.

Although Claude had established the use of work-producing expansion engines for air liquefaction as far back as 1902, it was not until 1934 that the first successful attempt was made to liquefy helium by the Claude process, by Kapitza. However, it was the monumental contribution of Sam Collins in 1946 which revolutionalized low temperature research to the extent that the period before 1946 is now referred to as BC (Before Collins) in cryogenic circles.

Collins built a practical, dependable helium liquefier using expansion engines which made helium available to most low temperature research centers. The design of the

Collins cryostat (Fig.1.3) was based on a second law analysis. By considering the flow of entropy in the cycle, he estimated the mass flow to be extracted and fed through the expansion engines. He was thereby able to derive a configuration for the liquefier which constitutes an efficient cycle. The design and fabrication of the cryostat also incorporated some ingenious features,[11] which made the cryostat reliable. The original cryostat used a Hampson-type heat exchanger but Collins later developed a compact and effective heat exchanger, called the Joy Tube . Thus the Collins contribution is significant for two reasons: the design was based on sound thermodynamic analysis demonstrating a clear insight into entropy flow, and the facility used well-designed, well-engineered components.

Improvements on this system have come from two directions. The cycle allows the flexibility of choosing the temperature levels (expander inlet or discharge temperatures to optimize the cycle performance). Therefore cycle optimization techniques have been developed and continually improved upon, to select these temperatures. Also efficient and reliable components have been and are still being developed. This research is a continuation of work in both directions.

1.3 Applications

Kamerlingh Onnes and his co-workers who first liquefied helium were interested in investigating the properties of materials at low temperatures and in checking the validity of known natural principles at cryogenic temperatures. Such investigation has led to a catalogue of unique cryogenic phenomena which have prompted several application ideas. Perhaps the most promising of these potential applications relate to superconductivity. There are two fundamental but related characteristics that underscore the potential use of superconductors. Superconductors are able to transmit enormous amounts of electric current without electrical resistance and therefore the heat associated with the losses. As a consequence of carrying large electric currents, they maintain intense and

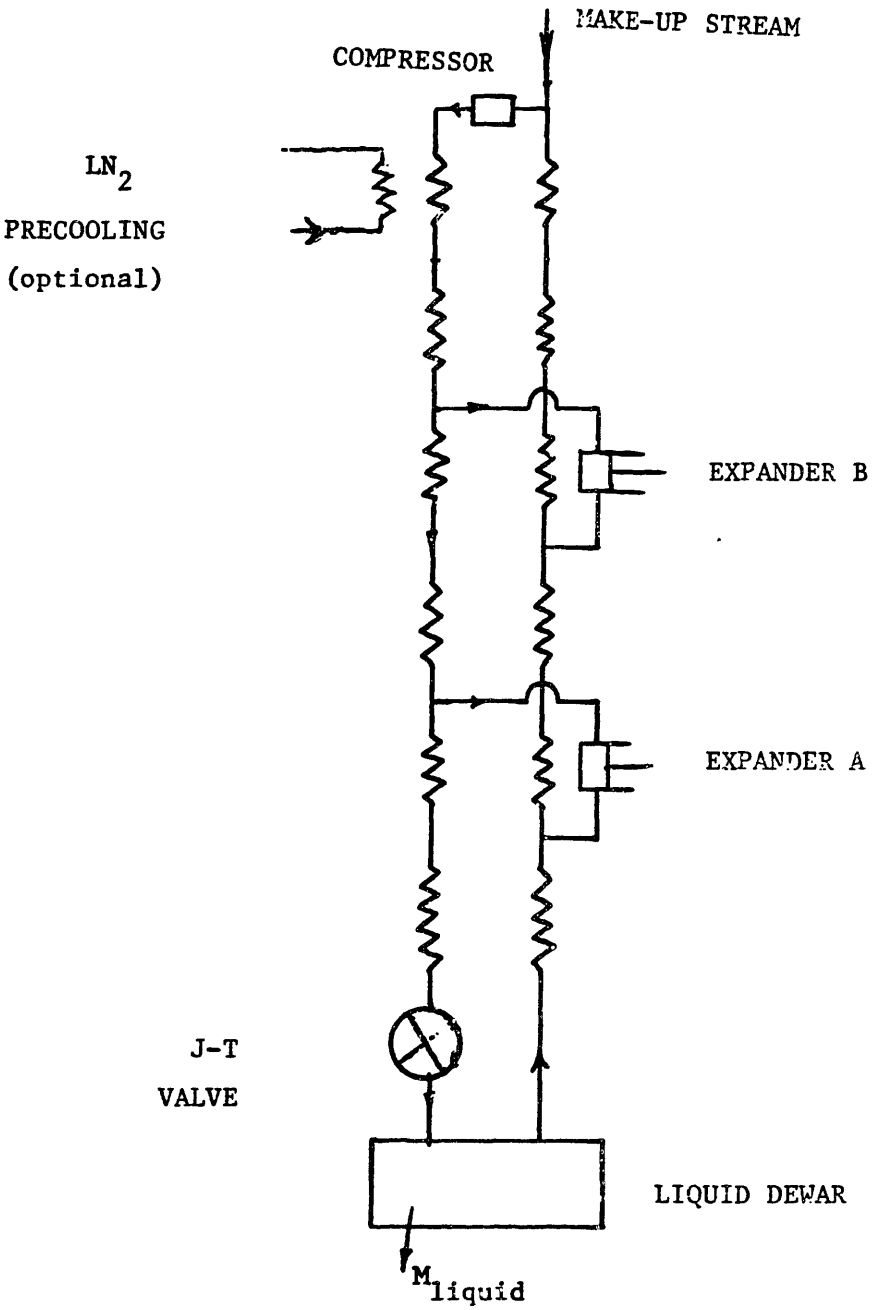


FIG. 1.3 COLLINS' CRYOSTAT (SHOWING OPTIONAL LN_2 PRECOOLING)

extremely steady magnetic fields. Some of the potential applications arising from these characteristics are discussed presently.

ELECTRICAL GENERATORS:[12 - 18] The basic superconducting generator concept has been demonstrated and advanced concept designs are being developed . Without the power losses associated with resistance heating, superconducting generators consume about two-third less energy than conventional generators with an equivalent power output; because of the high current density of the superconductors, the superconducting generator is only about two-thirds the size of a conventional generator, is lighter, and can generate higher voltages that conceivably could eliminate the use of step-up transformers in the power supply system. The superconducting generator is more resistant to short-lived line disturbances such as lightning because of its high fields.

ELECTRICAL ENERGY STORAGE:[7] This promises to be an efficient means of storing, in the form of magnetic energy, excess electrical energy produced by the utility companies. The utility companies can stockpile the excess electricity generated cheaply at night and use it to meet peak daytime demands. Currently the high daytime demands are handled by expensive oil or gas-fired plants.

ELECTRICAL POWER TRANSMISSION:[19 - 22] The use of superconducting cables for power transmission dramatically increases the current carrying capacity of cables of the same size.

TRANSPORTATION:[23,24] The use of superconducting magnets in the magnetically levitated train has been demonstrated, with the Japanese National Railways setting a world rail speed record in 1979 of 321 miles per hour with their experimental train. Superconducting magnets are mounted on the train and normally conducting magnets used as guideways. Levitation is provided by induced magnetic fields in the guideway magnets which repel the magnets on the train. Rapidly alternating magnetic fields from the guideway coils push and pull the train forward. Compact electric motors made from superconducting magnets are being considered to power ships. A 400 horsepower unit

was successfully tested by the U.S. Naval Ship R&D Center in late 1980.

PURIFICATION /SEPARATION PROCESSES:[23] The difference in magnetic susceptibility of various materials is the basis of several purification/separation processes. Thus a superconducting magnetic separator may be used to separate iron-containing components from low grade ore or in mining other hard-to-get minerals. In water purification, solids left after sewage treatments are first coagulated usually using alum. Magnetic particles are then added to the water and adhere to the coagulated solids. A strong magnet may subsequently be used to remove the solid particles. In fact, superconducting magnets can be used to replace conventional magnets in most separation processes.

NMR MEDICAL IMAGING SYSTEM:[25 - 26] The use of superconductors in NMR medical imaging systems may well be the first commercial application of superconductivity. The performance of NMR imaging systems is greatly enhanced by the use of superconductors because the associated magnetic fields are strong, spatially uniform and very steady. The use of superconductors result in image resolution of 1.3mm compared to 4mm when conventional magnets are used. Also contrasts up to 100:1 versus 32:1 and data collection time of 0.1s compared to 100s indicate the superior images that can be obtained with superconducting NMR. Capital cost of the superconducting NMR may be high but the operating cost will be low because of the minimal power consumption rate.

FUSION/HIGH ENERGY PHYSICS:[28] The high fields of superconducting magnets make them attractive in replacing conventional magnets in high energy physics experiments and in plasma heating for fusion devices. Also the small size makes them attractive, especially in aerospace applications where relatively small mass is of prime importance . Applications in the bio-medical/chemical field include control of chemical reactions (magnetocatalyses);and suspension/steering of magnetic objects such as the steering of magnetic catheters through the brain. Superconducting gyroscopes with

extremely small drift are also being developed.

CRYOPUMPING: This is used to create ultra high vacuum for space simulation tests, for high vacuum thermal insulation and for creating working environments in the semiconductor manufacturing industry.

ELECTRONIC DEVICES:[29,30] Several superconducting electronic devices are being developed. In addition to the low power dissipation, the performance characteristics of various solid state devices at cryogenic temperatures are stable, repeatable and insensitive to thermal cycling. These devices have wide applications such as in microwave receivers and as computer elements.

SQUIDS:[31-32] Superconducting Quantum Interference Devices reportedly are superior to all other magnetic sensors in sensitivity, frequency response, range and linearity. They can therefore perform unique functions not offered by conventional devices. But, in addition, they can also do less demanding jobs better than conventional instruments and are used in highly sensitive magnetometers, gradiometers, and amplifiers-particularly for applications requiring extreme voltage sensitivity.

There is a wide variety of potential applications for superconducting technology. This reflects on the demand for a wide range of refrigeration requirements from large plants, as for the superconducting generator program, to low values of refrigeration (fraction of watts) for cooling superconducting electronic devices. The commercialization of these and other cryogenic phenomena is contingent upon the availability of reliable and inexpensive refrigeration plants. The design of refrigeration devices therefore present challenging opportunities for technological innovations to the cryogenic engineer.

1.3.1 Cryogenic Refrigeration at the MIT Cryogenic Engineering Laboratory

The monumental contribution of Professor Sam Collins in the forties was the basis for the organization of the MIT Cryogenic Engineering Laboratory where Professor Collins continued to improve helium liquefaction equipment until 1964. After Professor Smith succeeded Professor Collins in 1964, improvement in helium liquefaction were continued and a more efficient liquefier which uses a supercritical wet expander in place of the J-T valve was installed. Refrigeration research was also broadened and several other methods of refrigeration were installed. Prominent among these are the analytical studies and extensive experimental work on Stirling cycle machines,[33,34] thermal regenerators [35-40] pulse tube refrigeration[41] and miniature refrigerators [42] using bellows engine. Contributions from this work have greatly enhanced our understanding of these systems, essentially redefining the basic theory of operation and providing appropriate methods for analyzing these systems. More recently, and especially since the energy crisis the focus of studies in cryogenic refrigeration by Prof. Smith has shifted to a fundamental study of the basic refrigeration process. This effort started with a comparative analysis of Collins-type liquefiers operating at elevated pressure levels[43] and also marked the entry of the author into cryogenic refrigeration and the MIT Cryogenic Engineering Laboratory. Current cryogenic refrigeration work in the laboratory includes magnetic refrigeration studies. It must be mentioned, however, that the laboratory has been at the forefront of other areas of cryogenic technology. The major work in the laboratory involves the superconducting generator. Since testing the world's first superconducting generator with a rotating cryostat in 1969[12] the laboratory has tested a 3mVA superconducting generator[12] and is currently involved in demonstrating advanced design concepts of the superconducting generator.[13]

1.3.2 Problem Statement

Our preliminary study of the performance of helium liquefaction cycles operating at elevated pressure levels indicated a superior performance over conventional cycles. The analysis used the conventional optimization scheme for the Collins-type liquefaction systems. In this conventional technique, a particular cycle configuration is first chosen. A system of equations with the state points (pressure and temperature) and the mass flow rates as the variables is obtained by applying the first law of thermodynamics to various components of the plant and also writing the continuity (mass conservation) equation at the various nodes of the flow schematic. The number of equations (n) is normally less than the number of variables (m) so that there is an infinite number of solutions to the system of equations, involving m-n arbitrary parameters. Consequently the system may be optimized by a straight forward mathematical parametric optimization technique. The resulting solution is then checked for violations of the second law of thermodynamics. An improvement on this technique by Toscano et al [44] incorporates the second law by computing the entropy generation associated with each component thereby identifying and quantifying the sources of irreversibilities in the cycle. Our preliminary analysis also used the second law of thermodynamics to judiciously initialize some of the optimizable parameters[45].

However, the short comings of this technique was soon apparent. The straight forward mathematical parametric optimization does not provide adequate insight into the physical factors driving the system. An even more limiting handicap is the fact that a cycle configuration had to be chosen first. In our analysis we thought of a number of cycle configurations and applied the procedure above to each one of them in turn. Although we had arrived at a more efficient cycle configuration in the form of the saturated vapor compression cycle, in the end there was no guarantee that we had exhausted all the possible configurations. Further the design of a thermodynamically efficient system requires a second law analysis but the conventional technique is

essentially based on a first law analysis.

These shortcomings of the conventional analysis are the basis for the final objective of this thesis: to develop an alternative design algorithm for cryogenic liquefaction cycles which is based on the second law and, in which the cycle configuration is an output rather than an input.

Our preliminary analysis had shown that the saturated vapor compression cycle is superior, in thermodynamic performance, to the conventional cycle. When used for the production of atmospheric pressure liquid helium, it allows the cycle pressures to be chosen independently of the liquid dewar pressure and thus allows these pressures to be selected for the best performance of the expanders and heat exchangers in the cycle and hence better overall performance.

For refrigeration at temperatures below 4.2K, the wet expander cold-compressor section is used to maintain subatmospheric pressure over the boiling liquid and thus allows the conversion of a standard helium liquefier to a 1.8K refrigerator without the addition of large low pressure heat exchangers and large displacement vacuum pumps. An approximate cost estimate also indicated that a saturated vapor compressor is worth developing. In view of these superior characteristics, the second objective of this thesis is to investigate, experimentally, the feasibility of implementing the saturated vapor compression.

Thus the objectives of this research are:

1. To develop an alternative optimization scheme for cryogenic liquefaction cycles, based on the second law of thermodynamics and in which the configuration is an output rather than an input.

2. To design and build a machine that can be used for investigations leading to the practical implementation of the saturated vapor compression cycle.

The thesis starts in chapter two with a discussion on the choice of entropy flow as the method of analysis and the generated entropy as the performance index, followed by a brief review of mechanical cryogenic refrigerators. In chapter three, reversible continuum models for the precooling stage of a typical refrigeration cycle are considered for synthesizing an optimum cycle configuration using the basic theory of chapter two. The new entropy flow optimization technique for designing helium liquefaction cycles is presented in chapter four. An account of the experimental work involving the design and fabrication of a reciprocating machine with a programmable hydraulic-pneumatic control and the evaluation of its performance is given in chapter five. Finally chapter six summarizes the salient points of the research.

Chapter 2

THERMODYNAMIC PRINCIPLES OF REFRIGERATION CYCLES.

This chapter discusses the use of entropy flow analysis in cryogenic refrigeration and the choice of generated entropy as the performance index for the analyses in subsequent chapters. A brief review of several mechanical refrigerators is also given.

2.1 Introduction

Refrigeration processes are essentially heat transfer processes. Invariably all practical heat transfer processes are accompanied by irreversibilities. Therefore since the keyword in this thesis is thermodynamic performance, it is important to quantify the irreversibilities in a way that lends itself to analytical optimization.

In this chapter, the generated entropy concept of the second law of thermodynamics[40] is shown to be an invaluable tool for quantifying the concept of thermodynamic irreversibility as well as efficiently identifying the origin and/or location of the irreversibilities (section 2.2.1). The cycle generated entropy is next shown to be equivalent to the coefficient of performance COP as a cycle performance index (section 2.2.2). Then a general requirement for refrigeration cycles is discussed which further underscores the role of entropy in refrigeration processes (section 2.3). Finally, examples of mechanical refrigeration cycles are presented in section 2.4 to contextualize the SVC cycle which is the main concern of this thesis.

2.2.1 Entropy Flow Analysis

The first law of thermodynamics defines energy as a property of a system and gives the interrelationship between the change in energy of a system and the energy transfer interactions associated with the system and its environment. Also the second law introduces entropy as a property. It is the entropy transfer which distinguishes between heat and work transfer interactions as parallel forms of energy transfer for a thermodynamic simple-system. It is only the transfer of energy as heat which is accompanied by entropy transfer. Further the second law directly imposes limits on the heat transfer between a system and its environment. Combining the first and second laws then reveals the limits imposed on the work transfer interaction. To illustrate, consider a closed system experiencing an isothermal change of state from initial state (1) to a final state (2). The first law gives the energy relationship:

$$Q_{1\to 2} - W_{1\to 2} = U_2 - U_1. \tag{2.1}$$

The second law gives the limit on the heat transfer

$$Q_{1\to 2} \leq T_o(S_2 - S_1), \tag{2.2a}$$

or alternatively

$$Q_{1\to 2} + T_o S_{gen} = T_o(S_2 - S_1). \tag{2.2b}$$

The generated entropy, S_{gen} is a path dependent variable. The difference between possible paths is described by the strength of the inequality sign in Eq. (2.2a) or by the magnitude of S_{gen} in Eq. (2.2b). For a reversible path, the equality holds in Eq. (2.2a) and $S_{gen} = 0$. Thus, S_{gen} gives a quantitative description of the degree of irreversibility of the process, which is missing in the inequality statement.

The corresponding limit on the work transfer is obtained by combining the first and second laws (i.e., Eqs. (2.1) and (2.2):

$$W_{1\to 2} \leq -[(U - T_oS)_2 - (U - T_oS)_1], \tag{2.3a}$$

or

$$W_{1\ldots 2} + T_o S_{gen} = -[F_2 - F_1] \tag{2.3b}$$

where F is the Helmholtz free energy and T_o is required to specify the final location on the thermal scale of the entropy generated by the irreversibility. By imposing the additional restriction that the environment is at constant pressure, P_o, the limit on the isothermal non-pdv work is given by the Gibbs free-energy:

$$(W_{1\ldots 2})_{non\ \ pdv} \leq -[(U + P_o V - T_o S)_2 - (U + P_o V - T_o S)_1]. \tag{2.4a}$$

The limit on the heat transfer is still given directly by the second law in Eq. (2.2). Further, if the environment is assumed to be the atmosphere, the maximum useful work available for the system atmosphere combination is given by the availability function Λ:[47]

$$(W_{1\ldots 2})_{useful} = \Lambda_2 - \Lambda_1, \tag{2.5a}$$

where

$$\Lambda = (U + P_{atm} V - T_{atm} S) - (U + P_{atm} V - T_{atm} S)_{minimum}. \tag{2.5b}$$

Similarly for an open system experiencing heat transfer only with a heat reservoir at T_{atm}, again the second law directly imposes a limit on the heat transfer interaction:

$$Q_v \leq \sum_{out} m T_{atm} S - \sum_{in} m T_{atm} S, \tag{2.6a}$$

or

$$Q_v + T_{atm} S_{gen} = \sum_{out} m T_{atm} S - \sum_{in} m T_{atm} S. \tag{2.6b}$$

To determine the limit imposed on the shear work transfer combine the first and second laws to get

$$(W_{cv})_{useful\,max} \leq -\left[\sum_{out} m(h - T_{atm}S) - \sum_{in} m(h - T_{atm}S)\right] = \tag{2.7a}$$

$$-\left[\sum_{out} \phi - \sum_{in} \phi\right], \tag{2.7b}$$

where

$$\phi = (h - T_{atm}S) - (h - T_{atm}S)_0. \tag{2.8}$$

Thus the maximum useful work obtainable is given by the change in the availability function, (also called exergy). Exergy is a relative quantity defined with reference to a dead state, usually the atmosphere.

In summary then, for refrigeration cycles the principal energy interaction of interest is heat transfer. Associated with this heat transfer is entropy transfer. Refrigeration cycles essentially absorb heat from some low temperature T_l and reject this heat at some higher temperature. Equivalently refrigeration cycles absorb entropy at T_l and move this entropy through a temperature gradient and reject it at some higher temperature. In the process of moving the entropy, irreversibilities occur at various temperature levels which are quantitatively given by the generated entropy. The entropy generated adds on to the entropy being moved through the temperature gradient. Thus there is a cascading effect. The total entropy eventually rejected at the hot end (or at any temperature level for that matter) indicates the degree of irreversibility of the cycle. Thus the path of the cycle determines the total value of non-property S_{gen} which indicates the degree of departure of the cycle from reversibility.

The entropy flow analysis is therefore the natural mode of analysis for such refrigeration cycles. Further for cryogenic refrigeration cycles several heat reservoirs may be used at different temperature levels such as in the cascade process. Heat may be rejected at more than one temperature level. It is therefore more appropriate to use the entropy flnow analysis which does not have the fixed reference temperature restriction of the

exergy analysis. Finally, the entropy flow analysis enables the entropy generated locally (and hence the irreversibilities) to be monitored thus facilitating continuum analysis. Entropy flow analysis is therefore invaluable in the design of efficient refrigeration cycles which requires minimizing irreversibilities generated over the temperature range of interest as discussed presently.

2.2.2 Generated Entropy as Performance Index

Cryogenic liquefaction/refrigeration cycles may be optimized based on several criteria such as maximum refrigeration (liquid extraction), minimum energy (busbar), minimum plant capital cost, minimum total input power per unit mass circulated or in terms of availability ratios. In general the various criteria do not necessarily result in the same optimum condition and the actual design condition involves trade-offs between some of these criteria. For example, designing for optimum thermodynamic performance requires expensive equipment: a reversible heat exchanger should have an infinite heat exchange area. The basic criterion used in this research is the thermodynamic performance of the cycle as measured by irreversibility. Trade-offs will then be based on the degree to which changes in a particular system parameter affects the thermodynamic performance.

The performance of thermodynamic cycles is traditionally given by an efficiency parameter or the coefficient of performance COP. An entropy flow analysis for evaluating the performance of a refrigeration system composed of a series of refrigerators (Fig. 2.1) is now discussed to establish in a simple case the relation between the generated entropy performance index and the conventional COP.

The refrigeration system shown in Fig. 2.1 is a cascade of differential refrigerators distributed between T_h and T_l with each refrigerator spanning a temperature dT. The work input for each stage is

$$\delta W = x\delta W_{rev}, \tag{2.9}$$

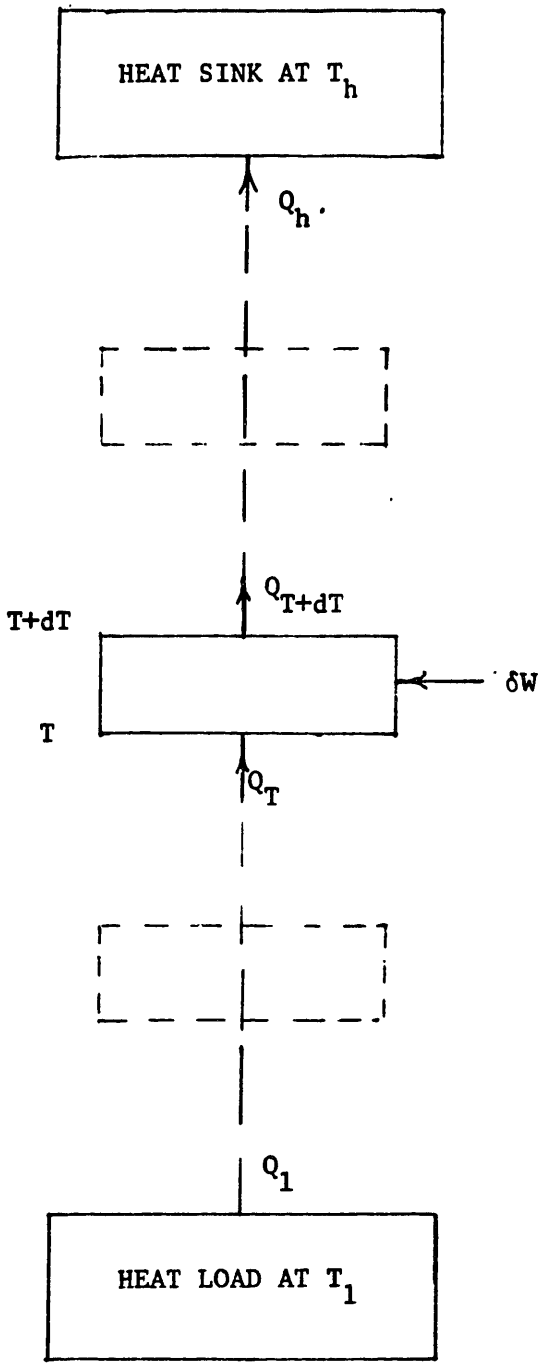


FIG. 2.1 REFRIGERATION SYSTEM COMPOSED OF A SERIES OF REFRIGERATORS.

where δW_{rev} is the reversible work for the differential refrigerator stage.

The overall performance of the refrigeration system is indicated by the COP which is derived in appendix A by integrating over the temperature span of the system

$$COP = \frac{Q}{W} = \frac{1}{(T_h/T_l)^x - 1}, \tag{2.10}$$

from which the COP for a reversible refrigerator is recovered for $x = 1$

$$COP_{rev} = \frac{1}{T_h/T_l - 1}. \tag{2.11}$$

The COP can be expressed in terms of entropy by substituting for the temperature ratio. The expression for this substitution is derived by first evaluating the heat transfer at any temperature T,

$$\frac{Q}{Q_l} = \left(\frac{T}{T_l}\right)^x. \tag{2.12}$$

The entropy–temperature relationship is then given by

$$\frac{S}{S_l} = \left(\frac{T}{T_l}\right)^{x-1}. \tag{2.13}$$

The temperature ratio in Eq. (2.10) may now be replaced by the entropy ratio in Eq. (2.13) to give

$$COP = \frac{1}{\frac{S_h}{S_l}\left(\frac{T_h}{T_l}\right) - 1}. \tag{2.14}$$

Finally substituting for

$$\frac{S_h}{S_l} = 1 + \frac{S_{gen}}{S_l}, \tag{2.15}$$

we can express Eq. (2.14) as:

$$COP = \frac{1}{\frac{T_h}{T_l}\left[1 + \frac{S_{gen}}{S_l}\right] - 1}. \tag{2.16}$$

Therefore maximizing COP is equivalent to minimizing $S_{gen}(T)$ given by

$$S_{gen} = \int_{T_l}^{T} \frac{dS_{gen}}{dT} dT. \tag{2.17}$$

Since S_{gen} is the integral over the precooling range of the local irreversibility, this example also illustrates the cascading effect of the irreversibilities associated with the refrigeration process.

The analyses in the next two chapters involve differential elements of a continuum model for the precooling stage of the refrigeration cycle. The local irreversibility given by dS_{gen} is integrated to determine the total irreversibility which is subsequently minimized. The equivalence established here between the COP and the generated entropy illustrates the use of the integrated entropy as a performance index.

2.3 General Requirement for Refrigeration

In order to further underscore the importance of the entropy flow concept in the analysis of refrigeration cycles, the dependence of refrigeration effect on the entropy changes associated with changes in a generalized variable of the refrigeration system is discussed in this section.

In the analysis of the common refrigeration cycles, the thermodynamic simple-system model is adequate for determining the cycle performance. Thus in applying the first law, only forces arising from the pressure have been taken into account in calculating the reversible work $\int Pdv$. The effects of body forces due to external force fields are neglected. Two independent variables are required to completely specify the state of the system: one thermal variable (T or S) and one mechanical work variable (P or v). By

choosing the intensive variables as independent variables, the entropy change is given by

$$dS = \left(\frac{\partial S}{\partial T}\right)_p dT + \left(\frac{\partial S}{\partial p}\right)_T dp \tag{2.18}$$

The refrigeration (δQ) provided by the mechanical refrigeration system at a given constant temperature level T_l is thus given by

$$\begin{aligned} \delta Q &\leq T_l dS \\ &\leq T_l \left(\frac{\partial S}{\partial p}\right)_T dp \end{aligned} \tag{2.19}$$

Thus the refrigeration effect depends on entropy changes associated with changes in the intensive mechanical work variable. This may be generalized to other refrigeration modes by relaxing the restrictions on the external force fields imposed on thermodynamic simple-systems.[48-50] The reversible work transfer may then be due to some other conservative force such as magnetic forces. (The change in magnetic field strength associated with magnetic work transfer is the basis of refrigeration by adiabatic demagnetization.) Thus a fundamental prerequisite for any refrigeration method is that there must be an identifiable property whose changes cause changes in entropy at constant temperature.

Magnetic refrigeration[51-54] is primarily used for providing refrigeration below 4K in a single cycle mode. Magnetic refrigerators that provide continuous refrigeration are not yet well developed. By far the most widely used cryocoolers/refrigerators use mechanical cooling effect. This research deals with the efficient design of these mechanical cooling devices. The underlying principles of various types of mechanical refrigerators are discussed presently.

2.4 Mechanical Refrigeration Cycles

2.4.1 Reversible Refrigeration Cycles

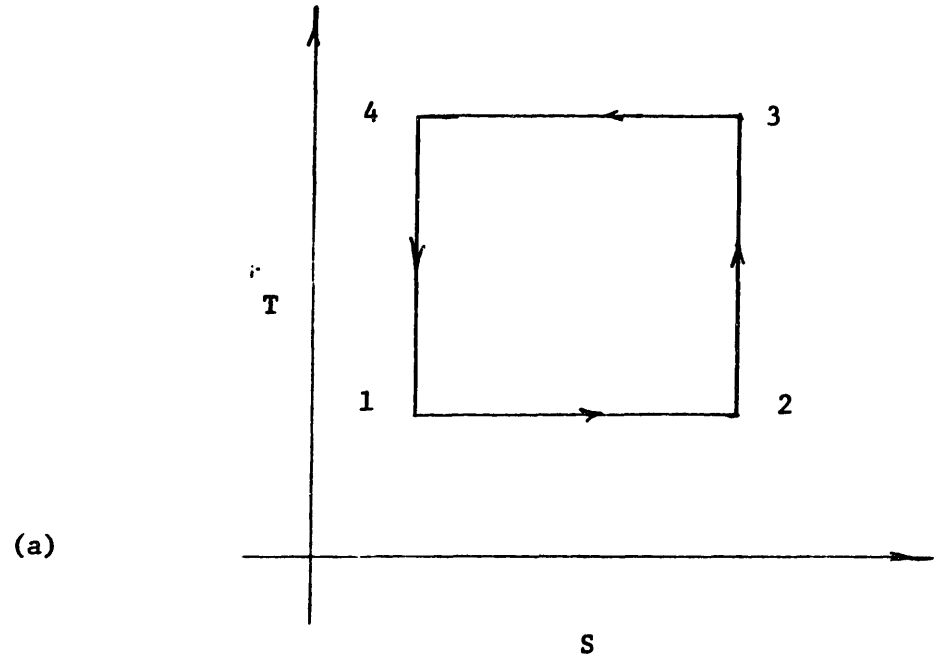
Typically, mechanical refrigeration cycles are fluid flow systems that absorb heat Q_l at the refrigeration temperature T_l and reject heat Q_h at a higher temperature T_h. For such two-heat reservoir cycles to be reversible, the entropy transferred at T_l (associated with the refrigeration effect) is transported, unchanged, against the temperature gradient, and rejected at T_h. Figures 2.4.1(a) and 2.4.2 show typical T-S diagrams for some reversible refrigeration cycles.[57-59] Historically, these cycles were first developed for power cycles and by reversing the direction of executing the cycle, the corresponding refrigeration cycle is derived. Consequently the cycles are often qualified by "reversed" as in reversed Carnot cycle.

2.4.2 Vapor Compression Cycle (VCC)

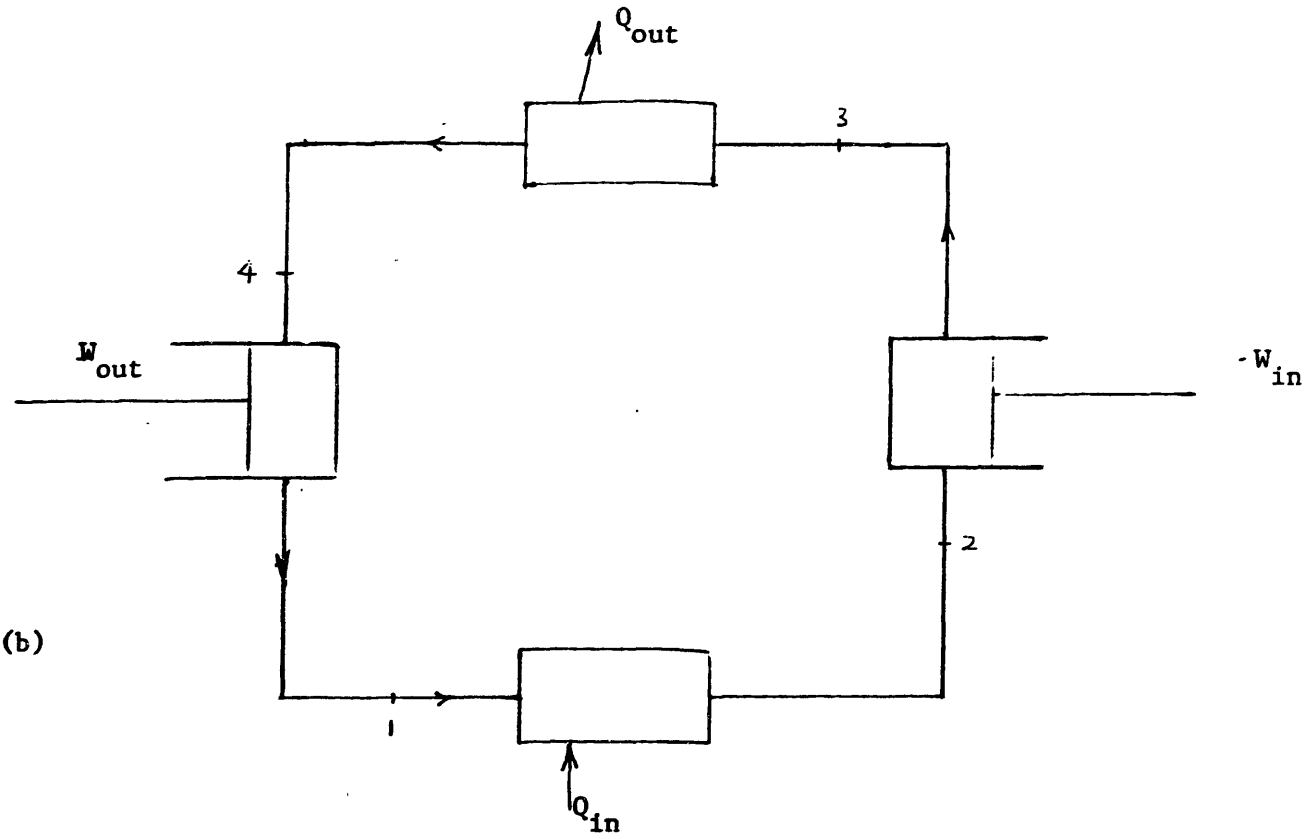
In the reversed Carnot cycle, the isotherms are joined by constant entropy processes 2-3 and 4-1. The arrangement of components in Fig. 2.4.1(b) can conceptually be used to effect this steady flow cycle if all component steady flow processes are reversible. This is the basis of the ideal vapor compression refrigeration cycle.[59,60] The working fluid is usually freon, ammonia, or hydrogen sulphide.

In the Carnot VCC, the refrigeration is provided by the latent heat of vaporization of the refrigerant. The expansion engine thus must operate in the two-phase region. This causes practical problems that degrade the performance of the engine. Therefore an expansion valve is routinely used for the expansion process. The valve also has the advantage of simplicity.

The resulting configuration and a typical T-S diagram are shown in Fig. 2.4.3. In this cycle the expansion process lies entirely in the two-phase region. This means

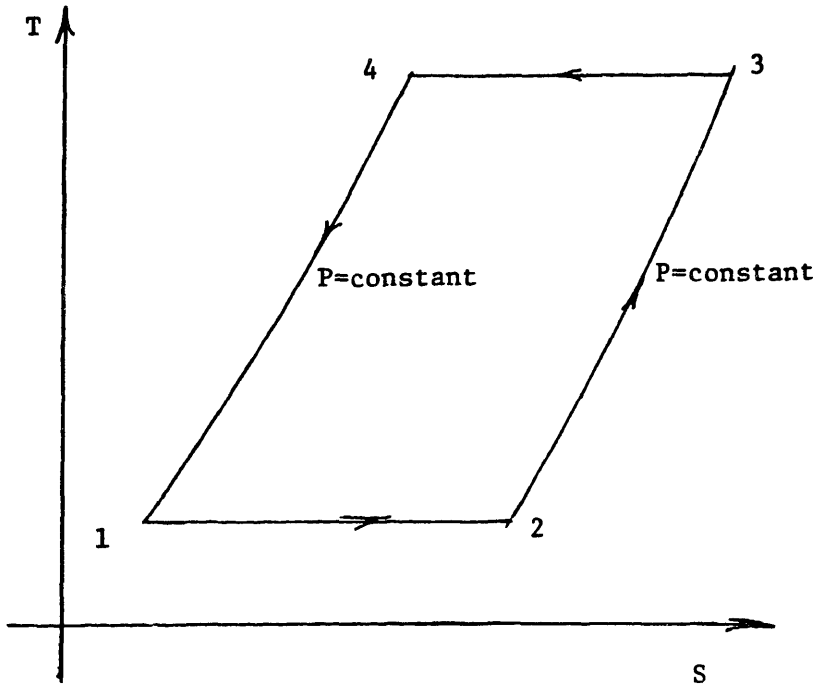


(a)

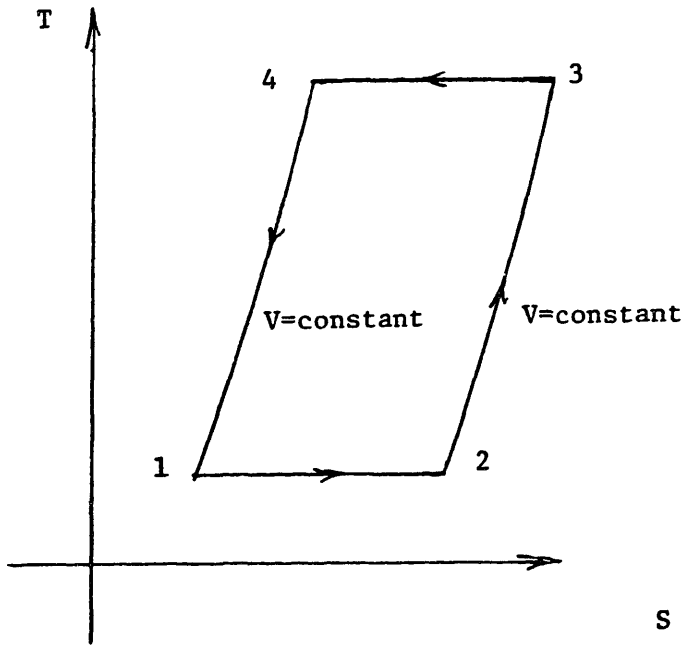


(b)

FIG. 2.4.1 REVERSED CARNOT CYCLE: (a) T-S DIAGRAM
(b) SCHEMATIC

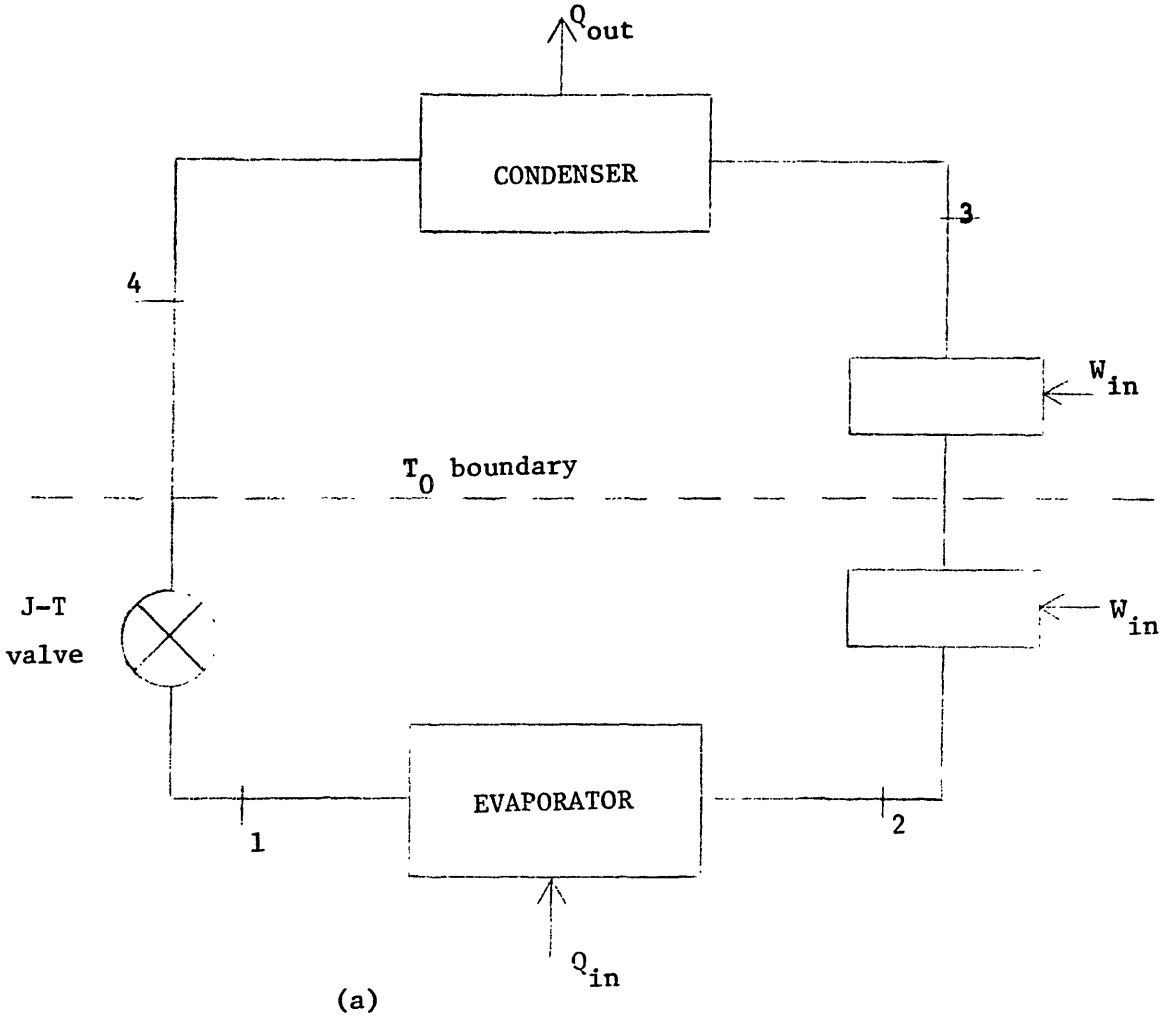


(a)



(b)

FIG. 2.4.2 REVERSIBLE REFRIGERATION CYCLES :
(a) ERICSSON; (b) STIRLING.



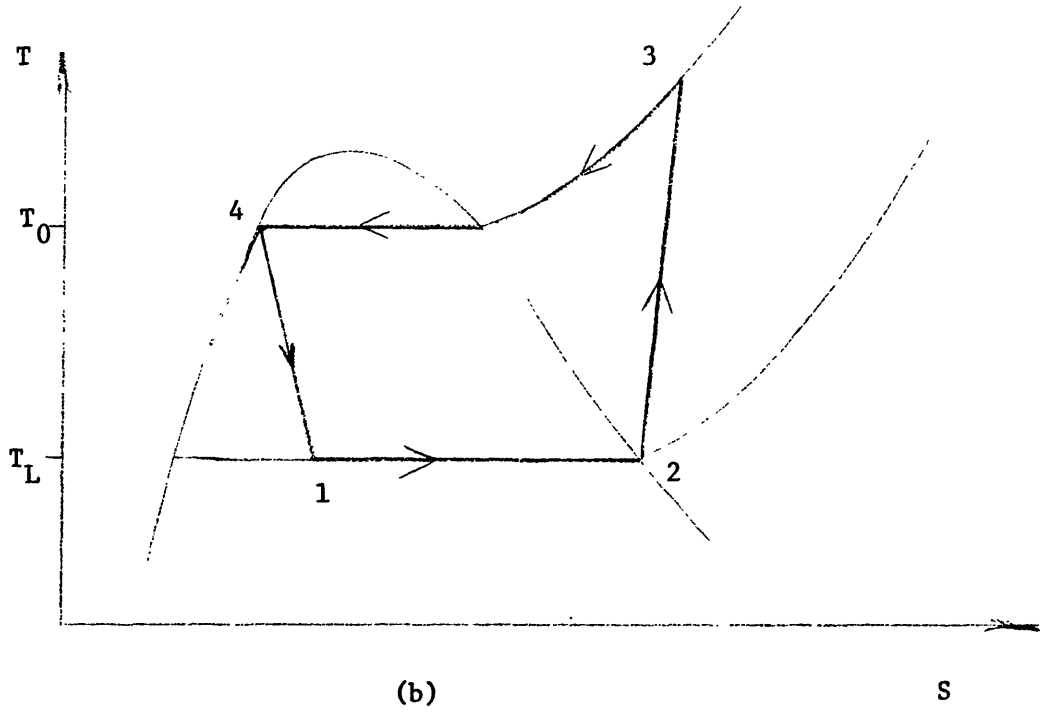


FIG. 2.4.3 VAPOUR COMPRESSION CYCLE : (a) SCHEMATIC
(b) T-S DIAGRAM

the critical temperature of the refrigerant is greater than the ambient temperature. This cycle is therefore commonly used for air-conditioning applications close to room temperature. Secondly, the cycle high temperature is less than the critical temperature of the working fluid so that the state of the working fluid is liquid after the heat rejection stage. This cycle is therefore used with non-cryogenic refrigerants.

2.4.3 Joule-Thompson Cycle

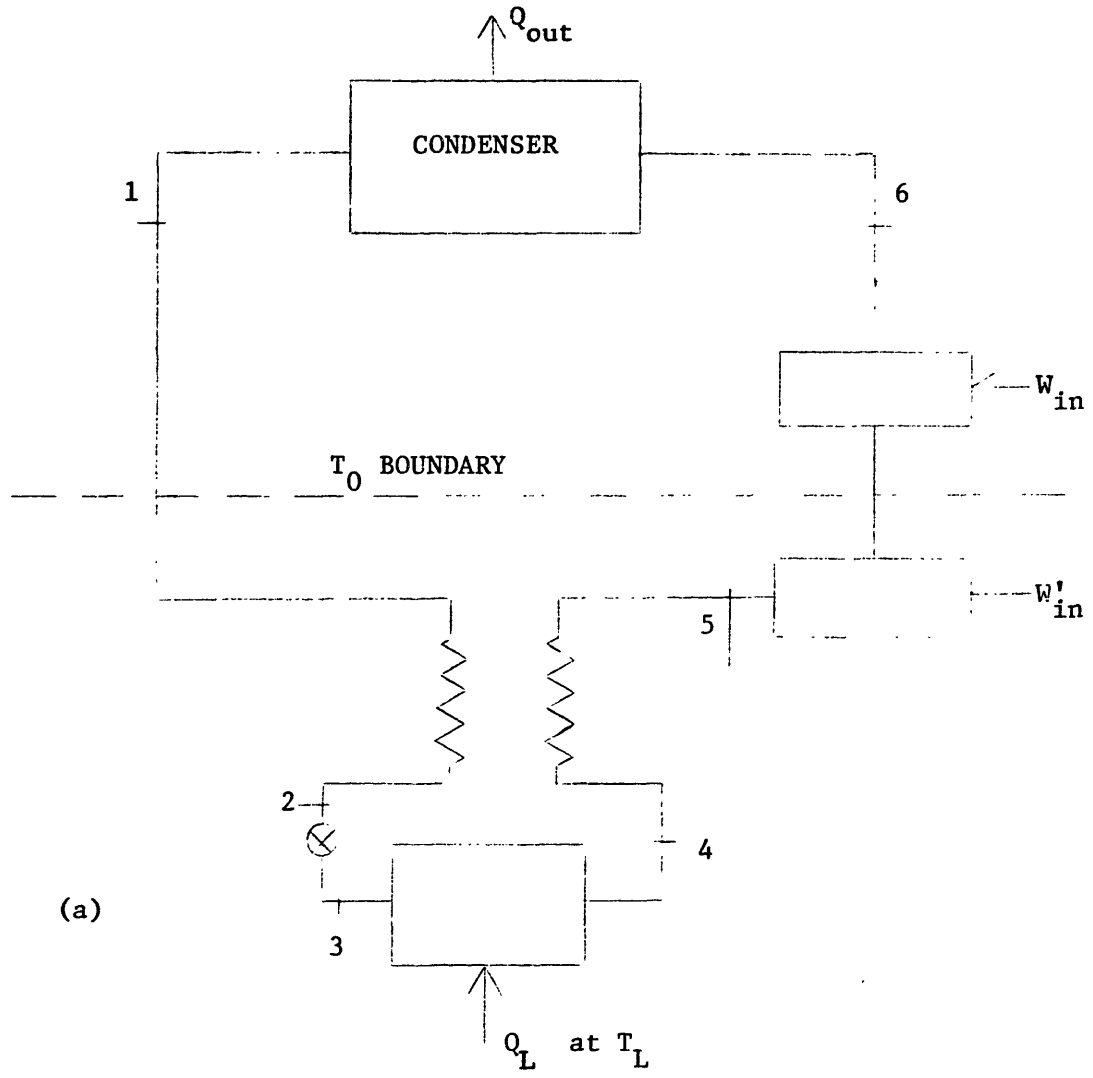
The Joule-Thompson cycle Fig. 2.4.4 is the analogous vapor compression scheme for gases with critical point temperatures far below ambient temperature[61,62]. Unlike the conventional vapor compression cycle this uses regenerative heat exchange to precool the high pressure gas before throttling. The T-S diagram for a typical Joule-Thompson cycle is shown in Fig. 2.4.4(b) and indicates a closer resemblance to the Ericsson rather than the Carnot cycle.

To understand what makes this cycle work, consider first the cold box Fig. 2.4.4 The temperature T_o is the boundary between the cold box and the hot end. In general the temperature T_5 is less than T_o by the heat exchange ΔT. Therefore much of the compressor work input is above T_o and in the limiting case of reversible heat exchange there is no work input below T_o. In this case the first law of thermodynamics applied to the cold box gives:

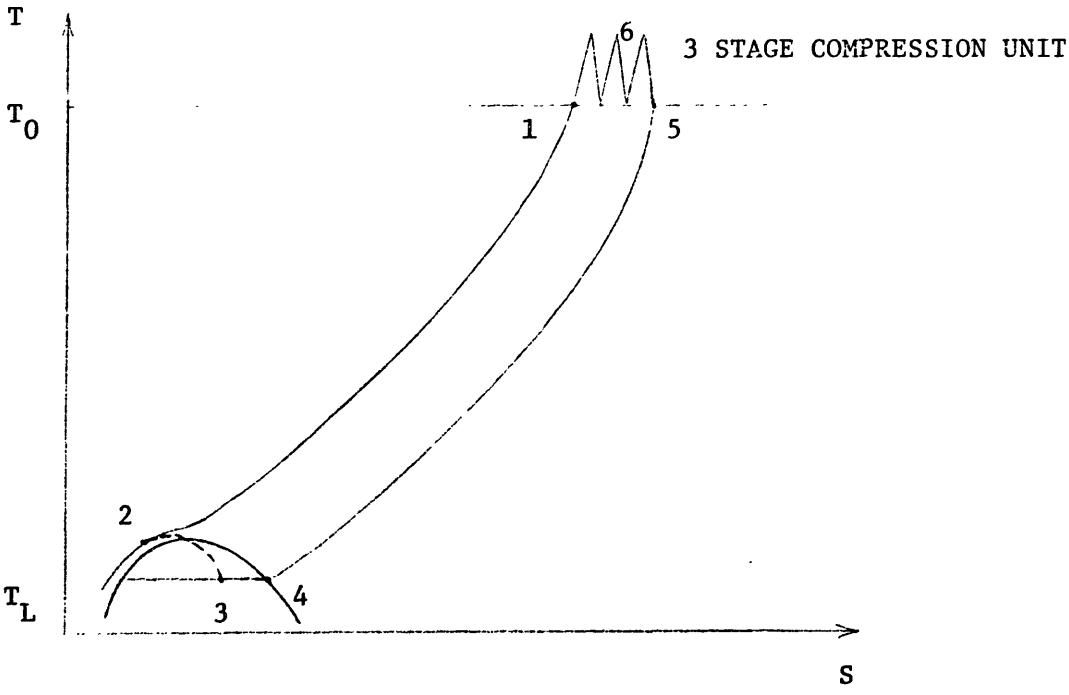
$$Q = -m(h_{hp} - h_{lp})_{T_o}. \tag{2.20}$$

Thus the enthalpy difference at the T_o boundary accounts for the refrigeration Q. In general the enthalpy change is due to a pressure effect as well as a temperature effect:

$$dh = \left(\frac{\partial h}{\partial P}\right)_T dT + \left(\frac{\partial h}{\partial T}\right)_P dP. \tag{2.21}$$



(a)



(b)

FIG. 2.4.4 J-T CYCLE: (a)SCHEMATIC; (b) T-S DIAGRAM

where

$$\left(\frac{\partial h}{\partial T}\right)_P = C_p \tag{2 22}$$

$$\left(\frac{\partial h}{\partial P}\right)_T = C_T \tag{2.23}$$

$$= -\left(\frac{\partial h}{\partial P}\right)_T \left(\frac{\partial P}{\partial T}\right)_h \tag{2.24}$$

$$= -\mu_{jt} C_p \tag{2.25}$$

Since $C_p > 0$, the heat exchange ΔT has a negative effect on the refrigeration potentially available diminishing it by $mC_p\Delta T$. If $\mu_{jt} > 0$ then the ΔP effect is positive and this is responsible for any refrigeration produced. Thus it is the non-ideality at T_o that makes the cycle work since $\mu_{jt} \neq 0$. The temperature T_o must lie below the Joule-Thompson inversion curve ($\mu_{jt} > 0$).

Joule-Thompson cycle refrigerators have been miniaturized with correspondingly low cool down times of the order of seconds.[63] These miniature J-T refrigerators (few millimeters diameter, few centimeters long) often use bottled high–pressure gas and are well-suited for cooling small electronic devices: they have negligible vibrational/magnetic noise since there are no moving mechanical parts. By incorporating an ejector into the cold end of the J-T cycle, lower temperatures may be reached.

Refrigeration with working fliuds which have low inversion temperatures uses a modified Joule-Thompson cycle, the cascade method, in which fluids with decreasing critical point temperatures are successively used to provide precooling Fig. 2.4.6. Nitrogen and hydrogen are used in succession in the liquefaction of helium by this method. This is the method used by Karmerlingh Onnes to liquefy helium in 1908.

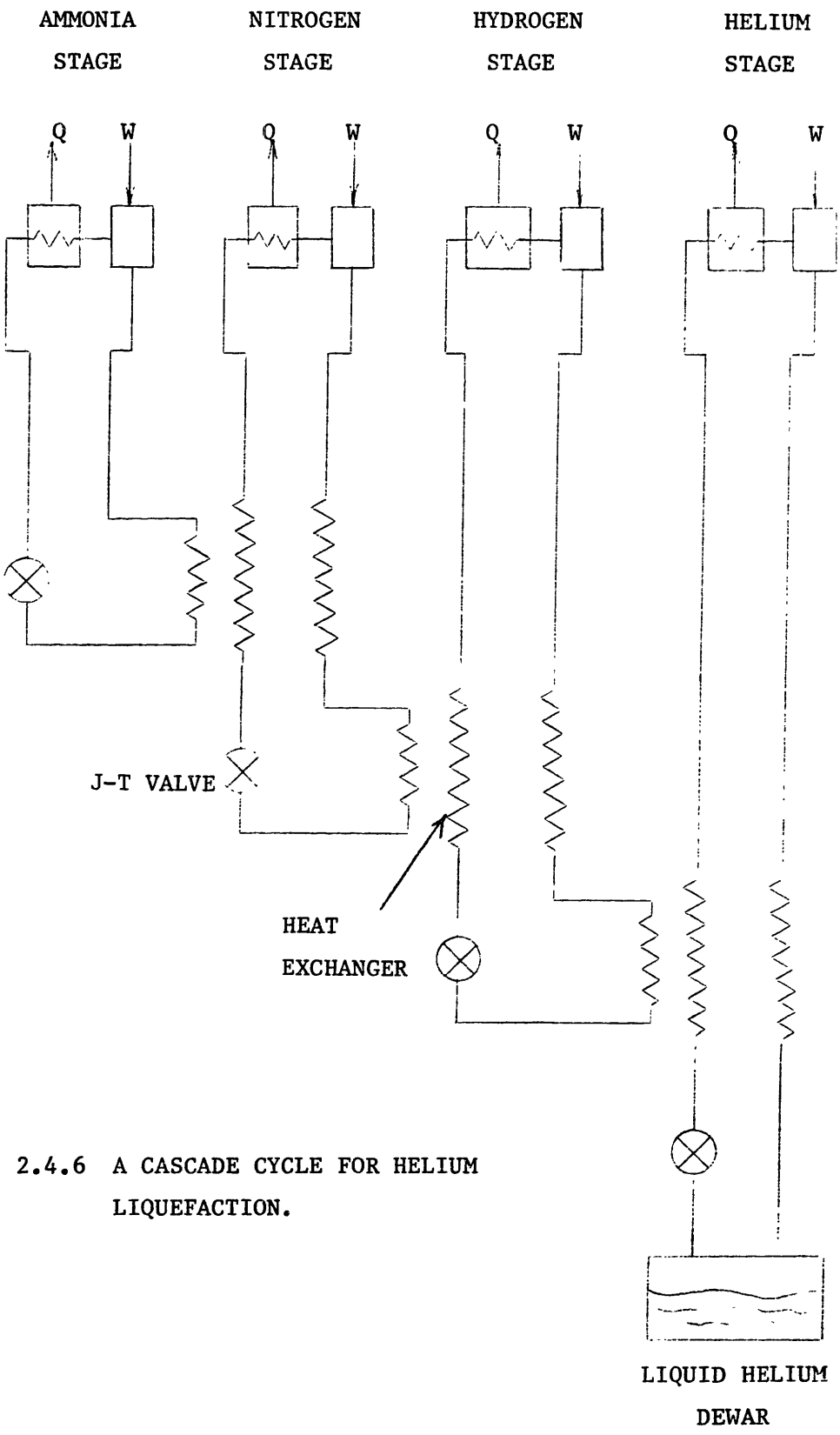


FIG. 2.4.6 A CASCADE CYCLE FOR HELIUM LIQUEFACTION.

2.4.4 Ideal Gas Cycle

It is the non-ideality effect of the working fluid, indicated by $\mu_{jt} > 0$, which provides the refrigeration in the J-T cycle. Therefore for helium refrigeration at temperatures above say 80 K, where helium approximates ideal gas behaviour, the J-T expansion process cannot be used. In general for an ideal gas cycle, mechanical work–producing–expansion processes are used as in the Carnot cycle configuration of Fig.2.4.1. Usually additional precooling is provided by regenerative heat exchange in counterflow heat exchangers.

There is a dependence of work distribution in the cold box on the fluid properties. For the reversible vapor compression cycle, the cold box requires work input whereas, in contrast, the reversible ideal gas cycle provides a work output. To determine the nature of this dependence, consider the cold box shown in Fig. 2.4.7. The expander work is derived from the first and second laws of thermodynamics and simplifies to

$$W_{ex} = m\left[(T_o - T_l)\int_{P_l}^{P_h} -\left(\frac{\partial S}{\partial P}\right)_{T_o} dP + \int_{P_l}^{P_h} v\,dP\right]. \tag{2.26}$$

The entropy term can be substituted from the Maxwell's relation

$$\left(\frac{\partial S}{\partial p}\right)_{T_o} = -\left(\frac{\partial v}{\partial T}\right)_{p}, \tag{2.27}$$

and the expander work becomes

$$W_{ex} = m\left[(T_o - T_l)\int_{P_l}^{P_h} -\left(\frac{\partial v}{\partial T}\right)_{P} dP + \int_{P_l}^{P_h} v\,dP\right]. \tag{2.28}$$

Therefore the isobaric coefficient $(\partial v/\partial T)_P$ (or equivalently $(\partial S/\partial P)_T$) of the working fluid determines whether the cold box requires work as input or output,

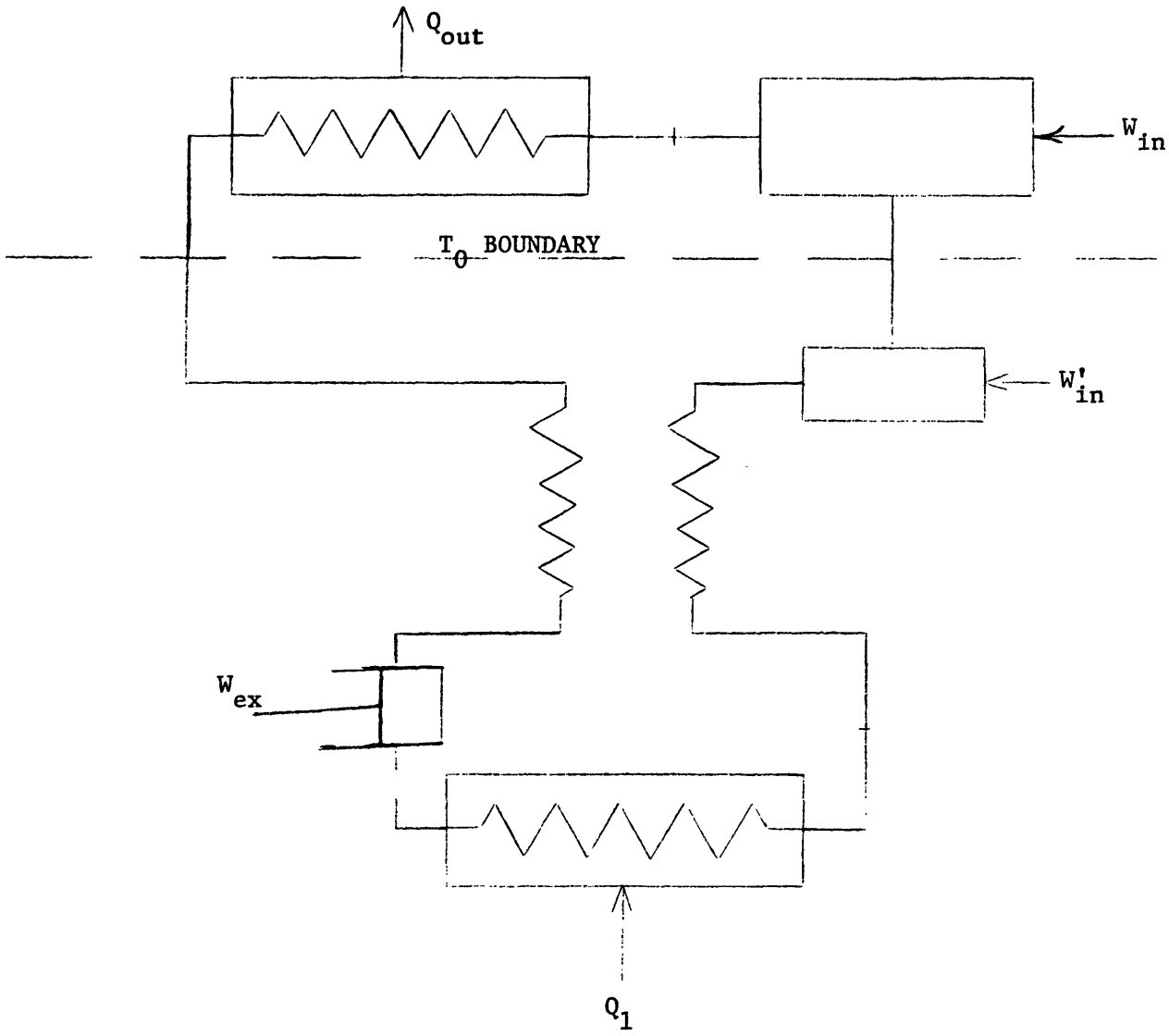


FIG. 2.4.7 SCHEMATIC OF AN IDEAL GAS CYCLE.

since (T_o – T_l) and v are both positive quantities. To illustrate, consider an ideal gas working fluid. From the ideal gas constitutive relation, the isobaric coefficient

$$\left(\frac{\partial v}{\partial T}\right)_p = \frac{v}{T} \tag{2.29}$$

Substitution in the expression for the expander work gives

$$W_{ex} = m\frac{T_l}{T_o}\int v\,dP, \tag{2.30}$$

$$> 0. \tag{2.31}$$

Thus for an ideal gas, there is a work output to heat input relationship for the cold box. Conversely, providing a work input into the cold box requires cooling–net heat rejection from the cold box.

2.4.5 Hybrid Cycles

The Claude cycle, Fig. 2.4.8, uses both mechanical work producing expansion and regenerative heat exchange to provide precooling before expansion through a J-T valve.[64] The Collin's cycle, Fig. 1.3, uses multiple expanders.[11,65]

2.4.6 Stirling Cycle

The Stirling cycle typifies a class of refrigerators with time separation, rather than space separation, of the high and low pressure stream.[66-71] In this cycle, (Fig. 2.4.9) the pressure, amplitude, frequency and phase are approximately the same at every geometric location at any given time. Point to point differences in each of these

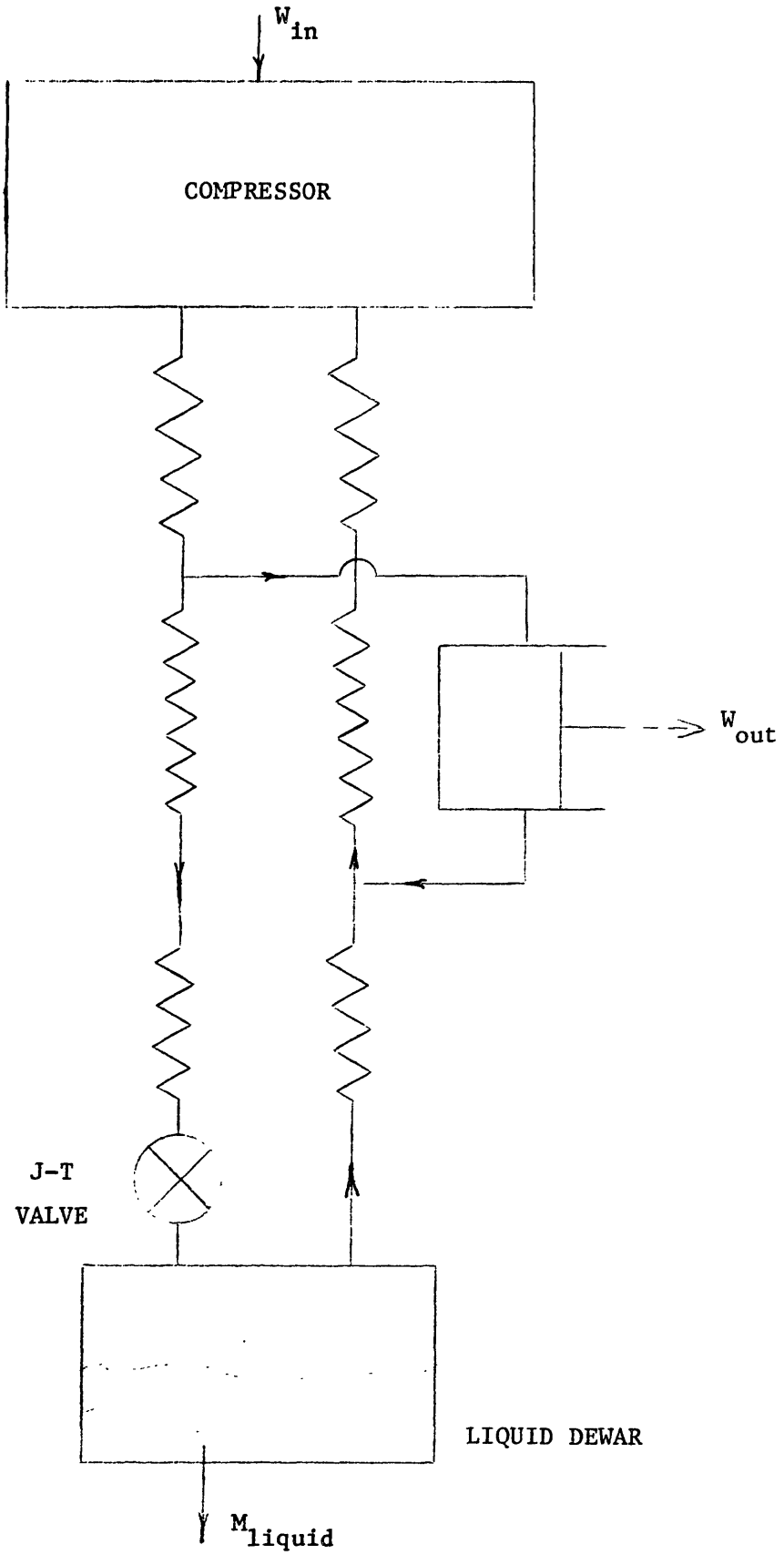


FIG.2.4.8 SCHEMATIC OF THE CLAUDE CYCLE

parameters are due to losses: for example, flow losses cause pressure differences. This class of cycles use regenerators in place of counterflow heat exchangers. A typical model for analytical Stirling cycles is shown in Fig. 2.4.9. A detailed account of the mathematical analysis of Stirling cycles is given by Rios in a PhD thesis.[66]

Several configurations are possible with Stirling cycles including 3-space Stirling cycle, 2-crankshaft configuration, and 4-cylinder double-acting Stirling. Figure 2.4.9 shows one of the simple configurations. The displacer and expander operate synchronously.

Stirling cycles are compact in size and have relatively high efficiencies because of low heat transfer losses. They are therefore widely used for cooling infra-red detectors especially at the 78 K level. However, in general they do have limited capacity (hence the use for electronic devices). A disadvantage with Stirling cycles is the lack of geometric flexibility: the compressor and expander must be close-coupled together. Also they are limited to refrigeration temperatures above 8-10K since most regenerator materials lose their ability to store heat below this temperature range.

2.4.7 Gifford-McMahon Cycle

The Gifford-McMahon cycle (Fig.2.4.10) uses warm valves to seperate the compressor from the displacer/regenerator arrangement.[72,73] The valves transform the "steady" flow from the compressor to a periodic flow through the regenerator/expander which have the same frequency. This is therefore a "hybrid" between steady and periodic flow.

The Gifford-McMahon cycle has several advantages for small refrigeration requirements.

1. Seperation of the expander from the compressor allows the use of a high speed compressor to drive a low speed expander and thus minimize losses in the cold expander.

2. It allows use of a compact remote compressor to drive the regenerator/expander.

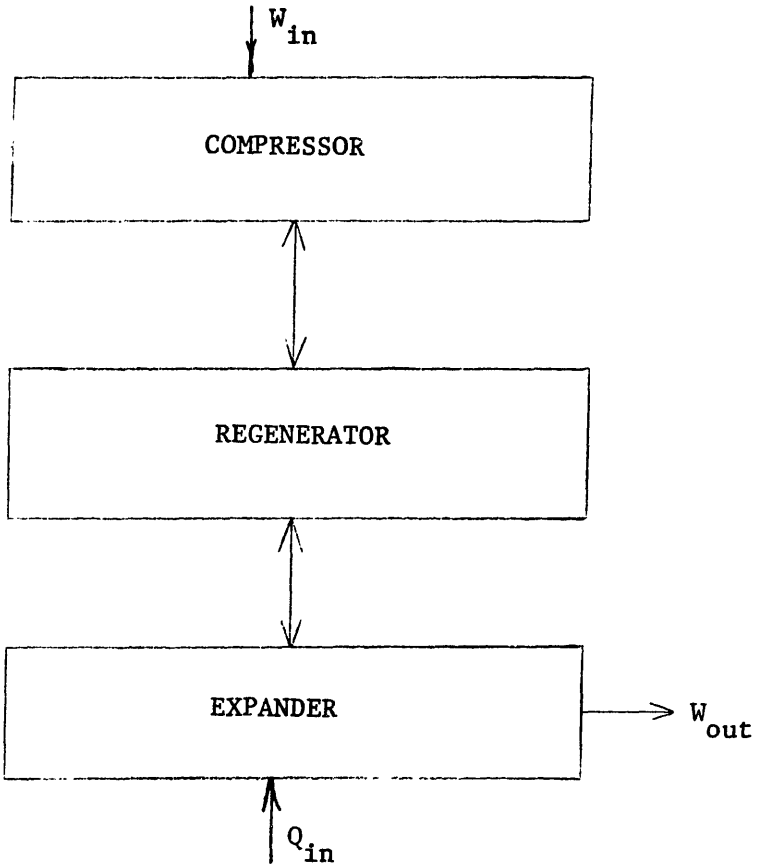


FIG. 2.4.9
STIRLING CYCLE.

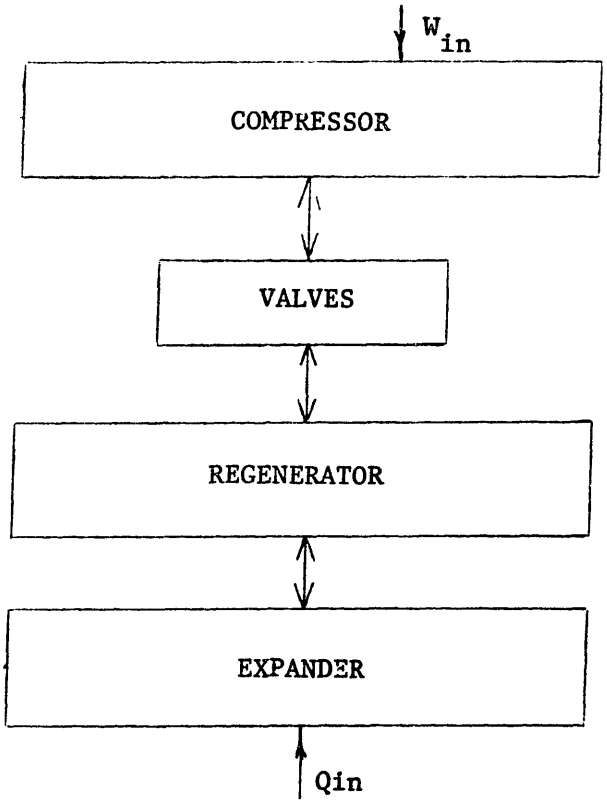


FIG. 2.4.10
GIFFORD-McMAHON CYCLE

3. The remote compressor can be of standard design.

However in contrast to the Stirling cycle this cycle has limited efficiency because the expander work is not recovered and there are losses asociated with the valves.

Multi-staging may be used in this cycle to reach low temperatures (6.5K) and a separate steady flow J-T cycle may be added to the cold end to reach 4.2K. However the system becomes complex and expensive.

2.4.8 Solvay Cycle

The Solvay cycle was invented in 1887 and was an answer to the problem of low-temperature valves. It is also a "hybrid" system between steady and periodic flow. However, unlike the Gifford-McMahon cycle, work is extracted from the cold gas. Modified versions of the original cycle have been discussed in the literature.[74-76]

2.4.9 Vuillemier Cycle

This is a Stirling cycle with the mechanical compressor replaced by a thermal compressor. This reduces the number of moving parts and tends to increase reliability.[77-80] However the thermal compressors operate with limited pressure ratios which affect the cycle efficiency.

2.4.10 Pulse Tube Refrigerator

This is also a mechanical refrigerator consisting of a thermal refrigerator, a heat exchanger and a void volume. By suitable arrangement of these components a refrigeration effect can be produced by rapid gas cycling at the closed end of the void (pulse) tube.[41,81-82] Temperature difference of the order of 100 K has been reached in a single stage. Multi-staging enables lower temperatures to be reached. The cycle has limited efficiency.

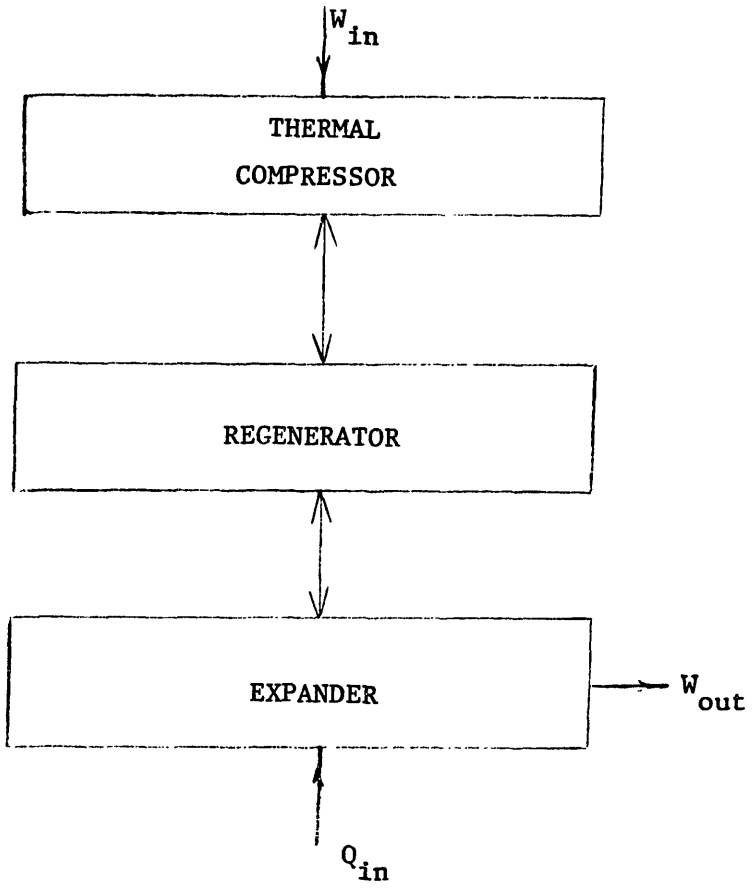


FIG.2.4.11
VM CYCLE: SCHEMATIC

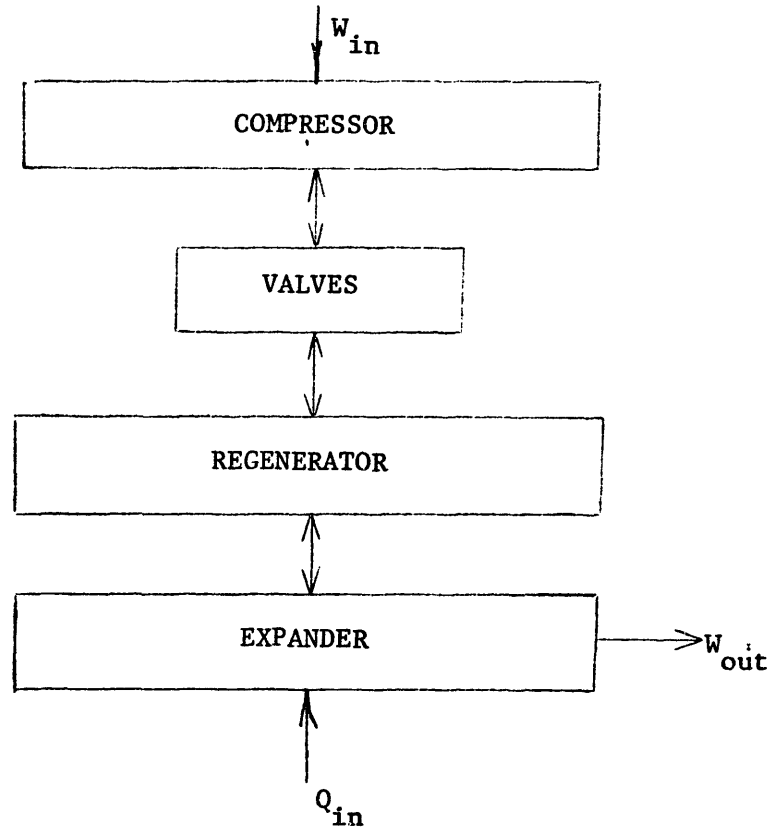


FIG. 2.4.12
SOLVAY CYCLE: SCHEMATIC

Chapter 3

AN OPTIMUM CONFIGURATION FOR HELIUM LIQUEFACTION CYCLES

This chapter discusses the cold end irreversibilities associated with helium liquefaction cycles and develops analytical models which provide a fundamental understanding of the competing effects of the various loss mechanisms characterising the cold end. The results of this analysis is an optimum cycle configuration consisting of the Saturated Vapor Compression configuration at the cold end and the Collins' multiple-expander precooling stage.

3.1 Introduction

A typical helium liquefaction cycle consists of a compression stage, a precooling stage and a cold end. Existing compressors for helium liquefaction cycles have rather low isothermal efficiencies (up to about 65%.) Therefore the compression stage represents the major source of irreversibilities in the cycle.[44,82] A major task of the continuing work in the design of efficient liquefier systems is to improve compressor efficiencies. With isothermal compressor efficiencies above 80%, the compression stage may no longer constitute the major source of cycle irreversibilities.

The precooling stage spans a wide temperature range from the refrigeration temperature to ambient, and consists of sets of counterflow heat exchangers and work producing expansion engines (in the Collins-type machine). There is a high penalty for the irreversibilities associated with the cold end of the cycle. To illustrate, consider a reversible refrigeration cycle rejecting heat at T_h and providing refrigeration at T_l. The coefficient of performance

$$COP = \frac{Q}{W_{net}}$$

$$= \frac{1}{(T_h/T_l - 1)} \qquad (3.1)$$

Thus the ratio of the ideal work required to remove a given quantity of heat Q at say 4.2 K and reject it at 300 K to that required to remove the same quantity of heat at 273.16 K and reject it at the same temperature 300 K is given by

$$\frac{(W_{rev})_{4.2K}}{(W_{rev})_{273.16K}} = \frac{COP_{273.16}}{COP_{4.2K}}$$

$$= 716.8 \qquad (3.2)$$

This high penalty for the cold end irreversibilities of helium liquefaction cycles is widely recognized. Yet conventional cycles still use the essentially irreversible J-T valve process as in the Linde cycle of 1895. The capital cost of large liquefiers is small compared with the operating costs and even small gains in overall cycle thermodynamic performance become important. Thus when the J-T valve is replaced by a wet expander, the liquid production rate of a liquefier is increased by over 30%.[83] Previously reported analyses include the use of a cold pump in a helium circulating loop for refrigeration loads.[84-87]

The discussion on basic thermodynamics of refrigeration processes in chapter 2 indicates that whether a particular cycle requires work input into or work out of the cold box depends on the thermodynamic behaviour of the fluid. Specifically, this depends on the behaviour of the isobaric coefficient $(\partial v/\partial T)_p$. For example, if the ideal gas model applies to the fluid behaviour, a work output from the cold box provides refrigeration whereas a work input into the cycle would reduce refrigeration. Helium exhibits non-ideal behaviour at low temperatures. It is therefore appropriate to investigate what the thermodynamic behaviour of the gas prescribes on the work transfer interaction to the

cycle. The models discussed here enable the effect of the thermodynamic behaviour on the cycle performance to be isolated from other effects and investigated.

3.2 Cold End Irreversibilities

The cold end irreversibilities are due primarily to the composite effect of the non-ideality of helium at low temperatures and the heat exchange (ΔT and ΔP) irreversibilities, in addition to the component irreversibilities fixed by the expander/compressor efficiencies. Heat exchangers may be designed to minimize irreversibilities for a given NTU and ΔP.[68,69] It thus remains to isolate the effect of the non-ideality of helium, decoupled from other loss mechanisms, on the cycle performance. The effect of these non-ideal properties, particularly the rapidly varying specific heat capacity requires special considerations in the design of efficient liquefiers. Collins considered this in discussing the basic theory of his precooling configuration. At low temperatures the effect of this variation is to cause an unbalanced heat capacity flow even in a balanced mass flow heat exchanger. Further because the specific heat capacity is a strong function of both temperature and pressure at very low temperatures, an appropriate analysis must necessarily invlolve differential elements of the two streams. Consequently, a continuum model for the precooling stage which decouples the two effects is considered. Two models are presented. In the first model portions of the high pressure stream are expanded across the full pressure ratio of the cycle whereas in the second model the full flow of either the high or low pressure stream is expanded in its channel.

3.3 Model I: Continuously Distributed Full-Pressure Ratio Expanders

3.3.1 Refrigeration mode

This model for the precooling process consists of a counterflow heat exchanger with reversible isothermal expanders continuously distributed over the precooling temperature range. At each temperature level an infinitesimal element of mass dM is extracted from the high pressure stream and expanded to the low pressure (Fig.3.1(a)). In order to use this model to capture the effect of the non-ideality of the gas, a reversible heat exchange process is considered. Thus the heat exchangers have infinite surface area and zero pressure drop. The model shown operates in a refrigeration mode so that the mass flow in the high pressure stream is the same as in the low pressure stream. The governing equations are derived from the first and second laws of thermodynamics. For the control volume shown in Fig. 3.1(a),

The first law simplifies to

$$\frac{dM}{M} = \frac{(C_{ph} - C_{pl})}{(S_l - S_h)} \frac{dT}{T} \tag{3.3}$$

and integrating gives the mass flow distribution over the precooling temperature range as:

$$\frac{M}{M_o} = \exp \int \left(\frac{C_{ph} - C_{pl}}{S_l - S_h} \right) \frac{dT}{T}. \tag{3.4}$$

Details of the analysis are given in appendix B.1. The second law also simplifies to:

$$dS_{gen} = 0. \tag{3.5}$$

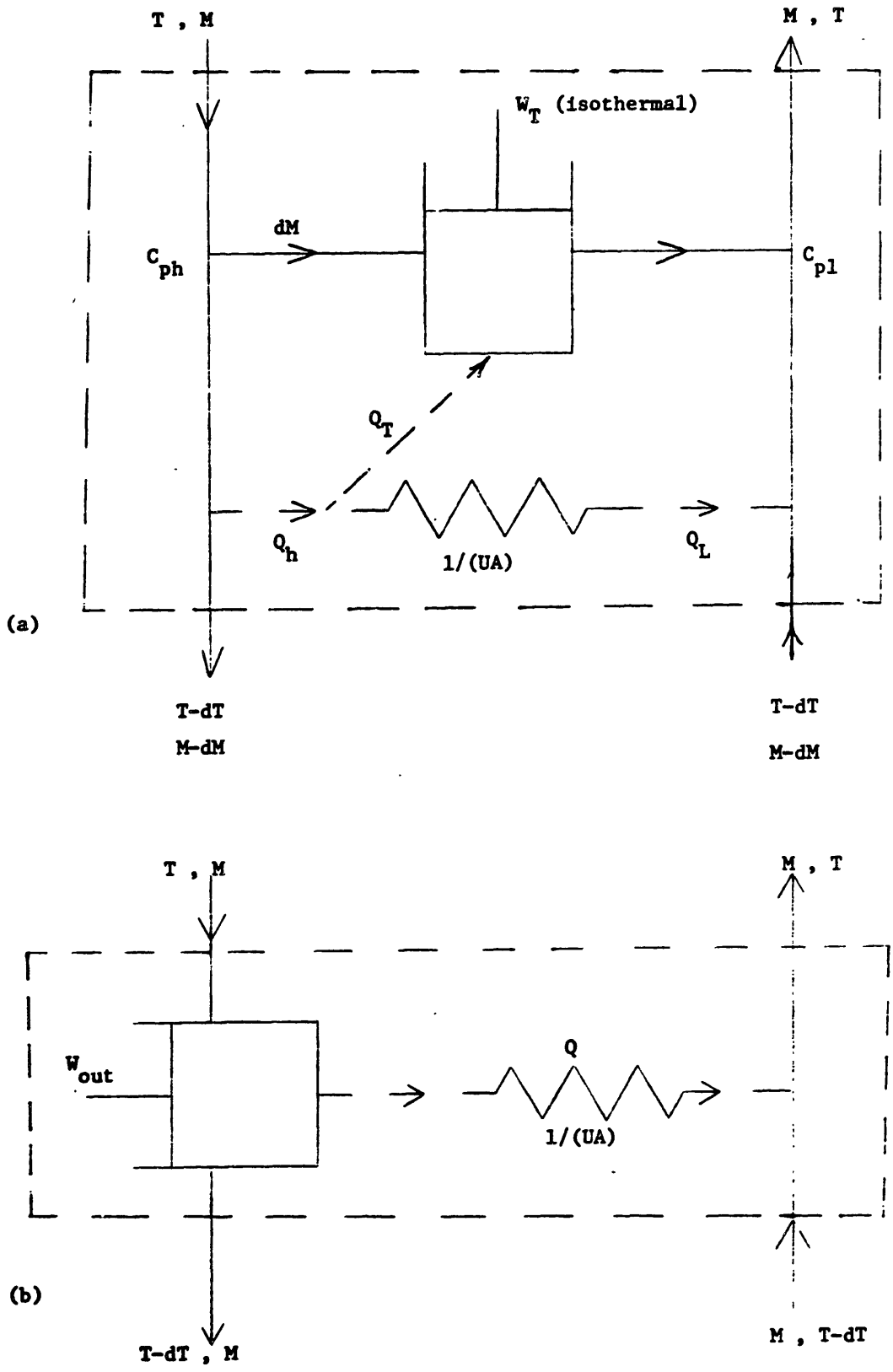


FIG.3.1 CONTINUUM MODEL FOR PRECOOLING STAGE: (a) MASS CROSSFLOW; (b) VARIABLE HIGH PRESSURE.

The mass flow rate is integrated using a Gauss-quadrature numerical integration algorithm. The thermodynamic properties of helium were obtained from the NBS Technical Note 631.[90] Figure 3.2 shows a typical curve of mass flow rate versus temperature. The well defined turning point occurs at the temperature T^* obtained by setting the first derivative of the mass flow rate to zero:

$$\frac{dM}{M} = \frac{C_{ph} - C_{pl}}{S_l - S_h} \frac{dT}{T} = 0 \tag{3.6}$$

This gives the condition that the specific heat capacity of the two streams must be equal ($C_{ph} = C_{pl}$) at the turning point.

Figure 3.3 shows results for various pressure ratios and Fig. 3.4 shows results for fixed pressure ratio but varying pressure level. These curves reflect the relative changes in the specific heat capacity of the two streams with temperature. The specific heat capacity at any pressure increases with decreasing temperature to a peak value, and then decreases. The peak value is maximum at the critical point. Also the specific heat capacity is higher at higher pressures at the warm end. Therefore for any two operating pressure levels, the difference in the specific heat capacity ($C_{ph} - C_{pl}$), which is the slope of the mass flow rate curve, is positive at the warm end, is zero at the turning point temperature T^* and negative thereafter. Consequently, the mass flow rate curve goes through a definite turning point at the temperature T^* which depends on the pair of pressures chosen. Typical values of this turning point temperature are given in Table 3.1.

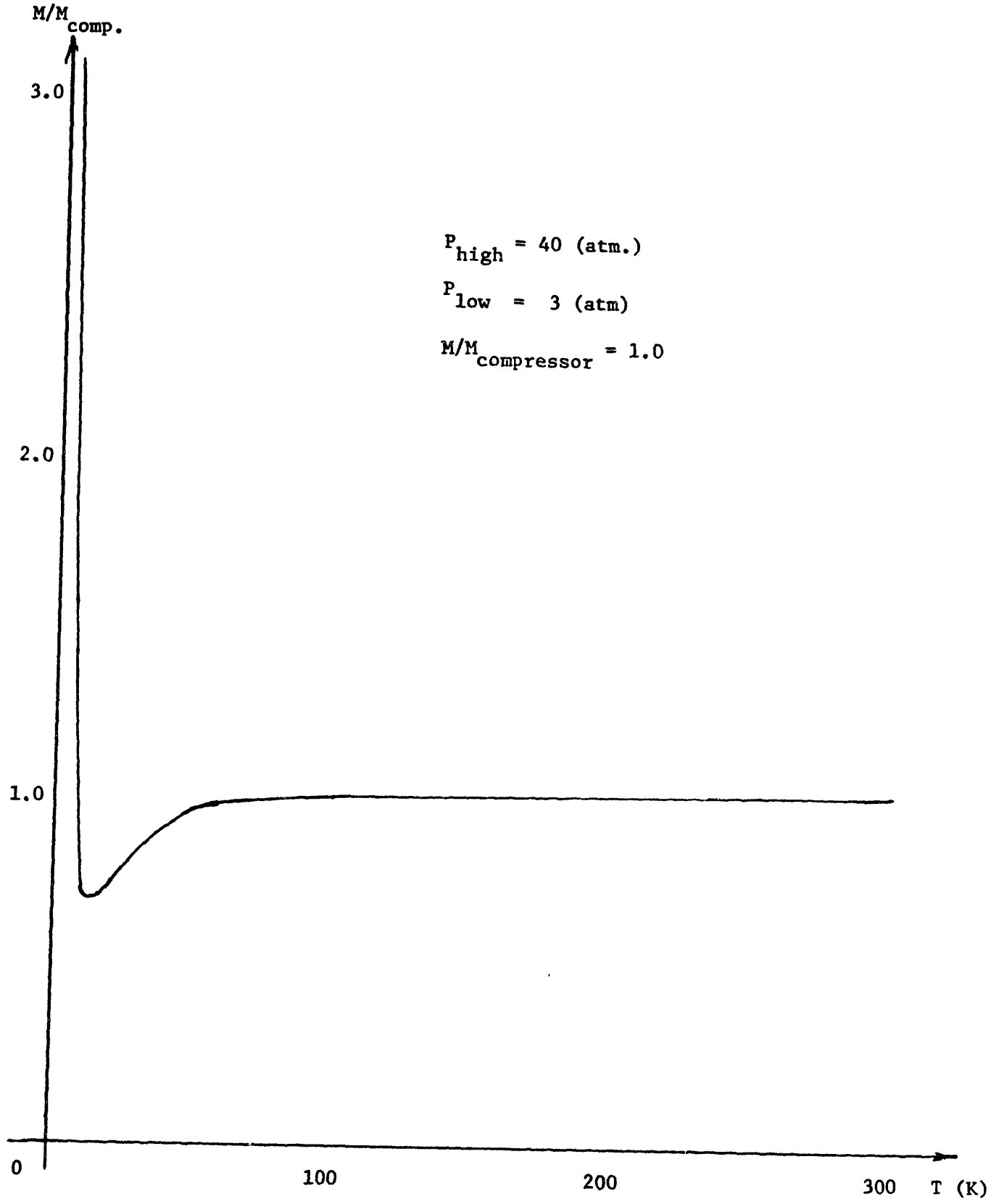


FIG. 3.2 TYPICAL PERFORMANCE CURVE FOR MASS CROSSFLOW MODEL : MASS FLOW RATE VERSUS TEMPERATURE.

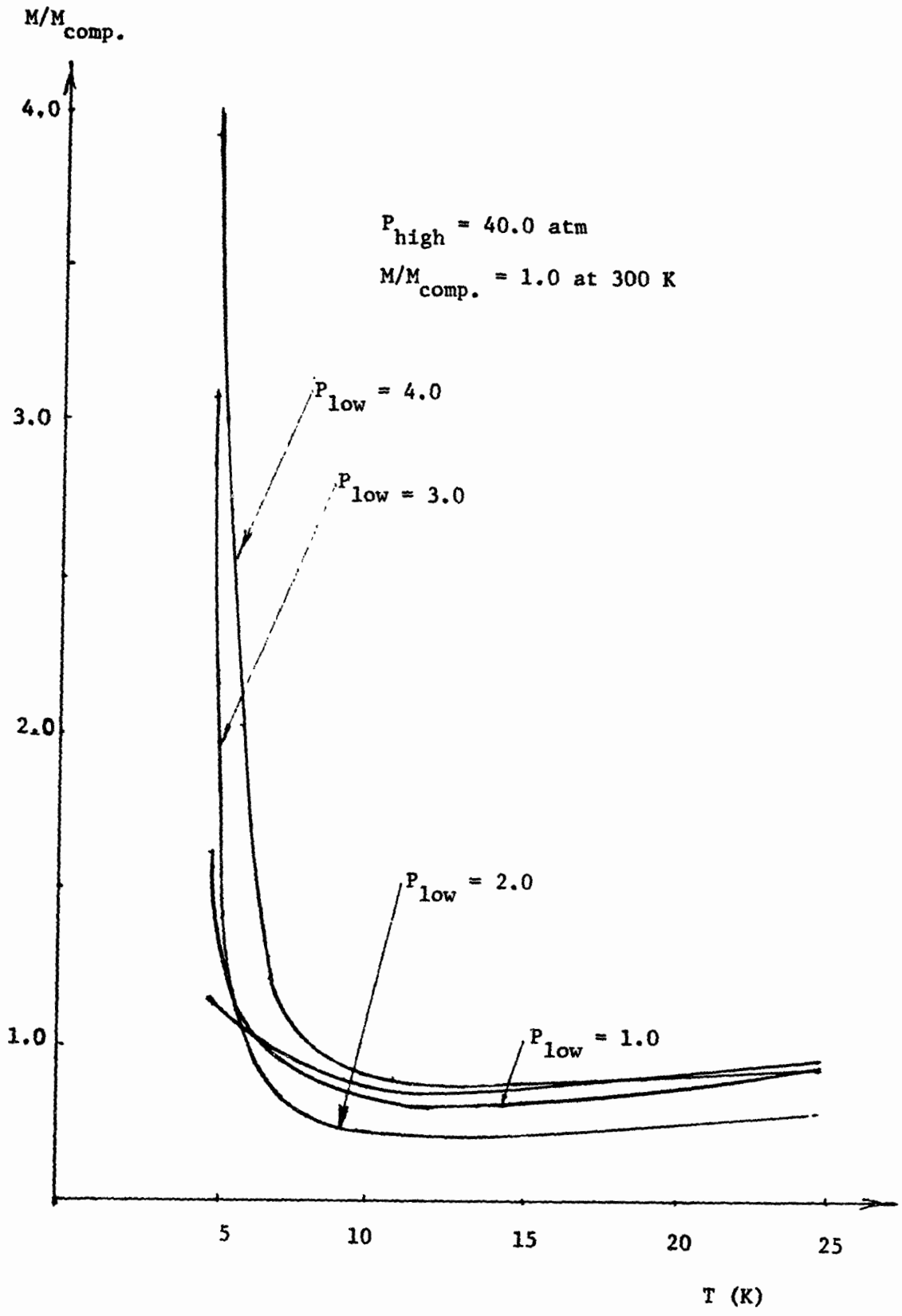


FIG. 3.3 COLD END PERFORMANCE CURVES FOR THE MASS CROSSFLOW MODEL (EFFECT OF PRESSURE RATIO).

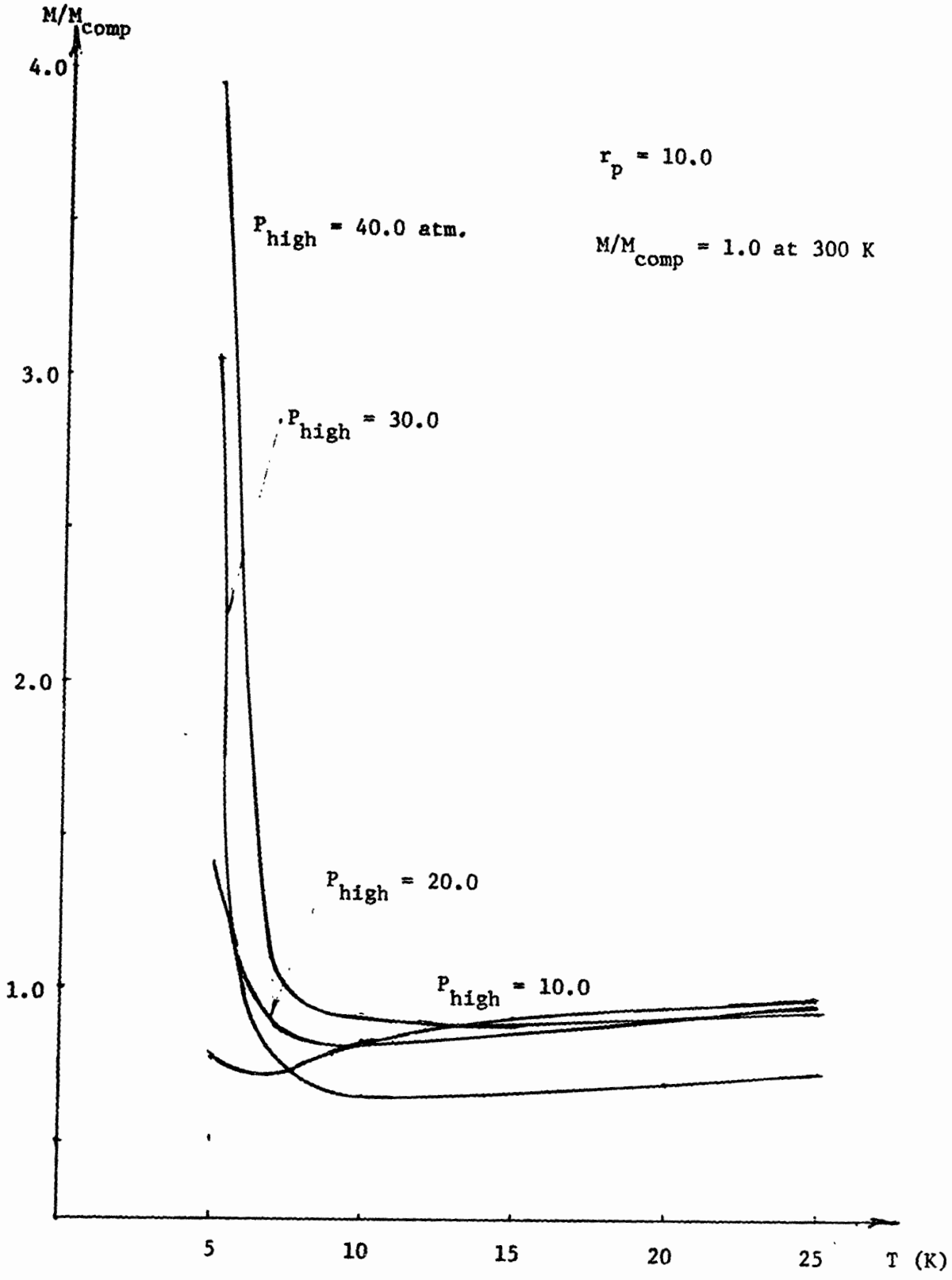


FIG. 3.4 COLD END PERFORMANCE CURVES FOR THE MASS CROSSFLOW MODEL : FIXED PRESSURE RATIO.

Table 3.1

Turning Point Temperatures

P_h(atm)	P_L(atm)	T^*(K)
40	4.0	13.8
40	1.6	12.5
30	3.0	11.5
30	1.4	10.7
20	2.0	9.2
20	1.2	8.8
10	1.0	6.7
5	0.5	5.3

3.3.2 Liquefaction Mode

In a liquefier, the mass flow rate is higher in the high pressure channel since a portion of this stream is liquefied. For the continuum precooling model in Fig. 3.1(a), suppose the mass flow rate in the low pressure channel is M and the ratio of the mass flow rate in the high pressure channel to that in the low pressure channel is ϵ. Then ϵ is a function of temperature. The low pressure stream flow rate for the continuum precooling model, derived from the first and second laws of thermodynamics in appendix B2 simplifies to:

$$\frac{dM}{M} = \left[\frac{\epsilon C_{ph} - C_{pl}}{S_l - S_h}\right]\frac{dT}{T}. \tag{3.7}$$

The temperature at the turning point, T^*, now depends also on the fraction of the flow into the warm end of the precooling section that is liquefied. The turning point

temperature T^* for the liquefaction mode is always lower than that for the refrigeration mode. To illustrate, consider a practical liquefier with pressure levels at 40 atm and 4.0 atm in which 39% of the flow through the wet expander is liquefied. A simple iteration gives the value of T^* as 8.75 K. At the same pressure level, $T^* = 13.8$ K for the refrigeration mode.

Figure 3.5 graphically explains why the turning point temperature T^* is lower in the liquefaction mode. The turning point is now determined by the condition $\epsilon C_{ph} = C_{pl}$ instead of $C_{ph} = C_{pl}$ for the refrigeration mode. Therefore the effect of the higher mass flow rate in the high pressure channel is to scale up the specific heat capacity of the high pressure stream relative to the low pressure stream. The intersection of the two curves is consequently shifted down to a lower temperature. The form of the mass flow rate versus temperature curves remains unchanged (Fig. 3.6 (a) and (b)). However the mass flow rate now decreases more rapidly, initially, because of the increased difference between the scaled-up high pressure stream specific heat capacity and the specific heat capacity of the low pressure stream. Consequently, the mass flow rate is always lower for the liquefier for the same mass flow rate into the warm end of the precooling stage.

3.4 Model II: Continuously Distributed Full-Flow Expanders

The counterflow heat exchanger in a precooler uses the cold low pressure return stream to precool the high pressure stream. The specific heat capacity of the high pressure stream is higher than that of the low pressure stream at high temperatures. Therefore, for comparable temperature drop in both streams, additional cooling is required for the high pressure stream. The pressure of the full-flow high-pressure stream

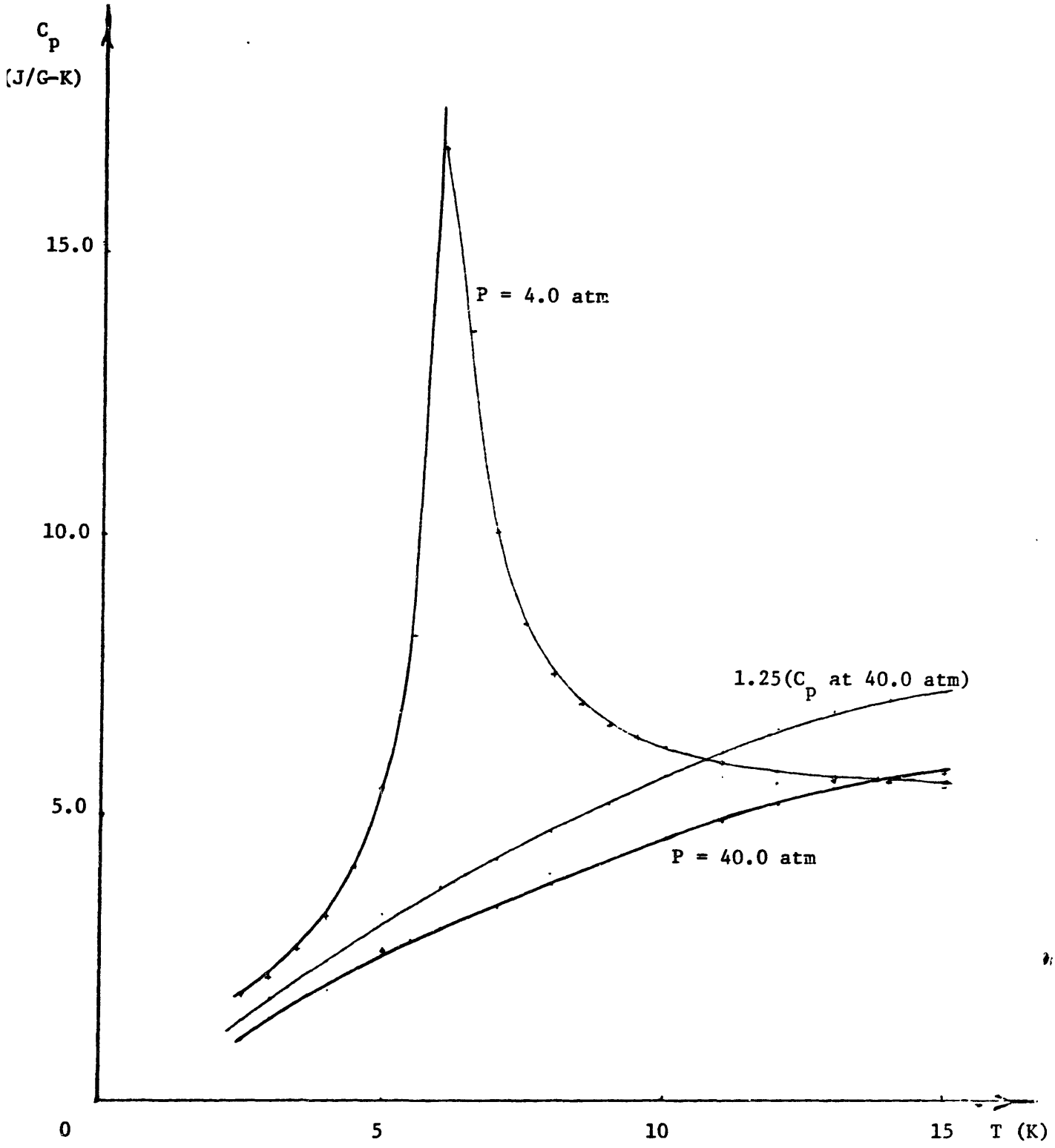


FIG. 3.5 SPECIFIC HEAT CAPACITY CURVE FOR HELIUM

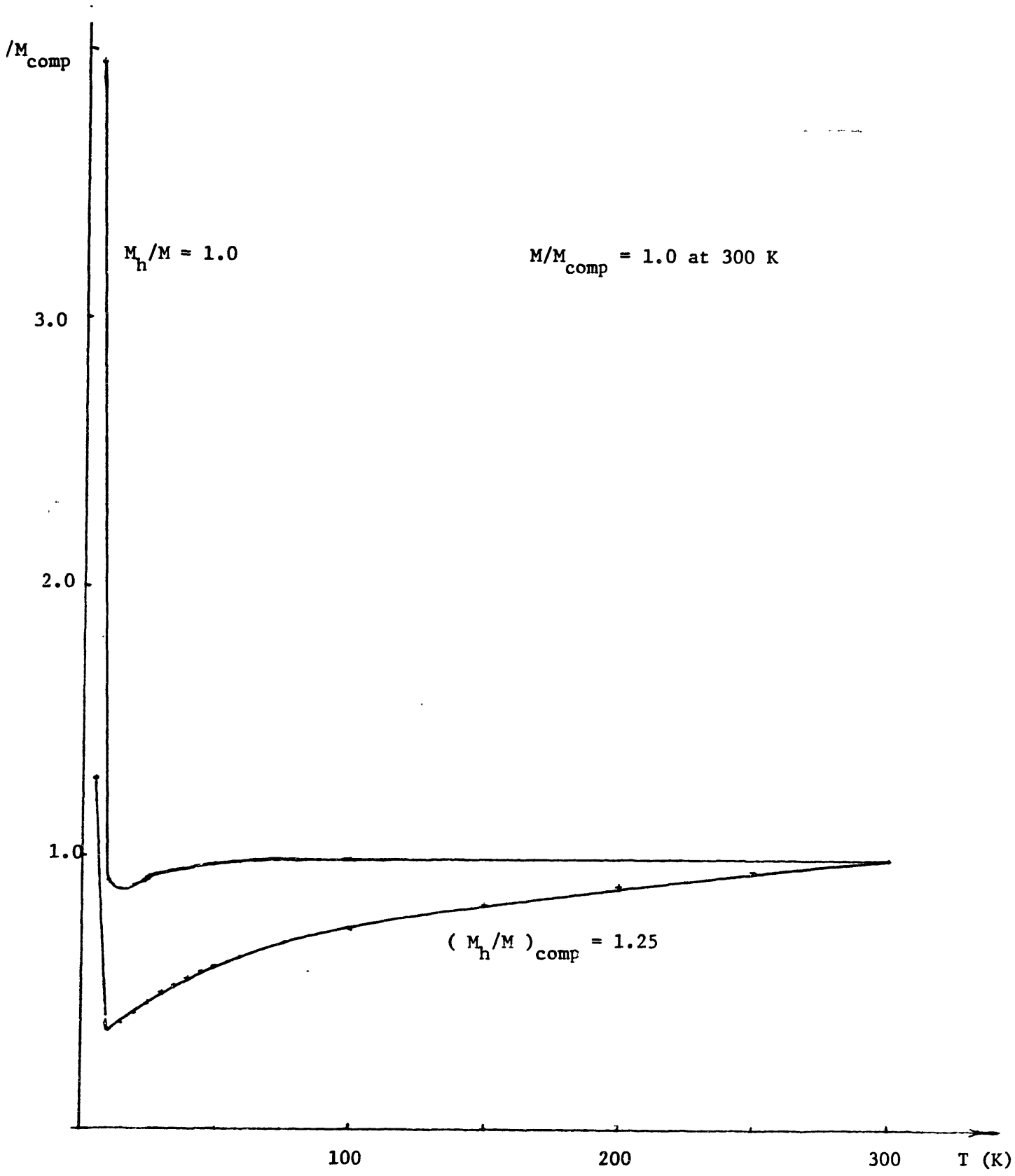


FIG. 3.6(a) PERFORMANCE CURVES FOR MASS CROSSFLOW MODEL: LIQUEFACTION MODE, REVERSIBLE HEAT EXCHANGE.

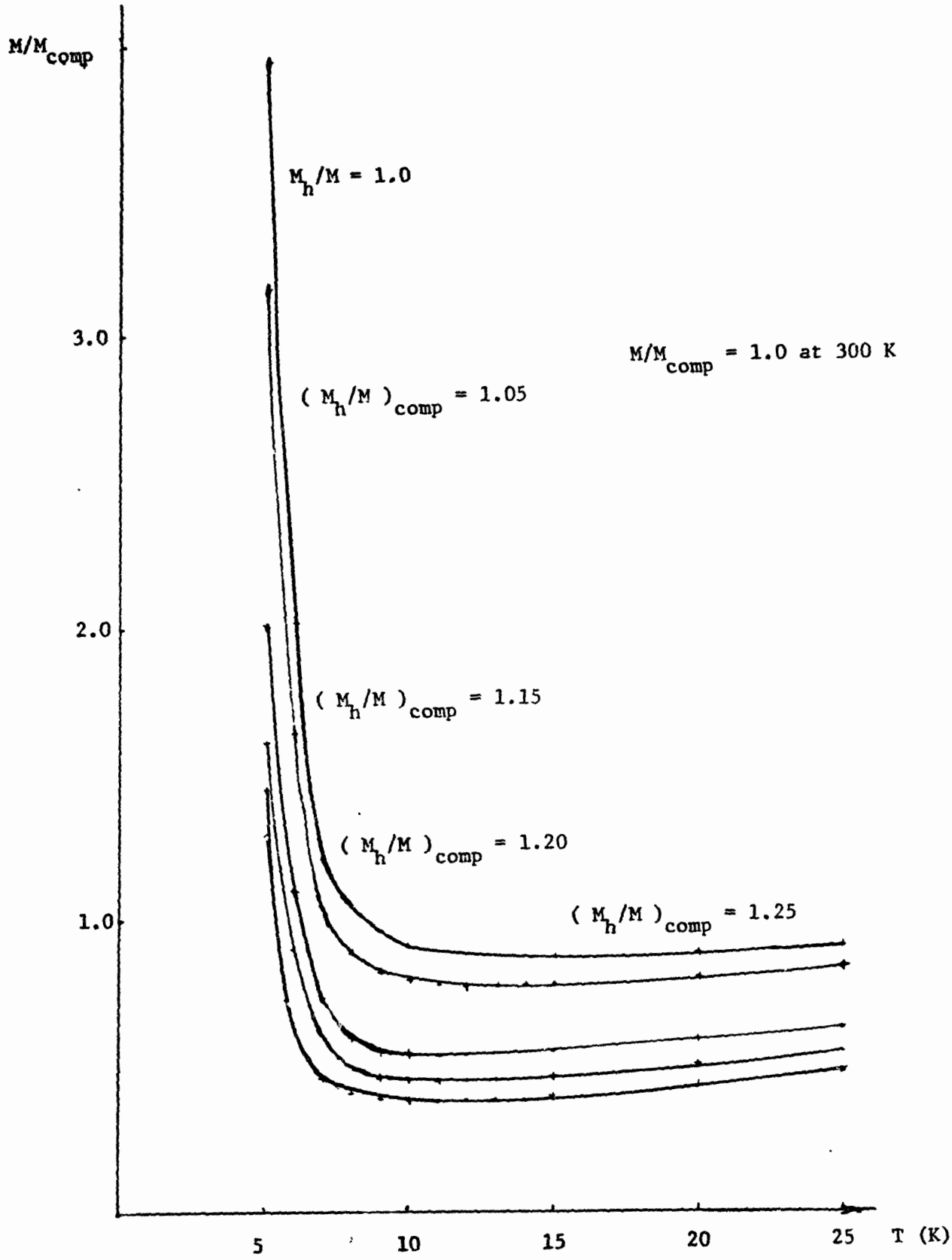


FIG.3.6 (b) COLD END PERFORMANCE CURVES FOR MASS CROSSFLOW MODEL: LIQUEFACTION MODE, REVERSIBLE HEAT EXCHANGE.

may be lowered in work producing reversible expansion steps to provide this cooling (Fig.3.1(b)). Similarly, the pressure of the full-flow cold stream may be varied by reversible compression to achieve the same end. Thus the heat exchanger may be considered as a regenerative work expander. The work of expansion in the high-pressure stream is removed, in the case of the variable high pressure, or the work of recompression is supplied to the low-pressure stream, in the case of the variable low pressure.

The second model involves continuously varying either pressure in the heat exchanger to match the cycle entropy flow and thereby produce a reversible precooling stage. The underlying assumptions governing this system are:

1. reversible expansion and compression processes;
2. infinite heat exchanger surface area;
3. zero heat exchange ΔT; and
4. zero flow irreversibilities.

3.4.1 Refrigeration Mode.

Figure. 3.1(b) depicts the second model for the precooling stage operating in a refrigeration mode with the low pressure kept constant and the high pressure varied. The governing equations for the control volume shown are derived by defining entropy S as a function of pressure P and temperature T:

$$dS = \left(\frac{\partial S}{\partial P}\right)_T dP + \left(\frac{\partial S}{\partial T}\right)_P dT \qquad (3.8)$$

Substituting for the partial derivatives in Eq. 3.8 gives:

$$dS = -\beta v dP + \left(\frac{C_v}{T}\right) dT, \tag{3.9}$$

where v is the specific volume and the coefficient of thermal expansion is defined as:

$$\beta = -\frac{1}{v}\left(\frac{\partial v}{\partial T}\right)_P.$$

The system equations are then obtained from the second law of thermodynamics:

$$dS_l = dS_h. \tag{3.10}$$

If the low pressure is kept constant, and the high pressure is varied, dP_l equals zero and the governing equation simplifies to:

$$\frac{dP_h}{dT} = \frac{C_{ph} - C_{pl}}{\beta_h v_h T} \tag{3.11}$$

Detailed derivation is given in appendix B3. Similarly for the variable low pressure case (constant high pressure),

$$\frac{dP_l}{dT} = \frac{C_{pl} - C_{ph}}{\beta_l v_l T} \tag{3.12}$$

Notice that the slope of the pressure curve dP/dT equals zero where the specific heat capacities match $C_{ph} = C_{pl}$. Thus the turning point temperature occurs at the same point as in the mass crossflow model discussed in the preceeding section. The gradient is

positive in the warm end and negative in the cold end for the constant low pressure case (Eq. 3.11). For the constant high pressure case the slope is negative in the warm end and positive in the cold end (Eq. 3.12).

The pressure is given in either case by direct numerical integration using Gauss quadrature and the thermophysical properties of the NBS Technical Note 631.[90] Thus

$$P_h - (P_h)_c = \int \frac{C_{ph} - C_{pl}}{\beta_h v_h T}\, dT. \tag{3.13}$$

$$P_l - (P_l)_c = \int \frac{C_{pl} - C_{ph}}{\beta_l v_l T}\, dT \tag{3.14}$$

Typical curves for the pressure are shown on Figs. 3.7 and 3.8.

Figure 3.7 shows the distribution of the pressure in the high pressure channel over the precooling temperature range while the low pressure is kept constant. This curve suggests that at the warm end, work of expansion should be removed from the high pressure stream and at the cold end work of recompression must indeed be supplied to the stream. Again this is consistent with the behaviour of the specific heat capacities. The higher specific heat capacity of the high pressure stream at the warm end requires that work be extracted from it to effectively reduce the heat capacity rate whereas at the cold end the lower value of the heat capacity rate requires that work of recompression be added.

Similarly, for the constant high pressure case (Fig.3.8), work of recompression must be added to the cold stream at the cold end but at the warm end, work of expansion

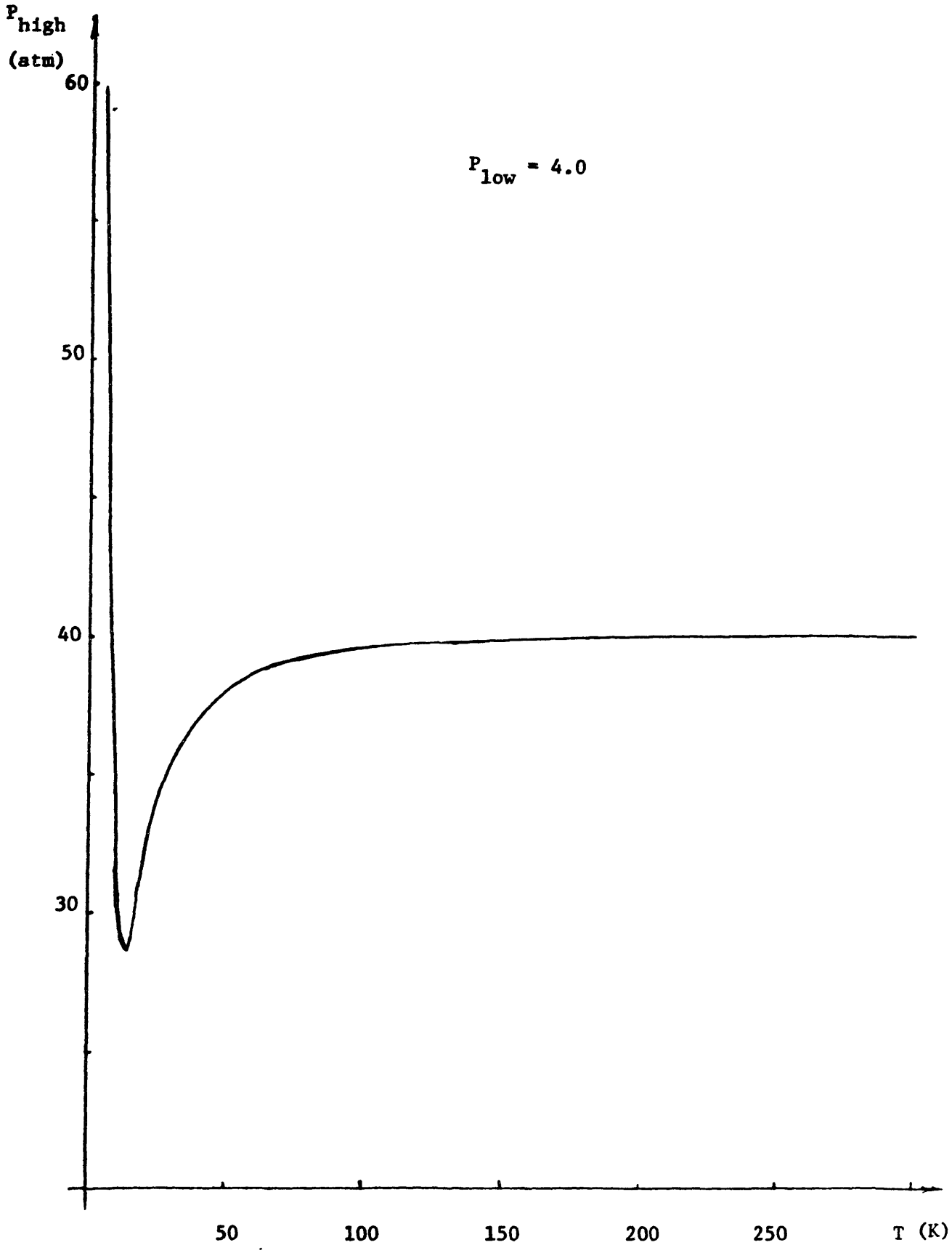


FIG. 3.7 PERFORMANCE CURVE FOR VARIABLE PRESSURE MODEL.

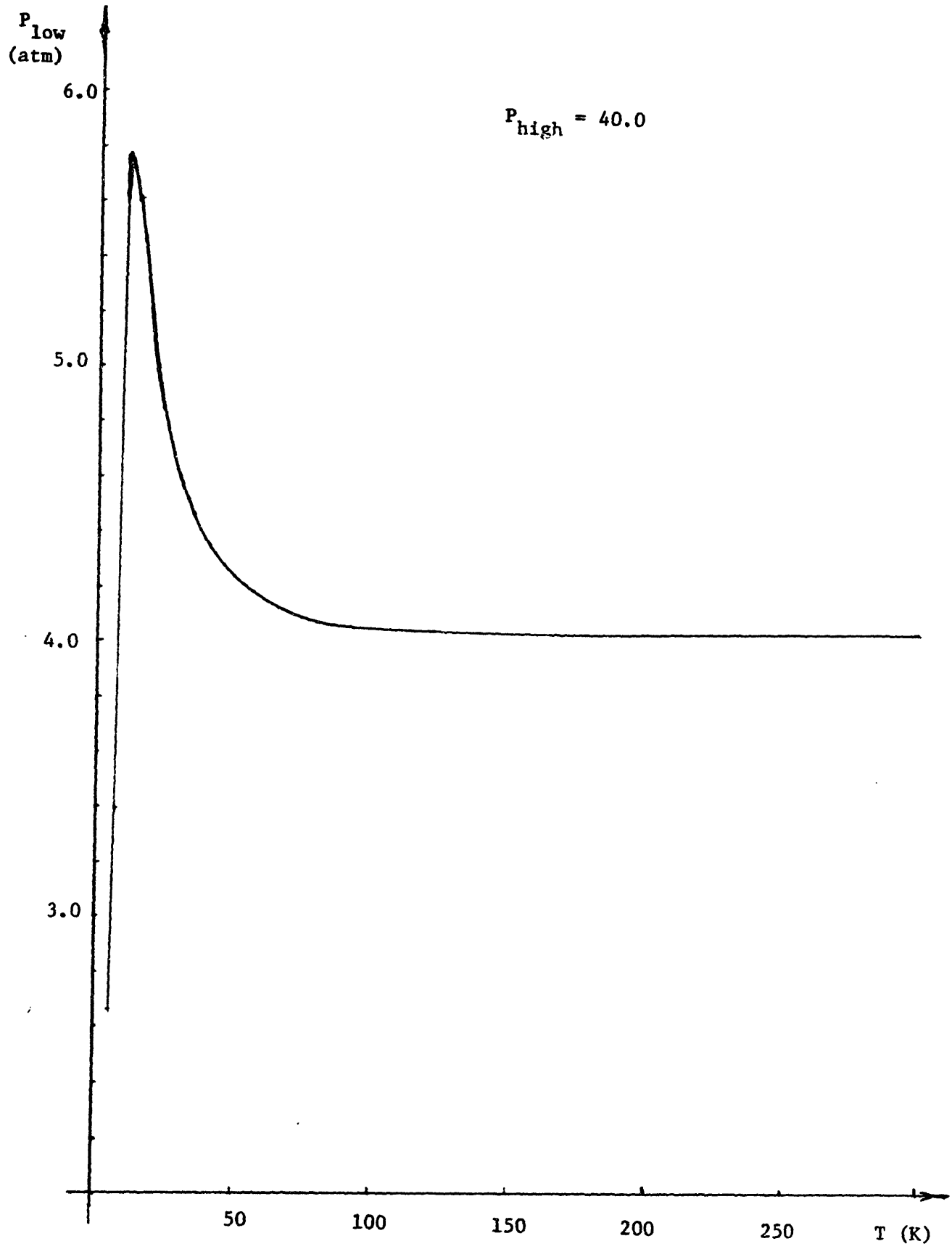


FIG. 3.8 TYPICAL PERFORMANCE CURVE FOR VARIABLE PRESSURE MODEL.

must be taken out

3.4.2 Liquefaction Mode

In a liquefier, the mass flow rate of the high pressure stream M_h is higher than that of the low pressure stream M. Therefore the governing equations for the continuum precooling stage contains an extra variable, the mass flow rate ratio $\epsilon = M_h/M$. For this case, the second law of thermodynamics simplifies to

$$dS_l = \epsilon dS_h \tag{3.15}$$

In this full-flow model, ϵ is not a function of temperature since the mass flow rate in either channel is constant. The pressure is now given by Eqs. 3.16 and 3.17 for the variable high and low pressure cases respectively.

$$P_h - (P_h)_c = \int \frac{\left(C_{ph} - \frac{C_{pl}}{\epsilon}\right)}{\beta_h v_h T} dT. \tag{3.16}$$

$$P_l - (P_l)_c = \int \frac{(\epsilon C_{ph} - C_{pl})}{\beta_l v_l T} dT. \tag{3.17}$$

Details of the derivation are given in appendix B4.

Once again the turning point temperature T^* is a function of the rate of liquid production and is always lower than the corresponding value for the refrigeration mode as explained in section 3.3.2.

3.5 Cold End Configuration

A practical cycle configuration may be derived from the curves resulting from the analysis by direct discretization. For the mass crossflow curves, this requires a finite number of expansion engines in the cycle above the transition temperature T^* to remove the work of expansion from the high pressure stream. The greater the number of expanders, the closer the practical cycle approaches the continuum mode. This arrangement is equivalent to the precooling configuration discussed by Collins. His practical cycle implementation used two expansion engines (*Fig.2.4.8*)

Below the transition temperature, the optimal curves require mass recirculation. Figure 3.9 shows a conceptual arrangement of components to approximate this behaviour. The mass recirculation compressor provides the cold end recirculating mass flow rate to approximate the mass flow rate curves. The wet expander is the final expansion stage of the cycle. The cold compressor is required to compress the saturated vapor if the cold channel pressure is above the dewar pressure.

The feasibility of this configuration as the cold end of a practical cycle is evaluated based on the following assumptions:

1. The refrigeration load is transferred reversibly at a refrigeration temperature T_l = 5.0 K.
2. The heat load is absorbed by a reversible isothermal expander.
3. The expansion and compression processes are reversible.

The refrigeration temperature and a given operating pressure fix the inlet state to

the vapor compressor. The states at the discharge to the vapor compressor and the mass recirculation compressor are fixed by the reversible compression processes. The wet expander inlet temperature equals the discharge temperature at the vapor compressor for zero heat exchange temperature difference ΔT.

Table 3.2

State point parameters for cold end configuration

P_{level}(atm)	T_{1h}(K)	T_{2h}(K)	T^*(K)
40 : 4.0	21.93	8.336	13.8
40 : 3.0	21.93	7.357	13.3
40 : 2.0	21.93	6.656	12.8
30 : 3.0	19.66	7.357	11.5
20 : 2.0	15.83	6.656	9.2

Table 3.2 summarizes the resulting state point parameters, defined on Fig.3.9, for a pressure ratio of ten. In all the cases considered, the exit temperature of the isentropic high pressure ratio compressor T_{1h} is much higher than the corresponding transition temperature. In contrast the wet expander inlet temperature T_{2h} is much closer to the transition temperature T^*. This means that the incorporation of the wet expander–vapor compressor arrangement in the cold end effectively eliminates the need for mass recirculation and the high pressure ratio compressor must be dispensed with. The resulting configuration simplifies to that shown in Fig. 3.10 which is the saturated vapor compression cycle. In the wet expander–cold compressor cold end configuration shown in Fig. 3.10, the wet expander inlet temperature T_{1h} is close to the turning point tempera-

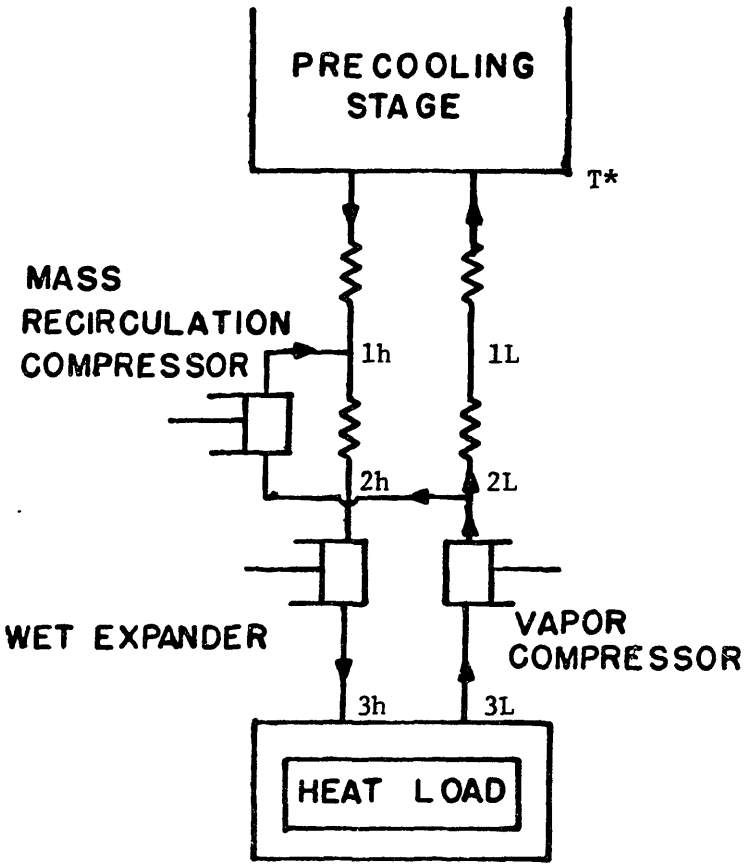


FIG. 3.9 MASS RECIRCULATION CONFIGURATION

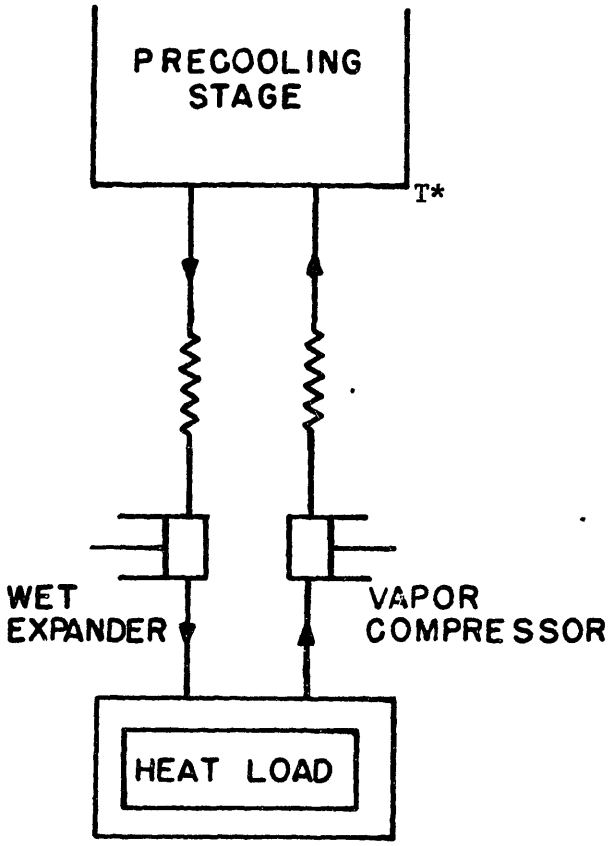


FIG. 3.10 SIMPLIFIED COLD END COFIGURATION ; SVC CONFIGURATION.

ture below which optimal precooling requires mass recirculation. This is what makes this configuration optimal. Since the wet expander inlet temperature is not necessarily equal to the turning point temperature, there is a trade-off between the irreversibilities associated with the precooling stage and the cold end for the optimized configuration.

If the assumption of reversible compression processes is relaxed, the discharge temperature of both compressors increases. Therefore for a practical cycle, the difference between the turning point temperature and the discharge temperature of the mass recirculation compressor is increased while the wet expander inlet temperature (vapor compressor discharge temperature) approaches the turning point temperature. Consequently the conclusion above still holds.

3.6 Summary

The analysis of the continuum models for the precooling stage of helium refrigeration or liquefaction cycles indicates that optimal performance requires mass recirculation at the cold end of the precooling stage. This is due to the unique behaviour of the specific heat capacity of helium at very low temperatures.

The cold end configuration derived from the optimal performance curves for the mass crossflow model by discretization simplifies to the saturated vapor compression (SVC) configuration. This configuration is optimal because the practical inlet temperature at the wet expander is close to the turning point temperature below which optimal precooling requires mass recirculation. In contrast, for a practical cold end configuration with discrete mass recirculation, the discharge temperature associated with the mass recirculation compressor is much higher than the turning point temperature and this discrete configuration no longer represents optimal precooling.

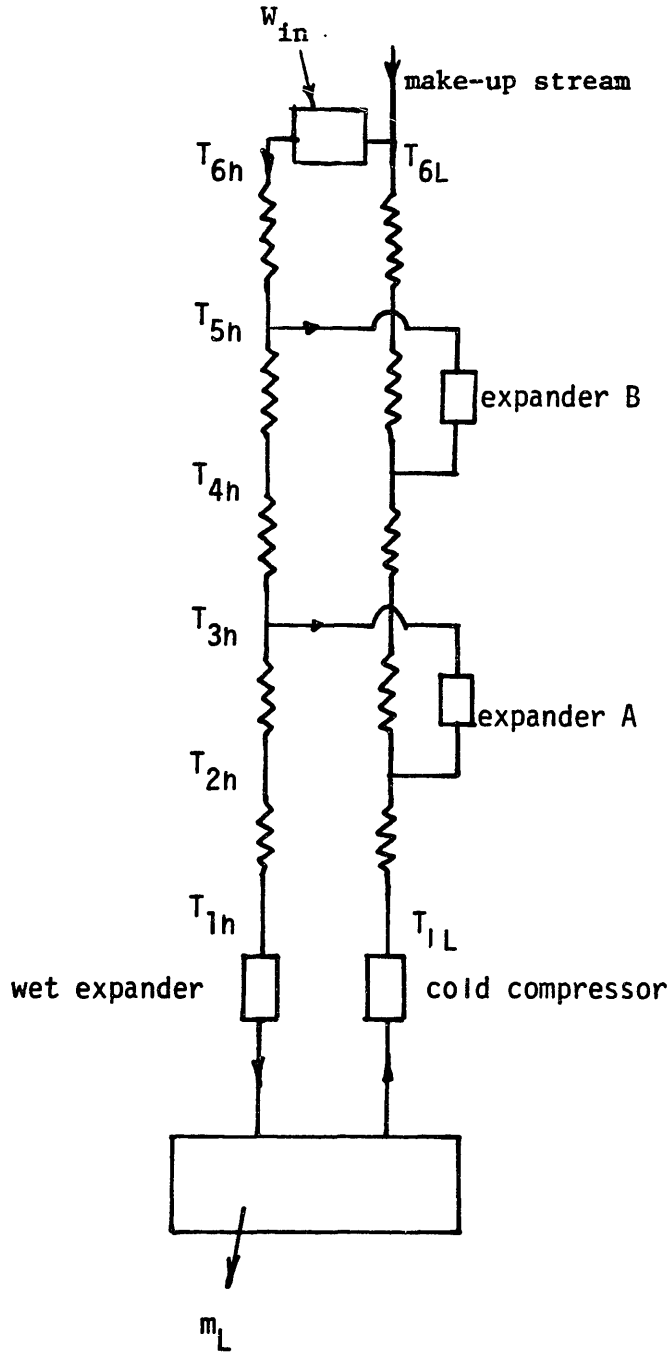


FIG. 3.11 2-EXPANDER COLLINS' PRECOOLER WITH OPTIMAL COLD END CONFIGURATION.

The combination of the SVC cold end configuration with the Collins' multiple-expander precooling stage represents an overall cycle optimal configuration. The greater the number of expansion processes, the closer the cycle approaches reversibility. A practical cycle will contain a finite number of these components from cost considerations. Figure 3.11 shows the SVC cycle with the Collins' two-expander precooling stage.

Chapter 4

AN ENTROPY FLOW OPTIMIZATION ALGORITHM FOR HELIUM LIQUEFACTION CYCLES

This chapter presents a new optimization technique for designing helium liquefaction cycles. The technique is based on the second law. The cycle configuration is an output of the design algorithm which also gives values to initialize the independent variables for final parametric optimization.

4.1 Introduction

Several of the potential applications of superconducting technology require large size refrigerators/liquefiers for cooling. The capital cost of such large size refrigerators is small compared with the operating cost. Therefore there is an emphatic need for highly efficient refrigerators. The intensity of the effort to design efficient cycles is reflected in the numerous discussions of optimization techniques in the literature.[44,82,91 - 93]

Although the idea of minimizing irreversibilities has been used to design efficient thermodynamic cycles, it has not been formalized in a design methodology for the whole cycle. In a conventional optimization scheme, a particular cycle configuration is first chosen. The cycle governing equations, a set of algebraic equations, are derived from the first law. Then a chosen performance index is optimized by varying each of a selected set of optimizable parameters– typically the state point pressures, the temperature levels and the critical heat exchange temperature differences. The state points are checked for any second law violations. An entropy flow technique has been used to identify and quantify the sources of cycle irreversibilities[44] and also to judiciously initialize some of the optimizable parameters.[45] Exergy methods of analysis have also been used.[82,93]

A new method of analysis based on continuous distribution of precooling over the

temperature range of the cycle is now introduced. Unlike the continuum model discussed in chapter 3, this model includes the heat exchange irreversibilities. Generated entropy flow is the chosen performance index and is minimized by variational calculus techniques. This is equivalent to maximizing the COP as discussed in Chapter 2. The method gives the optimum distribution of precooling over the temperature range of the cycle by specifying the mass flow to be expanded at each temperature. This result is used to select an optimum cycle configuration with discrete expansions. The method also indicates that the heat exchange temperature difference ratio $\Delta T/T$ must be constant for the refrigerator or liquefier and gives the influence of the pressure levels and pressure ratio on the cycle performance. These results are used to initialize the independent variables for final parametric optimization.

4.2 Description of Model

The precooling stage of the conventional cycle consists of regenerative heat exchange in a set of counterflow heat exchangers with discrete expansion of portions of the high pressure stream to augment the cooling provided by the low pressure return stream (Fig. 4.1.) The total heat exchange irreversibility is quantified by the total generated entropy and is obtained by integrating the local irreversibility over the temperature spanned by the heat exchanger. The heat capacity flow rates determine the distribution of internal heat exchange, ΔT. Therefore to capture the integrated loss accurately requires use of differential analysis and real gas properties. (The properties of helium depart substantially from ideal gas behavior at very low temperatures.) The continuum model described below facilitates differential analysis and therefore enables a more accurate evaluation of the irreversibilities. This model incorporates in the heat exchange irreversibility, the effect of non-ideal behaviour discussed in chapter 3 since the heat capacity rates determine the distribution of internal heat exchange ΔT.

The model (Fig. 4.2(a)), representing the precooling stage, depicts cooling the high pressure stream by continuously extracting infinitesimal portions of the high pressure

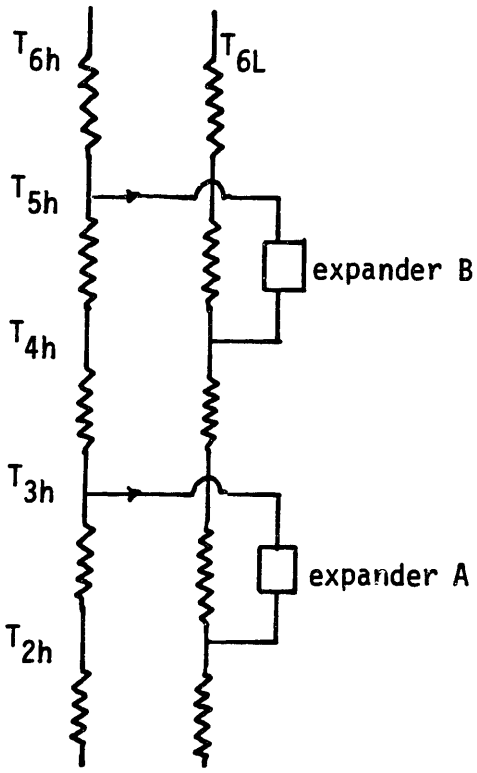


FIG. 4.1 TYPICAL PRECOOLING STAGE OF A HELIUM REFRIGERATION CYCLE.

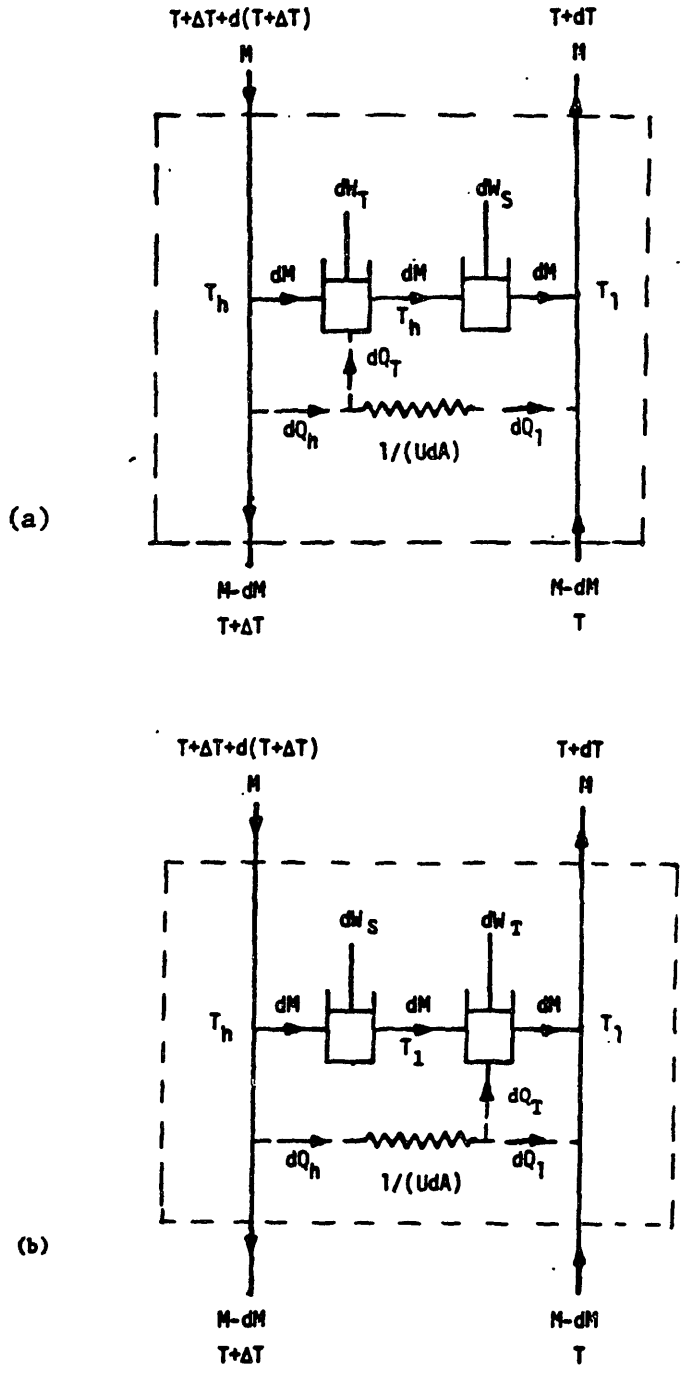


FIG. 4.2 MODEL FOR PRECOOLING STAGE: HEAT EXCHANGE WITH CONTINUOUS EXPANSION.

stream and expanding it to the low pressure in two stages: first through an isothermal expander to provide precooling to reduce ΔT and then through an adiabatic expander to drop the temperature by ΔT to T_l. The model shown applies to the refrigeration mode where the same mass is circulating in both streams. The level of complexity is reduced by first considering an ideal gas model for the working fluid. The results of this special case provide insight into the effects of the non-ideal behavior as well as guidance in solving the more complex case involving real properties.

4.2.1 Ideal Gas Model: Refrigeration Mode

The governing differential equations for the continuum model shown in Fig. 4.2a are derived in appendix C1 based on the following assumptions:

1. The working fliud is an ideal gas;
2. The expansion processes are reversible;
3. The pressure drop in the heat exchangers are negligible;
4. The overall heat transfer coefficient, U, is constant.
5. The pressure ratio is fixed.

The governing equations are a set of three differential equations derived from continuity, heat exchanger balance, and the second law of thermodynamics. For the control volume shown in Fig. 4.2(a), the first law and continuity of mass flow rate give the mass flow rate distribution as:

$$\frac{dM}{M} = \frac{d(\Delta T)}{(R/C_p)(1+\Delta T/T)[ln(P_h/P_l) - [\gamma/(\gamma-1)]ln(1+\Delta T/T)]}. \qquad (4.1)$$

The heat exchange rate equation simplifies to:

$$U\,dA = \frac{MC_p\,dT}{\Delta T}. \tag{4.2}$$

The entropy generated by heat exchange ΔT irreversibility is also given by:

$$dS_{gen} = MC_p\left(\frac{\Delta T}{T + \Delta T}\right)\frac{dT}{T}. \tag{4.3}$$

These three differential equations may be integrated over the precooling range. Integrating the first law expression gives the mass flow rate distribution over the precooling range. The heat exchange rate equation also integrates to give the total heat exchange area required for the precooling stage. Similarly the generated entropy expression derived from the second law of thermodynamics may be integrated to give the total generated entropy associated with the precooling stage. The resulting equations are further simplified if expressed in terms of the dimensionless mass flow rate Ψ, the temperature ratio η and the heat exchange temperature difference ratio y. Thus,

The mass flow rate equation becomes

$$\int_{\eta_o}^{\eta}\left[\frac{y + y'}{(1+y)[\beta - ln(1+y)]} - \Psi'\right]d\eta = \text{constant}. \tag{4.4}$$

The total heat exchange area

$$\frac{UA}{M_oC_p} = \int_{\eta_o}^{\eta}\frac{\exp\Psi}{y}\,d\eta, \tag{4.5}$$

and the total generated entropy is also given by

$$\frac{S_{gen}}{M_oC_p} = \int_{\eta_o}^{\eta}\frac{y\exp\Psi}{1+y}\,d\eta. \tag{4.6}$$

β is a constant representing the pressure ratio:

$$\beta = \frac{1}{\alpha} \ln r_p, \tag{4.7a}$$

and α is a constant which depends on the fluid properties:

$$\alpha = \frac{C_p}{R}. \tag{4.7b}$$

R is the gas constant for unit mass.

Optimal precooling for this model then requires minimizing the total generated entropy given by Eq. 4.6 subject to continuity of mass flow rate (Eq. 4.4) and a fixed total heat exchange area (Eq. 4.5.) This is a classical variational calculus problem whose solution gives the optimal distribution of the heat exchanger temperature difference, the mass flow rate, the total heat exchanger area and the total generated entropy respectively as follows:

$$\frac{\Delta T}{T} = \text{constant}, \tag{4.8}$$

$$\frac{M}{M_o} = \left(\frac{T}{T_o}\right)^{\Phi}, \tag{4.9}$$

$$\frac{AU}{M_o C_p} = \Phi_1 \left[\left(\frac{T}{T_o}\right)^{\Phi} - 1\right], \tag{4.10}$$

$$\frac{S_{gen}}{M_o C_p} = \Phi_2 \left[\left(\frac{T}{T_o}\right)^{\Phi} - 1\right], \tag{4.11}$$

where the index Φ is a dimensionless constant given by:

$$\Phi = \frac{y}{(1+y)[\frac{1}{n}lnr_p - ln(1+y)]}, \tag{4.12}$$

and the scaling constants for the total heat exchange area and the total generated entropy are given respectively by

$$\Phi_1 = \frac{1}{\Phi y}, \tag{4.13}$$

$$\Phi_2 = \frac{y}{\Phi(1+y)}. \tag{4.14}$$

These functions are shown graphically in Fig. 4.3 for several pressure ratios and Fig. 4.4 for several values of $\Delta T/T$. The performance of the continuous precooling stage improves with increasing pressure ratio for a fixed heat exchange temperature difference ratio. Also for a fixed pressure ratio, decreasing the heat exchange temperature difference ratio (equivalent to increasing the heat exchange area) improves the performance of the precooling stage.

4.2.2 Ideal Gas Model: Liquefaction Mode

In a liquefier, the mass flow rate of the high pressure stream is higher than that of the low pressure stream. If the ratio of the high pressure stream mass flow rate to the low pressure stream mass flow rate is represented by ϵ, then a parallel analysis for the precooling stage gives similar results as for the refrigeration analysis. Details of this analysis are given in appendix C2. The system equations are summarized as follows.

The first law of thermodynamics gives:

$$\frac{dM}{M} = \frac{\epsilon[dT + d(\Delta T)] - dT}{(R/C_p)(1+\Delta T/T)[ln(P_h/P) - [\gamma/(\gamma-1)]ln(1+\Delta T/T)]}. \tag{4.15}$$

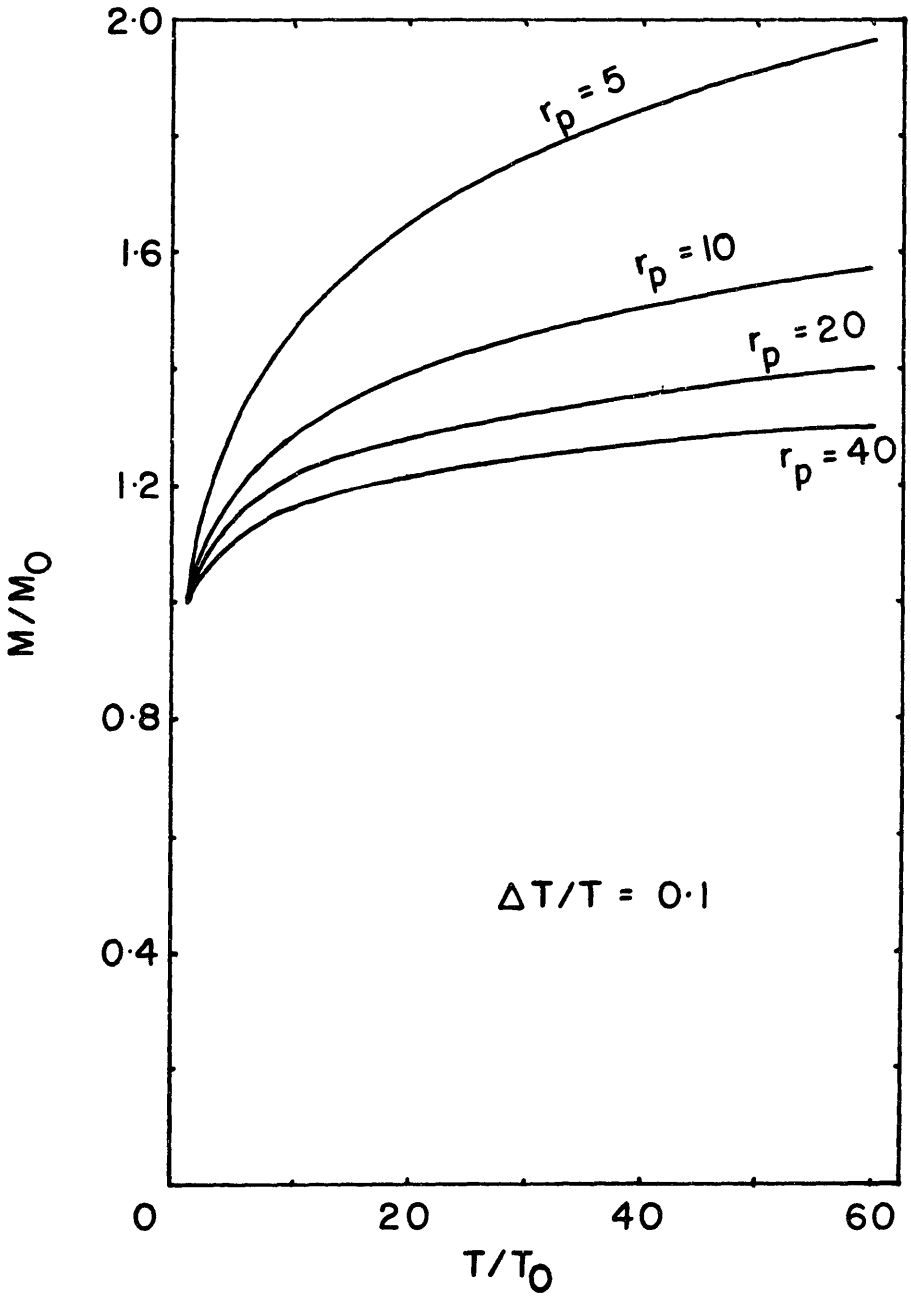


FIG. 4.3 PERFORMANCE CURVES FOR IDEAL GAS MODEL, REFRIGERATION MODE. (a) MASS FLOW RATE VERSUS TEMPERATURE.

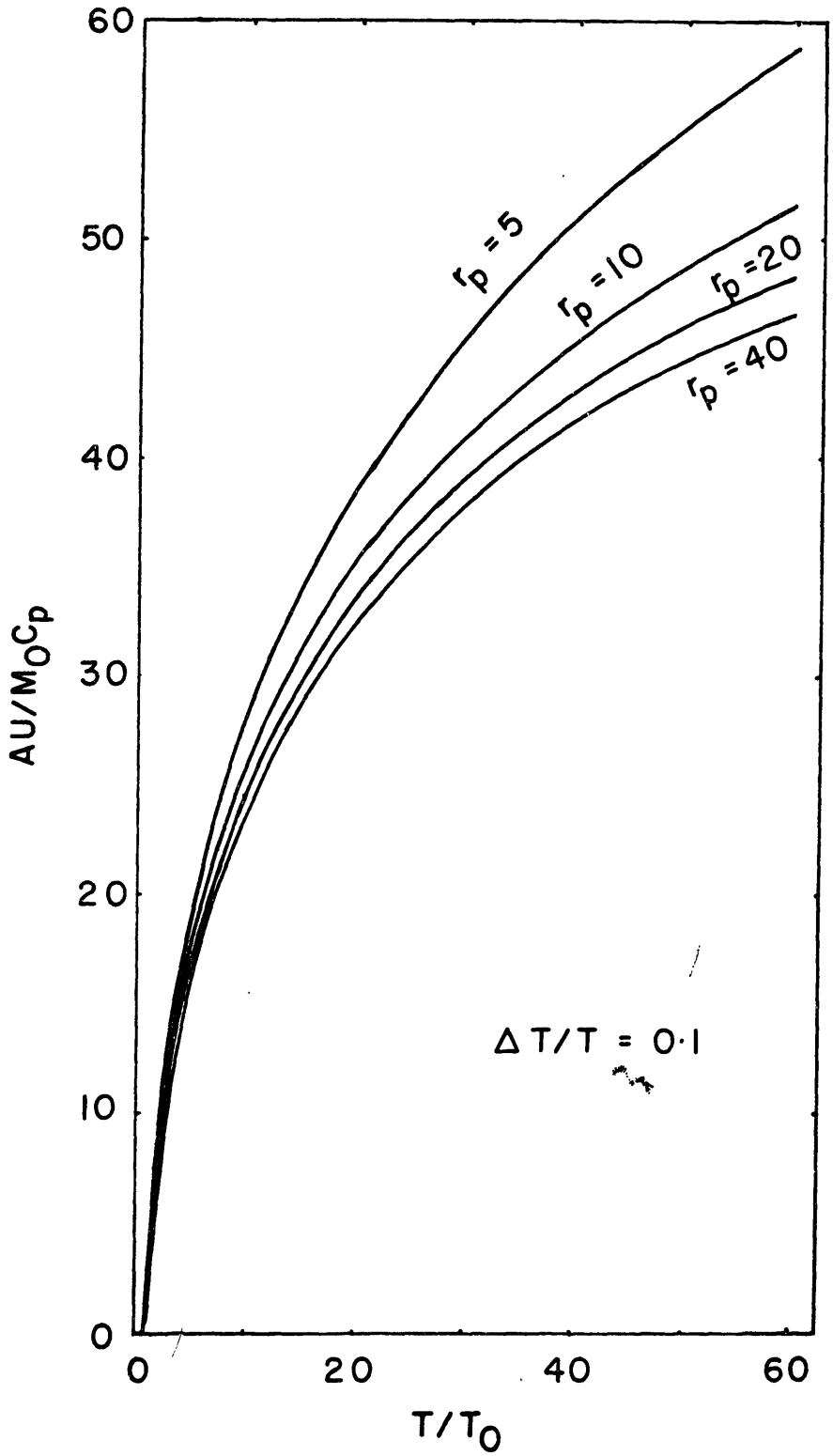


FIG.4.3 PERFORMANCE CURVES FOR IDEAL GAS MODEL, REFRIGERATION MODE: (b) HEAT EXCHANGE AREA VERSUS TEMPERATURE.

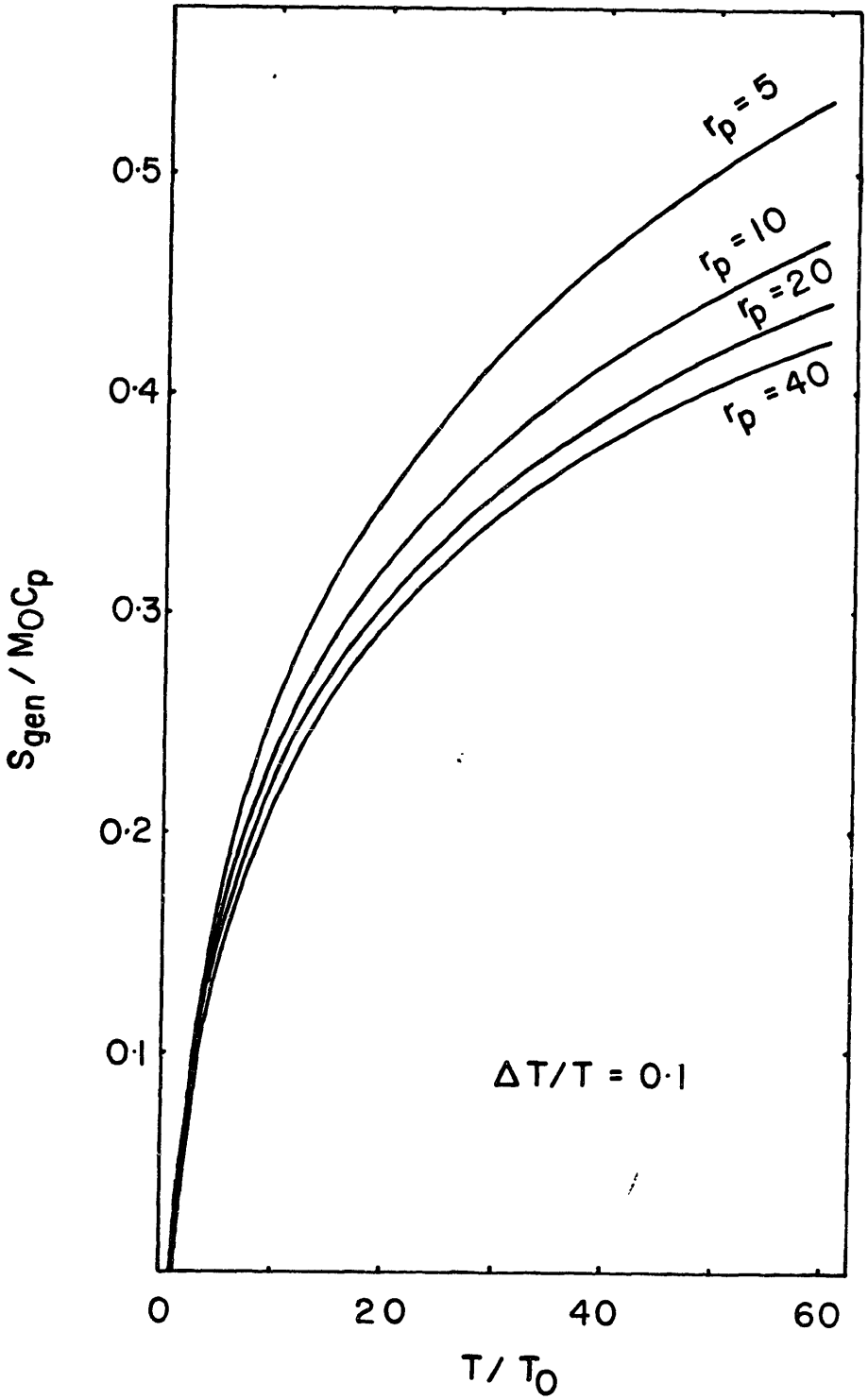


FIG. 4.3 PERFORMANCE CURVES FOR IDEAL GAS MODEL, REFRIGERATION MODE. (c) GENERATED ENTROPY VERSUS TEMPERATURE.

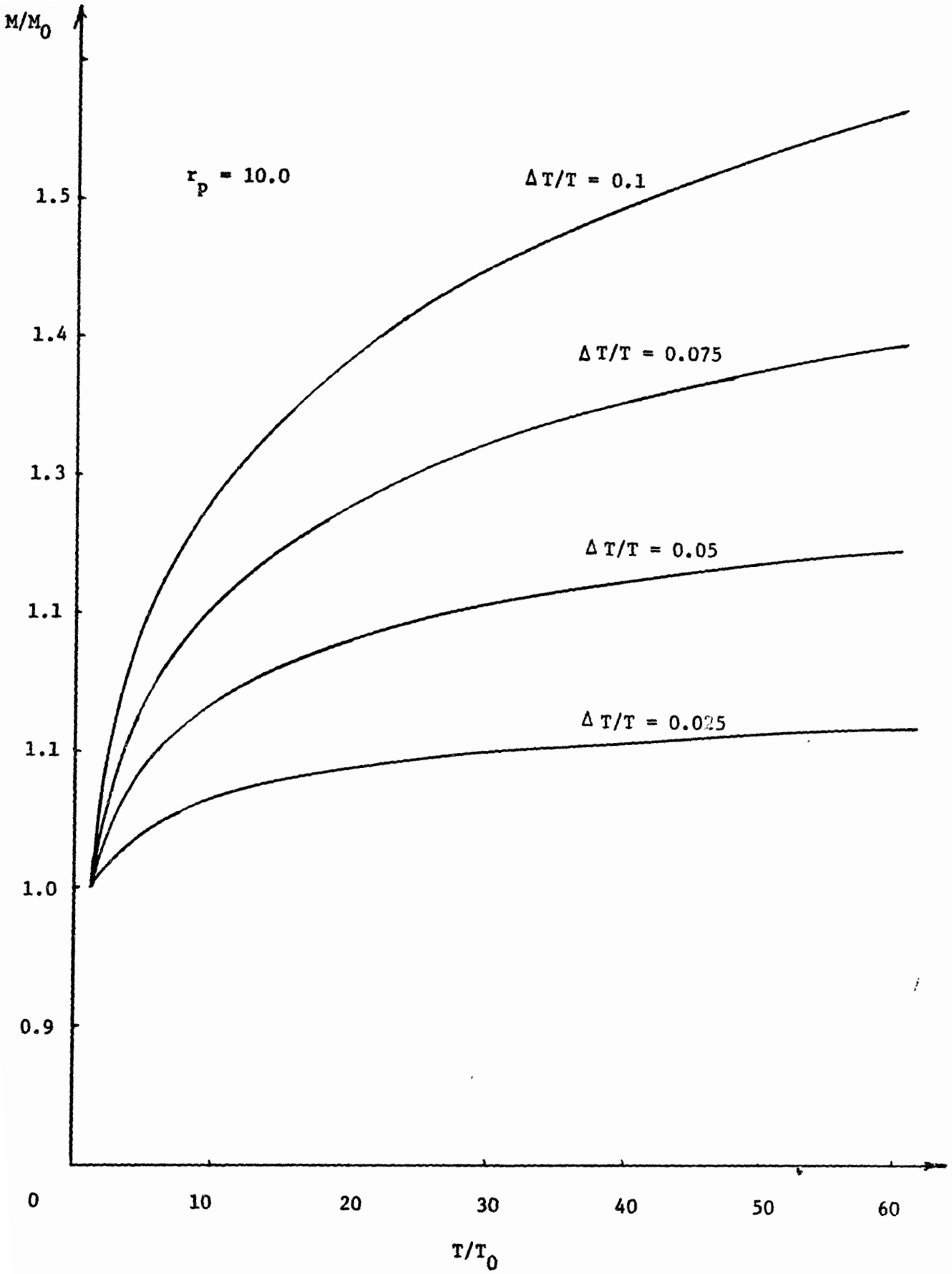


FIG. 4.4 PERFORMANCE CURVES FOR IDEAL GAS MODEL, REFRIGERATION MODE. (a) MASS FLOW RATE VERSUS TEMPERATURE.

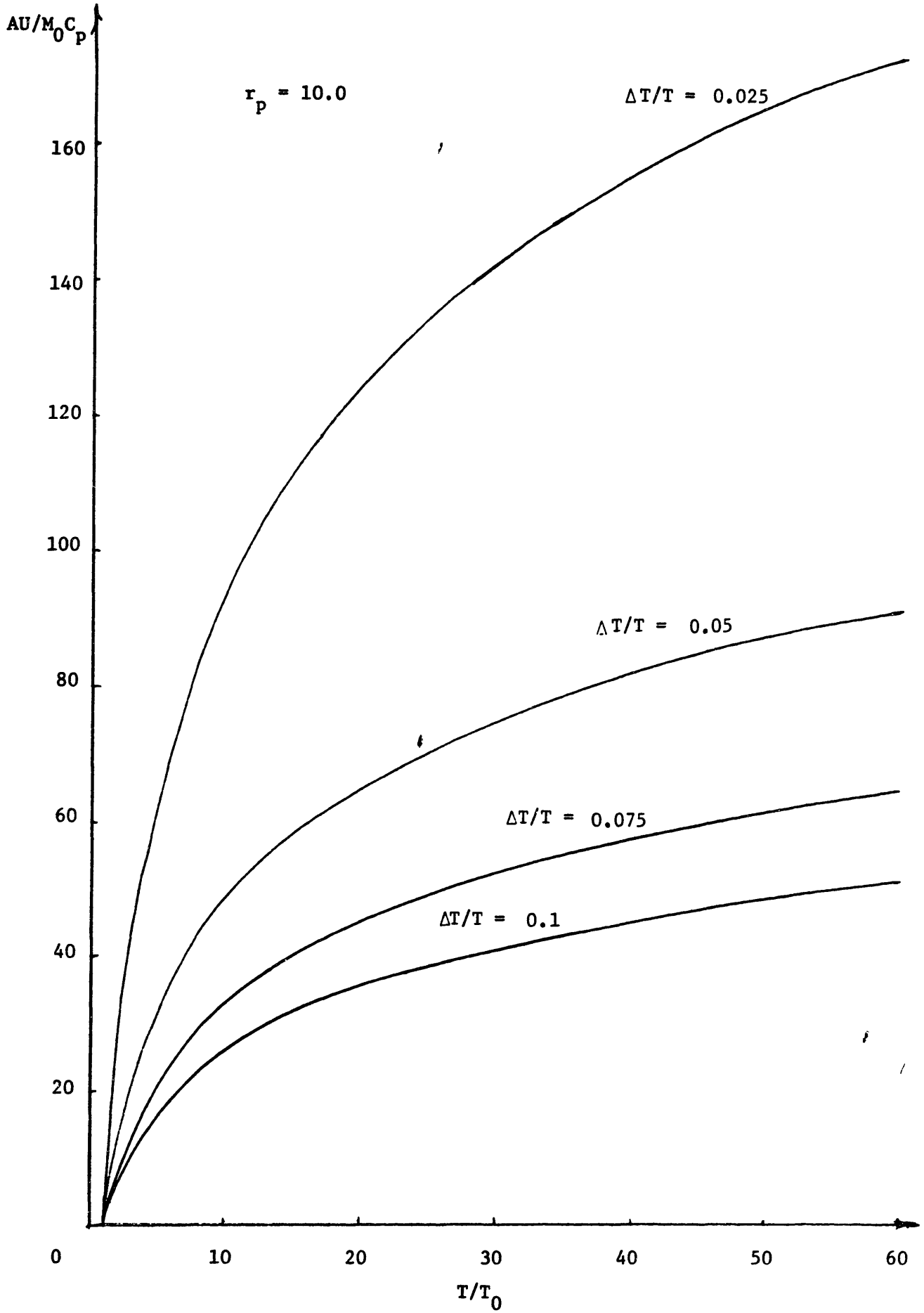


FIG. 4.4 PERFORMANCE CURVES FOR IDEAL GAS MODEL, REFRIGERATION MODE. (b) HEAT EXCHANGE AREA VERSUS TEMPERATURE.

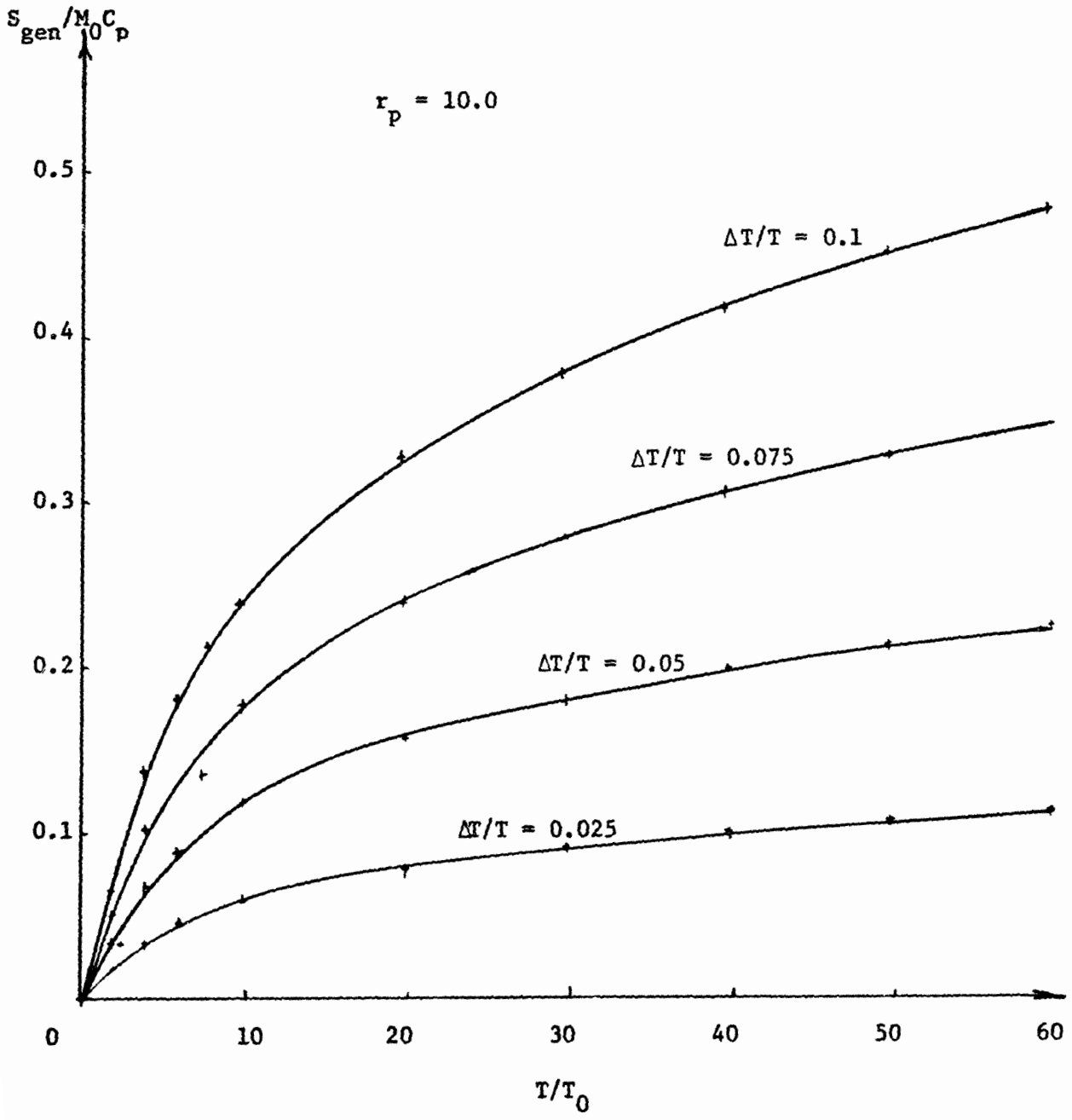


FIG. 4.4 PERFORMANCE CURVES FOR IDEAL GAS MODEL, REFRIGERATION MODE. (c) GENERATED ENTROPY VERSUS TEMPERATURE.

The heat exchanger rate equation gives:

$$U\,dA = \frac{MC_p\,dT}{\Delta T}. \tag{4.16}$$

The second law of thermodynamics also gives:

$$dS_{gen} = MC_p\left(\frac{\Delta T}{T + \Delta T}\right)\frac{dT}{T}. \tag{4.17}$$

The optimal distribution resulting from the variational calculus formulation reduces to:

$$\frac{\Delta T}{T} = \text{constant} \tag{4.18a}$$

$$\ln\frac{M}{M_o} = \frac{1+y}{\Phi}\int_{T_o}^{T}\epsilon\frac{dT}{T} - \frac{1}{\Phi}\frac{T}{T_o}; \tag{4.18b}$$

$$\frac{AU}{M_oC_p} = \frac{1}{y}\int_{T_o}^{T}\frac{M}{M_o}\frac{dT}{T}; \tag{4.18c}$$

$$\frac{S_{gen}}{M_oC_p} = \frac{y}{1+y}\int_{T_o}^{T}\frac{M}{M_o}\frac{dT}{T} \tag{4.18d}$$

The mass flow rate ratio ϵ is a function of temperature. However the similarity of the results for the refrigeration and liquefaction modes can be seen by considering this weak function of temperature as a constant. Then the resulting optimal functions are of the exact form as those for the refrigeration mode (Eqs. 4.7 through 4.14) except that the constant Φ is now given by Eq. 4.19 instead of Eq. 4.12

$$\Phi = \frac{\epsilon(1+y)-1}{(1+y)[\frac{1}{n}\ln r_p - \ln(1+y)]}. \tag{4.19}$$

Typical results for the liquefaction mode are shown in Fig. 4.5. The curves show the same trends as those obtained for the refrigeration mode (Fig. 4.4).

4.2.3 Real Gas Model: Refrigeration Mode.

The specific heat capacity of helium varies considerably at low temperatures. It is therefore appropriate, even necessary, to analyze the precooling model for the case of varying specific heat. Details of this analysis are given in appendix C3. The analysis is based on the following assumptions:

1. the expansion processes are reversible;
2. the pressure drop in the heat exchangers are negligible;
3. the overall heat transfer coefficient, U, is constant.
4. the pressure ratio is fixed.

The system equations derived from continuity of mass flow rate, heat exchanger heat balance and the second law of thermodynamics now become:

$$d\Psi = \frac{C_{ph}(1+y+y')-C_{pl}}{(1+y)(S_l - S_h)}\,d\eta, \tag{4.20}$$

$$\frac{U\,dA}{M_n C_p} = \frac{C_{pl}\exp\Psi}{C_{pn}y}\,d\eta, \tag{4.21}$$

$$\frac{dS_{gen}}{M_n C_p} = \frac{\frac{y}{1+y}C_{pl}}{C_{pn}\exp\Psi}\,d\eta, \tag{4.22}$$

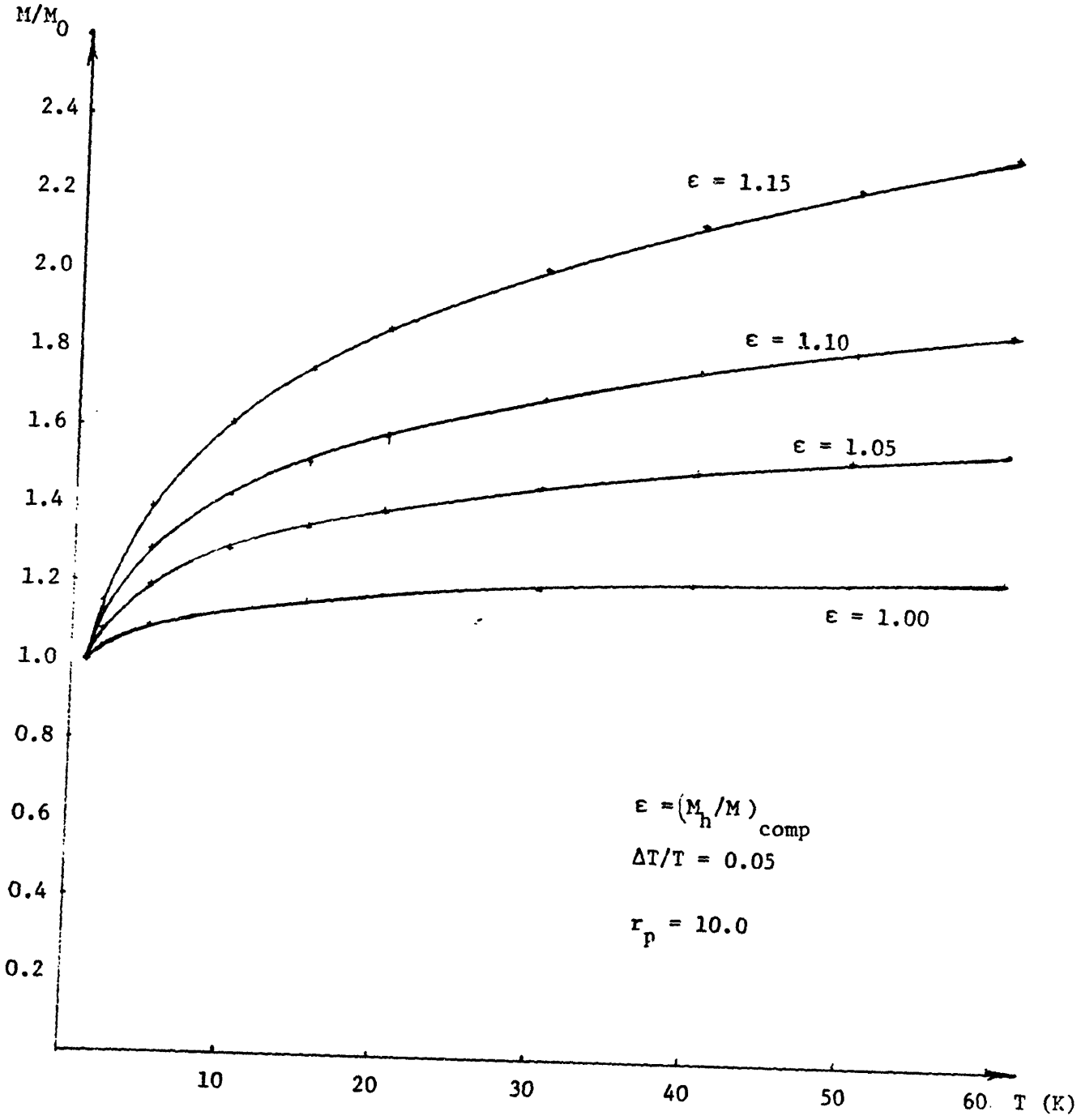


FIG. 4.5 PERFORMANCE CURVES FOR IDEAL GAS MODEL: LIQUEFACTION MODE
(a) MASS FLOW RATE VERSUS TEMPERATURE.

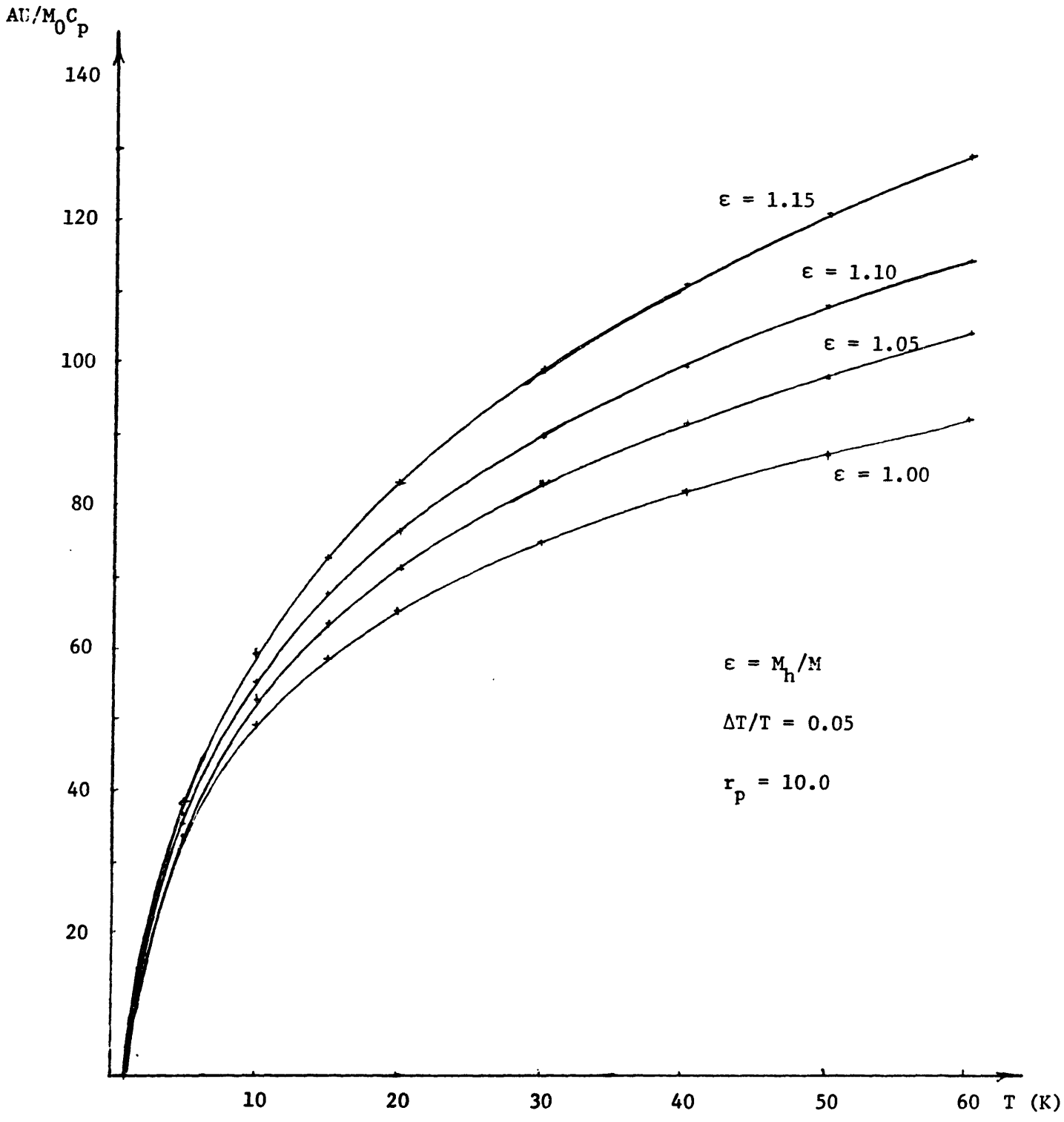


FIG. 4.5 PERFORMANCE CURVES FOR IDEAL GAS MODEL: LIQUEFACTION MODE
(b) HEAT EXCHANGE AREA VERSUS TEMPERATURE.

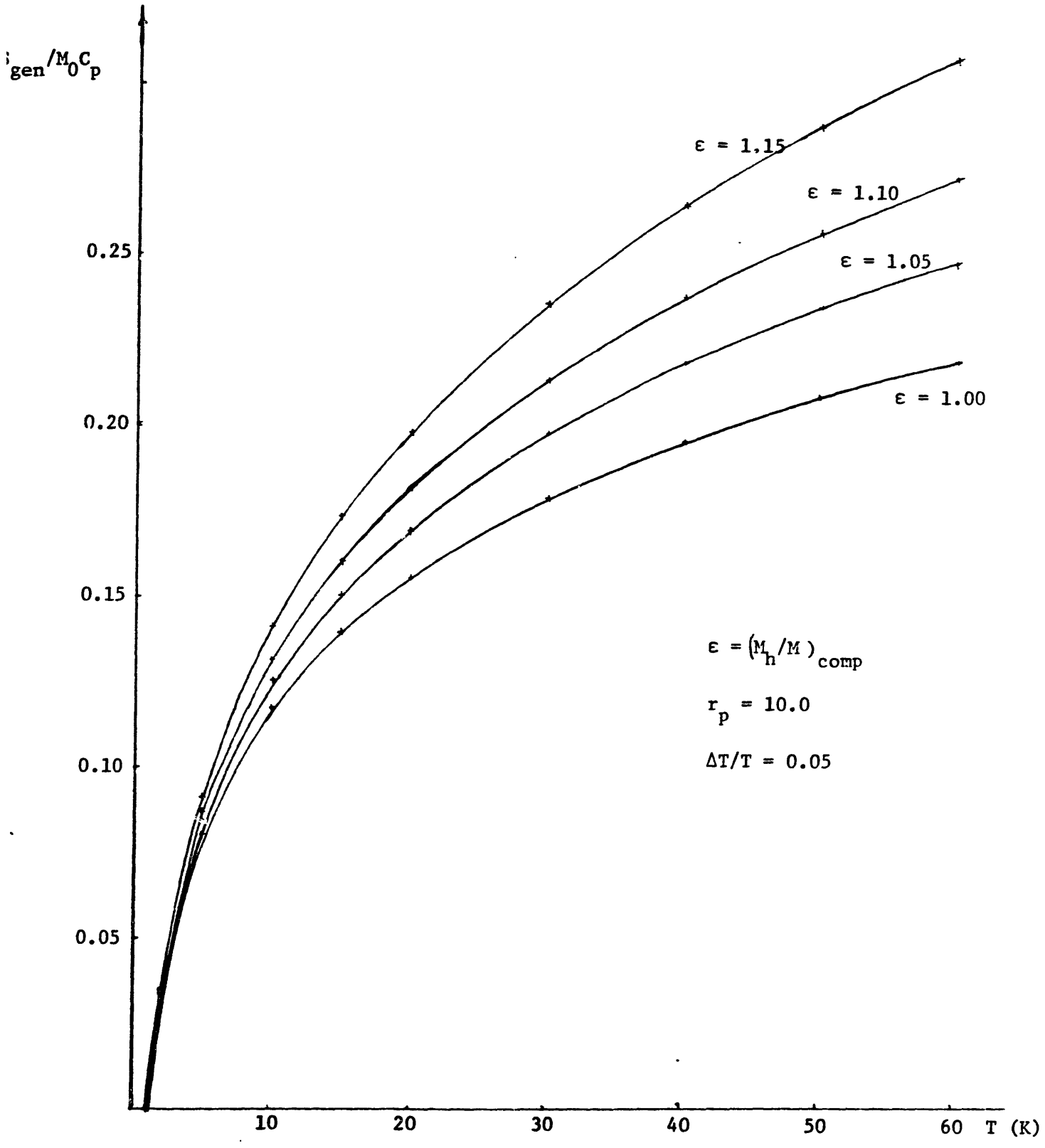


FIG. 4.5 PERFORMANCE CURVES FORIDEAL GAS MODEL: LIQUEFACTION MODE
(c) GENERATED ENTROPY VERSUS TEMPERATURE.

where Ψ is the dimensionless mass flow rate and n denotes normalizing constant.

Again invoking the variational calculus formulation to minimize the integrated generated entropy subject to continuity of mass flow rate and the total heat exchange area, the distribution of the performance parameters are derived:

The heat exchange temperature difference ratio,

$$\frac{\Delta T}{T} = \text{constant.} \tag{4.23}$$

The mass flow rate,

$$\frac{M}{M_n} = \exp\int \frac{C_{ph}(1+y) - C_{pl}}{(1+y)(S_l - S_h)} \frac{dT}{T}. \tag{4.24}$$

The total heat exchange area,

$$\frac{AU}{M_n C_{pn}} = \int \frac{C_{pl}}{C_{pn}} \frac{1}{y} \frac{M}{M_n} \frac{dT}{T}. \tag{4.25}$$

The total generated entropy,

$$\frac{S_{gen}}{M_n C_{pn}} = \int \frac{C_{pl}}{C_{pn}} \frac{y}{1+y} \frac{M}{M_n} \frac{dT}{T}. \tag{4.26}$$

These results are shown on Figs. 4.6-4.9. A Gauss quadrature numerical integration algorithm and the helium properties from the NBS Technical Note 631[90] are used for the numerical integration.

The mass flow rate curves show the trends due to non-ideal working fluid as discussed in chapter 3. However, for the same mass flow rate at the warm end, the mass flow rate is lower at the turning point for the model discussed in this chapter. This is because of the irreversibility due to non-zero heat exchange temperature difference.

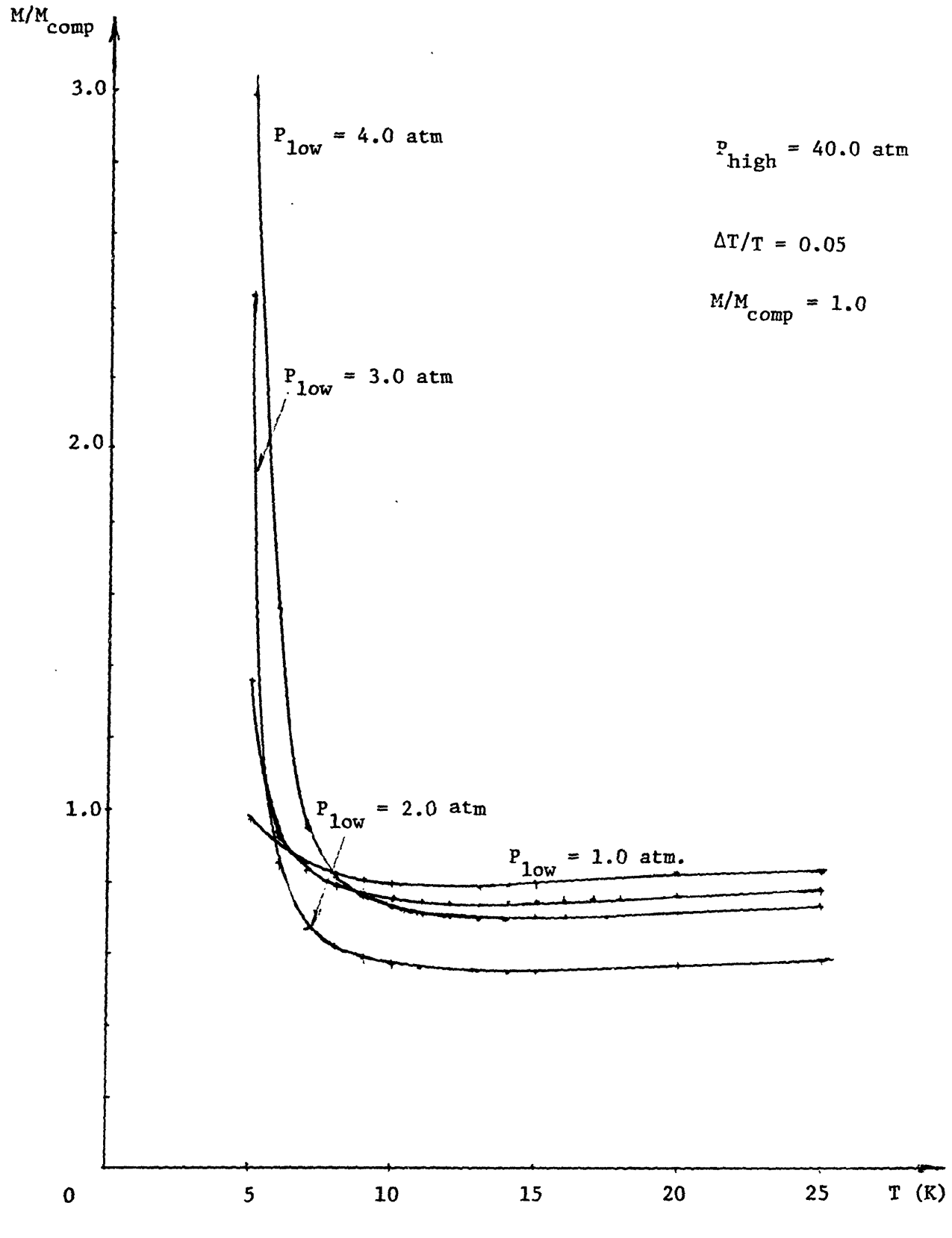


FIG. 4.6 COLD END PERFORMANCE CURVES FOR REAL GAS, REFRIGERATION MODE: INFLUENCE OF PRESSURE RATIO FOR FIXED ΔT/T.

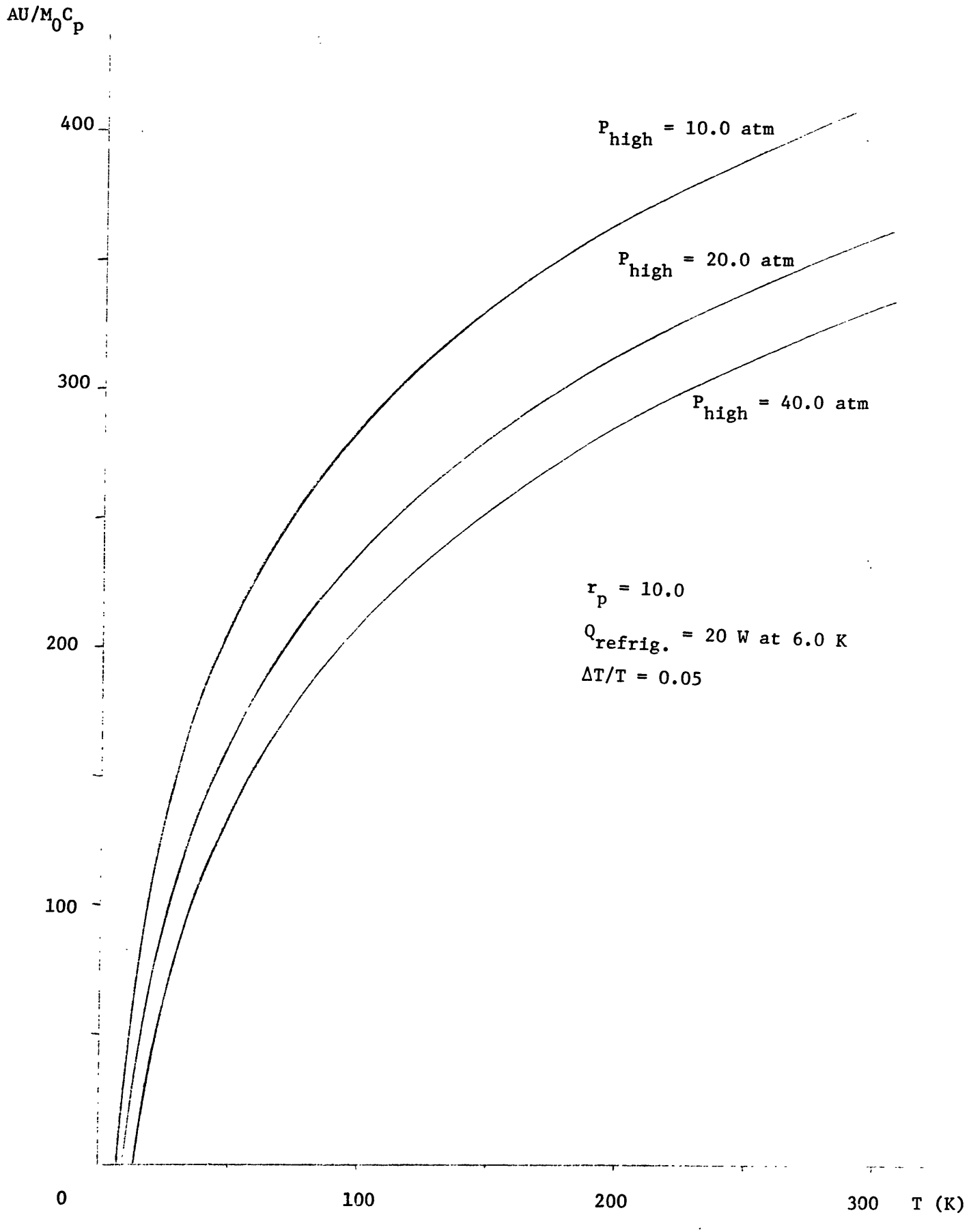


FIG. 4.7 PERFORMANCE CURVES FOR CONTINUOUS PRECOOLING, REFRIGERATION MODE.

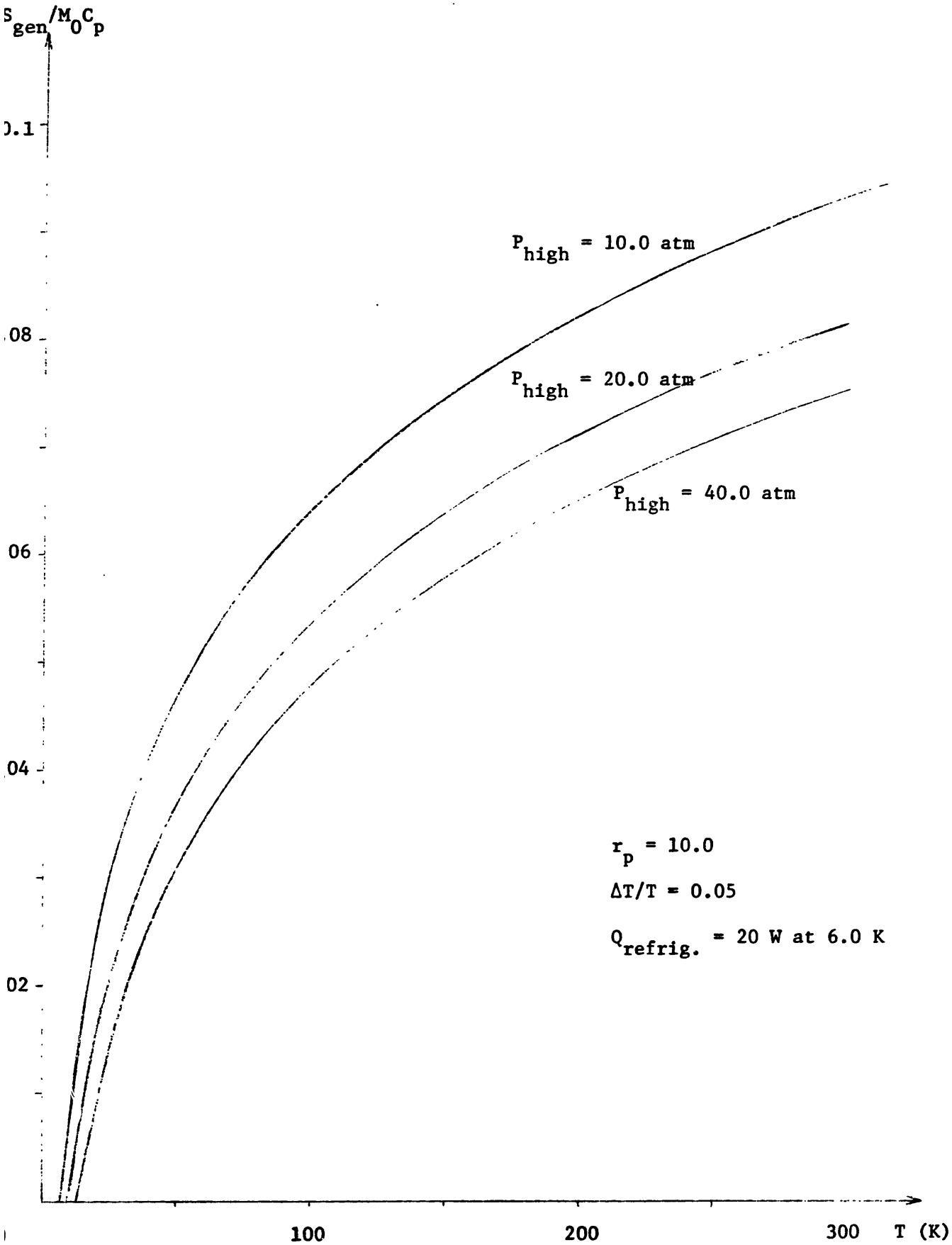


FIG. 4.8 PERFORMANCE CURVES FOR CONTINUOUS PRECOOLING, REFRIGERATION MODE.

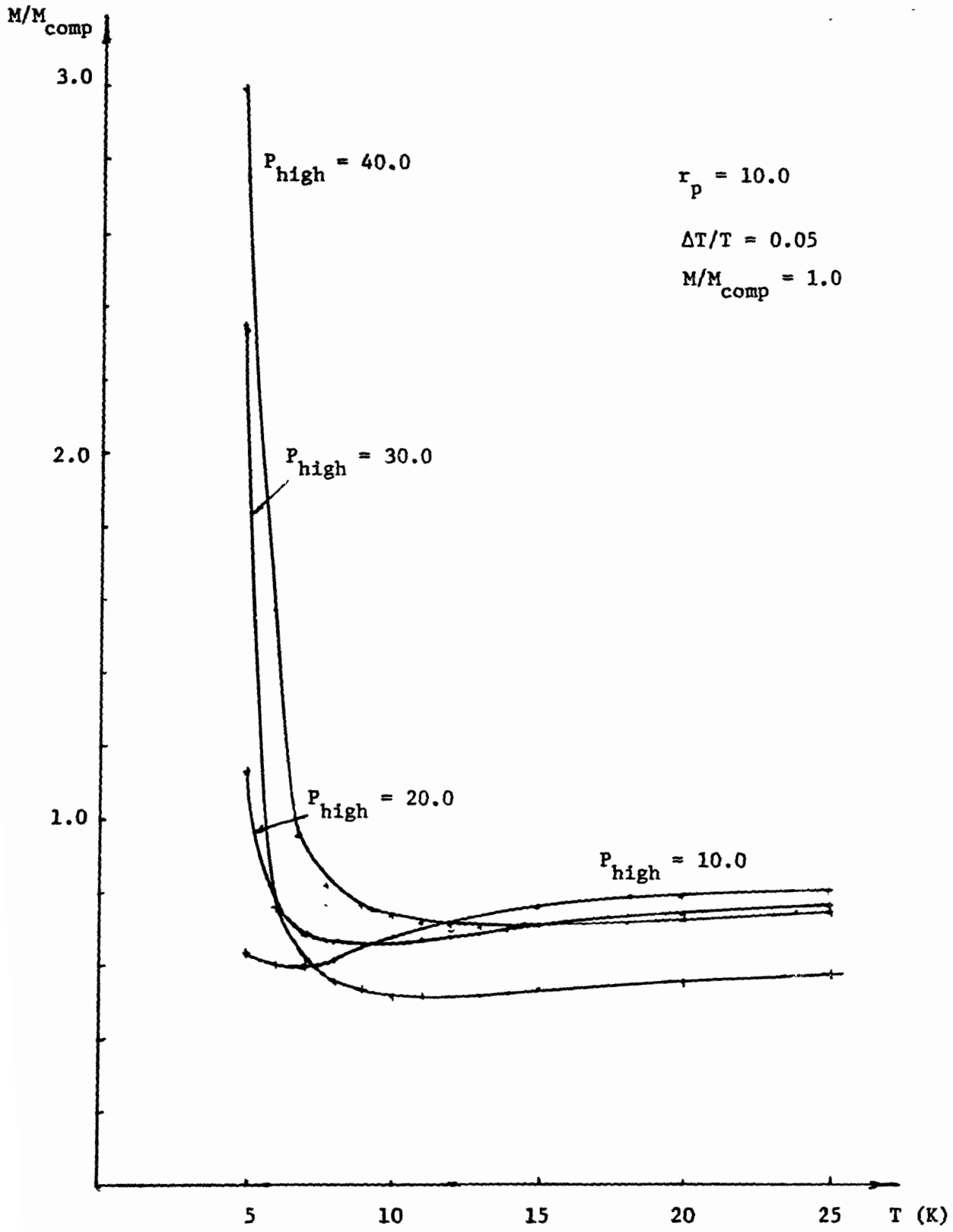


FIG. 4.9 COLD END PERFORMANCE CURVES FOR REAL GAS MODEL, REFRIGERATION MODE. $\Delta T/T = 0.05$

The turning point temperatures are also lower. The condition which determines the turning point temperature is now $(1+y)C_{ph} = C_{pl}$ instead of $C_{ph} = C_{pl}$ for the isolated effect of non-ideality. Thus the heat exchange temperature difference ratio scales up the specific heat capacity of the high pressure stream. Consequently, the turning point temperature is lowered for the same reason as discussed for the liquefaction mode in Sec. 3.3.2

4.2.4 Real Gas Model: Liquefaction Mode.

Again the higher mass flow rate of the pressure stream for the liquefier requires that the model be analyzed for the liquefaction mode. The same assumptions for the real gas model discussed in the preceeding section form the basis for deriving the governing equations. Details of the derivation are given in appendix C4. The final results are summarized below.

The heat exchange temperature difference ratio is given as:

$$\frac{\Delta T}{T} = \text{constant.} \tag{4.27}$$

The mass flow rate simplifies to the form:

$$\frac{M}{M_n} = \exp\int \frac{\epsilon C_{ph}(1+y) - C_{pl}}{(1+y)(S_l - S_h)} \frac{dT}{T}. \tag{4.28}$$

The total heat exchange area becomes,

$$\frac{AU}{M_n C_{pn}} = \int \frac{C_{pl}}{C_{pn}} \frac{1}{y} \frac{M}{M_n} \frac{dT}{T}. \tag{4.29}$$

The total entropy generated is of the form:

$$\frac{S_{gen}}{M_h C_{ph}} = \int \frac{C_{pl}}{C_{ph}} \frac{y}{1+y} \frac{M}{M_h} \frac{dT}{T}. \tag{4.30}$$

The parameter ϵ is defined as:

$$\epsilon = \frac{M_h}{M}$$
$$= 1 + \frac{M_{liq}}{M}. \tag{4.31}$$

Since the fraction of the high pressure stream liquefied and hence the value of the mass ratio ϵ is not known a priori, the solution requires iteration (the solution converges in about three iterations.) Figure 4.10 compares typical mass flow rate curves for the liquefaction mode and the refrigeration mode. Again the mass flow rate at the turning point is lower for the liquefaction mode because the factor ϵ scales up the specific heat capacity values for the high pressure stream relative to the low pressure stream.

4.2.5 Alternative Expander Arrangement

In the model of Fig. 4.2(a) discussed so far, the portion of the high pressure mass extracted is first expanded isothermally and then adiabatically. An alternative arrangement of the expanders is shown in Fig.4.2(b.) In this arrangement, the mass dM extracted from the high pressure stream is first expanded adiabatically to reduce the temperature by ΔT. Subsequently it is expanded isothermally to the low pressure.

Interchanging the order of the two expansion processes does not affect the basic form of the results. Naturally, the heat exchange area and the entropy generated trade off to a different set of optimal values because of the difference in the heat exchange thermal load.

A summary of the results follow for the ideal gas case and operation in a refrigeration mode. Details of the analysis are given in appendix C5.

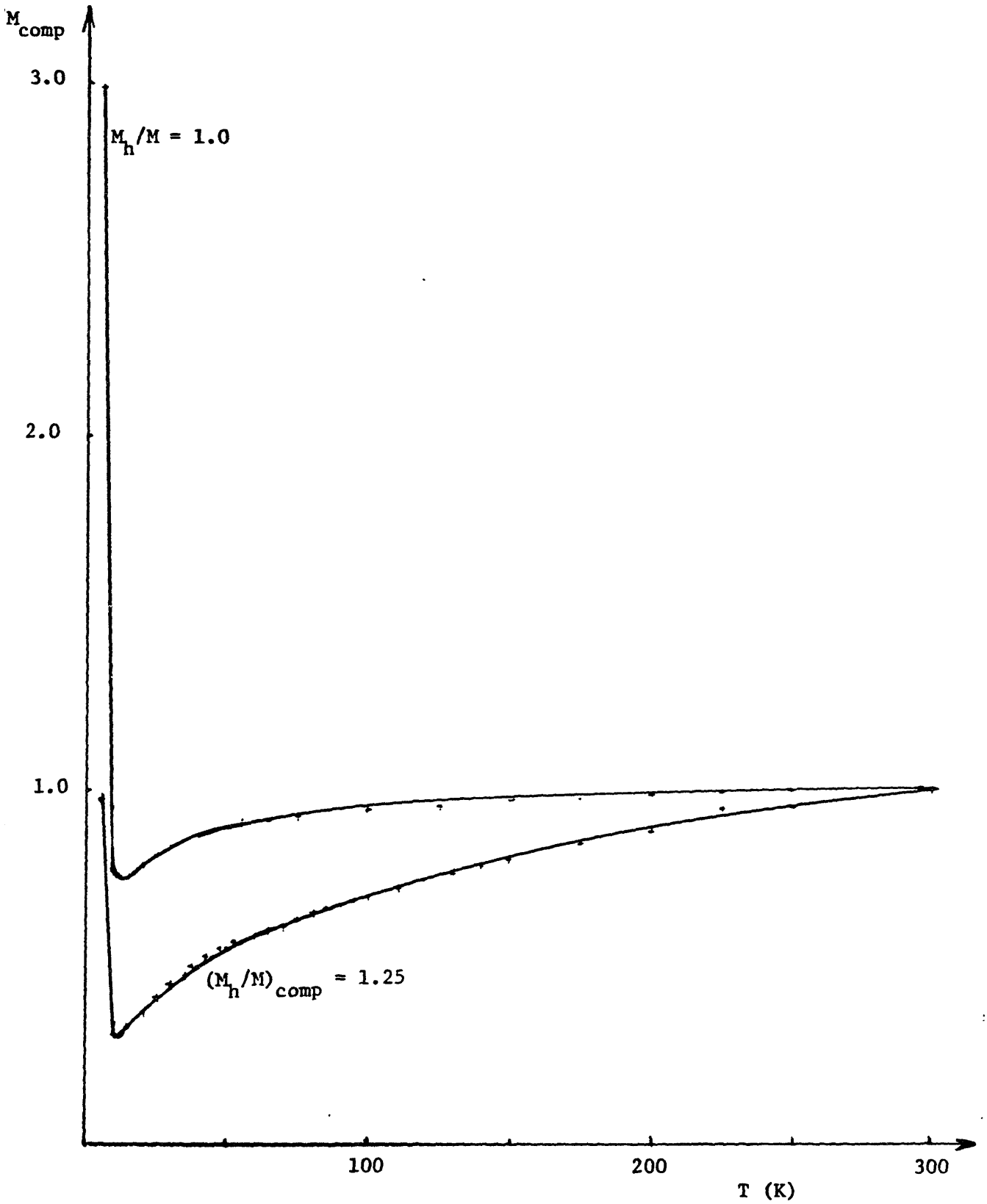


FIG.4.10 (a) PERFORMANCE CURVES FOR MASS CROSSFLOW MODEL: LIQUEFACTION MODE, $\Delta T/T = 0.05$, $r_p = 10.0$, $P_{high} = 40.0$ atm.

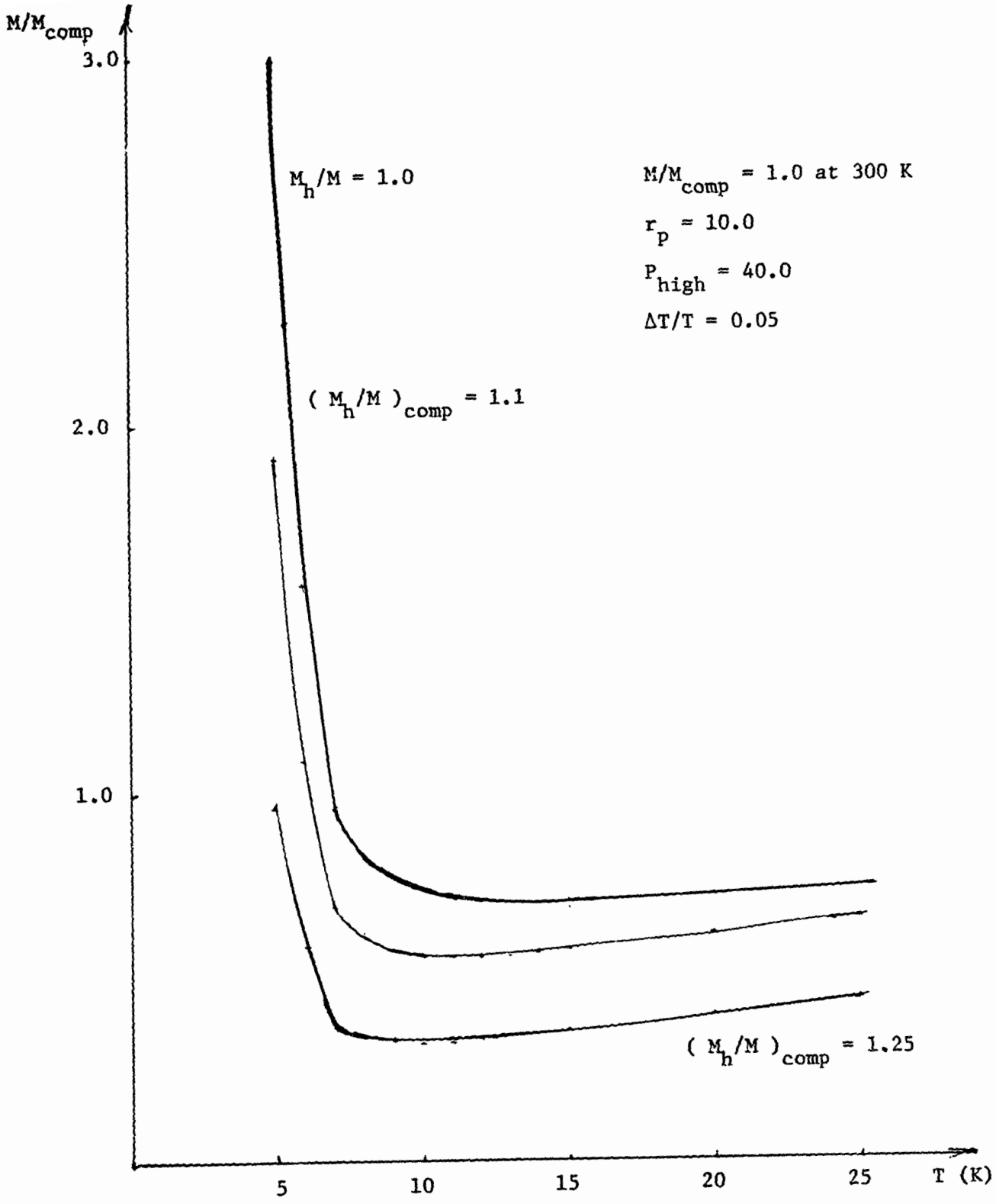


FIG. 4.10(b) COLD END PERFORMANCE CURVES FOR MASS CROSSFLOW MODEL: LIQUEFACTION MODE.

The heat exchange temperature difference ratio is given as:

$$\frac{\Delta T}{T} = \text{constant}, \tag{4.32}$$

The mass flow rate becomes

$$\frac{M}{M_o} = \left(\frac{T}{T_o}\right)^{\Phi}. \tag{4.33}$$

The total heat exchange area also becomes

$$\frac{AU}{M_o C_p} = \Phi_1\left[\left(\frac{T}{T_o}\right)^{\Phi} - 1\right]. \tag{4.34}$$

Finally the total generated entropy is given as:

$$\frac{S_{gen}}{M_o C_p} = \Phi_2\left[\left(\frac{T}{T_o}\right)^{\Phi} - 1\right]. \tag{4.35}$$

The index Φ is a dimensionless constant given by:

$$\Phi = \frac{y}{[\frac{1}{\alpha} ln r_p - ln(1+y)]}, \tag{4.36}$$

and the scaling constants for the total heat exchange area and the total generated entropy are given respectively by:

$$\Phi_1 = \frac{1+y}{\Phi y}, \tag{4.37}$$

$$\Phi_2 = \frac{y}{\Phi}. \tag{4.38}$$

These results are of the exact form as the results obtained for the alternative model discussed earlier in Sec. 4.3.1 (Eqs. 4.8-4.11.) The only difference is in the index and in the scaling constants. The heat exchange area scaling constant Φ_1 is increased by the factor $(1+\Delta T/T)$ while the generated entropy scaling constant Φ_2 is decreased by the same factor. The increased heat exchange surface area accounts for the decrease in the heat exchange irreversibility.

4.3 Discussion of Results.

The analysis shows that the heat exchange temperature difference ratio $\Delta T/T$ must be constant over the temperature span of the refrigeration or liquefaction cycle. This conclusion is independent of the working fluid. The heat exchange temperature difference ratio is an important parameter because it fixes the heat exchange area required. Figure 4.4 shows the effect of varying this temperature ratio on the performance of the cycle for a fixed pressure ratio and a fixed mass flow rate at the cold end of the precooling stage. A larger heat exchange area is required to decrease the temperature ratio. Also, the mass flow rate and the total entropy generated decrease with decreasing values of $\Delta T/T$. This is because the heat exchange irreversibilities decrease with increasing heat exchange area.

The mass flow rate curves for the real gas model Figs. 4.6, 4.7, 4.10 show the characteristic turning point discussed in chapter 3. These confirm the deductions made about the optimal configuration in Sec. 3.5.

The influence of pressure ratio on the performance of the precooling stage is shown in Fig. 4.3 for the ideal gas refrigerator. The mass flow rate, the generated entropy, and the total heat exchange area all show improved performance with increasing pressure ratio for fixed heat exchange temperature difference ratio. However, the performance of existing compressors also impose restrictions on practical values of the cycle pressure ratio which must be considered in a practical design.

The influence of pressure levels for fixed pressure ratio and fixed heat exchange temperature difference ratio $\Delta T/T$ is also shown in Figs. 4.8 and 4.9. The improved thermodynamic performance is due to the better matching of the specific heat capacities at the higher pressure levels. These curves may be used to trade-off heat exchange surface and cycle pressure level.

4.4 Design Algorithm Dased On The Continuum Precooling Model

The design procedure is illustrated by the design of an SVC cycle with a three-expander precooling stage (Fig.4.11.) The optimization parameters to be determined for a typical design are: pressure levels, heat exchanger critical temperature differences, temperature levels, and pressure ratio.

Pressure ratio: The performance of the precooling stage improves with increasing pressure ratio. In practice, however, the pressure ratio is fixed by the characteristics of the compressor and/or expander. Most helium compressors in use are retrofitted freon compressors . The development of helium compressors has not advanced to the level where their specifications become outputs of a design algorithm for the whole cycle. Rather the characteristics of these compressors are inputs to the design algorithm. Typically, reciprocating machines enable higher pressure ratios and a two stage compression from 1 atm to 18 atm seems to be a common choice. For the purpose of demonstrating the procedure, a pressure ratio of ten is chosen.

Pressure level: The performance curves for varying pressure levels and fixed pressure ratio indicate a consistently superior performance at the higher pressure levels. Consequently, the chosen operating pressures must be as high as practicable. Again the high pressure will be limited by the equipment performance, possibly the compressor. A high pressure of 40 atm. appear reasonable for this analysis.

Critical heat exchange ΔT: The critical heat exchange ΔT values are initialized using the constant value of $\Delta T/T$. The chosen value fixes the total heat exchange area

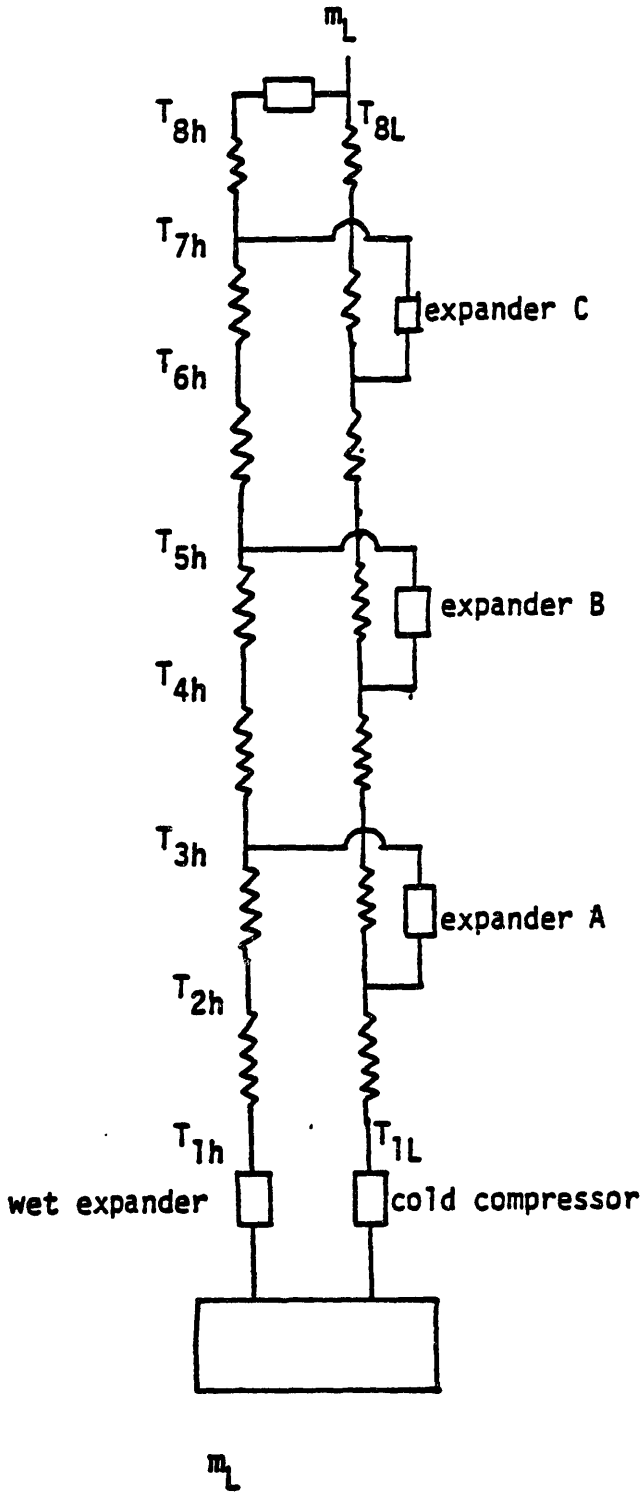


FIG. 4.11 3-EXPANDER SATURATED VAPOR COMPRESSION CYCLE

as well as losses due to heat exchange ΔT. Therefore the constant value is chosen to reflect trade-off in heat exchange area (and, hence cost) as well as heat exchange losses (thermodynamic performance of the precooling stage).

Temperature levels: The temperature levels, as determined by the expander inlet (or outlet temperatures, are directly related to the mass crossflow through the expanders. These may therefore be determined by the direct discretization of the mass flow rate curves. However, for three temperature levels and a liquefaction mode, this involves a tedious iteration. Therefore, each of the expander inlet temperatures is varied to obtain values that minimize the mass flow rate through the main compressor. This three-variable optimization problem is easily implemented on the computer.

Table 4

State point parameters for optimized 3-expander SVC cycle*

State Point	T_{high} (K)	T_{low} (K)	P_{high} (atm)	P_{low} (atm)	M_{high} (g/s)	M_{low} (g/s)
1	11.1	7.6	39.80	4.00	52.7	32.7
2	16.5	16.1	39.89	3.96	52.7	75.7
3	34.0	29.3	39.90	3.92	95.7	75.7
4	43.9	42.8	39.94	3.88	95.7	120.1
5	85.0	76.4	39.95	3.84	140.1	120.1
6	116.2	113.3	39.97	3.80	140.1	162.7
7	221.0	203.7	39.98	3.77	182.7	162.7
8	300.0	292.5	40.00	3.73	-	-

*Liquid production rate = 20 g/s;

Cold compressor power = 437 W;

Warm compressor power = 384.5 kW;

Heat exchange area = 347.2 m^2.

Sensitivity analysis: Figure 4.12 shows the variation of input (compressor) power and heat exchanger area with various values of $\Delta T/T$. From these curves, the power saving due to any additional heat exchanger area used can be determined. If the heat exchanger cost is known, these curves allow the operating value of $\Delta T/T$ to be determined. Optimal parameters for the SVC cycle corresponding to $\Delta T/T$ equal 0.05 are summarized in Table 4.

The results of Table 4 have been derived for a wet expander efficiency of 90% and a cold compressor efficiency of 85%. Figure 4.13 is a graphic representation of the sensitivity of the overall cycle performance to the efficiency of these components. The graph indicates that the cycle performance is more sensitive to changes in the wet expander performance than changes in the cold compressor performance. Thus a 20% decrease in cold compressor efficiency reflects in a 3% increase in total power input per unit liquid production rate whereas the same decrease in wet expander efficiency causes a dramatic 11% change in the power per unit liquid production.

4.5 Cost Analysis (for preceeding example)

The substantial improvement in thermodynamic performance reflects in savings in operating cost for the SVC cycle over the conventional cycle. This must however be compared to the additional capital cost required for the extra components (cold compressor/wet expander.) An appropriate cost analysis involves comparing the capital cost amortized over the estimated life of the machine with the operating cost for the same period. Lack of adequate documentation of components costs prevents such an accurate cost analysis.

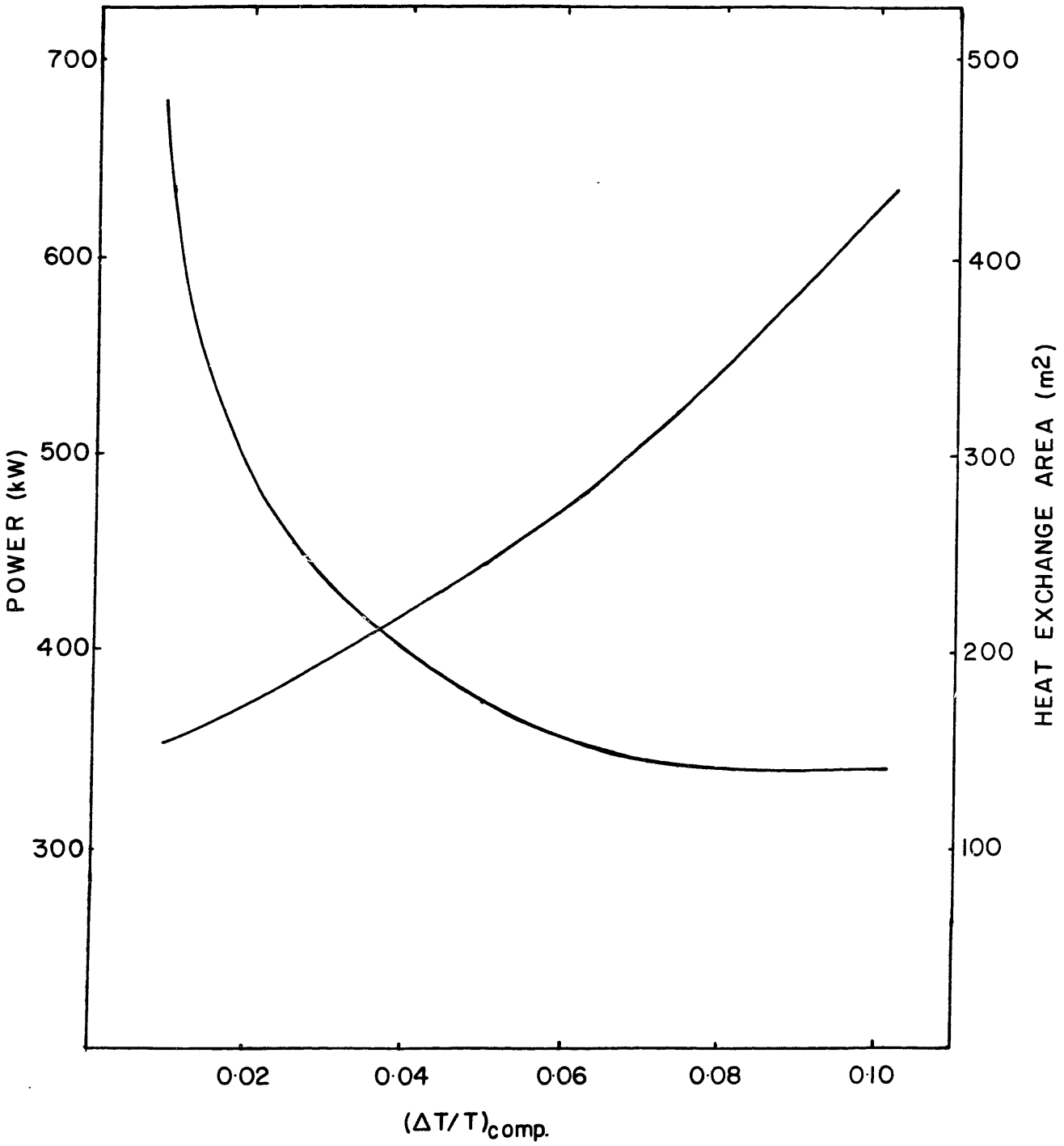


FIG. 4.12 PERFORMANCE CURVES FOR OPTIMAL 3-EXPANDER CYCLE.

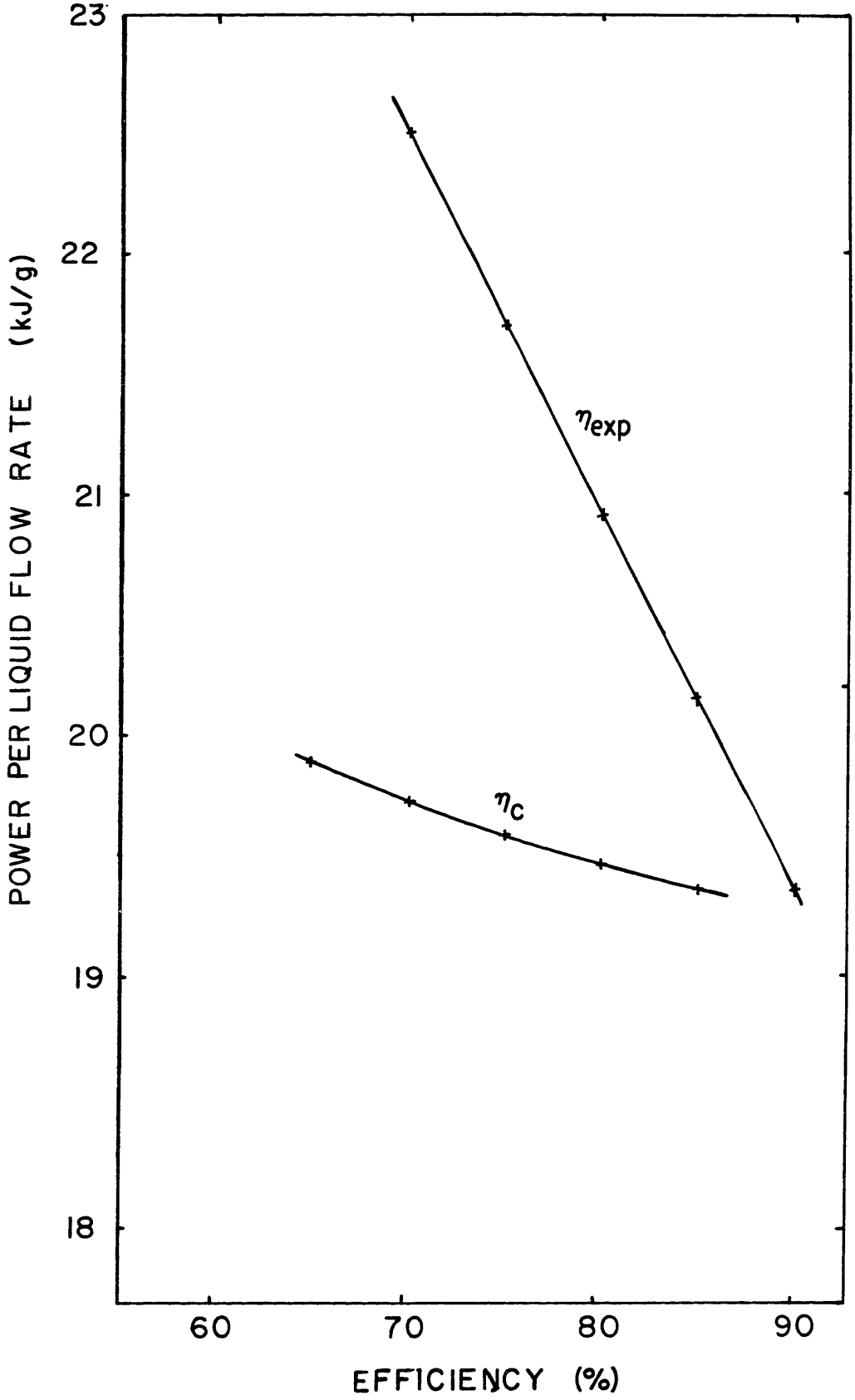


FIG. 4.13 SENSITIVITY OF CYCLE PERFORMANCE TO COLD END COMPONENT EFFICIENCIES.

Instead, a cost function is defined[45] which is a reasonable approximation to the effective cost: sum of operating cost and capital (installed) cost. As discussed in the reference, the cost function is given by:

$$CF = CHX + CPOWER + CLN_2 + CWATER, \tag{4.36}$$

where

CPOWER = power cost,

CLN_2 = liquid nitrogen cost,

CWATER = water cost,

CHX = heat exchanger cost.

The heat exchanger cost is obtained by an arbitrary cost correlating formula derived in terms of the total heat transfer area (representing the quantity of material used) and the frontal area (representing the size of the headers used.)

$$CHX = (42A_{fr} + 1.648A_{ht})(CPI)(I), \tag{4.37}$$

where

A_{fr} = frontal area,

A_{ht} = heat transfer area,

I = capital charge,

CPI = consumer price index (some of the data used had to be updated by the CPI.)

A scheduled operation of 80% (7008 hours per annum) is included to allow for maintenance periods and the plant is estimated to be in use for ten years.

Figure 4.14 shows the savings in the cost function for the SVC cycle over a conventional cycle with the J-T valve replaced by a wet expander. Thus the saving represents the breakeven cost of the cold compressor alone. The saving of order 0.5 million dollars demonstrates the economic viability of implementing the SVC cycle.

4.6 Conclusion

The analysis indicates that the optimal configuration for helium refrigeration or liquefaction cycles should have a multiple-expander precooling stage as suggested by Collins and the SVC configuration at the cold end. Also the heat exchange temperature difference ratio $\Delta T/T$ must be constant over the temperature span. This constant is used to initialize the heat exchange temperature pinch points in a final parametric optimization. Further the cycle pressure levels and cycle pressure ratio should be as high as practical.

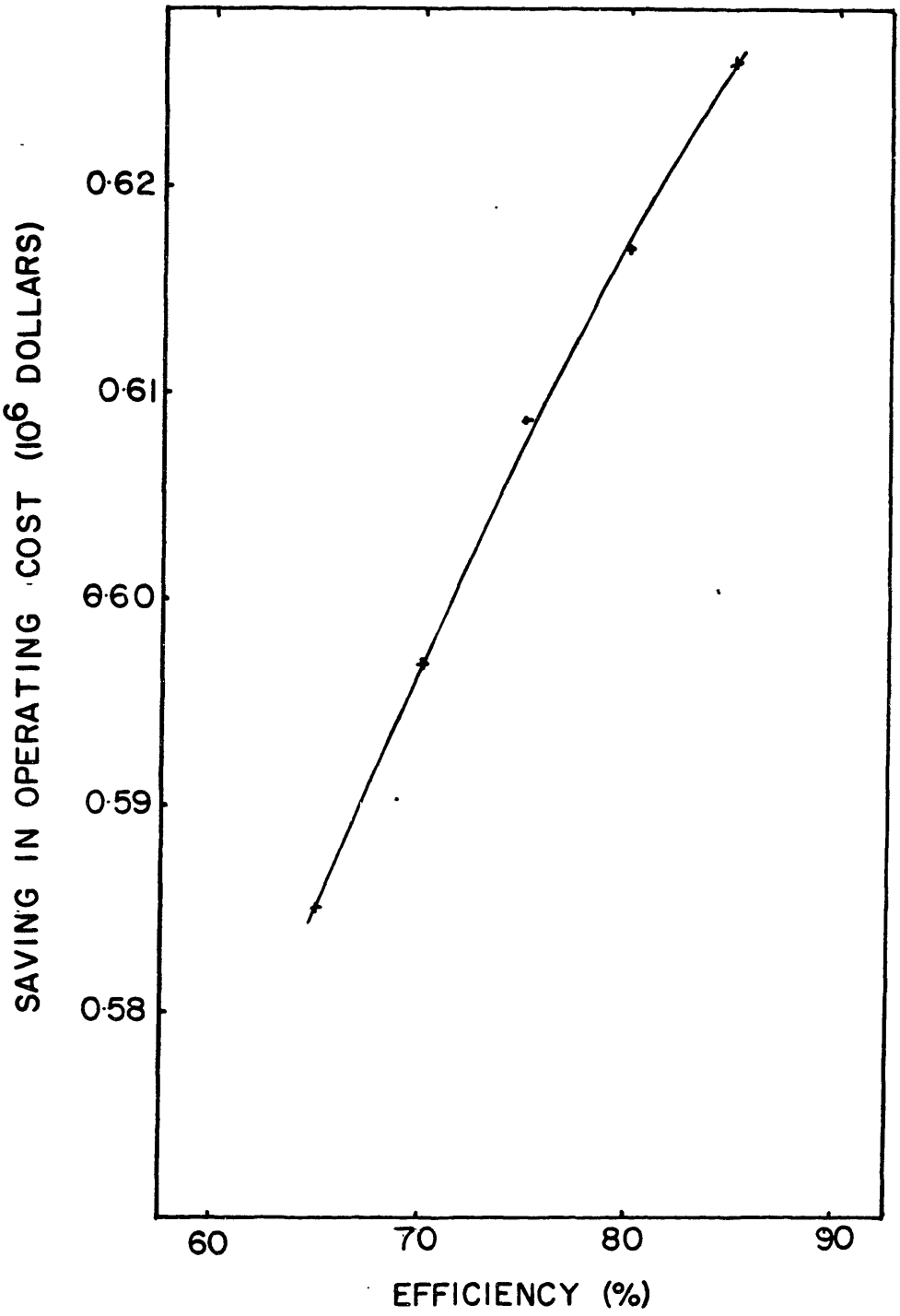


FIG. 4.14 SAVING IN COST FUNCTION VERSUS COLD COMPRESSOR EFFICIENCY FOR OPTIMIZED CYCLES.

Chapter 5

EXPERIMENTS

In this chapter, an experiment to evaluate the performance of a supercritical wet expander is presented together with a summary of results. The increase in the refrigeration capacity of a CTi model 1400 refrigerator as a result of replacing the Joule–Thompson valve with the supercritical wet expander is also reported. The chapter begins with the design of the experimental apparatus.

5.1 Introduction

5.1.1 SVC Program

The preceeding analyses confirm the SVC cycle as an optimal configuration for helium liquefaction systems. It is a more efficient thermodynamic cycle than conventional helium liquefaction cycles for several reasons. The irreversibilities associated with heat transfer through finite heat exchange temperature difference ΔT is reduced because of the better matching of the heat capacity rate values of the two streams. Moreover, the wet expander operates over a higher pressure ratio and thus has a greater refrigeration potential. Further, the cycle high pressure is no longer compromised between the performance of the J-T valve and the expanders: it can therefore be chosen for the best preformance of the expanders.

In addition to the thermodynamic superiority, there is a substantial reduction in the heat exchange area required for the SVC cycle because of the higher heat transfer coefficient available at the higher pressures, and the main (warm end) compressor size is reduced due to the increased suction pressure.

Further , the SVC cycle has a potential application for refrigeration at temperatures below 4.2 K. down to 1.8 K . In this case the cycle pressures may be maintained at the conventional levels and the wet-expander-cold-compressor section used to maintain subatmosphric pressures over the boiling liquid helium. Thus this SVC system will allow the conversion of a standard helium liquefier to a 1.8 K refrigerator without the addition of large low pressure (12 mbar) heat exchangers and large displacement vacuum pumps.

The foregoing impressive catalogue of the benefits associated with the SVC cycle naturally raises the question of implementing a prototype. There are two key additional components required over and above the standard components of the standard unit: the supercritical wet expander and the cold compressor. Although the use of wet expanders has been known to increase the liquefaction rate of helium liquefaction cycles, very little performance data has been documented to establish the efficiency and reliability of wet expanders. The performance of these expanders are still considered questionable even though the M.I.T. Cryogenic Engineering Laboratory has been operating a liquefier with a wet expander with great success for several years.[83] More recently a few large helium liquefaction/refrigeration plants have been built with wet expanders but small systems continue to use J-T valves without variation. The idea of a saturated vapor compressor with a considerable pressure ratio has not been investigated although there has been some experimental work on a "cold" circulating fan.[84]

The development of a prototype SVC cycle therefore involves demonstrating the practicability and reliability of cold compressors and wet expanders. In particular, the possible practically attainable efficiencies of these components are necessary for trade-off decisions on cost- savings versus development cost of these components. The ultimate goal of the SVC liquefaction cycle program at the M.I.T. Cryogenic Engineering Laboratory is to investigate and document the performance of these two components. The immediate goal, the objective of the experimental work for this research is to determine the performance of a wet expander for a fairly small helium liquefaction system. This involves the design and fabrication of an expansion engine operating in the cold

end of the cycle and expanding into the two-phase regime of the working fluid. The expander will be used in place of the J-T valve in a CTi model 1400 helium liquefier.

5.1.2 Turbine Versus Reciprocating Expanders

Both reciprocating and turbine expansion machinery are successfully used in helium liquefaction/refrigeration systems.[95] [96] Traditionally turbo-expanders are used in large plants while reciprocating machines are used in small plants. The dividing area between large and small plants occur in the range of about 100 to 300 liters per hour liquid production rate. These are general trends: both types of machines may be found in the same plant and the dividing area may be extended (for example by using components in parallel). More recently miniature turbo-expanders have been introduced.[99] - [101] There are several considerations that determine which type of expander may be used in a particular application.

Turbine expanders have the advantage of compactness. They can also be totally hermetic, even to mass spectrometer limits. They exhibit low noise and vibration levels. Conceptually, they can be made very reliable. (But this is under rather stringent conditions which are not easily attainable.) They must be well designed and they must meet precise balancing requirements. The stream of gas fed through it must be pure, and the flow throughput must be constant. Conditions of unstable load/supply are difficult to eliminate completely and, in fact, the flexibility of changing the operating mode from liquefier to refrigerator, for example, is a desirable feature of helium liquefaction systems).

There are also limitations to turbine-machinery use. They are capable of peak efficiencies only over a limited range of operating conditions and off-design performance is rather poor, especially if they have fixed nozzles. The use of variable nozzles adds to the complexity of the machine but somewhat broadens the range of acceptable efficiencies about the design point. The practical pressure ratio that may be achieved

in a single stage machine is mach number limited at low temperatures and wheel stress limited at higher temperatures. Disk friction and circulation losses are developed as the turbine wheel spins in the working fluid. These viscous dissipation losses increase with decreasing Reynolds number and hence decreasing size. Similarly the seal leakage and tip clearance losses do not scale proportionally with the size of the machine. Thus for low flows or small machines, the efficiency of the turbo-machine is rather low. Further turbine machines generally handle two-phase flows rather inefficiently.

There are practical constraints on the experiment which dictate the type of expander to be chosen. The wet expander in the SVC cycle operates over a high pressure ratio and also expands into the two-phase region. The estimated flow rate through the expander (based on the capacity of the CTi model 1400 liquefier available for the experiment) is small. The wet expander required is therefore correspondingly small. Because of the high premium on the cold end irreversibilities, it is imperative that the cold end components be highly efficient. Therefore, in the light of the preceeding discussion, the choice of a turbo-machine for the experiment would be inappropriate.

In contrast to the turbo-machine, the principal losses associated with the reciprocating machine are heat transfer losses which may be minimized by proper design. Unlike reciprocating air engines processing two-phase fluid, small quantities of liquid helium remaining in the cycle after the discharge stroke do not degrade the performance of the wet expander significantly because of the large heat capacity ratio of the incoming compressed gas charge to the latent heat of the liquid residue. Further the cylinder wall heat capacity is very low at the low operating temperatures[102] so that the cyclic heat loss is correspondingly low. Finally, noise and vibration levels of the reciprocating expander may be reduced by an appropriate choice of the means of mechanical energy conversion/dissipation. Therefore a reciprocating-type expander is preferred to the turbo-expander for the experiment.

5.2 Expander Design

5.2.1 Historical Evolution of Reciprocating Expanders

The first expansion engine used successfully in cryogenic liquefaction was a judicious adaptation of the steam engine by Georges Claude.[10] By incorporating several ingenious improvements, Claude was able to develop durable and reliable reciprocating expansion engines for cryogenic applications. However these engines used leather cups as piston seals in the cold region with no lubrication. Therefore there was significant friction generated by this seal which reduced the efficiency of the machine.

In order to improve upon the efficiency of the engine, Heylandt[10] increased the length of the piston and cylinder and relocated the seal at the warm end of the arangement. The heat generated by the seal is then discharged into the atmosphere, instead of the cold space, resulting in an improved efficiency.

As the piston length is increased, a slight veritical misalignment causes a lateral force on the piston. This results in rubbing (between piston and cylinder) and hence heat leak into the cold space. Kapitza made use of two universal joints to align the piston in his helium engine built in 1934.[10] He also tried to dispense with the leather seal altogether by reducing the diametral clearance between the piston and cylinder . This required a rapid power stroke to minimize the leakage rate through the clearance volume. The use of a hydraulic work-absorbing mechanism instead of the conventional crankshaft arrangement enabled speeds of about 120 strokes per minute to be achieved. In order to prevent piston seizure small grooves 0.010" deep and 0.010" wide at distances of about 0.25" were cut around the circumference of the piston. The grooves helped to equalize the pressure around the piston and thus prevent hydrodynamic side loads which cause rubbing and seizure.

The real break through in the use of expanders below 20K was the Collins' flexible-

rod expansion engine.[10] This incorporated several innovative designs. The engine has a single acting cylinder with the piston rod passing through the expansion space, contrary to conventional designs. The piston is mostly in tension and all forces are colinear in the low temperature region, enabling the use of thin and slender rods by promoting elastic stability in the thin cross-section. The use of thin cross-section rods drastically reduces conduction losses associated with the piston. Further the piston–rod can be long and hence the piston can be self-aligning: therefore frictional forces developed between the piston and cylinder are minimal.

The flex-rod engine uses cold clearance seals: the annular gap between the piston and cylinder is approximately 0.0002" for a 1" diameter piston. The piston and cylinder were first made of hard nitrided alloy steel that will not gall and were closely fitted together by successively lapping and fitting until they fit together when cold. The principal problems associated with such restricted tolerances are: the generation of friction by solid air or carbon dioxide in the annular space; impurities, like iron filings or even dirt particles which tend to lock the piston; and warping of the cylinder due to improper fitting of the cylinder head causes rubbing and the associated heat generation. An alternative arrangement which has been very successful uses the good wear characteristics of micarta: a steel piston is fitted with a micarta sleeve; and the cylinder is made of chromium plated bronze. The bronze was chosen to match the thermal expansion characteristics of the micarta-steel piston assembly.

The pioneering effort of these and other early workers has provided the general framework for designing fairly efficient reciprocating engines and these improvements are taken into consideration in the design. Recent advances, especially in heat transfer analysis and experimentation[103 - 105], have enhanced our understanding of the losses associated with the expander and analytical models of varying sophistication and adequacy are now available for the losses. The losses may be grouped, generally, into those affecting the power and those directly manifesting themselves as heat leaks to the working fluid.

Power Losses

Valve Flow Losses. These occur when the flow through the valves causes the cylinder pressure to be different from the inlet or exhaust pressure.

Leakage Losses. These are losses associated with gas leaking past the piston seals.

Mechanical Friction Losses. Rubbing between the piston and cylinder may occur generating heat which is dumped into the cold space. Also the piston seals may generate some heat but for warm end seals this heat is dumped into the atmosphere and does not detract from the refrigeration capacity of the engine.

Blow Down Losses. These occur when the gas pressure inside the cylinder is higher than the exhaust pressure when the exhaust valve opens.

Blow In Losses. This is similar to the blow down losses and occurs when the gas pressure in the clearance vlolume is lower than the inlet pressure when the inlet valve opens.

Cyclic Heat Transfer Loss. This is the result of periodic heating and cooling of the working gas by the cylinder walls. The incoming gas is warmer than the cylinder walls and is therefore cooled while the cold gas after the expansion process is warmed by the walls. The net effect is that the expander processes more gas without a corresponding increase in expander work per stroke.

Heat Input Losses

Static Heat Leak. This includes the thermal conduction from the hot sections to the cold parts of the engines as a result of a steady state temperature gradient along the cylinder wall, piston, valve pull rods, valve sheaths etc.; and the radiation of heat to the cold parts.

Shuttle Heat Transfer Loss. This is a mechanism for transporting heat from the

warm atmosphere to the cold parts as a result of relative motion between the piston and cylinder. Both have axial temperature gradients. At top dead center, there is heat transfer from the hot, upper part of the cylinder wall to the piston wall. At bottom dead center, this heat is transferred back to the cylinder wall. Thus the heat flux is transported along the cylinder a distance equal to the stroke of the engine during every cycle until it is finally rejected into the coldest part of the cylinder.

Cylinder-Piston Gap Pumping Loss. This is caused by the periodic flow in the gap between the piston and cylinder wall as the working space is alternately pressurized and depressurezed. The loss is due to the flow resistance to the gas motion and heat transfer between the flowing gas and the walls which causes a temperature difference between the gas which goes in and the gas which comes out of the gap. Thus there is a net enthalpy flux discharged into the cold gas. Further, the flow from the cold to the warm end is induced by the increase in pressure which in turn produces an increase in gas temperature due to adiabatic compression. This is the pulse-tube effect and it reduces the heat transfer required to bring the gas to the local gap-wall temperature.

Estimates of most of these losses are incorporated in the design to determine the expander parameters.

5.2.2 General Description of Expander

The reciprocating expansion engine, shown in the photographs (Plate 1), consists of a long tubular cylinder which hangs from a base plate–the top plate of the vacuum chamber(not shown). Above the base plate is a programmable hydraulic–pneumatic system for piston motion and valve control. The valves stick out from below the cylinder. A single two–channel co–axial transfer tube interconnects the expansion engine and the CTi liquefier. Surge chambers are located at the inlet and discharge ends of the expan-

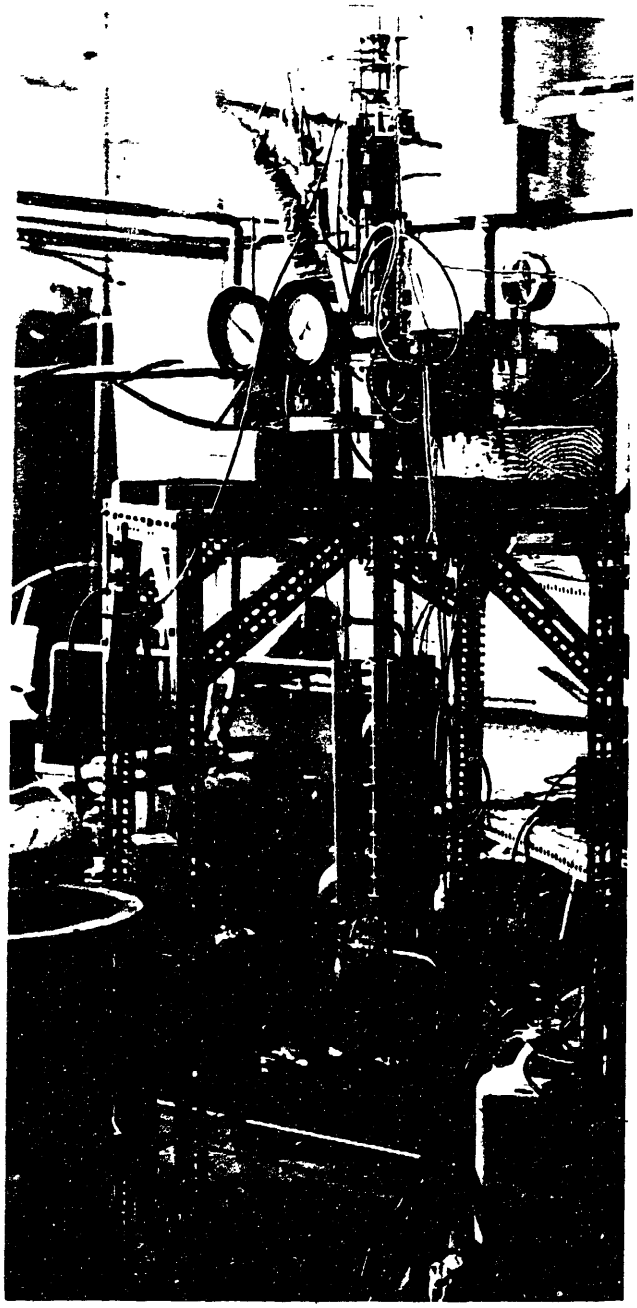


PLATE 1A EXPOSED ENGINE WITH CONTROL MECHANISM.

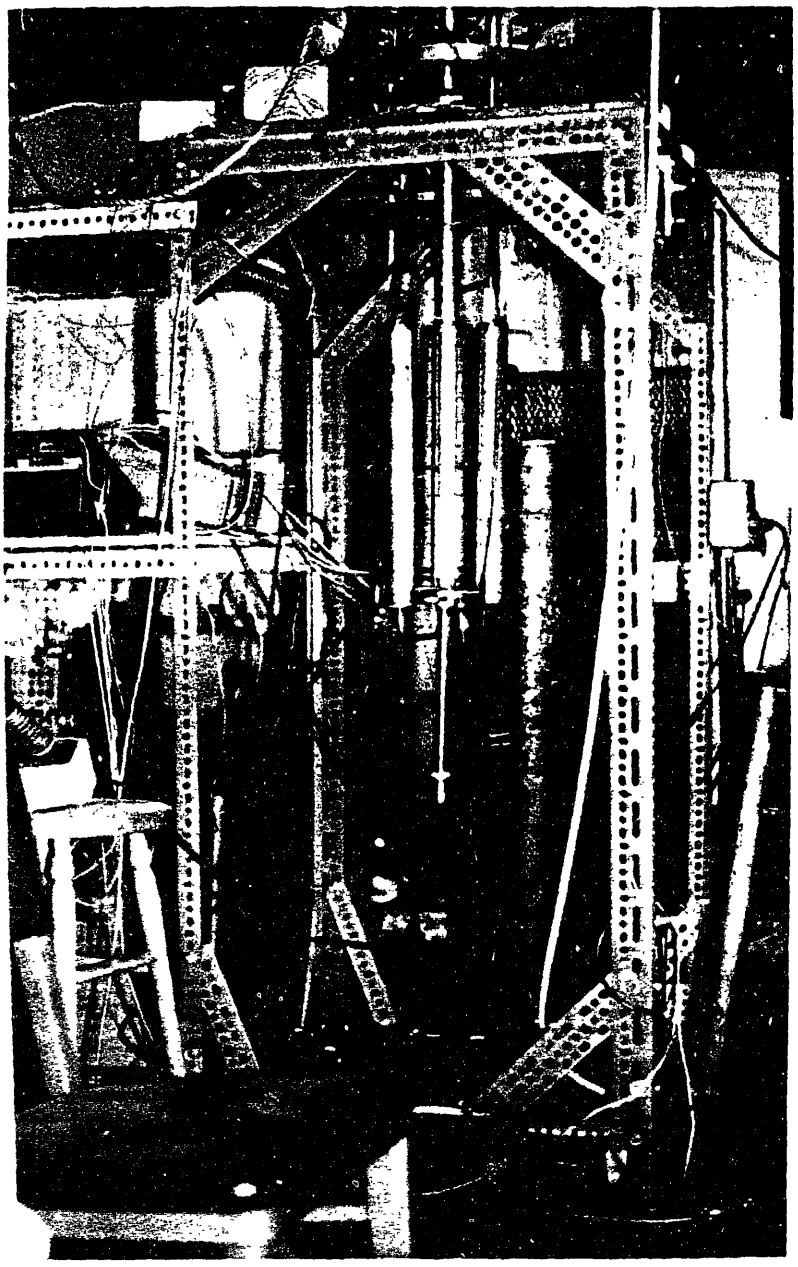


PLATE 1B EXPOSED ENGINE WITH VACUUM JACKET IN THE BACKGROUND.

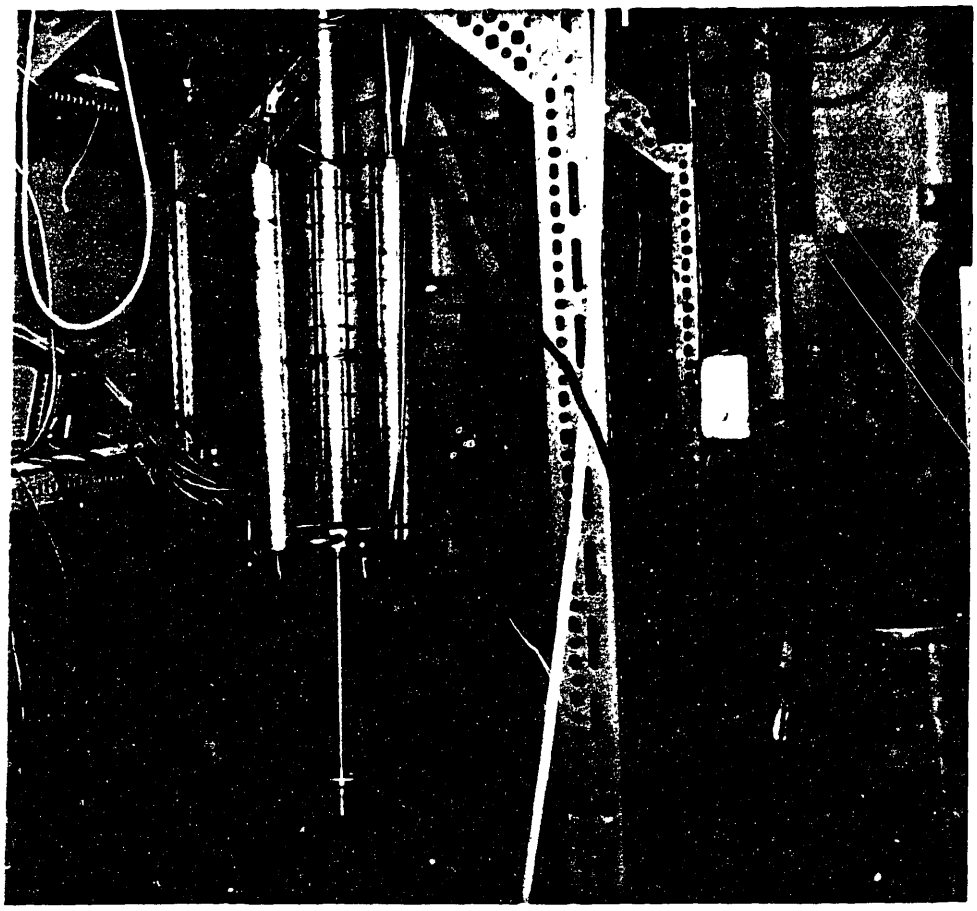


PLATE 1C CLOSE-UP OF ENGINE.

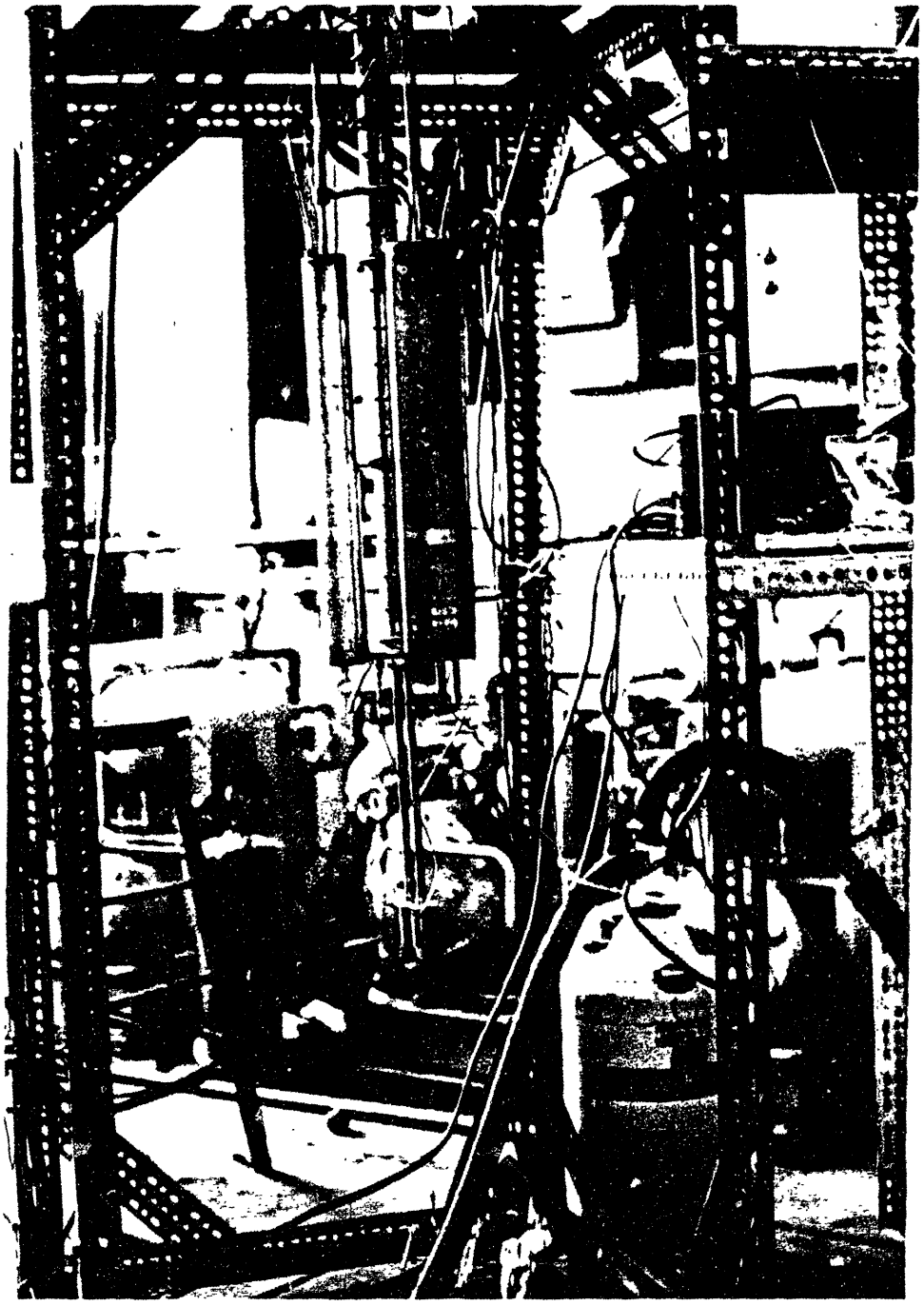


PLATE 1D ANOTHER CLOSE-UP VIEW OF THE ENGINE .

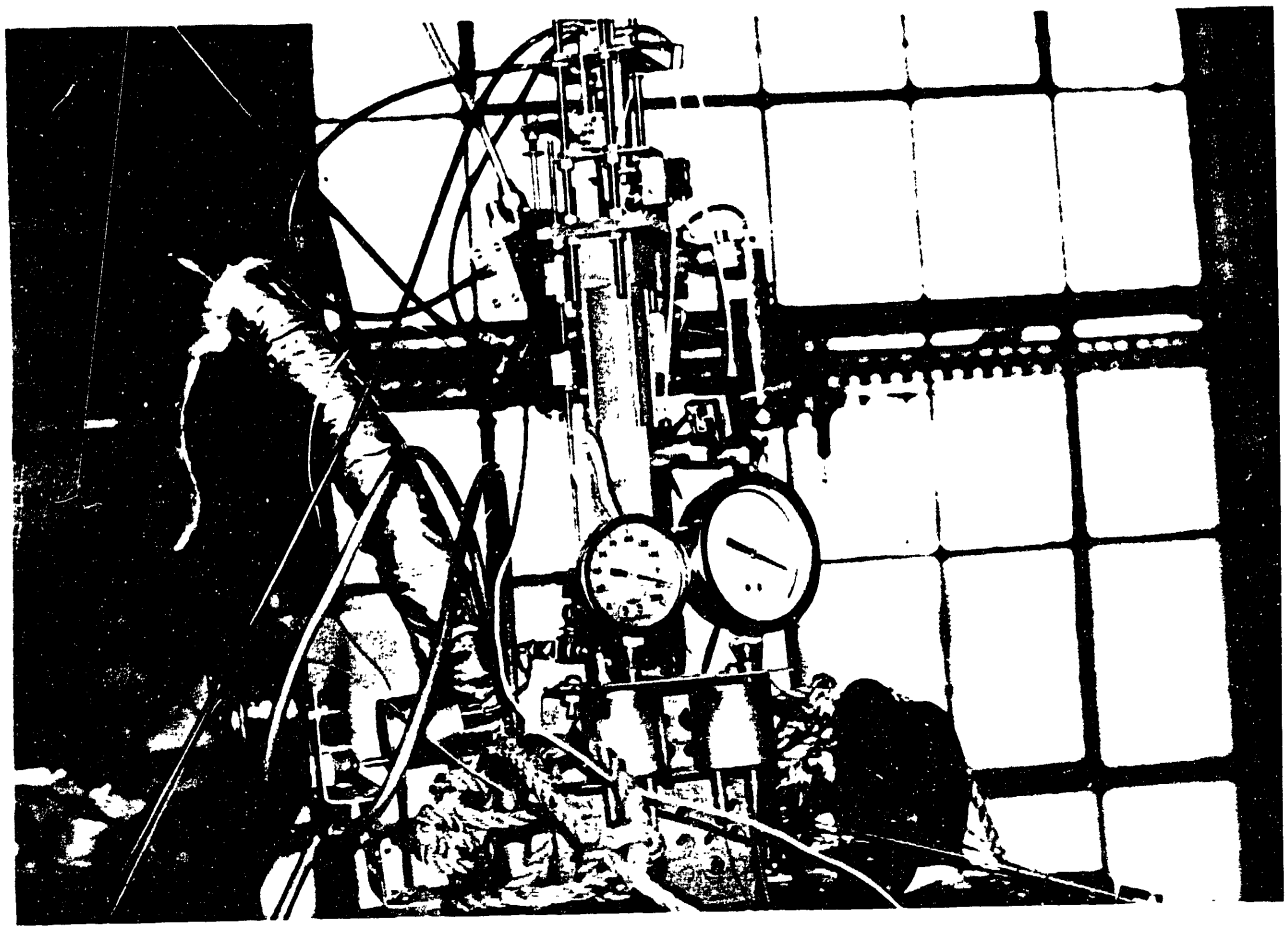


PLATE 1E PISTON MOTION CONTROL MECHANISM.

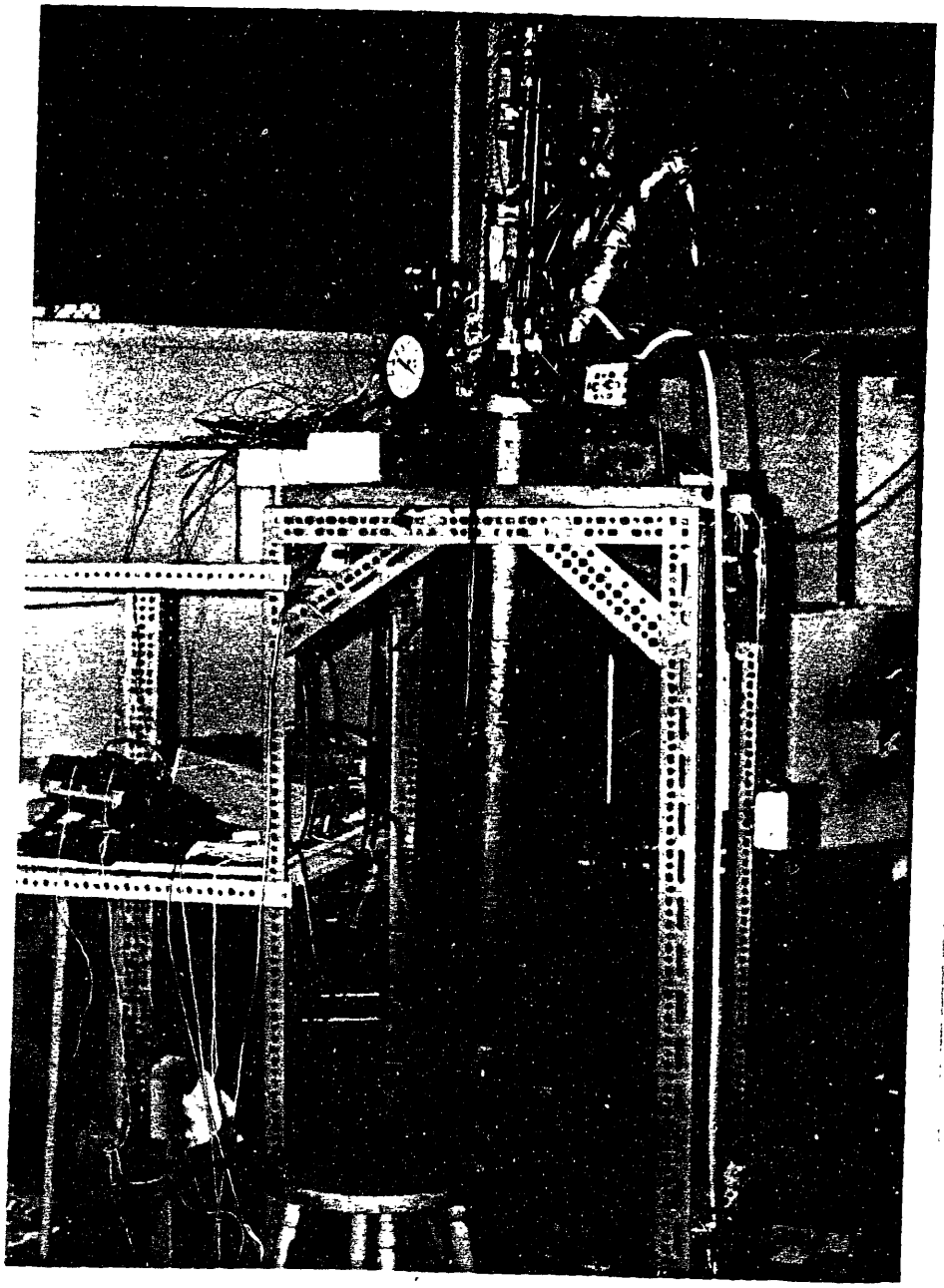


PLATE 1F ENGINE WITH VACUUM JACKET BEING MOUNTED.

sion engine and a heater tank is located after the discharge tank. Detailed description of these components follow.

Displacer-Cylinder: The cylinder is made of stainless steel 304 because of its low thermal conductivity, high strength, low specific heat capacity and lack of brittleness at low temperatures. The high strength tubing with a long thin wall tubing (0.020 inches wall thickness) and a low thermal conductivity reduces the conduction loss. Stiffening rings spaced 1 1/ 2 inches apart around the outside diameter keep the tubing round. The thin wall tubing is TIG welded to the valve block (cylinder head containing the valve ports) at one end and a thick wall tubing at the warm end used for mounting the engine. A solid micarta rod stock, F, (Fig. 5.2.1) is used for the displacer because of its good wear characteristics. Also the thermal contraction characteristics closely match those of the stainless steel. The diametral clearance between the piston and cylinder is 0.006 inches and is chosen by consideration of the shuttle heat transfer loss, the possibility of seizure due to small solid impurities and the possibility of displacer- cylinder contact.

Sealing:(Fig. 5.2.1) The engine uses a single buna O-ring seal E at the warm end of the displacer-cylinder assembly. An oily felt washer D provides 'continuous' lubrication for the O-ring. Thus there is minimal wear which reduces the possibility of wear material contamination. Also the small frictional heat generated is dumped into the atmosphere and does not detract from the cooling power of the engine.

Alignment: (Fig. 5.2.1) The radial clearance on the 33 inch-long displacer F is 0.003 inch. Therefore only 0.005 degree misalignment is required to cause displacer-cylinder contact. To ensure that the alignment stays within the tolerance provided, the displacer-cylinder assembly is mounted vertically. In a horizontal orientation, the effect of gravity would force the displacer into contact with the cylinder causing wear and rubbing . To maintain the displacer in vertical alignment, it is

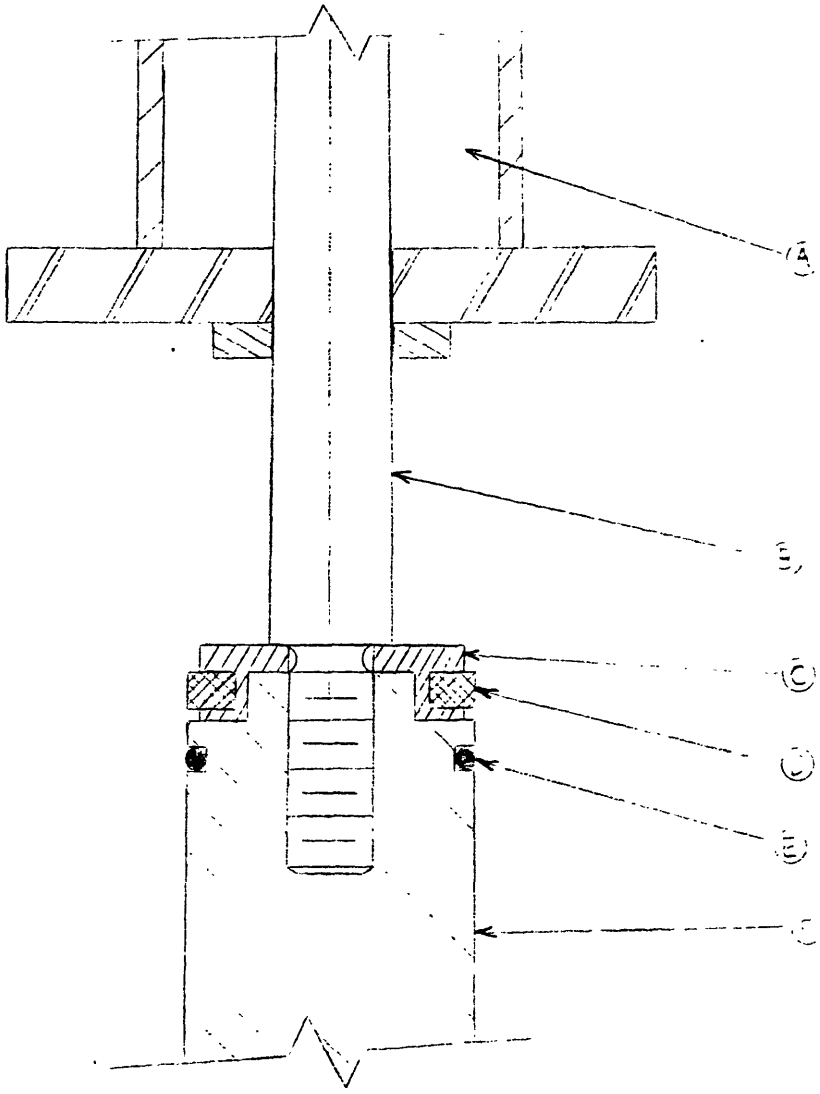


FIG. 5.2.1 DISPLACER-PISTON ROD CONNECTION SHOWING ENGINE SEALS.

rigidly connected to the piston rod B of a tandem cylinder assembly A for the drive mechanism. (The threaded end of the piston is connected to the displacer through a helicoil insert). The tandem cylinder has four rod seals and two piston seals. Therefore the integral unit consisting of the tandem piston rod and the engine displacer ride on a total of seven supports of close tolerances. By proper initial positioning, the unit can be maintained reasonably well aligned in the vertical. The axes of the engine cylinder and the tandem cylinder are also colinear. This alignment is achieved through a copper alignment piece C (Fig.5.2.2) which fits inside the engine cylinder E and outside the bushing B at the end of the tandem cylinder.

Mounting: (Fig. 5.2.2) In order to reduce heat transfer losses associated with convection currents, the engine employs vacuum insulation. Also in order to allow for thermal contraction during cooldown, at least one end of the engine must be free. Consequently the warm end of the cylinder is rigidly supported on a base plate (the top plate of the vacuum chamber) and the cold finger hangs into the inner part of the vacuum chamber. The warm end of the cylinder E is made up of 1/4 inch wall stainless steel which enabled an 1/8 inch deep and 1/8 inch wide groove to be cut in it. A tight fitting split ring, G, 1/4 inch wide fits into the groove and is firmly secured on the top surface of the base plate H by a bracket F that supports the tandem cylinder A.

Valves: (Fig. 5.2.3) Throttling in the valves degrade the performance of the engine. Therefore the valve port size is a prime consideration in the valve design. The valve ports are located at the closed end of the cylinder rather than the side of the cylinder. This allows a reasonably large-size ports for the engine which together with a slow engine speed substantially reduce the throttling effects. This port location also helps to reduce the residual liquid that might remain in the clearance volume. The ports are 1/4 inch holes drilled through the valve block A which also serves as the cylinder head and is TIG welded to the tubular part F of

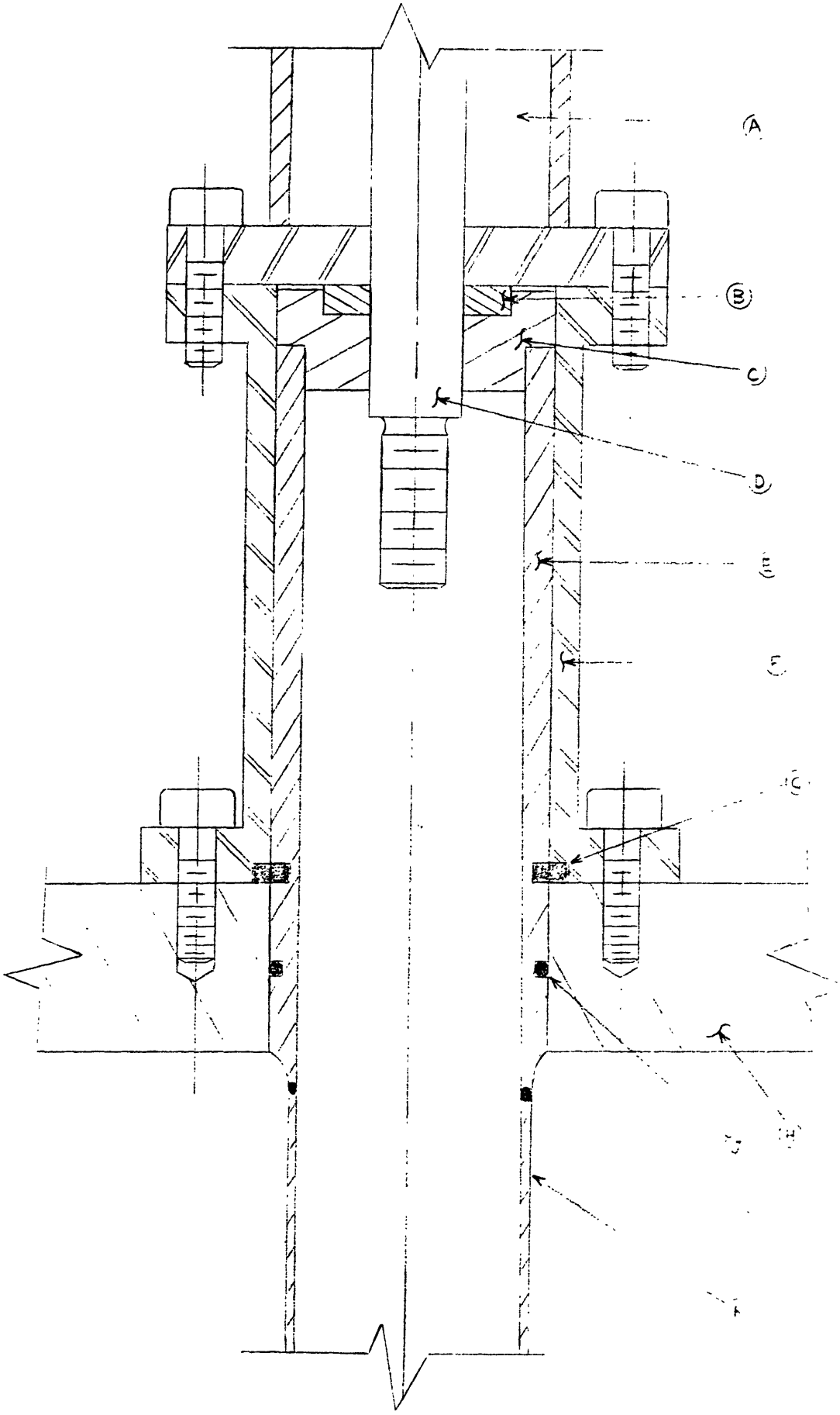


FIG. 5.2.2 CYLINDER MOUNTING

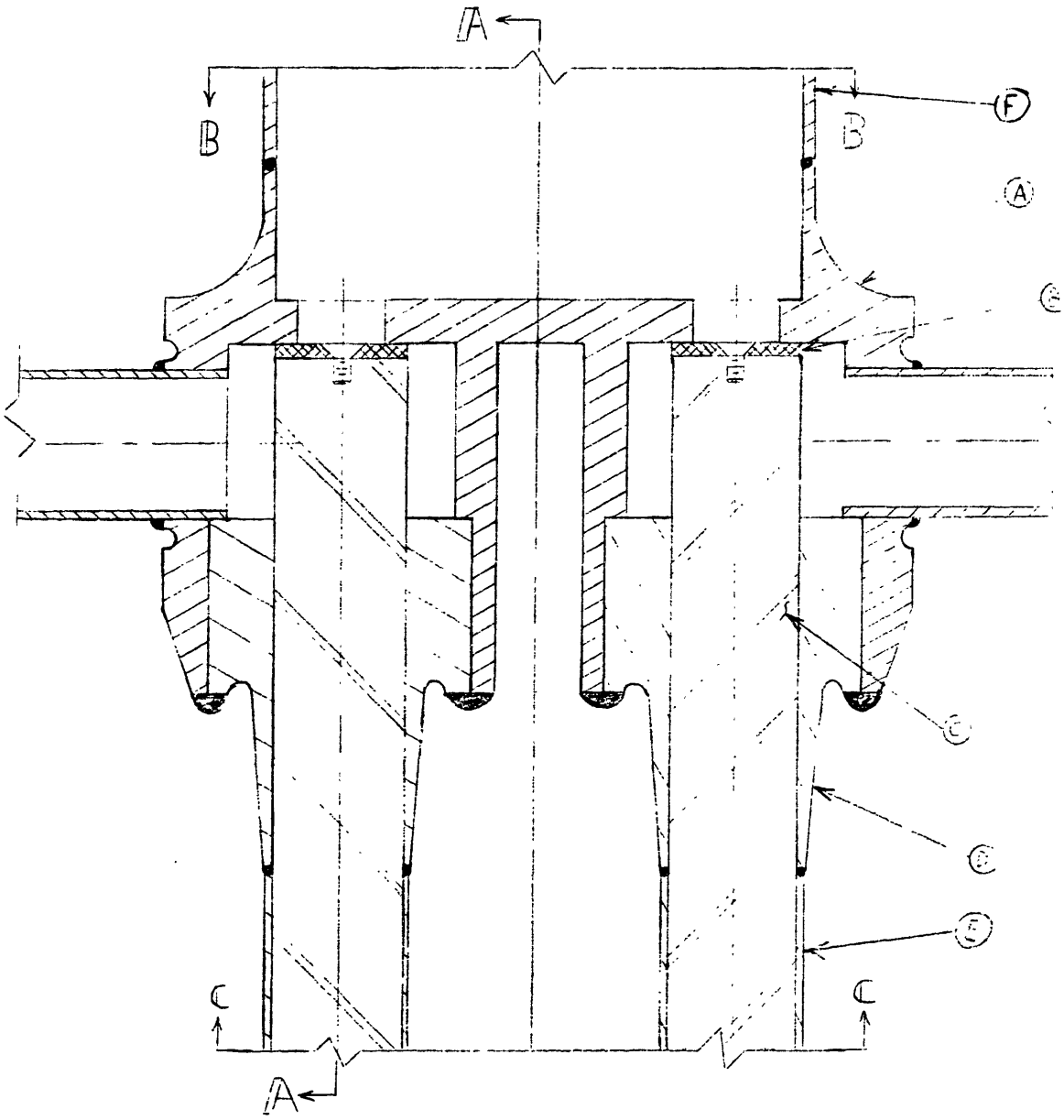


FIG. 5.2.3(a) VALVE BLOCK

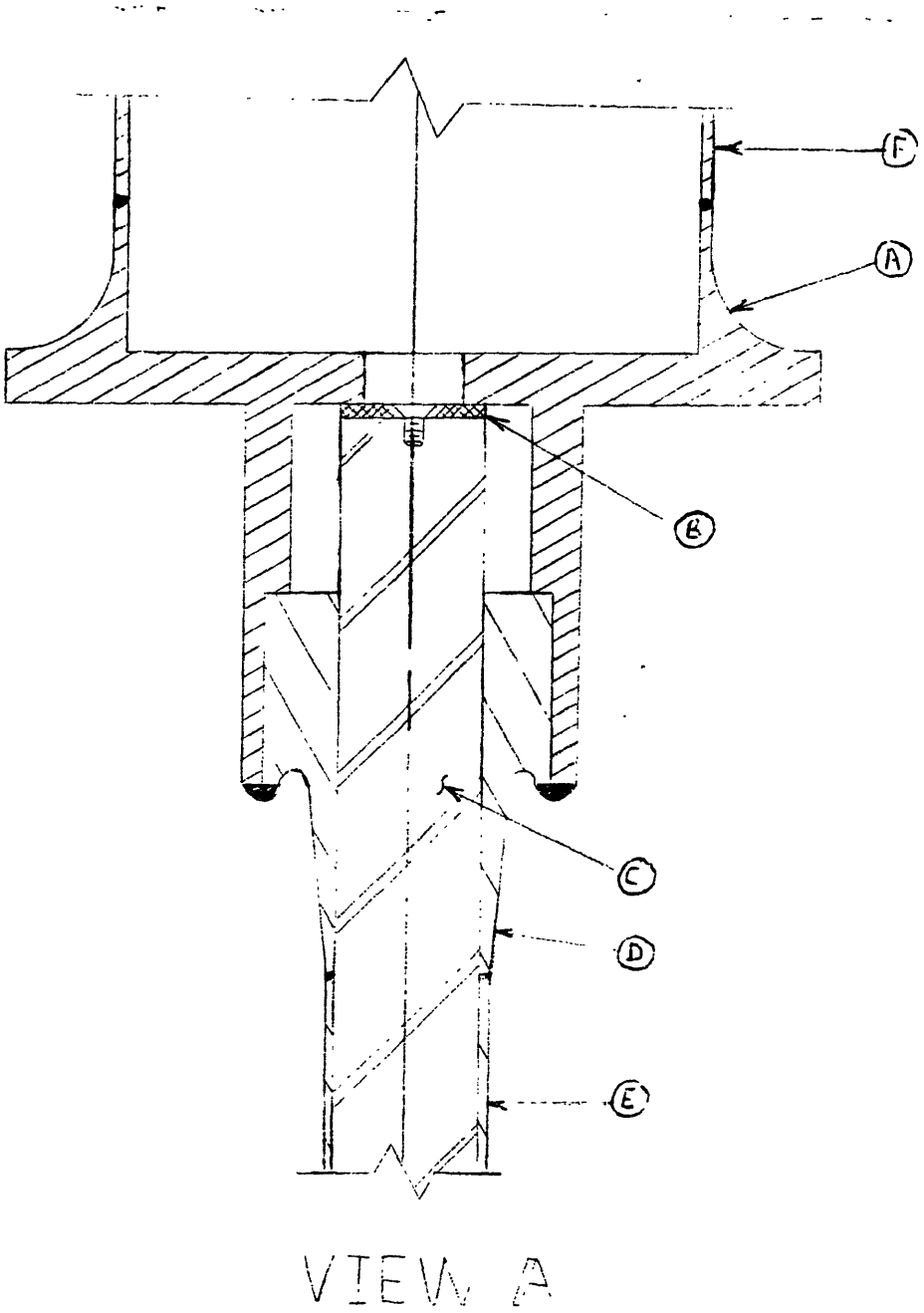


FIG. 5.2.3(b) VIEW A OF VALVE BLOCK.

the cylinder. Tubular sheaths F of 304 stainless steel are also welded to the valve block and stick out from the bottom side of the engine. These tubular sheaths enclose the valve pull-rods,C. The teflon valve seal disk is mounted on the cold end of the micarta pull-rod with a screw and is locked with a belleville washer. The valves open outward against strong springs of a miniature air cylinder. A buna O-ring serves as the warm end seal on the valve rod which fits closely into the stainless steel tubular sheath. Because of the rather short travel of the pull rods, no lubrication is provided for the O-ring . Also no extra piece is required to keep the pull rod centered over the valve port because the annular gap between the pull rod and sheath is small (0.003 inch) on the diameter.

Hydraulic-Pneumatic Piston Motion Control System

The overall schematic for the control system is shown in Fig. 5.2.4. Air limit switches feedback signals into the programmable air controller at various points in the cycle. Signals to sequentially operate directional air valves and a 3- way hydraulic valve are fed out of the programmable air controller. Also signals from the programmable hydraulic controller to control the speed of the piston, are fed to the hydraulic ports of the tandem cylinder.

Hydraulic Controller. The purpose of the hydraulic controller is two-fold: to absorb the expander work; and to maintain three different speeds during the discharge stroke, the intake (charging) part of the power stroke and during the expansion stroke. The expander work is dissipated in resistive elements in the fluid flow circuit which dissipate energy ($\int vdp$.), analogous to the I^2R heating in electrical circuits.

The principal components of the hydraulic controller are three adjustable flow control valves A,B,C and a three-way hydraulic valve E (Fig. 5.2.5). The three- way valve is a two-position. single air piloted, spring return valve. The oil supply through this valve is either through valve A when there is air pressure at the

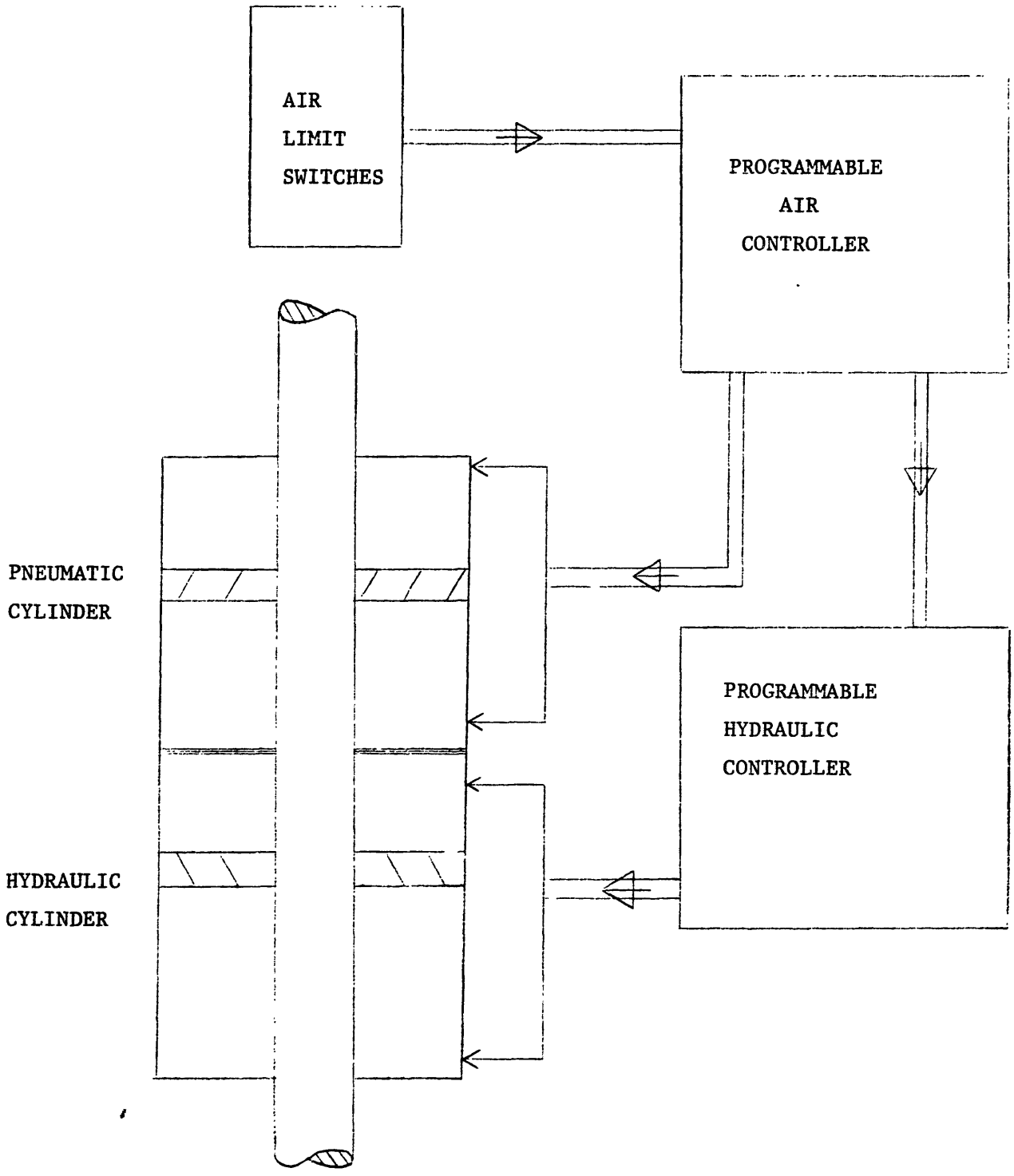


FIG. 5.2.4(a) OVERALL LAYOUT OF PISTON MOTION CONTROL SYSTEM.

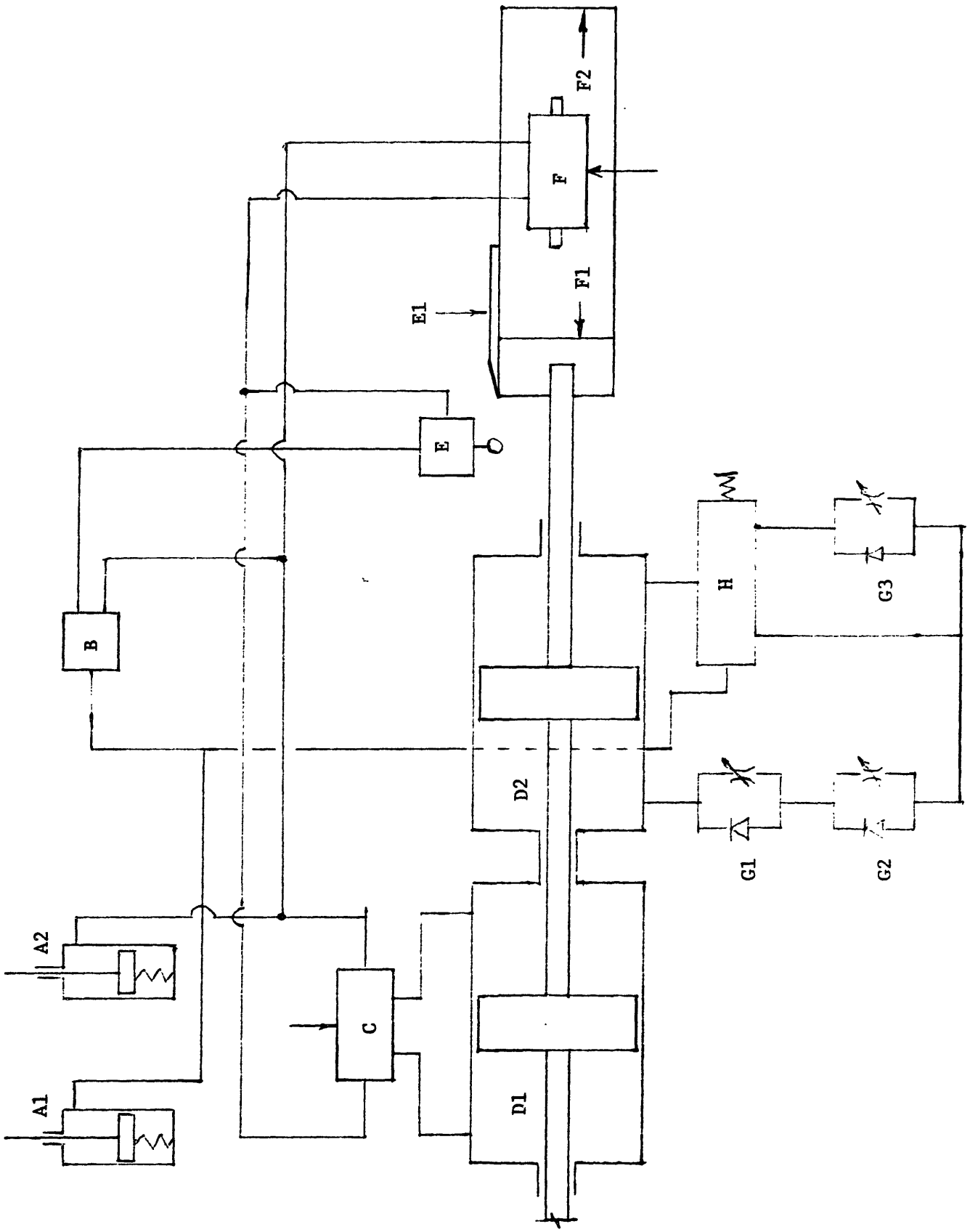


FIG. 5.2.4 (b) OVERALL SCHEMATIC OF PISTON MOTION CONTROL SYSTEM

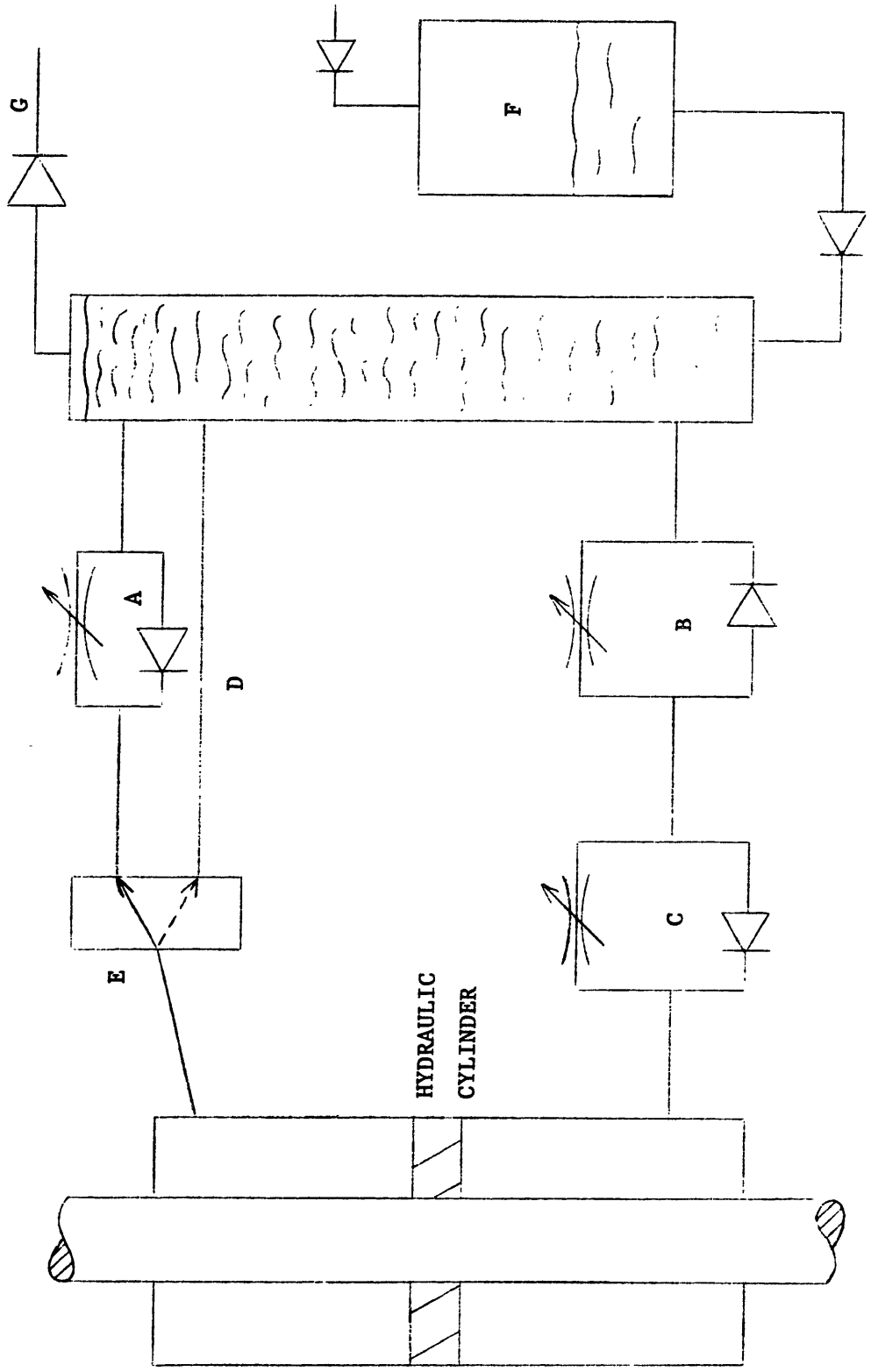


FIG. 5.2.5 HYDRAULIC CONTROLLER (NOT TO SCALE).

pilot, or through line D when there is no air pressure (spring return mode).

The adjustable flow control valve is a needle and check valve combination which allows flow control in one direction and full flow in the other. Valves A and B restrict flow in the same direction (during the power stroke) while valve C restricts flow in the other direction (during the discharge stroke). Therefore the setting on valve C determines the engine speed during the discharge stroke. Valve A is by-passed during this stroke. During the charging stroke, air pressure at the three-way valve E switches the oil input to valve A which has metered flow together with valve B. The valve setting on these two valves therefore determine the piston speed during the charging process. Finally, at cut off, air pressure is released on the three-way valve and the spring returns the oil input to line D. Valve A is now by-passed. There is full flow in valve C and metered flow in valve B which consequently determines the piston speed during the expansion process.

A bleedline G is provided for the hydraulic circuit. Also an oil reservoir under air pressure F is provided which maintains the oil under pressure throughout the cycle. This eliminates the possibility of air leaks into the hydraulic ciruit which degrades the performance of the engine. The effectiveness of the arrangement is reflected in the smooth operation of the piston in marked contrast to the rapid piston motion as it changes direction which characterised operation with air in the hydraulic circuit. The tank also provides additional capacitance to the hydraulic circuit.

Air Limit Switches: The heart of the air limit switch system is a miniature double-plunger two-position fully ported four-way spool valve D (Fig. 5.2.6). The valve is supported by a pair of stainless steel plates (not shown) mounted on four threaded rods connected to the top flange of the tandem-cylinder assembly. The free end of the piston rod (of the control circuit) G is threaded into a small brass block F with an actuating surface E to actuate the plunger at top dead center.

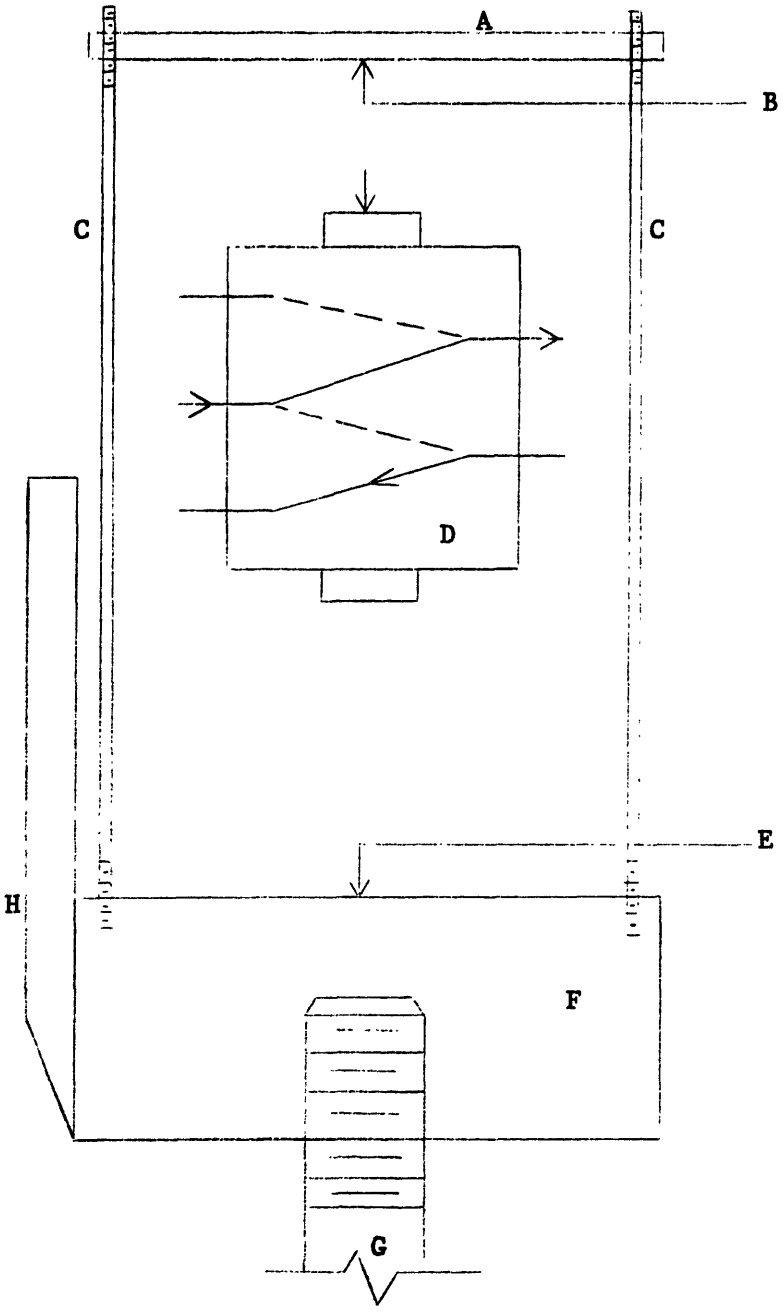


FIG. 5.2.6 LAYOUT OF LIMIT SWITCH ARRANGEMENT (NOT TO SCALE).

A thin steel plate A fastened to two threaded rods C projecting from the brass block act as the other plunger actuator at bottom dead center. The stroke of the machine is adjusted by adjusting the vertical position of the four-way valve as well as the BDC acutuator. The threaded-rod -nut mounting for these parts facilitate easy and fine adjustment of the stroke.

Cut -Off Switch: (Fig.5.2.7) The cut-off switch sends a signal to the pneumatic control at the end of the intake process. It is a heavy duty miniature air limt switch. It is a two-position, plunger-actuated, normally closed valve. The integral plunger actuator B is a pivoted lever D with a roller E , supported on ball bearings, at the free end. During the intake process. the roller rides on a cam H (Fig.5.2.6) silver-soldered to the brass block at the free end of the piston rod. This depresses the plunger and opens the valve. The valve is supplied with air pressure only during the power stroke.

The output signal from this switch is used as pilot for the expander inlet valve which remains open only during the charging process; and the three-way hydraulic valve which directs oil flow through the intake process speed control valve A Fig. 5.2.5

The cut-off switch is rigidly fastened to threaded rods projecting form the control cylinder. The position of the switch determines the cut-off point on the power stroke. This is easily changed by adjusting the set of nuts on the threaded rods used for mounting the switch.

Pneumatic Controller and Stroker: There are two principal components of the pneumatic controller: a directional valve Fig. 5.2.9 and a NOT element Fig. 5.2.8 The directional valve provides compressed air to drive pneumatic driver piston (and hence the engine displacer). It is a heavy duty two-position double air piloted fully ported four-way spool valve. Signals to sequentially operate the valve are fed out of the limit switches to the pilot ports. The two valve positions facilitate

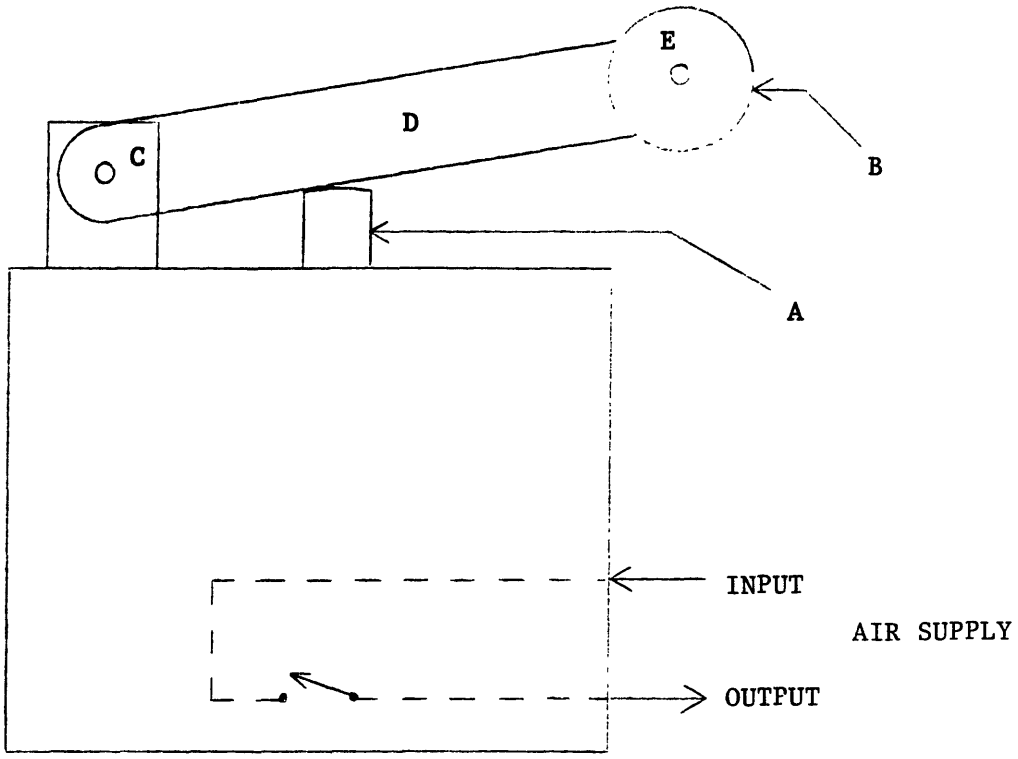


FIG. 5.2.7 CUT-OFF SWITCH (NOT TO SCALE).

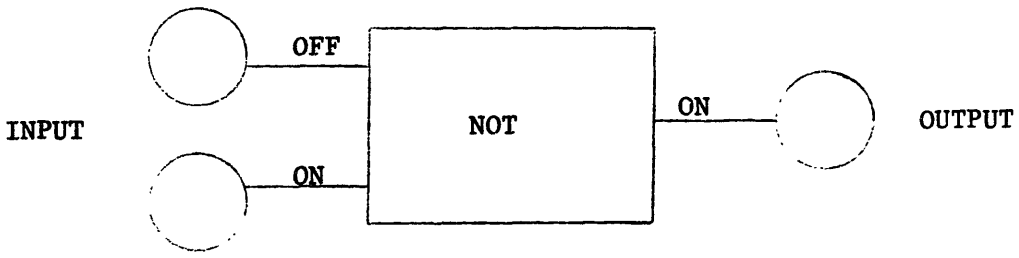


FIG. 5.2.8 NOT ELEMENT

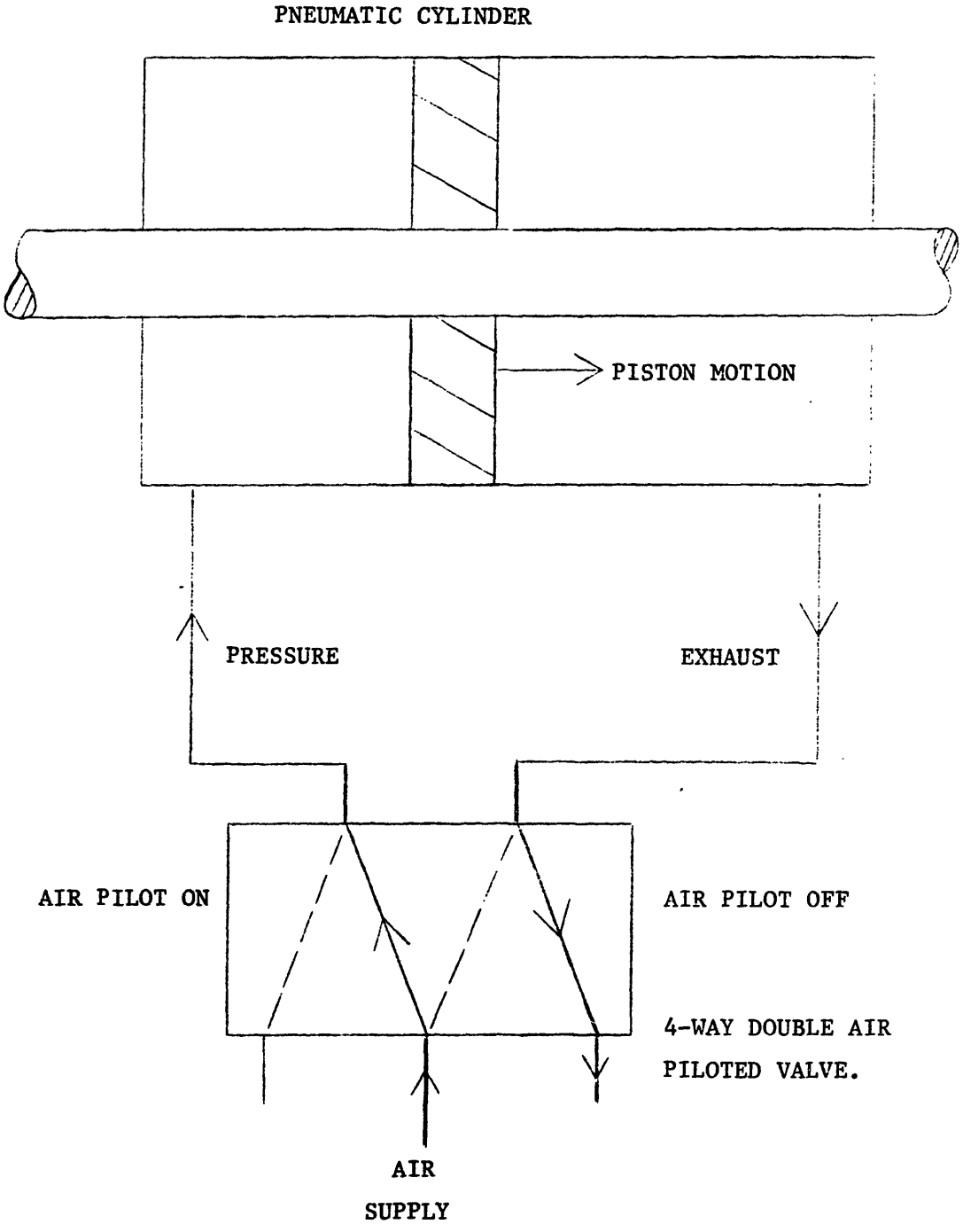


FIG. 5.2.9 DIRECTIONAL VALVE (NOT TO SCALE).

piston motion in one of two directions at a time by maintaining air pressure in one port while exhausting the other port. The two output ports are connected to the two sides of a double-acting pneumatic cylinder therefore pressurising one port while exhausting the other results in a net force on the piston rod which causes the motion. Thus the pneumatic driver can drive the piston even when no cold helium is being processed by the expander. This feature allows a later adaptation of the expander as a compressor. Exhaust ports provided on the valve result in fast system response.

The purpose of the NOT element is to provide the signals to open the engine inlet valve at the end of the discharge stroke, after the discharge valve has been closed and to close the inlet valve at the cut-off point of the power stroke. There are two input signals to this element: a signal from the cut-off switch to input port 2 and another from the TDC limit switch to input port 1. The output pressure signal at port 3 is on if there is pressure at input 2 and if there is no pressure at input port 1. Consequently, there is an output pressure signal only during the charging process–after the discharge valve is closed and until the piston moves up to the cut-off set point.

5.2.3 Expander Sizing

Bore/Stroke: The sizing of the bore and stroke of the expander is based on the following estimated values and assumptions.

1. Expander inlet condition: P_{in} = 11 atm, T_{in} = 6.5 K
2. Piston Speed = 60 Strokes/Minute
3. Bore-to-stroke ratio = 50%
4. Refrigeration capacity at 1.2 atm (4.5 K) = 72 W. (This is the refrigeration produced by the CTi 1400 liquefier using two compressors and LN_2 precool-

ing. Since the experimental plan is to use one compressor, the design specification resulting from this assumption should be an upper bound).

5. The refrigeration is produced by the latent heat of vaporization.

From 4 and 5, the mass flow rate is estimated to be 3.76 g/s.

The isentropic expansion line from the expander inlet condition intersects the saturated liquid curve at the release pressure $P_r = 1.91$ atm. The saturated liquid density at this release point ρ_r implies a cut-off volume ratio $\rho_{in}/\rho_r = .80$. Also the release point density and the estimated mass flow rate M and the cycle time T give the displacement volume

$$\begin{aligned} V &= MT/\rho_r \\ &= \frac{\pi d^2 L_s}{4} \\ &= 4.5\,\text{in}^3 \end{aligned} \tag{5.16}$$

giving

Expander bore $d = 1.42$ in.

Expander stroke $L_s = 2.84$ in.

where subscript in denotes expander inlet condition and subscript r denotes release point condition. Based on these results, a bore of 1.5" and a variable stroke of up to 3" are chosen.

Length: The length of the displacer is determined from heat transfer consideration. Vacuum insulation is employed to minimize heat transfer loss due to convection. Layers of superinsulation wound around the engine together with a radiation shield positioned between the cold parts and the vacuum jacket drastically reduce the radiant energy loss. The displacer length is then determined from thermal conduction loss considerations.

The Fourier's law for conduction heat transfer is given by

$$\left(\frac{q}{A}\right) dx = k dT$$

at steady state, q = constant. Hence integrating

$$L = \frac{A(F_{Tw} - F_{Tc})}{q} = \frac{\epsilon}{q}$$

where

$$F_T = \int_{T_o} k dT$$

A = constant cross-sectional area

q = heat flux

Table 5.1 gives values of q and L for the piston and cylinder. The room temperature value of the thermal conductivity for micarta is used for lack of low temperature values.

An approximate estimate of the shuttle heat transfer loss is obtained using the equation derived by Rios[105] for thin walls and assuming sinusoidal displacer motion:

$$q_{shuttle} = \frac{1}{4}\left(\frac{s}{l}\right)\left(\frac{d}{\delta}\right)\left(\frac{1}{1+\sigma}\right) k_g s \Delta T \qquad (5.17)$$

where

s = stroke

L = dispacer length

d = displacer diameter

δ = radial clearance

k_g = thermal conductivity of the gas

ΔT = temperature difference between warm seal and cold space.

$\sigma = (\frac{d}{\delta})(\frac{k_g s}{d J})(\frac{1}{(\rho C t)_{piston}} + \frac{1}{(\rho C t)_{cyl}})$

C = specific heat capacity of solid

t = wall thickness

ρ = density

J = circular frequency

substitution gives:

σ = 0.00128 (dimensionless)

$q = 18.72/L$ W

The shuttle heat transfer loss is shown with the conduction losses on Table 5.1.

Table 5.1

Heat loss as function of displacer length.

L (in)	q_{cyl} (W)	q_{piston} (W)	$q_{shuttle}$ (W)	q_{total}(W)
L	6.92/L	4.123/L	18.72/L	29.76/L
3	2.30	1.38	6.24	9.92
15	0.46	0.28	1.25	1.98
30	0.23	0.14	0.62	0.99
45	0.15	0.092	0.42	0.66
60	0.115	0.069	0.312	0.50

The estimated reversible enthalpy drop across the expander = 33 W

For L = 36", the conduction and shuttle heat loss together is 2.5% of this estimated enthalpy drop which appears reasonable. Therefore an expander length of 36" is chosen.

5.3 Experimental Procedure

Objective. Two objectives are addressed in the experimental work. In the context of investigating the feasibility of implementing the SVC cycle, the principal goal of the experiment is to evaluate the performance of the wet expander. This is in view of the inadequate documentation of the performance of wet expanders. As a secondary objective, the effect of the wet expander on the overall cycle performance is also investigated.

Experimental Setup: In order to measure the refrigeration capacity of the liquefier operating with the expansion engine, an apparatus to simulate a heat load is required. A tank with a resistance heating element to simulate the heat load is connected to the discharge end of the expansion engine (Fig. 5.3).

To simplify the experimental apparatus, the same vacuum jacket encloses both the engine and the heater tank. A single two-channel coaxial transfer tube interconnects the model 1400 liquefier and the expander. The high pressure gas from the liquefier flows through the innermost tube of the transfer line. This tube is made of 304 stainless steel and is TIG welded to a surge tank which feeds the intake port of the engine with a uniform stream. Another surge tank is located at the discharge end of the engine to convert the pulsatile flow from the engine to a relatively smooth and continuous flow to the heater tank connected to it. All interconnecting tubing are made of 3/8 " OD

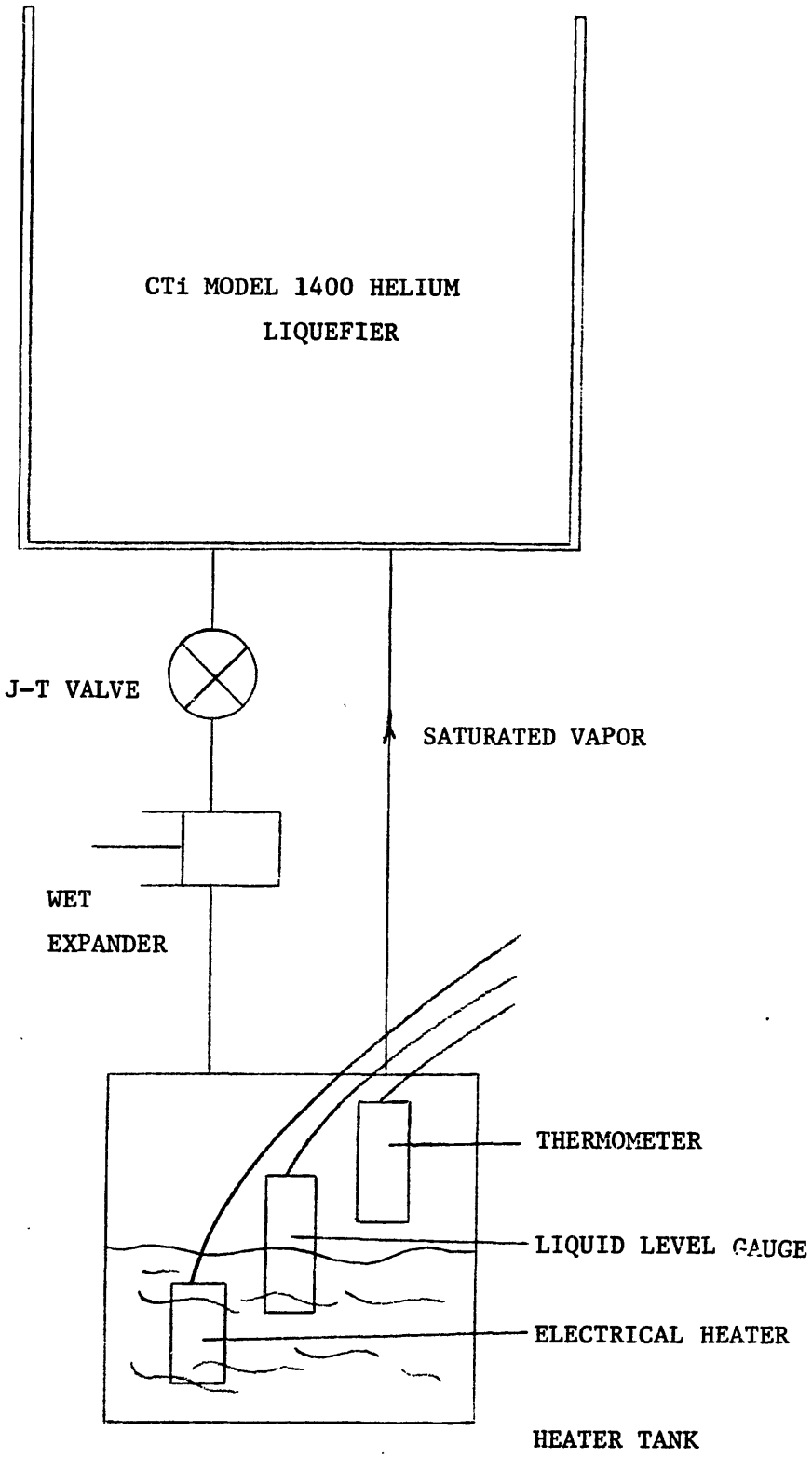


FIG. 5.3 LAYOUT OF EXPERIMENTAL SET-UP: DETERMINATION OF REFRIGERATION CAPACITY.

stainless steel and all joints are TIG welded.

The saturated vapor from the heater tank is returned to the liquefier through the annular flow passage in the two-channel transfer tube. The outer tube of this annulus is insulated from ambient by vacuum as well as several layers of superinsulation. The vacuum space of the transfer tube is connected to the main vacuum space of the engine. The preparation at the end of the transfer tube which is inserted into the liquefier is a duplicate of that on the CTi transfer tube supplied with the liquefier. This ensures a leak-free connection at the liquefier.

5.4 Instrumentation

5.4.1 Required Measurements.

Refrigeration Capacity. The resistance heating element for simulating the heat load is made of a short strip of chromel wire wound into a cylindrical coil spring and insulated using kapton tape. Thin copper wires with film insulation are used as electrical leads to minimize conduction heat loss.

The heater power supplied must be just sufficient to balance the latent heat of vaporization of the liquid resulting from the expansion process so the leaving stream is saturated vapor. Therefore a temperature sensor in the form of a helium vapor pressure thermometer is provided to monitor that the gas is not overheated. It was also found necessary to use a liquid level gauge to monitor a steady liquid level in the heater tank.

Evaluation of Engine Peformance. The efficiency of the wet expander is defined as (Fig. 5.4.1):

$$\eta = \frac{W_{act}}{W_{rev}},$$

where

the actual work, $W_{act} = m(h_1 - h_3) + Q_{act}$

the reversible work, $W_{rev} = m(h_1 - h_3) + Q_{rev}$

The reversible heat input $Q_{rev} = T_{sat}(S_3 - S_1)$

Q_{act} = the actual resistance heat input

m = mass flow rate

h_1, h_3 = inlet and saturated vapor enthalpy respectively

The actual work W_{act} is also given by the difference between the indicated work W_{ind} and the heat leak:

$$W_{act} = W_{ind} - Q_{leak}$$

Therefore the measurements required to evaluate the performance are:

- the inlet state (temperature and pressure)
- the fluid state leaving the heater tank (temperature and pressure)
- the refrigeration capacity Q_{act}

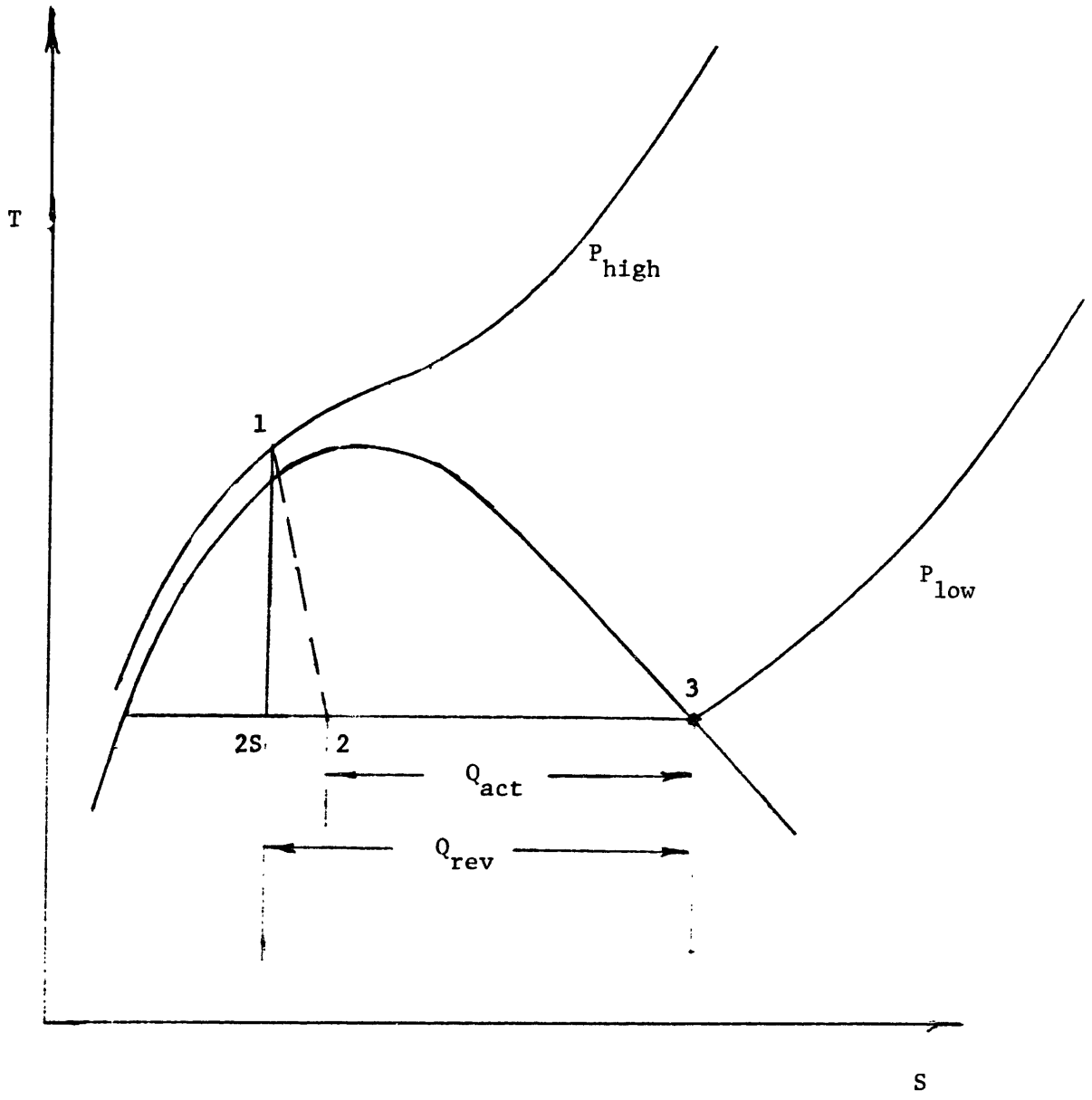


FIG. 5.4.1 TEMPERATURE-ENTROPY DIAGRAM FOR DEFINING WET EXPANDER EFFICIENCY.

- the indicated work from a P-V trace
- heat leaks - static heat leak and heat generated due to piston motion.

State Points: Pressure gauges are connected to the inlet and the heater tanks, through 1/8" capillary tubing, to measure the pressure in these places. The temperature is measured using vapor pressure thermometers. The warm volume is connected to the cold bulb by AWG16 capillary tubing.

Refrigeration Capacity: The refrigeration capacity is measured as before. A linear motion position transducer (model SLF-75 from the Waters Manufacturing Inc.) is used to obtain a displacement and hence volume versus time signal. The transducer is a simple resistive potentiometer consisting of a translational movable contact and a conducting plastic resistance element. A 3VDC excitation voltage gives a 3VDC output voltage at the maximum stroke of 3.0". The free end of the movable element of the transducer is connected to the free end of the control rod.

Indicated Work: The pressure inside the expander working space is measured using a high impedance piezoelectric miniature pressure transducer from Kistler Instruments. The transducer operated at the expander temperature. The charge output of the sensing element, a quartz crystal, is fed to a signal conditioning module and is converted into a proportional voltage signal. The transducer threads into a mounting adaptor which is connected to the cylinder through a short capillary tube. One end of the capillary tube is soft-soldered to the expander valve block and the other end is TIG welded to the mounting adaptor. The connecting cable between the transducer and the signal conditioning module is taken out of the vacuum jacket through a hermetic feed through.

Static Heat Leak Test: Figure 5.4.2 shows a schematic arrangement of the setup used to measure the static heat leak. The engine valves were propped open. The expander and the peripheral apparatus were then cooled down to the operating temperature. The two-phase flow from the J-T valve was gradually reduced until a small temperature rise was detected across the expander. The temperatures were recorded from vapor pressure thermometers.

To measure the mass flow rate, the cold gas is first warmed up by heat exchange with a pool of warm water and then passed through a mass flow transducer (TSi model 2012). This transducer is the heated sensor type. A factory calibration curve was used to read off the mass flow rate corresponding to a given output DC voltage.

Piston Motion Heat Transfer Loss: The setup shown schematically on Fig. 5.3 was used for measuring the heat transfer loss associated with the piston motion. The engine was first cooled down to the operating temperature. Both valves were propped open and the refrigeration capacity of the liquefier operating with the J-T valve determined by measurement of heater power required to achieve saturated vapor at the heater tank discharge. With the valves still propped open, the piston was shuttled by means of the piston motion control system. Because of the heat loss through this piston motion, the heater supply power (indicating the refrigeration capacity) is reduced. The difference between the two measured capacities gives the loss due to the piston motion.

5.4.2 Pneumatic Circuit (Debugging)

The factors affecting the dynamic behaviour of the pneumatic circuit includes: the internal design and port sizes of the pneumatic valves and switches as well as the inertial,

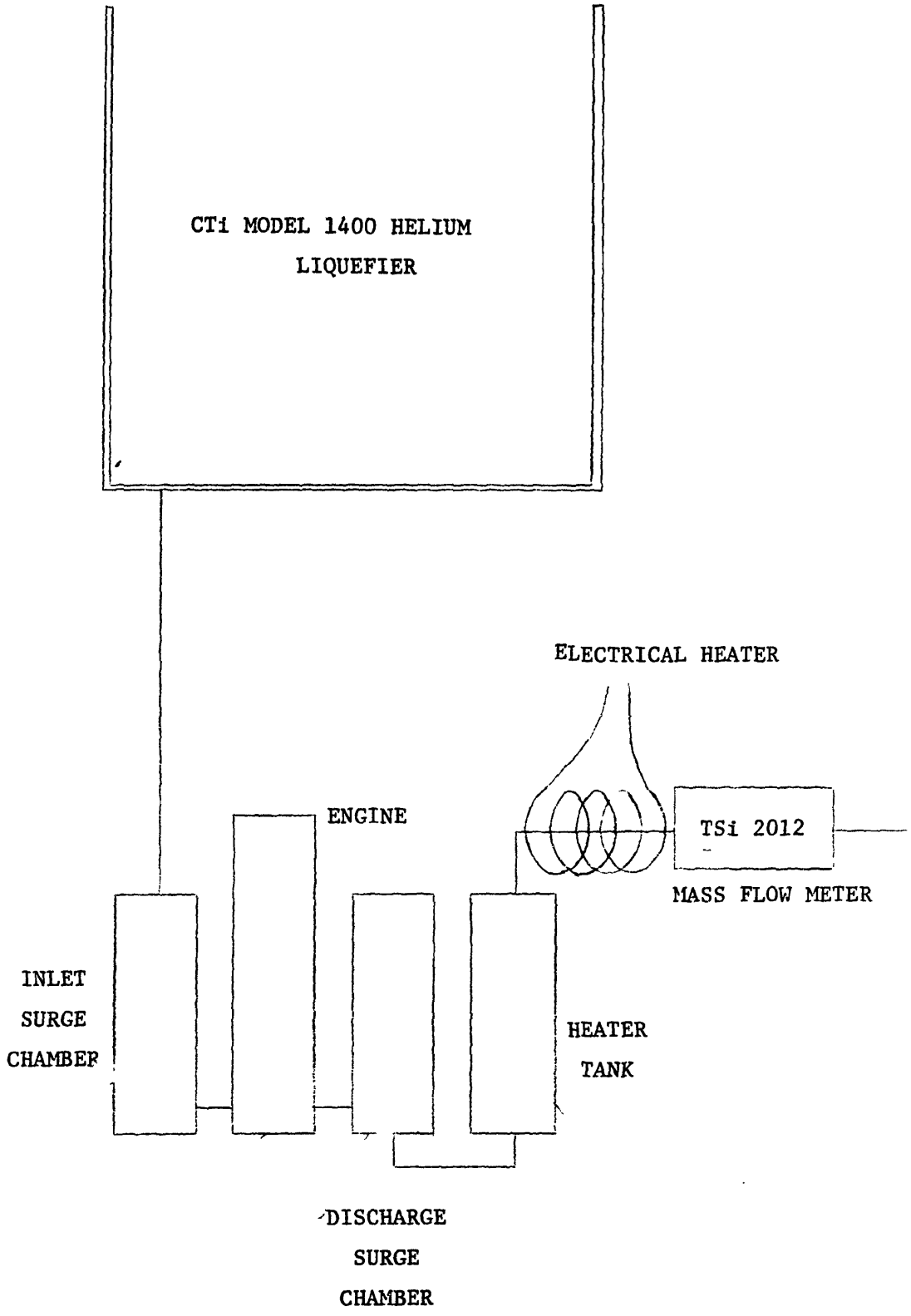


FIG. 5.4.2 LAYOUT OF EXPERIMENTAL SET-UP: STATIC HEAT TEST.

capacitive and resistive effects in the long plastic tubing interconnecting the components of the circuit. The lack of adequate information about the internal details of the valves and switches mitigates against the use of analytical modelling to determine the dynamic response of the circuit. Consequently an experimental approach to determining the circuit behaviour and hence tuning the circuit was developed.

The method consisted essentially of instrumenting the pneumatic circuit – with pressure transducers – which together with pressure and displacement information from the working space of the engine represented a diagnostic tool for debugging the control circuit. The pressure transducers used are the strain-gauge type with a 20 mV DC maximum output voltage corresponding to a 250 psi pressure in some cases and 125 psi pressure in other cases. The voltage signals from these pressure transducers, as well as those from the pressure and displacement transducers on the engine, are monitored by means of a Nicolet Explorer III digital oscilloscope with disk memory capabilities and subsequently transferred to the JCF VAX computer for analysis. Typical curves showing the phase relationships are shown in Figs. 5.4.3 through 5.4.7.

One principal change effected in the initial design of the pneumatic circuit was raising the operating pressure level to 80 psig. The pneumatic valves and switches are all rated at 40 psig. However the circuit response is too slow at this pressure level. For example, the 3-way hydraulic valve is air piloted. Air pressure switches the 3-way valve to slow the engine down during the charging process. However, at the 40 psig pneumatic pressure level, there is a long delay before this valve switches due to the long time constant required to build up the pressure at the pilot, and the charging speed control is thus overridden. Elevating the pressure level to 80 psig cuts down on the time constant

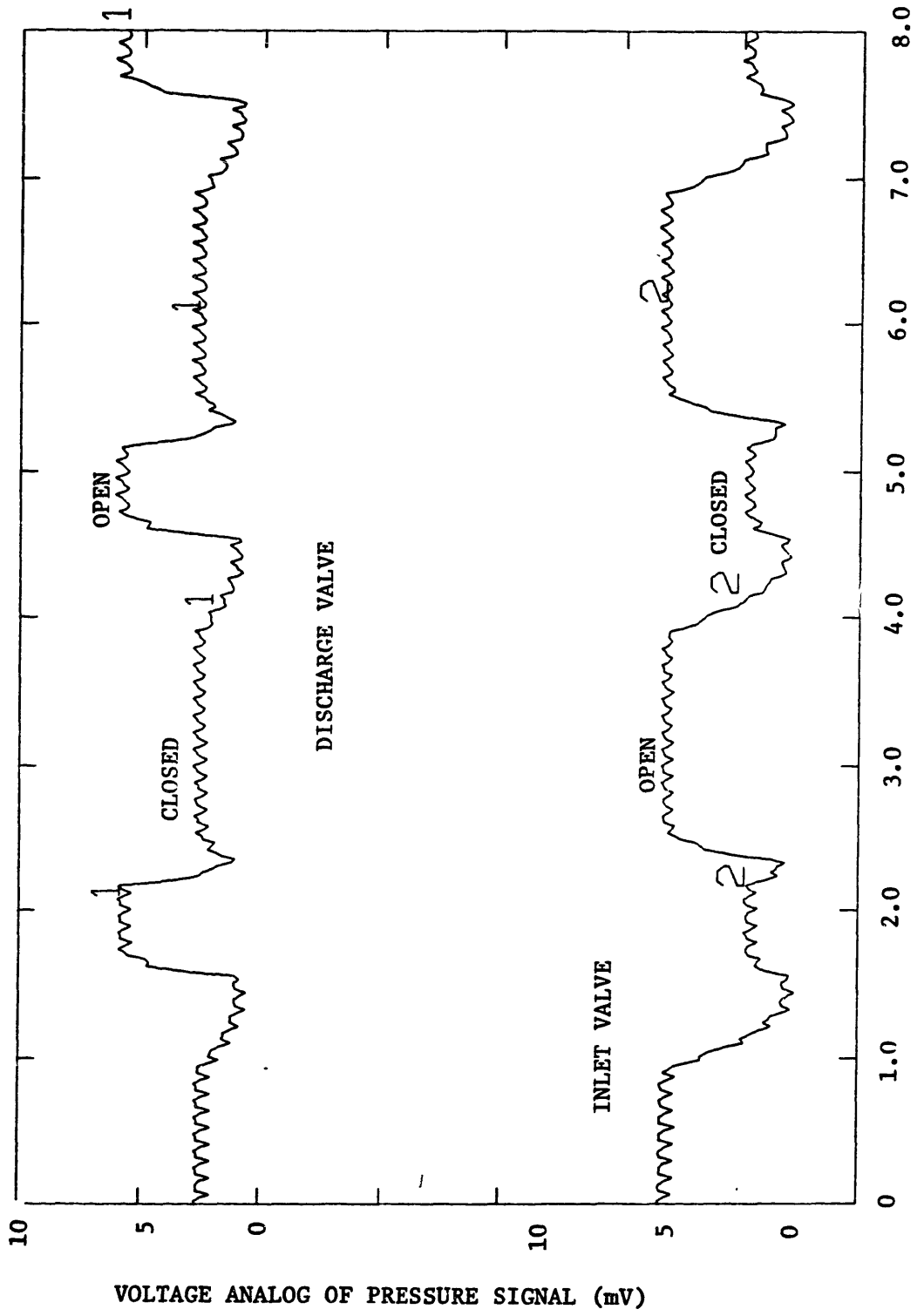


FIG. 5.4.3 PHASE RELATIONSHIP BETWEEN PRESSURE AT THE DISCHARGE VALVE ACTUATOR AND INLET VALVE ACTUATOR.

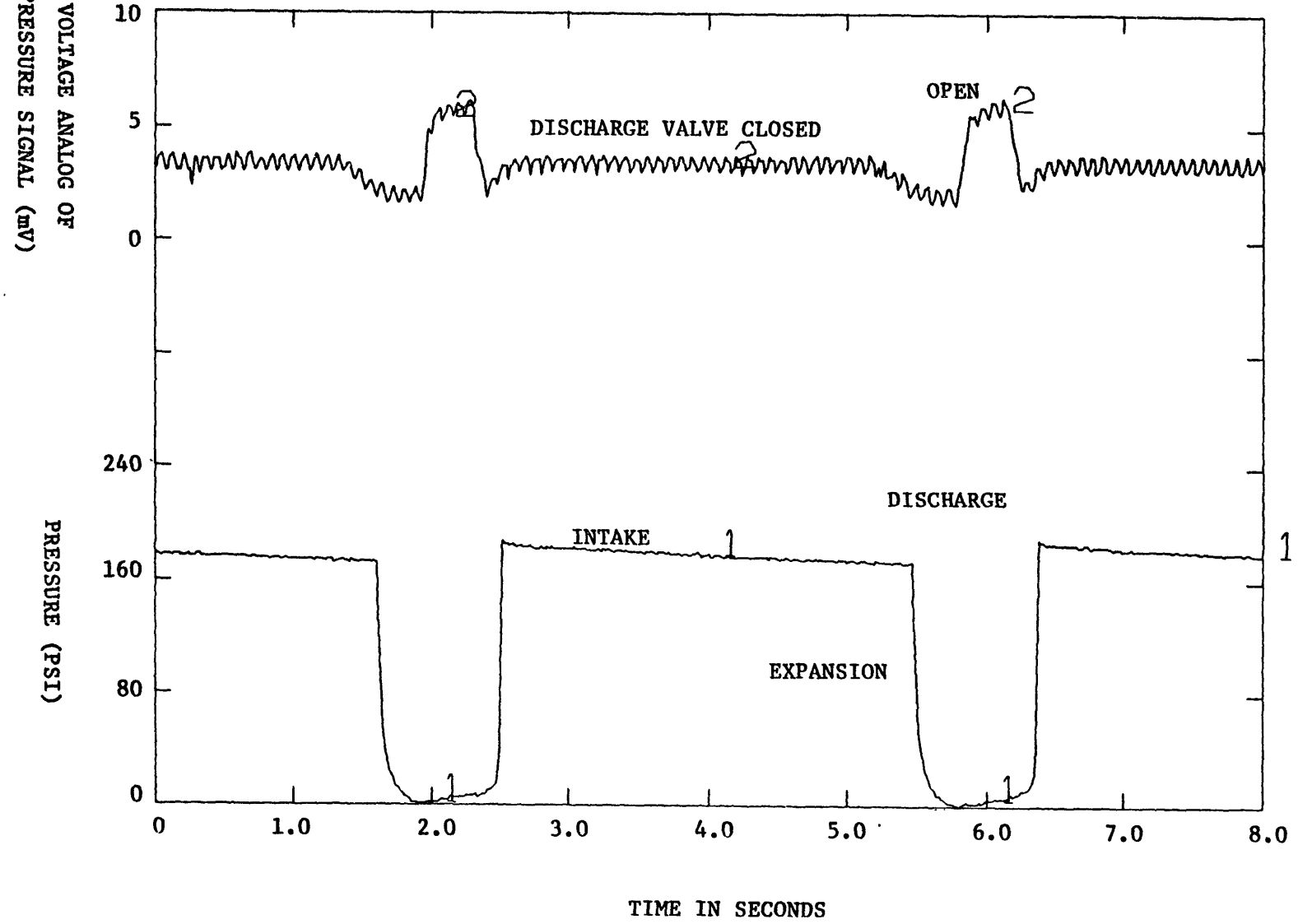


FIG. 5.4.4 PHASE RELATIONSHIP BETWEEN PRESSURE IN THE EXPANDER (1) AND AT THE DISCHARGE VALVE ACTUATOR (2).

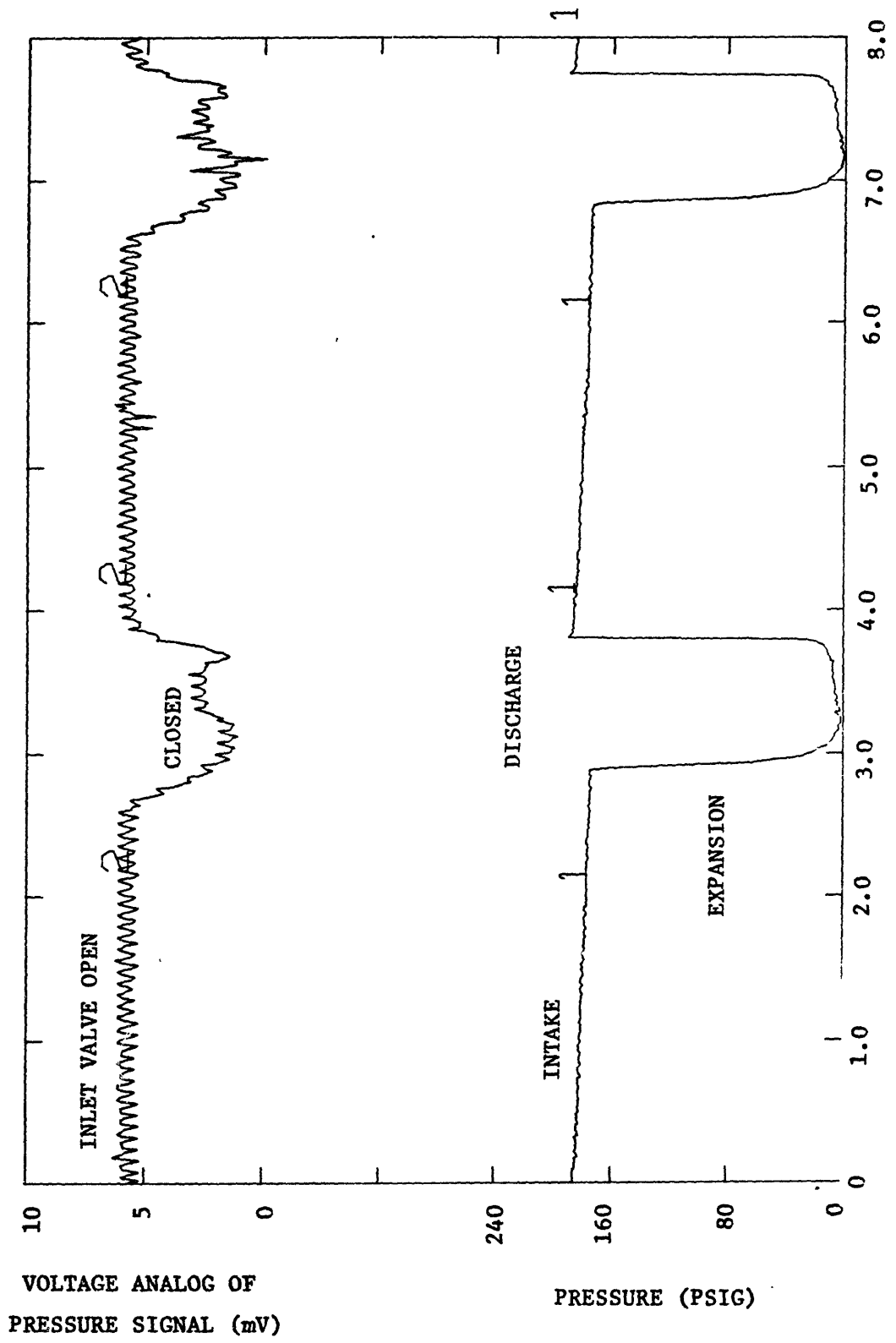


FIG. 5.4.5 PHASE RELATIONSHIP BETWEEN PRESSURE IN THE EXPANDER (1) AND AT THE INLET VALVE ACTUATOR (2).

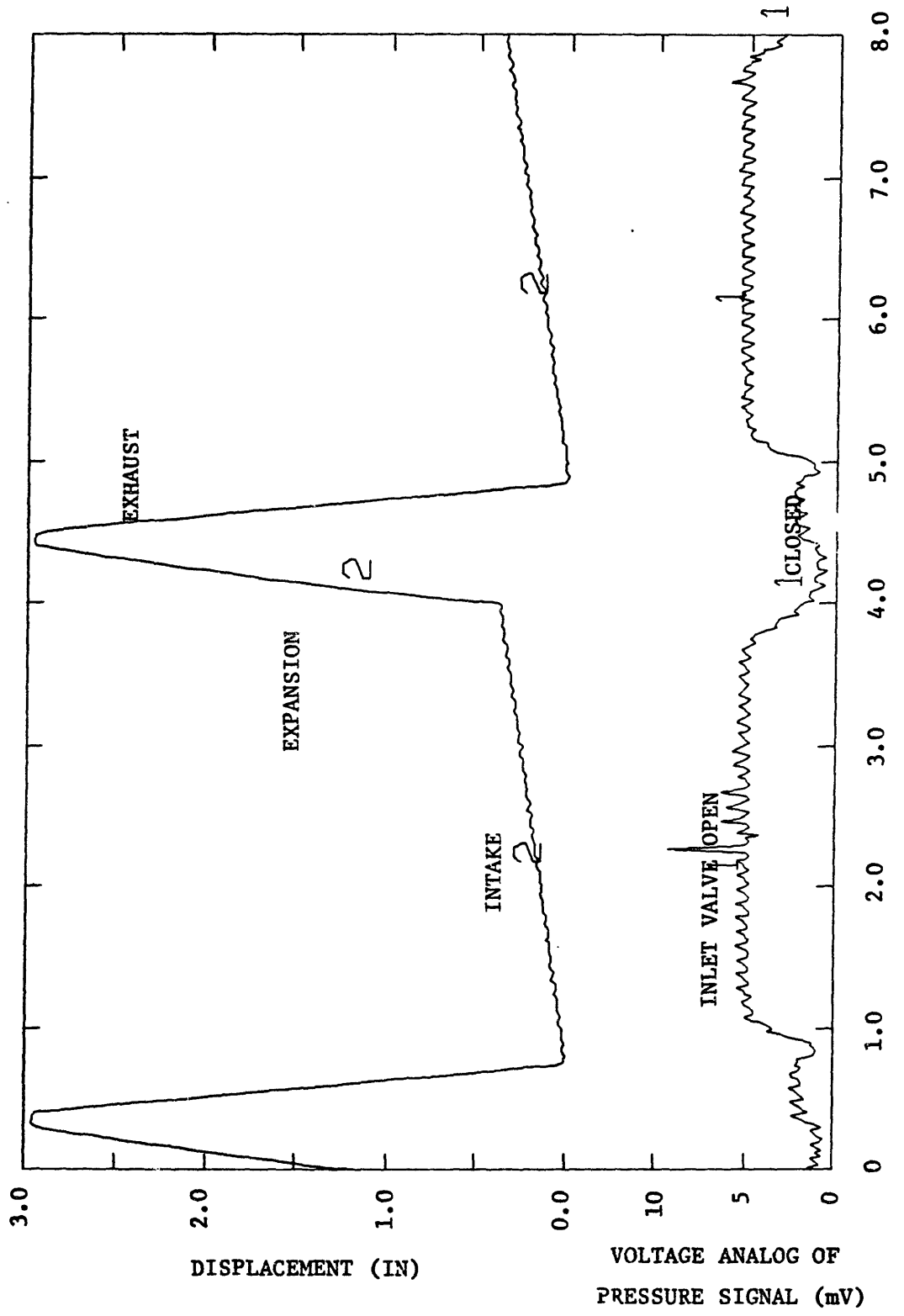


FIG. 5.4.6 PHASE RELATIONSHIP BETWEEN PRESSURE AT THE INLET VALVE ACTUATOR (1) AND DISPLACEMENT (CYLINDER VOLUME) (2).

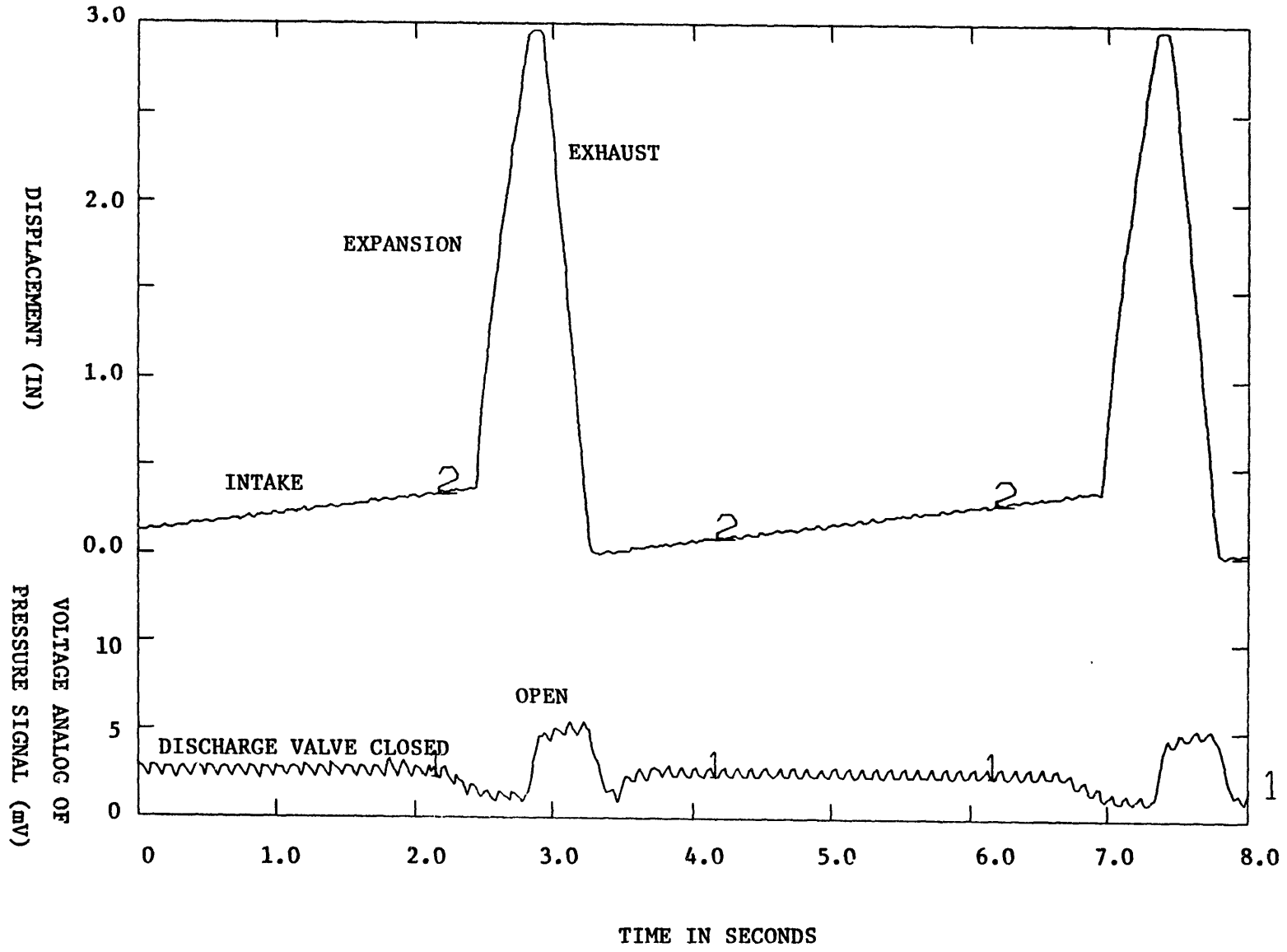


FIG. 5.4.7 PHASE RELATIONSHIP BETWEEN PRESSURE AT THE DISCHARGE VALVE ACTUATOR (1) AND DISPLACEMENT (CYLINDER VOLUME) (2).

sufficiently to facilitate speed control during the charging process.

Time Sequence of Events in Pneumatic Circuit

A typical phase relationship between the inlet valve actuator pressure signal and that of the discharge valve actuator is shown in Fig. 5.4.3. Also other phase relationships based on signals from the expander pressure transducer and the displacement transducer are shown (Figs. 5.4.4-5.4.7). The digital oscilloscope enabled fairly good estimates of the sequence of events as follows:

- The pressure at the inlet valve actuator takes about 0.14 s to 0.16 s to build up to its full value (80 psig). However it takes about 0.06 to 0.085 to reach the level high enough to switch the valve. On the other hand the complete discharge process takes about 0.20 to 0.24 s to complete. Again the valve closes after about 0.16 s.

- Similarly, the pressure at the discharge valve actuator takes between 0.10 and 0.12 s to build up to full value and about 0.14 s to discharge completely.

The quicker response of the discharge valve actuator time is because it is connected directly to the limit switch whereas the inlet valve actuator is connected to the limit switch through a NOT element with a smaller port size than the air limit switch (see Fig. 5.2.10).

The curves also indicate that there is always a residual pressure at one of the actuators whenever there is pressure in the other line. The residual pressure is about 6 psig for the inlet valve actuator and 12 psi at the discharge valve actuator. There is no

pressure in either actuator only during the expansion process (and also briefly at the end of the discharge stroke before the inlet valve opens).

Time Sequence of Cycle Events

An ideal cylinder-pressure, cylinder-volume curve is shown in Fig. 5.4.8. In this idealized cycle, there is:

- no blow in losses;
- no blow down losses;
- no clearance volume;
- and the charging pressure is constant.

To ensure a fairly constant charging pressure, a surge chamber is provided at the inlet to the engine. Also the piston speed during the charging process is kept minimal. A fairly constant charging pressure is obtained in Fig. 5.4.9. For this figure, time is spent charging the working space with the high pressure gas as is clearly shown in the time plots shown in Figures 5.4.6 and 5.4.7. This also reduced the flow losses associated with the inlet valve. Table 5.2 summarizes time and speed distribution for this cycle.

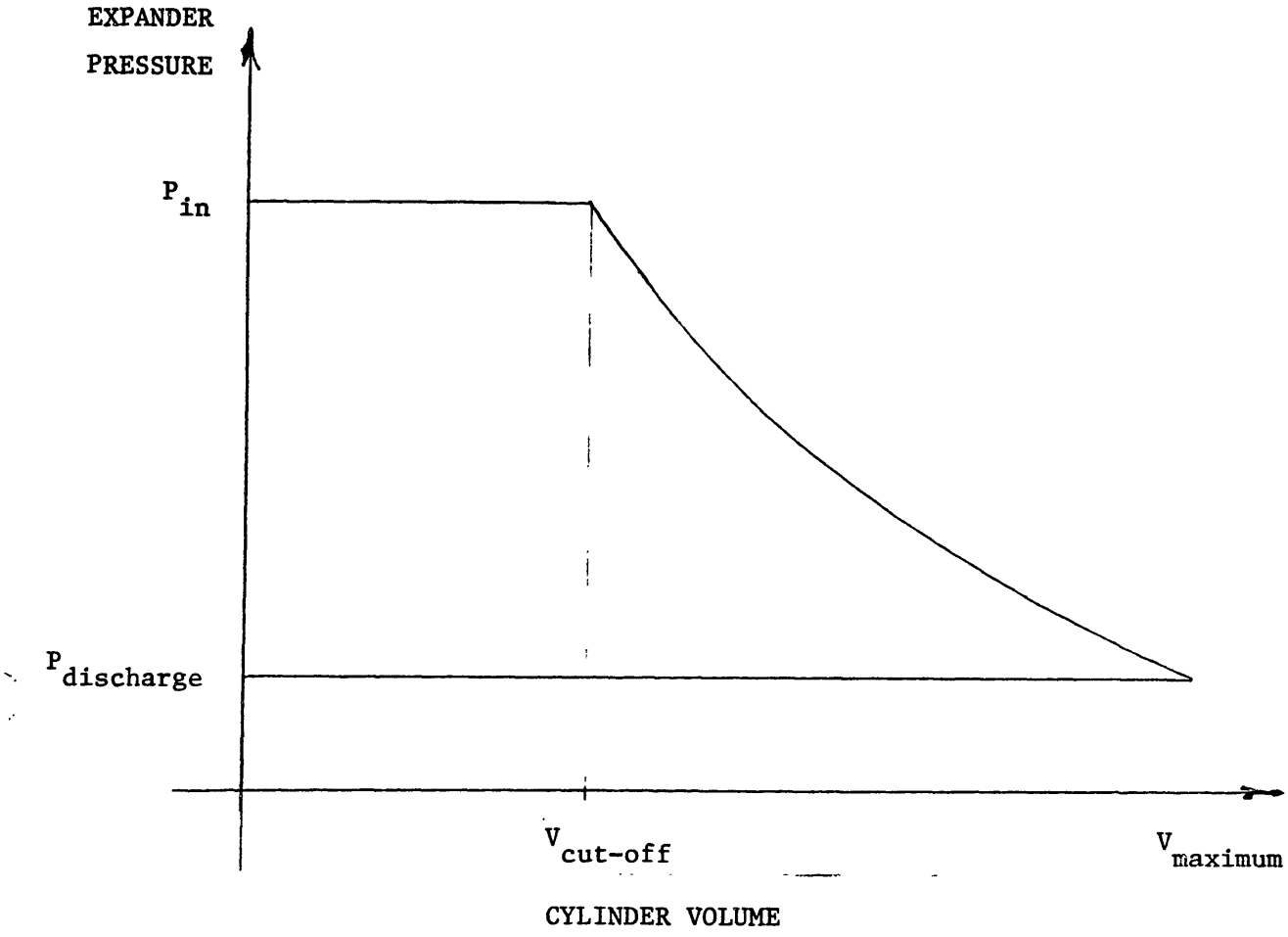


FIG. 5.4.8 IDEAL P-V DIAGRAM FOR EXPANDER

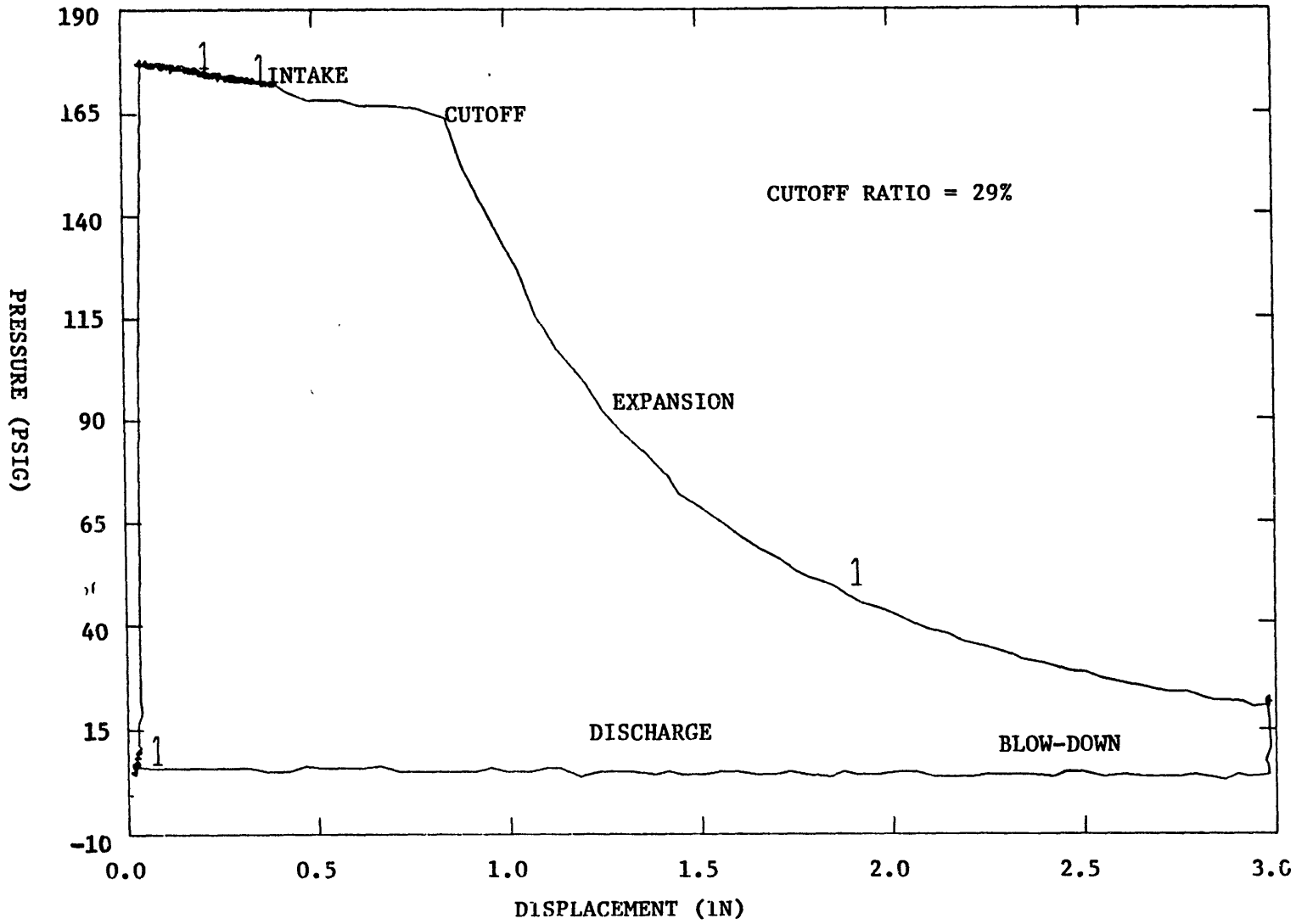


FIG. 5.4.9 PRESSURE-VOLUME (DISPLACEMENT) DIAGRAM FOR SINGLE PHASE EXPANDER MODE, WITH BLOW DOWN.

Table 5.2

Typical Time Distribution for Cycle Processes

Process	Piston Speed (in/s)	Time (s)
Charging	0.21	1.87
Expansion	9.14	0.28
Discharge	7.76	0.38
Dwell at TDC	-	0.10
Dwell at BDC	-	0.04
	Total	2.67

The capacity of the surge chamber was exceeded at the flow rate required. Thus, it was not possible to keep the charging pressure constant during the intake stroke as shown.

The cycle just described has a blow down loss associated with it. In contrast, the cycle in Fig. 5.4.10 shows complete expansion. It is possible to adjust the cut-off point to ensure negligible blow down loss.

The two cycles just described (Figs. 5.4.9, 5.4.10) are obtained for single phase operation of the expander. The cut-off ratio is about 20%. The P-V diagram of Fig. 5.4.11 was obtained for a comparable cut-off ratio and for operation in a two-phase expander mode. The P-V curve indicates an overexpansion followed by a small recompression.

The maximum charging pressure tested was about 190 psig. The primary limitation against testing at any higher pressure level was the pressure drop in the heat exchanger

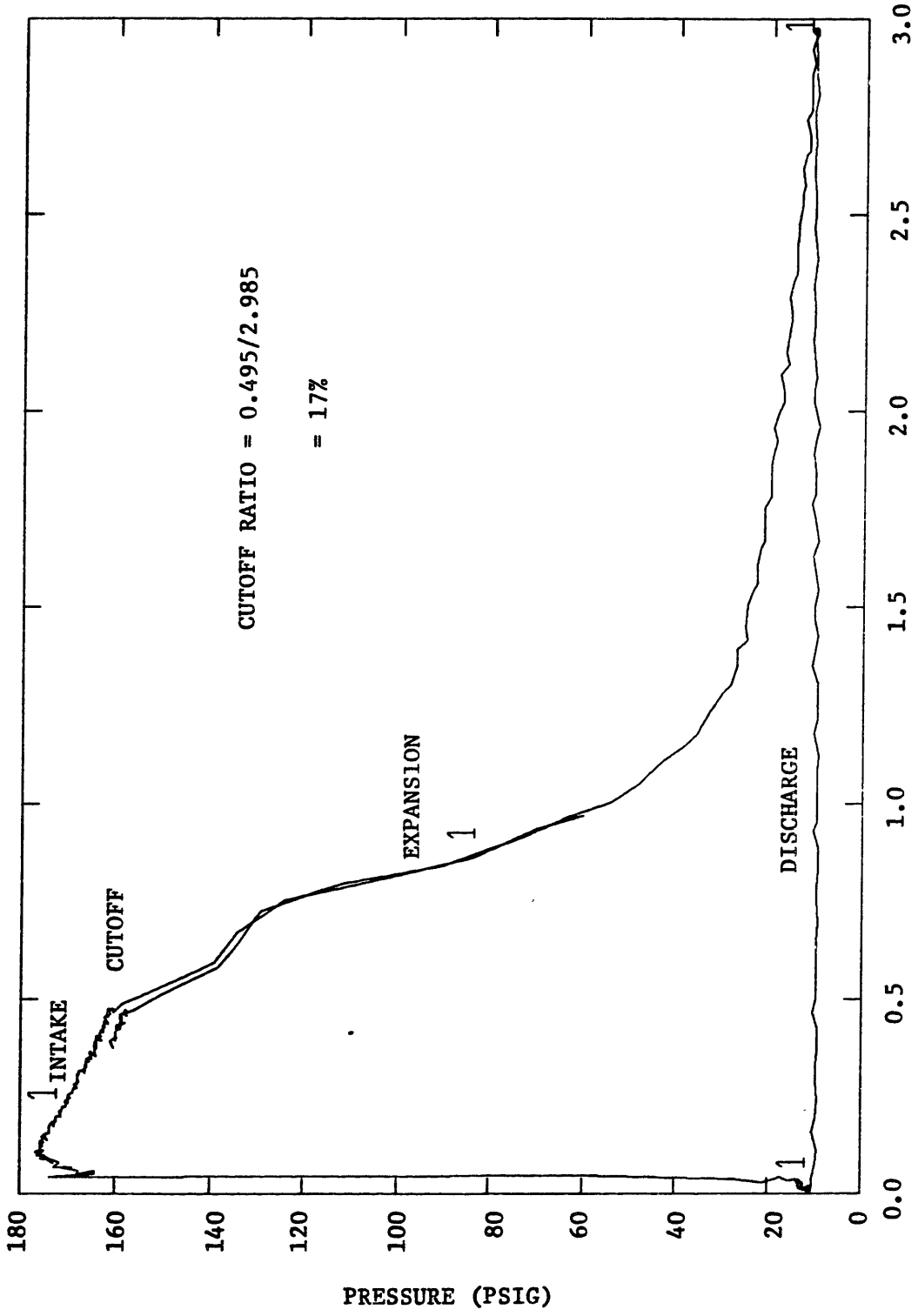


FIG. 5.4.10 PRESSURE-VOLUME DIAGRAM FOR SINGLE PHASE EXPANDER MODE, WITHOUT BLOWDOWN

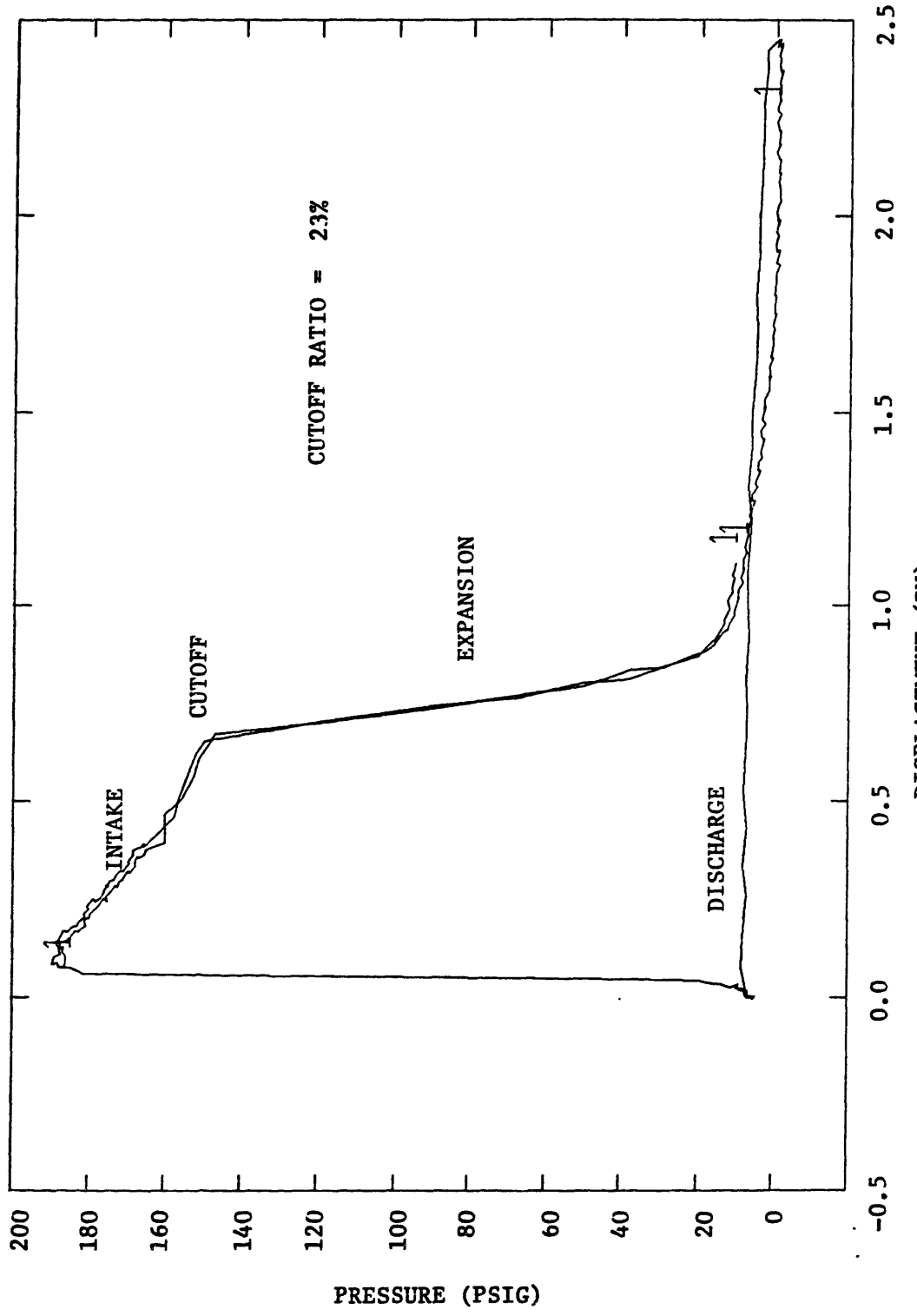


FIG. 5.4.11 PRESSURE-VOLUME DIAGRAM FOR TWO-PHASE EXPANDER.

stack in the helium liquefier and also the pressure ratio limits on the helium compressors on the liquefier. This maximum pressure was obtained while running the liquefier with one compressor and without liquid nitrogen precooling.

5.5 Summary Of Test Results

5.5.1 Refrigeration capacity

The refrigeration capacity was determined from the experimental data summarized on Table 5.3. The refrigeration capacity increased from 18.5 W when using the J-T valve, to 33.4 W when the J-T valve was replaced by the supercritical wet expander. This represents an increase of over 80%.

Also the piston motion loss was found to be 1.3 W (appendix E2). The measured resistance of the heating element was 10.7Ω when cold.

Table 5.3

Typical results for refrigeration capacity

	J-T mode	J-T+ piston motion	Wet expander mod
Comp. disch. pres (psig)	209	212	212
Comp. suction pres (in H_2O)	92	84	87
J-T pressure (psig)	188	190	180-190
J-T valve setting (μin)	65	65	fully open
Engine inlet temp (K)	4.42	4.42	6.55
Engine discharge temp (K)	4.42	4.42	4.42
Heater voltage (V)	14.07	13.566	18.9
Heater power (W)	18.5	17.2	33.4

5.5.2 Wet expander performance

The following values are also extracted from the analysis of results given in Appendix E2. The mass flow rate is calculated from the cylinder volume and the state of the working fluid at the cut-off point:

$$M = 2.18 \text{ g/s.}$$

The reversible expander power $W_{rev} = 21.8$ W.

The actual power calculated from the mass flow rate $W_{act} = 20.4$ W.

The ratio gives the expander efficiency $\eta = 94\%$

The actual power was also calculated from the indicated power and the heat losses.

Indicated power $W_{ind} = 21.4$ W

Static heat loss rate = 1.6 W

Piston motion loss rate = 1.3 W

These three values give the actual work

$$W_{act} = 18.5 \text{ W}$$

which gives the expander efficiency

$$\eta = 84.5\%$$

The agreement between the two values for the actual work is 10%. The uncertainty associated with the measured value of the expander inlet temperature contributes to the different values obtained.

5.5.3 Single Phase Expander Performance:

The device was also tested as a single phase expander with a typical performance summarized below:

Table 5.4

Results for single phase expander test

	Test 1	Test 2
Expander inlet pressure (atm)	13.21	10.32
Expander inlet temperature (K)	11.51	10.22
Expander discharge pressure (atm)	1.2	1.2
Expander discharge temperature (K)	4.72	4.6
Expander efficiency η (%)	93	91

5.6 Conclusion

The measured efficiency of the supercritical wet expander lies between 84%and 93%. As a single phase gas expander, the measured efficiency is between 91%and 93%. These high efficiencies are indications that even for moderate vapor compressor efficiencies the Saturated Vapor Compression cycle may be viable.

Chapter 6

CONCLUSION

6.1 Summary

The following objectives for this thesis have been achieved:

1. To develop an alternative optimization scheme for cryogenic liquefaction cycles,based on the second law of thermodynamics and in which the configuration is an output rather than an input.
2. To design and build a machine that can be used for investigations leading to the practical implementation of the saturated vapor compression cycle.

An entropy flow (second law) analysis of a continuum model for the precooling stage of helium refrigeration/liquefaction cycles has been introduced. The model adjusts the heat capacity flow in the cycle such that the irreversibilities associated with the heat exchange, quantified by the generated entropy flow, is minimum. This is achieved either by extracting work of expansion from the stream with the higher heat capacity rate or by adding work of compression to the stream with the lower heat capacity rate. The result of this adjustment is that starting from the warm end of the precooling stage, work of expansion must be extracted from the high pressure stream, up to a point where the heat capacity rates match; thereafter work of compression must be added to the high pressure stream which now has a lower specific heat.

An optimal configuration is synthesized from the performance curves of the continuum model by discretization. For the precooling stage, this optimum configuration

involves use of heat exchangers and expanders as discussed by Collins11. The greater the number of expansion stages, the ecloser the precooling stage approaches reversibility (for reversible expansion processes). In practice, however, the cost of the expanders may against the use of so many expansion stages. The Collins' cryostat contains two expansion stages (Fig. 3.11).

The analysis also confirms the saturated vapor compression (SVC) arrangement as the optimal cold end configuration based on a second law analysis. Thus together with the multiple-expander precooling stage, an optimal cycle configuration has been derived. This SVC cycle has several advantages over the conventional helium liquifaction cycle.

1. The overall cycle thermodynamic performance is improved due to better matching of the heat capacity rates of the two streams. Also, the wet expander operates over a much higher pressure ratio, and therefore its potential is more fully utilized.
2. The required heat exchange area is substantially reduced. This is due to the improved heat transfer coefficient at the higher pressure levels resulting from increased mass velocities for the same loss of pressure ratio in each channel.
3. The cycle pressure level can be chosen for the best performance of the expansion engines and heat exchangers alone, rather than by compromise with the performance of the J-T value.
4. The increased suction pressure results in a reduced compressor size.
5. The SVC cold end may be used as a bottoming cycle to convert a conventional refrigerator to a 1.8 K refrigerator without the addition of large low pressure heat exchangers and large displacement vacuum pumps.

One of the novelties in the optimization procedure developed is in providing the configuration as an output rather than an input to the design algorithm. The following general trends in the cycle design parameters are also deduced from the procedure.

1. **Critical heat exchange ΔT:** The analysis indicates that for optimal cycle performance, the heat exchange $\Delta T/T$ must be constant over the entire precooling temperature range for either operation mode (refrigeration or liquefaction) and using ideal or real gas properties. Thus in designing a cycle with discrete expansion, the critical heat exchange temperature differences must be initialized to a constant value for $\Delta T/T$. Each value of $\Delta T/T$ corresponds to a specific heat exchange area. Thus, this allows a trade-off decision between heat exchange surface and thermodynamic performance..

2. **Pressure ratio/level:** The cycle pressure ratio and pressure level must be as high as possible. These must therefore be fixed by the structural integrity and/or the performance of the cycle components.

3. **Temperature levels:** In general the temperature levels, indicated by the expander inlet (or discharge) condition can be obtained by direct discretization of the mass flow rate curve. However this may involve a tedious iteration. Therefore a parametric optimization scheme may be used to obtain these temperature levels.

In the experimental work an experimental reciprocating engine has been constructed and operated at efficiencies between 84% and 93% as a wet expander and between 91% and 93% as a single phase expander at temperatures near 4.2 K. The

static heat loss and the piston motion loss account for the major part of the expander losses. Cyclic heat transfer loss which substantially affect the performance of Stirling machines do not have a significant effect on the wet expander because of the reduced specific heat capacity of stainless steel at the operating temperature. The programmable hydraulic/pneumatic piston motion control unit enabled fine-adjustment of the valves and the clearance volume essentially eliminating blow down and blow in losses.. The operating hours for the expansion engine are not yet long enough to facilitate a determination of the reliability of the machine. The only problem so far seems to be small oil leaks at the miniature pneumatic fittings used for the hydraulic circuit. Replacement of these fittings would be recommended.

6.2 Suggestions For Further Work

Optimization Technique: The total heat exchange area available has been incorporated in the overall cycle design through the choice of $\Delta T/T$ used for initiating the critical heat exchange temperature differences. However, the overall design is still a 2-step procedure involving the heat exchanger design and then the overall cycle design. The heat exchanger ΔP losses and axial conduction losses are not included in the model. An extension of this work would be to develop a model that includes these two effects.

Cold Compressor Test: Two simple changes are required to convert the expansion engine into a cold compressor interfaced with the CTi Model 1400 liquefier. These are:

1. Reprogramming the piston motion control system for the appropriate valve opening and closing sequence; and

2. Replumbing the engine end of the two-channel coaxial transfer line interconnecting the engine and the CTi liquefier.

Thus the machine may be used to run experiments as a cold compressor. The performance will be useful in determining the viability of implementing the SVC cycle.

Experiments: Analytical models for the shuttle heat transfer loss, piston gap pumping loss and cyclic heat transfer loss associated with reciprocating displacers, have been developed for Stirling cycles. These models are invariably used for the design of cryogenic expanders. However no experimental verification of these models at cryogenic temperatures has been documented. Experiments to model these losses would be very useful to the designer of cryogenic expanders and can be easily carried out with minor modification of the experimental apparatus.

Appendix A

GENERATED ENTROPY AS A PERFORMANCE INDEX

The performance of thermodynamic refrigeration cycles is traditionally given by the coefficient of performance COP. Details of an entropy flow analysis for evaluating the performance of a refrigeration system consisting of a series of refrigerators each spanning a temperature dT and rejecting heat to the next higher temperature (Fig. 2.1) is presented in this appendix. It is shown that minimizing the generated entropy is equivalent to maximizing the COP for the refrigeration system, as discussed in chapter 2.

Suppose the work input per stage (see Fig. 2.1)

$$\delta W_{act} = x\delta W_{rev} \tag{A.1}$$

where δW_{rev} is the reversible work input per stage.

For each stage,

$$\begin{aligned} \frac{1}{COP_{rev}} &= \frac{\delta W_{rev}}{Q_T} \\ &= \frac{T + dT}{T} - 1 \\ &= \frac{dT}{T} \end{aligned} \tag{A.2}$$

Also,

$$\begin{aligned} \frac{1}{COP_{act}} &= \frac{\delta W}{Q_T} \\ &= \frac{x\delta W_{rev}}{Q_T} \\ &= \frac{xdT}{T} \end{aligned} \tag{A.3}$$

Further, from the first law

$$\delta W_{act} = Q_T \cdot {}_{dT} - Q_T = dQ \tag{A.4}$$

hence

$$\frac{dQ}{Q} = x\frac{dT}{T} \tag{A.5}$$

Integrating,

$$\frac{Q}{Q_i} = \left(\frac{T}{T_i}\right)^x \tag{A.6}$$

The entropy transfer at temperature T,

$$S = \frac{Q}{T} \tag{A.7}$$

Therefore

$$S = S_i\left(\frac{T}{T_i}\right)^{x-1} \tag{A.8}$$

To find the overall COP we note that

$$W = Q_h - Q_i$$
$$= Q_i[\frac{Q_h}{Q_i} - 1] \tag{A.9}$$

hence the performance of the refrigeration system

$$COP = \frac{Q}{W} \tag{A.10}$$

becomes

$$COP = \frac{1}{\left[\left(\frac{Q_h}{Q_l}\right) - 1\right]} \tag{A.11}$$

which simplifies to

$$COP = \frac{1}{\left(\frac{T_h}{T_l}\right)^x - 1} \tag{A.12}$$

from which the COP for a reversible refrigerator is recovered for $x = 1$

$$COP_{rev} = \frac{1}{\frac{T_h}{T_l} - 1} \tag{A.13}$$

In terms of entropy, the COP becomes

$$COP = \frac{1}{\frac{S_h}{S_l}\left(\frac{T_h}{T_l}\right) - 1} \tag{A.14}$$

but

$$\frac{S_h}{S_l} = 1 + \frac{S_{gen}}{S_l} \tag{A.15}$$

hence

$$COP = \frac{1}{\frac{T_h}{T_l}\left[1 + \frac{S_{gen}}{S_l}\right] - 1} \tag{A.16}$$

Therefore maximizing COP is equivalent to minimizing $S_{gen}(T)$ given by

$$S_{gen} = \int_{T_l}^{T} \frac{dS_{gen}}{dT} dT \tag{A.17}$$

as used in chapter 2.

Appendix B

REVERSIBLE CONTINUUM MODELS FOR THE PRECOOLING STAGE OF HELIUM REFRIGERATORS

An optimal configuration for helium refrigeration cycles was synthesized from the performance curves of two models for the precooling stage of the refrigeration cycle. In this appendix details of the analysis for deriving these performance curves are presented for these models. The mass crossflow model is first considered for the refrigeration mode and then the liquefaction mode in sections B1.1 and B1.2 respectively. Similarly, sections B2.1 and B2.2 address the variable pressure model in the two operating modes: refrigeration and liquefaction respectively. There are three basic assumptions underlining the analyses:

1. all expansion and/or compression processes are reversible;

2. the heat exchanger has infinite heat transfer area;

3. the pressure drop in the heat exchangers is zero.

Thus there is zero heat exchange ΔT and zero flow irreversibility.

B1 Continuously Distributed Full-Pressure Ratio Expanders

B1.1 Refrigeration Mode

Fig. 3.1(a) is a model representing the precooling stage of the refrigeration cycle. It consists of a counter flow heat exchanger with reversible isothermal expanders continuously distributed over the temperature spanned the precooling stage. The governing equations are derived from the first law applied succesively to the components and processes as follows.

The heat balance for the two streams gives

$$Q_h = Q + Q_r. \qquad (B.1)$$

For the isothermal expansion process,

$$W_T = Q_T, \tag{B.2}$$

$$= T(S_l - S_h)dM. \tag{B.3}$$

Also for the low pressure stream,

$$Q_l = MC_{pl}dT. \tag{B.4}$$

Similarly for the high pressure stream,

$$Q_h = MC_{ph}dT. \tag{B.5}$$

Substitution in the heat balance equation (Eq. B.1) gives the describing equation for the model as:

$$M(C_{ph} - C_{pl})dT = T(S_l - S_h)dM. \tag{B.6}$$

Rearranging terms:

$$\frac{dM}{M} = \frac{(C_{ph} - C_{pl})}{(S_l - S_h)}\frac{dT}{T}. \tag{B.7}$$

Finally, integrating (Eq. B.7) gives the mass flow rate distribution as:

$$\frac{M}{M_o} = \exp\int\left(\frac{C_{ph} - C_{pl}}{S_l - S_h}\right)\frac{dT}{T}. \tag{B.8}$$

Equation B1.8 is integrated numerically, using a Gauss integration algorithm, RGQIS, to obtain the results plotted in Sec 3.3.1. The computer program is listed in appendix D.

B1.2 Liquefaction Mode

In the refrigeration mode, the same mass circulates in both the high and the low pressure channels of the heat exchanger. This section details the derivation of the system equations for the model when operating in the liquefaction mode. The principal difference between the analysis for the liquefaction mode and that for the refrigeration mode is the factor ϵ (the ratio of the mass flow rate through the two channels) which modifies the specific heat capacity of the high pressure stream. The assumptions underlining the derivation of the following equations are as stated in the preceeding section. These equations are again derived from succesive application of the first and second laws of thermodynamics.

The heat balance for the two streams gives

$$Q_h = Q_l + Q_T. \tag{B.9}$$

For the isothermal expansion process,

$$W_T = Q_T, \tag{B.10}$$

$$= T(S_l - S_h)dM. \tag{B.11}$$

Also for the low pressure stream,

$$Q_l = M_l C_{pl} dT. \tag{B.12}$$

Similarly for the high pressure stream,

$$Q_h = M_h C_{ph} dT. \tag{B.13}$$

Substitution in the heat balance equation (B.9) gives the describing equation for the model as:

$$M(\epsilon C_{ph} - C_{pl})dT = T(S_l - S_h)dM. \tag{B.14}$$

where

$$\epsilon = M_h/M, \tag{B.15}$$

and

$$M_l = M. \tag{B.16}$$

Equation (B.14) may be rearranged to give:

$$\frac{dM}{M} = \frac{(\epsilon C_{ph} - C_{pl})}{(S_l - S_h)}\frac{dT}{T}, \tag{B.17}$$

and subsequent integration gives the final result as:

$$\frac{M}{M_o} = \exp\int\left(\frac{\epsilon C_{ph} - C_{pl}}{S_l - S_h}\right)\frac{dT}{T}. \tag{B.18}$$

as presented in Sec. 3.3.2.

In Eq. B.18, ϵ is a function of temperature which is not known a priory. The numerical integration therefore requires iteration on ϵ. The mass flow rate curve for the refrigeration mode is used to initialize ϵ. Subsequently, the resulting mass flow rate curve is used for the next iteration on ϵ.

B2 Model II: Continuously Distributed Full-Flow Expanders

The second model discussed in Chapter 3 involves continuously varying either pressure in the heat exchanger to match the cycle entropy flow and thereby produce a reversible precooling stage. Figure 3.1(b) shows the model with variable high pressure and constant low pressure in the heat exchanger. The governing equations are based on the same three assumptions listed in the introduction to this appendix.

The derivation of the governing equations start with the definition of entropy s as a function of pressure P and temperature T. Thus,

$$ds = \left(\frac{\partial S}{\partial P}\right)_T dP + \left(\frac{\partial S}{\partial T}\right)_P dT. \tag{B.19}$$

The partial derivative of the characteristic thermodynamic function $h(S, P)$ is

$$dh = T\,dS + v\,dP, \tag{B.20}$$

from which

$$\left(\frac{\partial h}{\partial T}\right)_P = T\left(\frac{\partial S}{\partial T}\right)_P,$$

$$= \frac{C_p}{T}. \tag{B.21}$$

Further from the Maxwell relation

$$\left(\frac{\partial S}{\partial P}\right)_T = -\left(\frac{\partial v}{\partial T}\right)_P, \tag{B.22}$$

and the definition of the coefficient of thermal expansion,

$$\beta = \frac{1}{v}\left(\frac{\partial v}{\partial T}\right)_P, \tag{B.23}$$

we obtain

$$\left(\frac{\partial S}{\partial P}\right)_T = -\beta v. \tag{B.24}$$

Substitution for the partial derivatives in equation (B.19) then gives

$$dS = -\beta v\, dp + \left(\frac{C_p}{T}\right) dT. \tag{B.25}$$

This expression for the change in entropy is substituted in the statement of the second law to derive the differential equations for the model as demonstrated presently.

B2.1 Refrigeration mode

For the refrigeration model shown in Fig. 3.1(b), the second law of thermodynamics applied to the control volume is

$$dS_l = dS_h, \tag{B.26}$$

where

$$dS_l = -\beta_l v_l\, dP_l + \frac{C_{pl}}{T}\, dT, \tag{B.27}$$

$$dS_h = -\beta_h v_h\, dP_h + \frac{C_{ph}}{T}\, dT. \tag{B.28}$$

Case 1. P_l = constant

Consider first the case of varying the high pressure to match the entropy flow while the low pressure is kept constant. Thus,

$$dP_l = 0, \tag{B.29}$$

and substitution of Eqs. (B.27) and (B.28) in Eq. (B.26) gives the equation for the variable high pressure case as:

$$-\beta_h v_h\, dP_h \quad C_{ph}\frac{dT}{T} = C_{pl}\frac{dT}{T}, \tag{B.30}$$

which simplifies to:

$$\frac{dP_h}{dT} = \frac{C_{ph} - C_{pl}}{\beta_h v_h T}. \tag{B.31}$$

Case 2. P_h **= constant**

Similarly if the low pressure is varied and the high pressure is kept constant, then

$$dP_h = 0, \tag{B.32}$$

and substitution in the second law now gives the governing equation for the variable low pressure case as:

$$-\beta_l v_l\, dP_l + C_{pl}\frac{dT}{T} = C_{ph}\frac{dT}{T}, \tag{B.33}$$

which simplifies to:

$$\frac{dP_l}{dT} = \frac{C_{pl} - C_{ph}}{\beta_l v_l T}. \tag{B.34}$$

Notice that for

$$\frac{dP}{dT} = 0, \tag{B.35}$$

$$C_{ph} = C_{pl}. \tag{B.36}$$

This is the condition for the turning point in the pressure versus temperature curves. The gradient is positive in the warm end and negative in the cold end for the constant low pressure case. Conversely, the gradient is negative in the warm end and positive in the cold end for the constant high pressure case as shown in Figs. 3.7 and 3.8 of Chapter 3.

The pressure is given in either case by direct numerical integration using Gauss quadrature and the thermophysical properties of helium from the NBS Technical Note 631.[90]

Thus for the variable high pressure we get

$$P_h - (P_h)_c = \int \frac{C_{ph} - C_{pl}}{\beta_h v_h T}\, dT, \qquad (B.35)$$

and for the variable low pressure we get the result

$$P_l - (P_l)_c = \int \frac{C_{pl} - C_{ph}}{\beta_l v_l T}\, dT. \qquad (3.28)$$

Typical curves for the pressure are shown in Chapter 3.

B2.2 Liquefaction mode

In the liquefaction mode the mass flow rate of the high pressure stream M_h is greater than the low pressure stream mass flow rate M. The second law of thermodynamics now gives:

$$M_l\, dS_l = M_h\, dS_h, \qquad (B.37)$$

which simplifies to

$$dS_l = \epsilon\, dS_h, \qquad (B.38)$$

where $\epsilon = M_h/M = 1 + M_{liq}/M$.

Then for P_l = constant,

$$\epsilon((-\beta_h v_h)dP_h + C_{ph}\frac{dT}{T}) = C_{pl}\left(\frac{dT}{T}\right), \tag{B.39}$$

which simplifies to:

$$\frac{dP_h}{dT} = \frac{C_{ph} - C_{pl}/\epsilon}{\beta_h v_h T}. \tag{B.40}$$

Similarly for P_h = constant,

$$(-\beta_l v_l)dP_l + C_{pl}\frac{dT}{T} = \epsilon C_{ph}\left(\frac{dT}{T}\right), \tag{B.41}$$

which simplifies to:

$$\frac{dP_l}{dT} = \frac{\epsilon C_{ph} - C_{pl}}{\beta_l v_l T}. \tag{B.42}$$

Integrating Eqs. B.40 and B.42 gives the variation of the high and low pressure values respectively as:

$$P_h - (P_h)_c = \int \frac{\left(C_{ph} - C_{pl}/\epsilon\right)}{\beta_h v_h T}, \tag{B.43}$$

and

$$P_l - (P_l)_c = \int \frac{(\epsilon C_{ph} - C_{pl})}{\beta_l v_l T}. \tag{B.44}$$

The gradients behave in the same way as before in both cases but the condition at the turning point, obtained by setting the pressure gradient to zero, now becomes

$$\epsilon C_{ph} = C_{pl}. \tag{B.45}$$

Thus the turning point temperature is now a function of the rate of liquid production and is always lower than the corresponding value for the refrigeration mode as explained in Chapter 3.

In this full-flow expansion model, the mass flow rate in either channel is constant. Therefore the mass flow rate ratio ϵ is also a constant.

Appendix C

In chapter 4, a continuum model for the precooling stage of the refrigeration cycle was introduced together with the results of the optimal distribution of the system parameters. In this appendix, details of the derivation of system equations as well as their solutions are presented. The analysis covers both refrigeration and liquefaction operating modes. An ideal gas model for the working fluid is first considered (appendix C1 details the refrigeration mode analysis and appendix C2 presents the parallel analysis for the liquefaction mode). The corresponding analyses for the real gas model are presented in appendices C3 and C4 for the refrigeration mode and the liquefaction mode respectively. Finally the analysis is repeated for an alternative expander arrangement for the ideal gas case (C5). Only the refrigeration mode version is presented. The liquefaction mode analyses, as demonstrated in C2 and C4 are similar to the refrigeration mode analyses differing only by the parameter ϵ which is the ratio of the mass flow rate of the high pressure stream to the mass flow rate of the low pressure stream.

C1 Ideal Gas Model: Refrigeration Mode

The model for the refrigeration mode is shown in Fig. 4.2(a) and described in Sec. 4.2. The fractional mass extracted from the high pressure stream is expanded in two steps: first through a reversible isothermal expander and then through a reversible adiabatic expander.

The governing equations for the continuum model, are derived based on the following assumptions:

1. The working fluid is an ideal gas;

2. The expansion process are reversible;

3. The pressure drop in the heat exchangers are negligible;

4. The overall heat transfer coefficient. U, is constant.

5. The pressure ratio is fixed.

The first law is first applied successively to the various processes and/or components.

Heat Balance for the stream gives:

$$\delta Q_h - \delta Q_l = \delta Q_T. \tag{C1.1}$$

The isothermal expansion process gives:

$$\delta Q_T = \delta W_T, \tag{C1.2}$$

$$\delta W_T = dMR(T + \Delta T)\ln\frac{P_h}{P_l}. \tag{C1.3}$$

Similarly,for the adiabatic expansion process,

$$\frac{P_l}{P_l} = \left(\frac{T + \Delta T}{T}\right)^{\frac{\gamma}{\gamma - 1}}. \tag{C1.4}$$

For the low pressure stream,

$$\delta Q_l = MC_p\,dT, \tag{C1.5}$$

and for the high pressure stream,

$$\delta Q_h = MC_p d(T + \Delta T). \tag{C1.6}$$

Also the heat exchanger heat balance is:

$$\delta Q_l = U\,d\Lambda\Delta T. \tag{C1.7}$$

Finally,the second law of thermodynamics gives the entropy balance in the form:

$$dS_{sys} = \frac{\delta Q}{T} - \frac{\delta Q}{T + \Delta T}. \qquad (C1.8)$$

These equations may be reduced to a system of three equations. Thus substitution in the heat balance for the streams gives an equation for the mass flow rate:

$$MC_p(dT + d\Delta T) - MC_p\,dT = dMRT(1 + \frac{\Delta T}{T})\Big[\ln(\frac{P_h}{P_h}) - \frac{\gamma}{\gamma - 1}\ln(1 + \frac{\Delta T}{T})\Big] \qquad (C1.9)$$

or equivalently,

$$\frac{dM}{M} = \frac{d(\Delta T)}{(\frac{R}{C_p})(1 + \frac{\Delta T}{T})[\ln\frac{P_h}{P_l} - \frac{\gamma}{\gamma - 1}\ln(1 + \frac{\Delta T}{T})]}. \qquad (C1.10a)$$

Similarly,the heat exchange rate equation reduces to:

$$U\,dA = \frac{MC_p\,dT}{\Delta T}. \qquad (C1.10b)$$

and the entropy balance becomes:

$$dS_{sys} = MC_p\Big(\frac{\Delta T}{T + \Delta T}\Big)\frac{dT}{T}. \qquad (C1.10c)$$

The three equations are further simplified when expressed in terms of the dimensionless parameters:

$$y = \frac{\Delta T}{T}$$

$$\eta = \ln \frac{T}{T_o}$$

$$\Psi = \ln \frac{M}{M_o}$$

$$\alpha = \frac{\gamma - 1}{\gamma}$$

$$= \frac{C_p}{R}$$

$$r_p = \frac{P_h}{P_l}$$

In terms of these parameters, the equations take the following form:

Continuity of mass flow:

$$d\Psi = \frac{(y + y')}{(1+y)[\frac{1}{\gamma}\ln r_p - \ln(1+y)]}\, d\eta \qquad (C1.11a)$$

Heat exchange area,

$$\frac{U\, dA}{M_o C_p} = \frac{\exp\Psi}{y}\, d\eta \qquad (C1.11b)$$

Entropy balance,

$$\frac{dS_{gen}}{M_o C_p} = \frac{y \exp\Psi}{1+y}\, d\eta \qquad (C1.11c)$$

A set of integral equations can now be obtained for the mass flow rate,the total heat exchange area and the total generated entropy respectively as:

$$\int_{\eta_o}^{\eta} \left[\frac{y + y'}{(1+y)[\beta - \ln(1+y)]} - \Psi \right] d\eta = \text{constant}, \qquad (C1.12a)$$

$$\frac{UA}{M_o C_p} = \int_{\eta_o}^{\eta} \frac{\exp\Psi}{y}\, d\eta, \qquad (C1.12b)$$

$$\frac{S_{gen}}{M_o C_p} = \int_{\eta_o}^{\eta} \frac{y \exp\Psi}{1+y}, \qquad (C1.12c)$$

where the constant β is given by the pressure ratio $\beta = \frac{1}{\alpha} \ln r_p$

Optimal precooling for this model then requires minimizing the generated entropy subject to continuity of mass flow and the total heat exchange area constraint (Eq. C1.12b). This is a classical variational calculus problem.

Variational calculus formulation

To minimize the total generated entropy

$$\frac{S_{gen}}{M_o C_p} = \int \frac{y \exp\Psi}{1+y}\, d\eta, \qquad (C1.13)$$

subject to the two constraints: equations (C1.12a) and (C1.12b), we define the functional with

$$I = \int (F + \lambda_1 G_1 + \lambda_2 G_2)\, d\eta, \qquad (C1.14)$$

where

$$F = \frac{y \exp \Psi}{1 + y}, \tag{C1.15a}$$

$$G_1 = \frac{\exp \Psi}{1 + y}, \tag{C1.15b}$$

and

$$G_2 = \frac{y + y'}{(1 + y)[\beta - \ln(1 + y)]} - \Psi'. \tag{C1.15c}$$

Thus

$$I = \int H(\eta, y, y', \Psi, \Psi')d\eta \tag{C1.16}$$

The Euler equations for this functional with two dependent variables (y, Ψ) and one independent variable η are:

$$\frac{\partial H}{\partial y} = \frac{d}{d\eta}\left(\frac{\partial H}{\partial y'}\right), \tag{C1.17a}$$

and

$$\frac{\partial H}{\partial \Psi} = \frac{d}{d\eta}\left(\frac{\partial H}{\partial \Psi'}\right). \tag{C1.17b}$$

The components of the Euler equation are first evaluated:

$$\frac{\partial H}{\partial \Psi} = \exp \Psi[\frac{y}{1+y} + \frac{\lambda_1}{y}]. \qquad (C1.18)$$

$$\frac{\partial H}{\partial \Psi'} = -\lambda_2. \qquad (C1.19)$$

$$\frac{d}{d\eta}\left(\frac{\partial H}{\partial \Psi'}\right) = 0. \qquad (C1.20)$$

$$\frac{\partial H}{\partial y} = \exp \Psi\left(\frac{1}{(1+y)^2} - \frac{\lambda_1}{y^2} + \frac{\lambda_2}{(1+y)[\beta - \ln(1+y)]} + \right.$$

$$\left. \frac{\lambda_2(y+y')}{(1+y)^2[\beta - \ln(1+y)]^2} - \frac{\lambda_2(y+y')}{(1+y)^2[\beta - \ln(1+y)]}\right). \qquad (C1.21)$$

$$\frac{\partial H}{\partial y'} = \frac{\lambda_2}{(1+y)[\beta - \ln(1+y)]}. \qquad (C1.22)$$

$$\frac{d}{d\eta}\left(\frac{\partial H}{\partial y'}\right) = \frac{\lambda_2 y'}{(1+y)^2[\beta - \ln(1+y)]^2} - \frac{\lambda_2 y'}{(1+y)^2[\beta - \ln(1+y)]}. \qquad (C1.23)$$

The equations describing the optimal performance of the model can now be obtained by direct substitution in the Euler equations. The results of substitution in equations C1.17(a and b) are given respectively by:

$$\exp \Psi[\frac{y}{1+y} + \frac{\lambda_1}{y}] = 0. \qquad (C1.24)$$

$$\exp\Psi\left(\frac{1}{(1+y)^2}-\frac{\lambda_1}{y^2}+\frac{\lambda_2}{(1+y)[\beta-\ln(1+y)]}+\frac{\lambda_2(y+y')}{(1+y)^2[\beta-\ln(1+y)]^2}-\right.$$

$$\left.\frac{\lambda_2(y+y')}{(1+y)^2[\beta-\ln(1+y)]}\right)+\frac{\lambda_2 y'}{(1+y)^2[\beta-\ln(1+y)]}-\frac{\lambda_2 y'}{(1+y)^2[\beta-\ln(1+y)]^2}=0. \quad (C1.25)$$

Solution

The resulting simple algebraic equation (Eq. C1.24) has the unique solution:

$$\frac{y}{1+y}+\frac{\lambda_1}{y}=0, \quad (C1.26)$$

since

$$\exp\Psi\neq 0$$

Equation $C1.26$ thus gives the distribution of y over the precooling temperature range in the quadratic form:

$$y^2+\lambda_1 y+\lambda_1=0 \quad (C1.27)$$

with the simple solution

$$y=\frac{-\lambda_1+\sqrt{\lambda_1^2-4\lambda_1}}{2}$$

$$=\text{constant} \quad (C1.28)$$

This constant value for y may be substituted into Eq. C1.2 to obtain the distribution of Ψ as a function of the Lagrange multiplier λ_1. Subsequently, the Lagrange multiplier λ_1 may be evaluated from the heat exchange area constraint (or the first law constraint) to complete the solution.

Alternatively, for a given constant value for y, the continuity equation may be integrated directly to give

$$\Psi = \Phi\eta \tag{C1.29}$$

where

$$\Phi = \frac{y}{(1+y)[\frac{1}{\alpha}\ln r_p - \ln(1+y)]} \tag{C1.30}$$

The initial conditions are Ψ_0 and $\eta_o = 0$.

Subsequently, the heat exchange area and the generated entropy are also obtained by direct integration after substituting for y and Ψ in equation C1.12b and C1.12c respectively:

$$\frac{AU}{M_oC_p} = \frac{1}{y}\int_{\eta_o}^{\eta} \exp\phi\eta\, d\eta \tag{C1.31a}$$

$$= \frac{\exp\phi\eta - 1}{\phi y}; \tag{C1.31b}$$

and

$$\frac{S_{gen}}{M_oC_p} = \frac{y}{1+y}\int_{\eta_o}^{\eta} \exp\phi\eta\, d\eta, \tag{C1.32a}$$

$$= \frac{y}{\phi(1+y)}[\exp\phi\eta - 1]. \qquad (C1.32b)$$

Substituting for the dimensionless variables gives the distribution of the heat exchange temperature difference ratio, the mass flow rate, heat exchange area and the generated entropy in terms of temperature:

$$\frac{\Delta T}{T} = \text{constant} \qquad (C1.33)$$

$$\frac{M}{M_o} = \left(\frac{T}{T_o}\right)^{\Phi} \qquad (C1.34)$$

$$\frac{AU}{M_o C_p} = \Phi_1\left[\left(\frac{T}{T_o}\right)^{\Phi} - 1\right] \qquad (C1.35)$$

$$\frac{S_{gen}}{M_o C_p} = \Phi_2\left[\left(\frac{T}{T_o}\right)^{\Phi} - 1\right] \qquad (C1.36)$$

where the scaling constants for the heat exchange area and the generated entropy are given respectively by:

$$\Phi_1 = \frac{1}{\Phi y} \qquad (C1.37)$$

$$\Phi_2 = \frac{y}{\Phi(1+y)} \qquad (C1.38)$$

and Φ is given by equation (1.30). These functions are shown and discussed in Chapter 4.

Appendix C2

Ideal Gas Model: Liquefaction Mode

In a liquefier,the mass flow rate of the high pressure stream M_h is higher than that of the low pressure stream M. Therefore the governing equations for the continuum precooling stage contains an extra variable, the mass flow rate ratio $\epsilon = M_h/M$ which is a function of temperature. This section gives detailed derivation of the governing equations for the precooling stage of a liquefaction cycle. The analysis is essentially a repeat of the derivation in Sec. C1 except for the parameter ϵ, and is based on the same assumptions.

Heat balance for the two streams gives:

$$\delta Q_h - \delta Q = \delta Q_T. \tag{C2.1}$$

The isothermal expansion process gives:

$$\delta Q_T = \delta W_T. \tag{C2.2}$$

$$\delta W_T = dMR(T + \Delta T)\ln\frac{P_h}{P_l}, \tag{C2.3}$$

Similarly for the adiabatic expansion process,

$$\frac{P_l}{P_l} = \left(\frac{T + \Delta T}{T}\right)^{\frac{\gamma}{\gamma-1}}. \tag{C2.4}$$

For the low pressure stream,

$$\delta Q = MC_p\,dT, \tag{C2.5}$$

and for the high pressure stream,

$$\delta Q_h = M_h C_p d(T + \Delta T). \tag{C2.6}$$

Also the heat exchange rate equation gives:

$$\delta Q = U\, dA\Delta T. \tag{C2.7}$$

Finally the second law of thermodynamics gives the entropy balance in the form:

$$dS_{gen} = \frac{\delta Q}{T} - \frac{\delta Q}{T + \Delta T} \tag{C2.8}$$

These equations may be reduced to a system of three equations. Thus substitution in the heat balance for the streams gives an equation for the mass flow rate:

$$\epsilon MC_p(dT + d\Delta T) - MC_p\, dT = dMRT(1 + \frac{\Delta T}{T})[ln(\frac{P_h}{P_l}) - \frac{\gamma}{\gamma - 1} ln(1 + \frac{\Delta T}{T})] \tag{C2.9}$$

or equivalently,

$$\frac{dM}{M} = \frac{\epsilon(dT + d(\Delta T)) - dT}{(\frac{R}{C_p})(1 + \frac{\Delta T}{T})[\ln \frac{P_h}{P_l} - \frac{\gamma}{\gamma - 1} \ln(1 + \frac{\Delta T}{T})]}. \tag{C2.10}$$

Similarly,the heat exchange rate equation reduces to:

$$U\, dA = \frac{MC_p\, dT}{\Delta T}, \tag{C2.11}$$

and the entropy balance becomes:

$$dS_{gen} = MC_p\left(\frac{\Delta T}{T + \Delta T}\right)\frac{dT}{T} \tag{C2.12}$$

where $\epsilon = M_h/M = 1 + M_{f,q}/M$.

The three equations are further simplified when expressed in terms of the following dimensionless parameters:

$$
\begin{aligned}
y &= \frac{\Delta T}{T};\\
\eta &= \ln\frac{T}{T_o};\\
\Psi &= \ln\frac{M}{M_o};\\
\alpha &= \frac{\gamma-1}{\gamma};\\
&= \frac{C_p}{R};\\
r_p &= \frac{P_h}{P_l};
\end{aligned}
$$

In terms of these parameters, the equations take the following form:

Continuity of mass flow:

$$d\Psi = \frac{\epsilon(1+y+y')-1}{(1+y)[\frac{1}{\alpha}\ln r_p - \ln(1+y)]}\,d\eta \qquad (C2.13)$$

Heat exchange area:

$$\frac{U\,dA}{M_oC_p} = \frac{\exp\Psi}{y}\,d\eta, \qquad (C2.14)$$

Entropy balance:

$$\frac{dS_{gen}}{M_oC_p} = \frac{y\exp\Psi}{1+y}\,d\eta, \qquad (C2.15)$$

A set of integral equations can now be obtained for the mass flow rate,the total heat exchange area and the total generated entropy respectively in the form:

$$\int_{\eta_o}^{\eta} [\frac{\epsilon(1+y+y')-1}{(1+y)[\beta-ln(1+y)]} - \Psi'] d\eta = \text{constant}, \qquad (C2.16)$$

$$\frac{UA}{M_o C_p} = \int_{\eta_o}^{\eta} \frac{\exp\Psi}{y} d\eta, \qquad (C2.17)$$

$$\frac{S_{gen}}{M_o C_p} = \int_{\eta_o}^{\eta} \frac{y \exp\Psi}{1+y} \qquad (C2.18)$$

where the constant β is given by the pressure ratio

$$\beta = \frac{1}{\alpha} \ln r_p. \qquad (C2.19)$$

Optimal precooling for this model then requires minimizing the generated entropy subject to continuity of mass flow and the total heat exchange area constraint (Eqs. C2.16 and C2.17). This is a classical variational calculus problem.

Variational Calculus Formulation

To minimize the total generated entropy

$$\frac{S_{gen}}{M_o C_p} = \int \frac{y \exp\Psi}{1+y} d\eta, \qquad (C2.20)$$

subject to the two constraints: equations (C2.16) and (C2.17), we define the functional with

$$I = \int (F + \lambda_1 G_1 + \lambda_2 G_2) d\eta, \qquad (C2.21)$$

where

$$F = \frac{y \exp \Psi}{1 + y}, \qquad (C2.22)$$

$$G_1 = \frac{\exp \Psi}{1 + y}, \qquad (C2.23)$$

and

$$G_2 = \frac{\epsilon(1 + y + y') - 1}{(1 + y)[\beta - ln(1 + y)]} - \Psi'. \qquad (C2.24)$$

Thus

$$I = \int H(\eta, y, y', \Psi, \Psi') d\eta \qquad (C2.25)$$

The Euler equations for this functional with two dependent variables (y, Ψ) and one independent variable η are:

$$\frac{\partial H}{\partial y} = \frac{d}{d\eta}\left(\frac{\partial H}{\partial y'}\right), \qquad (C2.26)$$

and

$$\frac{\partial H}{\partial \Psi} = \frac{d}{d\eta}\left(\frac{\partial H}{\partial \Psi'}\right). \tag{C2.27}$$

The components of the Euler equation are first evaluated:

$$\frac{\partial H}{\partial \Psi} = \exp \Psi[\frac{y}{1+y} + \frac{\lambda_1}{y}] \tag{C2.28}$$

$$\frac{\partial H}{\partial \Psi} = -\lambda_2 \tag{C2.29}$$

$$\frac{d}{d\eta}\left(\frac{\partial H}{\partial \Psi'}\right) = 0 \tag{C2.30}$$

$$\frac{\partial H}{\partial y} = \exp \Psi\left(\frac{1}{(1+y)^2} - \frac{\lambda_1}{y^2} + \frac{\lambda_2}{(1+y)[\beta - ln(1+y)]} + \right.$$

$$\left. \frac{\lambda_2[\epsilon(1+y+y')-1]}{(1+y)^2[\beta - ln(1+y)]^2} - \frac{\lambda_2[\epsilon(1+y+y')-1]}{(1+y)^2[\beta - ln(1+y)]}\right) \tag{C2.31}$$

$$\frac{\partial H}{\partial y'} = \frac{\lambda_2 \epsilon}{(1+y)[\beta - ln(1+y)]} \tag{C2.32}$$

$$\frac{d}{d\eta}\left(\frac{\partial H}{\partial y'}\right) = \frac{\epsilon \lambda_2 y'}{(1+y)^2[\beta - ln(1+y)]^2} - \frac{\epsilon \lambda_2 y'}{(1+y)^2[\beta - ln(1+y)]} +$$

$$\frac{\lambda_2 \epsilon'}{(1+y)[\beta - \ln(1+y)]}. \tag{C2.33}$$

The equations describing the optimal performance of the model can now be obtained by direct substitution in the Euler equations. The results of substitution in equation C2.27 is:

$$\exp\Psi[\frac{y}{1+y} + \frac{\lambda_1}{y}] = 0. \qquad (C2.34)$$

Solution

The resulting simple algebaic equation (Eq. C2.34) has the unique solution:

$$\frac{y}{1+y} + \frac{\lambda_1}{y} = 0, \qquad (C2.35)$$

since

$$\exp\Psi \neq 0 \qquad (C2.36)$$

Equation C2.35 thus gives the distribution of y over the precooling temperature range in the quadratic form:

$$y^2 + \lambda_1 y + \lambda_1 = 0 \qquad (C2.37)$$

with the simple solution

$$y = \frac{-\lambda_1 + \sqrt{\lambda_1^2 - 4\lambda_1}}{2}$$

$$= \text{constant} \qquad (C2.38)$$

For a given constant value for y, the first law equation may be integrated directly to give

$$\Psi = \frac{1+y}{\Phi}\int_{T_o}^{T} \epsilon\, d\eta - \frac{\eta}{\Phi} \qquad (C2.39)$$

where

$$\Phi = \frac{1}{(1+y)[\frac{1}{\alpha}\ln r_p - \ln(1+y)]} \qquad (C2.40)$$

The initial conditions are $\Psi_o = 0$ and $\eta_o = 0$.

Subsequently, the heat exchange area and the generated entropy are also obtained by direct integration after substituting for y and Ψ in equation C2.17 and C2.18, respectively. Thus

$$\frac{AU}{M_o C_p} = \frac{1}{y}\int_{\eta_o}^{\eta} \exp\Psi\, d\eta \qquad (C2.41)$$

and

$$\frac{S_{gen}}{M_o C_p} = \frac{y}{1+y}\int_{\eta_o}^{\eta} \exp\Psi\, d\eta, \qquad (C2.42$$

Substituting for the dimensionless variables gives the distribution of the heat exchange temperature difference ratio, mass flow rate, heat exchange area and the generated entropy in terms of temperature:

$$\frac{\Delta T}{T} = \text{constant} \tag{C2.43}$$

$$\ln \frac{M}{M_o} = \frac{1+y}{\Phi} \int_{T_o}^{T} \epsilon \frac{dT}{T} - \frac{1}{\Phi} \frac{T}{T_o}; \tag{C2.44}$$

$$\frac{AU}{M_o C_p} = \frac{1}{y} \int_{T_o}^{T} \frac{M}{M_o} \frac{dT}{T}; \tag{C2.45}$$

$$\frac{S_{gen}}{M_o C_p} = \frac{y}{1+y} \int_{T_o}^{T} \frac{M}{M_o} \frac{dT}{T} \tag{C2.46}$$

The parameter ϵ is a function of temperature which is not known a priori. An initial guess value is calculated from the mass flow rate distribution curve for the refrigeration mode.

The similarity between this result and that for the refrigeration mode can be seen clearly if the slowly varying parameter ϵ is assumed to be a constant. Then the integral equations for the mass flow rate, heat exchange area and generated entropy reduce to those obtained for the refrigeration mode. The scaling constants remain the same and the index Φ now depends on ϵ and is given by

$$\Phi = \frac{\epsilon(1+y) - 1}{(1+y)[\frac{1}{\alpha} \ln r_p - \ln(1+y)]} \tag{C2.46}$$

Real Gas Model: Refrigeration Mode

The continuum model for the precooling stage operating in the refrigeration mode (Fig. 4.2(a)) is now analyzed using a real gas model for the working fluid. Thus the system equations are derived based on the following assumptions:

1. Real gas model for the working fluid – variable specific heat.
2. The expansion processes are reversible.
3. The pressure drop in the heat exchangers is negligible.
4. The overall heat transfer coefficient, U, is constant.
5. The pressure ratio is fixed.

From these assumptions the following equations are derived for the model. The heat balance for the two streams gives:

$$\delta Q_h - \delta Q_l = \delta Q_T. \qquad (C3.1)$$

For the isothermal expansion process,

$$\delta Q_T = \delta W_T, \qquad (C3.2)$$

$$\delta W_T = (T + \Delta T)\Delta S dM, \qquad (C3.3)$$

and for the adiabatic expansion,

$$S_i = S_i. \qquad (C3.4)$$

Also for the low pressure stream,

$$\delta Q_l = MC_{pl}dT, \tag{C3.5}$$

and for the high pressure stream,

$$\delta Q_h = MC_{ph}d(T + \Delta T). \tag{C3.6}$$

Further the heat exchange rate equation gives:

$$\delta Q_l = UdA\Delta T, \tag{C3.7}$$

and the second law gives the entropy balance as:

$$dS_{gen} = \frac{\delta Q_l}{T} - \frac{\delta Q_l}{T + \Delta T}. \tag{C3.8}$$

Substitution in the heat balance equation gives the first law expression for the mass flow rate:

$$C_{ph}d(1 + \frac{\Delta T}{T}) - C_{pl}dT = \frac{dM}{M}(1 + \frac{\Delta T}{T})\Delta S. \tag{C3.9}$$

The heat exchange balance also simplifies to:

$$UdA = \frac{MC_{pl}dT}{\Delta T}, \tag{C3.10}$$

and the entropy balance reduces to:

$$dS_{gen} = \frac{MC_{pl}\Delta T}{T + \Delta T}\frac{dT}{T}. \qquad (C3.11)$$

In terms of the dimensionless mass flow rate Ψ, the heat exhange temperature difference ratio y and the temperature ratio η, these three equations become:

$$d\Psi = \frac{C_{ph}(1 + y + y') - C_{pl}}{(1 + y)\Delta S}d\eta. \qquad (C3.12)$$

$$\frac{UdA}{M_n C_{pn}} = \left(\frac{C_{pl}}{C_{pn}}\right)\frac{\exp\Psi}{y}d\eta. \qquad (C3.13)$$

$$\frac{dS_{gen}}{M_n C_{pn}} = \frac{C_{pl}}{C_{pn}}\frac{y\exp\Psi}{1 + y}d\eta. \qquad (C3.14)$$

where n denotes normalizing constant. Integrating these exprcssions over the precooling temperature range gives the following set of integral equations.

The total generated entropy is:

$$\frac{S_{gen}}{M_n C_{pn}} = \int_{\eta o}^{\eta}\frac{C_{pl}}{C_{pn}}\frac{\exp\Psi}{y}d\eta. \qquad (C3.15)$$

The total heat exchange area is

$$\frac{UA}{M_n C_{pn}} = \int_{\eta o}^{\eta}\frac{C_{pl}}{C_{pn}}\frac{\exp\Psi}{y}d\eta. \qquad (C3.16)$$

Continuity of mass flow rate:

$$\int_{\eta c}^{\eta'} \left[\Psi' - \frac{C_{ph}(1+y+y') - C_{pl}}{(1+y)\Delta S} \right] d\eta = constant. \qquad (C3.17)$$

Variational Calculus Formulation

The minimization of the generated entropy subject to the two integral constraints derived from the first law and the heat exchange area is again a classical variational calculus problem. Therefore define the functional H with

$$I = \int (F + \lambda_1 G_1 + \lambda_2 G_2) d\eta. \qquad (C3.18)$$

$$= \int H(\eta, y, y', \Psi, \Psi') d\eta. \qquad (C3.19)$$

where

$$F = \frac{C_{pl}}{C_{pn}} \frac{y \exp \Psi}{1+y}. \qquad (C3.20)$$

$$G_1 = \frac{C_{pl}}{C_{pn}} \frac{\exp \Psi}{y}. \qquad (C3.21)$$

and

$$G_2 = \frac{C_{ph}(1+y+y') - C_{pl}}{(1+y)\Delta S} - \Psi'. \qquad (C3.22)$$

The two Euler's equations for the variational calculus problem are:

$$\frac{\partial H}{\partial y} = \frac{d}{d\eta}\left(\frac{\partial H}{\partial \eta'}\right); \qquad (C3.23)$$

$$\frac{\partial H}{\partial \Psi} = \frac{d}{d\eta}\left(\frac{\partial H}{\partial \Psi'}\right). \qquad (C3.24)$$

The components of the Euler's equations are evaluated first:

$$\frac{\partial H}{\partial \Psi} = \frac{C_{pl}}{C_{pn}}\left[\frac{y \exp \Psi}{1+y} + \frac{\exp \Psi}{y}\right]; \tag{C3.25}$$

$$\frac{\partial H}{\partial \Psi'} = -\lambda_2; \tag{C3.26}$$

$$\frac{d}{d\eta}\left(\frac{\partial H}{\partial \Psi'}\right) = 0; \tag{C3.27}$$

$$\frac{\partial H}{\partial y} = \frac{C_{pl}}{C_{pn}} \exp \Psi\left\{\frac{1}{(1+y)^2} - \frac{\lambda_1}{y^2}\right\} + \frac{\lambda_2 C_{ph}}{(1+y)\Delta S} - \frac{C_{ph}(1+y+y') - C_{pl}}{(1+y)^2 \Delta S}; \tag{C3.28}$$

$$\frac{\partial H}{\partial y'} = \frac{\lambda_2 C_{ph}}{(1+y)\Delta S}; \tag{C3.29}$$

$$\frac{d}{d\eta}\left(\frac{\partial H}{\partial y'}\right) = \frac{\lambda_2}{1+y}\frac{d}{d\eta}\left(\frac{C_{ph}}{\Delta S}\right) - \frac{\lambda_2 C_{ph}}{(1+y)^2 \Delta S} y'. \tag{C3.30}$$

Then substitution in Eq. (C3.24) gives

$$\frac{C_{pl}}{C_{pn}} \exp \Psi\left\{\frac{y}{1+y} + \frac{1}{y}\right\} = 0. \tag{C3.31}$$

This is a simple algebraic equation with the solution

$$\frac{y}{1+y} + \frac{\lambda_1}{y} = 0 \quad \text{or} \quad y = \textit{constant}, \tag{C3.32}$$

since

$$\frac{C_{pl}}{C_{pn}} \exp \Psi \neq 0. \tag{C3.33}$$

By analogy with the ideal gas analysis, the distribution of the performance parameters are given by direct substitution into Eqs. (C3.15 - C3.17) resulting in the simple integral expressions:

$$\frac{S_{gen}}{M_n C_{pn}} = \frac{y}{1+y} \int_{\eta o}^{\eta} \frac{C_{pl}}{C_{pn}} \exp \Psi d\eta; \tag{C3.34}$$

$$\frac{AU}{M_n C_{pn}} = \frac{1}{y} \int_{\eta o}^{\eta} \frac{C_{pl}}{C_{pn}} \exp \Psi d\eta; \tag{C3.35}$$

$$\Psi = \ln \frac{M}{M_n} = \int_{\eta o}^{\eta} \frac{C_{pn}(1+y) - C_{pl}}{(1+y)\Delta S} d\eta; \tag{C3.36}$$

In terms of the physical variables of the problem the following optimal distribution of the performance parameters are obtained.

The mass flow rate is given as:

$$\frac{M}{M_n} = \exp \int_{To}^{T} \frac{C_{ph} - \chi C_{pl}}{S_i - S_n} \frac{dT}{T}. \tag{C3.37}$$

The total heat exchange area is also given as:

$$\frac{AU}{M_n C_{pn}} = \frac{1}{M_n C_{pn} y} \int_{To}^{T} \frac{M C_{pl}}{T} dT. \tag{C3.38}$$

Finally, the total generated entropy becomes:

$$\frac{S_{gen}}{M_n C_{pn}} = \frac{y}{M_n C_{pn}(1+y)} \int_{To}^{T} \frac{MC_{pl}}{T} dT. \qquad (C3.39)$$

The constant χ depends on the temperature difference ratio y:

$$\chi = \frac{1}{1+y}. \qquad (C3.40)$$

These equations are integrated numerically using a Gauss quadrature algorithm and the results are as presented in Section 4.4.2.

Appendix C4

Real Gas Model: Liquefaction Mode

Again the higher mass flow rate of the high pressure stream for the liquefier requires that the model be analyzed for the liquefaction mode. The same assumptions for the real gas model discussed in the preceeding section form the basis for deriving the following equations.

The heat balance for the two streams gives:

$$\delta Q_h - \delta Q_l = \delta Q_T. \qquad (C4.1)$$

For the isothermal expansion process,

$$\delta Q_T - \delta W_T. \qquad (C4.2)$$

$$\delta W_T = (T + \Delta T)\Delta S dM. \qquad (C4.3)$$

Also for the adiabatic expansion process,

$$S_i = S. \qquad (C4.4)$$

Further for the low pressure stream,

$$\delta Q_l = MC_{pl}dT. \qquad (C4.5)$$

Similarly, for the high pressure stream,

$$\delta Q_h = M_h C_{ph} d(T + \Delta T). \qquad (C4.6)$$

The heat exchange rate equation gives:

$$\delta Q = U dA \Delta T. \qquad (C4.7)$$

Finally the second law gives the entropy balance as:

$$dS_{gen} = \frac{\delta Q}{T} - \frac{\delta Q}{T + \Delta T}. \qquad (C4.8)$$

Let

$$\epsilon = \frac{M_h}{M}. \qquad (C4.9)$$

Then substitution in the heat balance equation gives the first law expression for the mass flow rate:

$$\epsilon C_{ph} d(T + \Delta T) - C_{pl} dT = \frac{dM}{M}(T + \Delta T)\Delta S. \qquad (C4.10)$$

The heat exchange balance also simplifies to

$$U dA = \frac{M C_{pl} dT}{\Delta T}. \qquad (C4.11)$$

The entropy balance also reduces to:

$$dS_{gen} = \frac{M C_{pl} \Delta T}{T + \Delta T} \frac{dT}{T}. \qquad (C4.12)$$

In terms of the dimensionless variables y, Ψ, η these equations become respectively:

$$d\Psi = \frac{\epsilon C_{pn}(1+y+y') - C_{pl}}{(1+y)\Delta S} d\eta. \qquad (C4.13)$$

$$\frac{UdA}{M_n C_{pn}} = \left(\frac{C_{pl}}{C_{pn}}\right) \frac{\exp\Psi}{y} d\eta. \qquad (C4.14)$$

$$\frac{dS_{gen}}{M_n C_{pn}} = \frac{C_{pl}}{C_{pn}} \frac{y \exp\Psi}{1+y} d\eta. \qquad (C4.15)$$

where n denotes normalizing constant. Again intergrating these expressions over the precooling temperature range gives the total generated entropy, the total heat exchange area and the continuity equations in the form:

$$\frac{S_{gen}}{M_n C_{pn}} = \int_{\eta o}^{\eta} \frac{C_{pl}}{C_{pn}} \frac{\exp\Psi}{y} d\eta. \qquad (C4.16)$$

$$\frac{UA}{M_n C_{pn}} = \int_{\eta o}^{\eta} \frac{C_{pl}}{C_{pn}} \frac{\exp\Psi}{y} d\eta. \qquad (C4.17)$$

$$\int_{\eta o}^{\eta} \left[\Psi' - \frac{\epsilon C_{pn}(1+y+y') - C_{pl}}{(1+y)\Delta S}\right] d\eta = constant. \qquad (C4.18)$$

Variational Calculus Formulation

The minimization of the generated entropy subject to the two integral constraints:continuity of mass flow rate: and fixed total heat exchange area is again a classical variational calculus problem. Therefore define the functional H with

$$I = \int (F + \lambda_1 G_1 + \lambda_2 G_2) d\eta. \qquad (C4.19)$$

$$= \int H(\eta, y, y', \Psi, \Psi') d\eta. \qquad (C4.20)$$

where

$$F = \frac{C_{pl}}{C_{pn}} \frac{y \exp \Psi}{1 + y}. \qquad (C4.21)$$

$$G_1 = \frac{C_{pl}}{C_{pn}} \frac{\exp \Psi}{y}. \qquad (C4.22)$$

and

$$G_2 = \frac{\epsilon C_{ph}(1 + y + y') - C_{pl}}{(1 + y)\Delta S} - \Psi'. \qquad (C4.23)$$

The two Euler's equations for the problem are:

$$\frac{\partial H}{\partial y} = \frac{d}{d\eta}\left(\frac{\partial H}{\partial \eta'}\right). \qquad (C4.24)$$

$$\frac{\partial H}{\partial \Psi} = \frac{d}{d\eta}\left(\frac{\partial H}{\partial \Psi'}\right). \qquad (C4.25)$$

First we evaluate the components of the Euler equations:

$$\frac{\partial H}{\partial \Psi} = \frac{C_{pl}}{C_{pn}}\left[\frac{y \exp \Psi}{1+y} + \frac{\exp \Psi}{y}\right]. \tag{C4.26}$$

$$\frac{\partial H}{\partial \Psi'} = -\lambda_2. \tag{C4.27}$$

$$\frac{d}{d\eta}\left(\frac{\partial H}{\partial \Psi'}\right) = 0. \tag{C4.28}$$

$$\frac{\partial H}{\partial y} = \frac{C_{pl}}{C_{pn}} \exp \Psi \left\{\frac{1}{(1+y)^2} - \frac{\lambda_1}{y^2}\right\} + \frac{\lambda_2 \epsilon C_{ph}}{(1+y)\Delta S} - \frac{\epsilon C_{ph}(1+y+y') - C_{pl}}{(1+y)^2 \Delta S}. \tag{C4.29}$$

$$\frac{\partial H}{\partial y'} = \frac{\lambda_2 \epsilon C_{ph}}{(1+y)\Delta S}. \tag{C4.30}$$

$$\frac{d}{d\eta}\left(\frac{\partial H}{\partial y'}\right) = \frac{\lambda_2}{1+y}\frac{d}{d\eta}\left(\frac{\epsilon C_{ph}}{\Delta S}\right) - \frac{\lambda_2 \epsilon C_{ph}}{(1+y)^2 \Delta S} y'. \tag{C4.31}$$

Then substitution in Eq. (C4.25) gives

$$\frac{C_{pl}}{C_{pn}} \exp \Psi \left\{\frac{y}{1+y} + \frac{1}{y}\right\} = 0. \tag{C4.32}$$

This is a simple algebraic equation for y with the solution

$$\frac{y}{1+y} + \frac{\lambda_1}{y} = 0 \quad \text{or} \quad y = \text{constant}, \tag{C4.33}$$

since

$$\frac{C_{pl}}{C_{pn}} \exp \Psi \neq 0. \tag{C4.34}$$

By analogy with the ideal gas model analysis, the distribution of the performance parameters are given by direct substitution into Eqs. (C4.16 - C4.18) to give

$$\frac{S_{gen}}{M_n C_{pn}} = \frac{y}{1+y} \int_{\eta o}^{\eta} \frac{C_{pl}}{C_{pn}} \exp \Psi d\eta. \tag{C4.35}$$

$$\frac{AU}{M_n C_{pn}} = \frac{1}{y} \int_{\eta o}^{\eta} \frac{C_{pl}}{C_{pn}} \exp \Psi d\eta. \tag{C4.36}$$

$$\Psi = \ln \frac{M}{M_n} = \int_{\eta o}^{\eta} \frac{\epsilon C_{ph}(1+y) - C_{pl}}{(1+y)\Delta S} d\eta. \tag{C4.37}$$

In terms of the physical variables of the problem, the performance curves are derived.

The mass flow rate is given as:

$$\frac{M}{M_n} = \exp \int_{To}^{T} \frac{\epsilon C_{ph} - \chi C_{pl}}{S_i - S_h} \frac{dT}{T}. \tag{C4.38}$$

The total heat exchange area is also given as:

$$\frac{AU}{M_n C_{pn}} = \frac{1}{M_n C_{pn} y} \int_{To}^{T} \frac{M C_{pl}}{T} dT. \tag{C4.39}$$

Finally, the total generated entropy is given as:

$$\frac{S_{gen}}{M_n C_{pn}} = \frac{y}{M_n C_{pn}(1+y)} \int_{To}^{T} \frac{MC_{pl}}{T} dT. \qquad (C4.40)$$

where

$$x = \frac{1}{1+y}. \qquad (C4.41)$$

These equations are integrated numerically using a Gauss quadrature algorithm and the results are as presented in Section 4.4.2. The mass flow rate ratio ϵ is a function of temperature and is not known a priori. An initial guess is calculated from the results for the refrigeration mode. The mass flow rate for the liquefaction mode obtained is then used for the next iteration on ϵ. The solution converges in about four iterations.

Ideal Gas Model: Refrigeration Mode, Alternative Expander Arrangement

It was stated in chapter 4 that the order of the isothermal and adiabatic expanders in the model does not affect the principal results of the analysis. The analysis to validate the assertion is now presented. This alternative model is shown in Fig. 4.2(b) and the assumptions for the analysis are:

1. The working fluid is an ideal gas;
2. The expansion processes are reversible;
3. The pressure drop in the heat exchangers are negligible;
4. The overall heat transfer coefficient, U, is constant.
5. The pressure ratio is fixed.

To derive the governing equations, the first law is first applied successively to the various processes/components as follows.

The heat balance for the two streams gives:

$$\delta Q_h - \delta Q_l = \delta Q_T. \tag{C5.1}$$

For the isothermal expansion process,

$$\delta Q_T = \delta W_T; \tag{C5.2}$$

$$\delta W_T = dMR(T + \Delta T)\ln\frac{P_i}{P_h}. \tag{C5.3}$$

Also for the adiabatic expansion process,

$$\frac{P_h}{P_i} = \left(\frac{T + \Delta T}{T}\right)^{\frac{\gamma}{\gamma - 1}}. \tag{C5.4}$$

Further for the low pressure stream,

$$\delta Q_l = MC_p\, dT. \tag{C5.5}$$

Similarly, for the high pressure stream,

$$\delta Q_h = MC_p d(T + \Delta T). \tag{C5.6}$$

The heat exchange rate equation is given as:

$$\delta Q_h = U\, dA\Delta T. \tag{C5.7}$$

Finally the second law gives the entropy balance as:

$$dS_{gen} = \frac{\delta Q_h}{T} - \frac{\delta Q_h}{T + \Delta T}. \tag{C5.8}$$

These equations may be reduced to a system of three equations.

Continuity of mass flow rate gives:

$$MC_p(dT + d\Delta T) - MC_p\, dT = dMRT[\ln(\frac{P_h}{P_h}) - \frac{\gamma}{\gamma - 1} ln(1 + \frac{\Delta T}{T})]. \tag{C5.9}$$

or equivalently,

$$\frac{dM}{M} = \frac{d(\Delta T)}{(\frac{R}{C_p})[ln\frac{P_h}{P_l} - \frac{\gamma}{\gamma - 1} ln(1 + \frac{\Delta T}{T})]}. \tag{C5.10a}$$

Also the heat exchange rate equation becomes:

$$U\,dA = \frac{MC_p\,(dT + d(\Delta T)}{\Delta T}. \qquad (C5.10b)$$

The entropy balance reduces to:

$$dS_{gen} = MC_p\left(\frac{\Delta T}{T + \Delta T}\right)\frac{d(T + \Delta T)}{T}. \qquad (C5.10c)$$

The three equations are further simplified when expressed in terms of the dimensionless parameters:

$$y = \frac{\Delta T}{T}$$

$$\eta = ln\frac{T}{T_o}$$

$$\Psi = \ln\frac{M}{M_o}$$

$$\alpha = \frac{\gamma - 1}{\gamma}$$

$$= \frac{C_p}{R}$$

$$r_p = \frac{P_h}{P_l}$$

In terms of these parameters, the equations take the following form:

Continuity of mass flow rate:

$$d\Psi = \frac{(y + y')}{[\frac{1}{\gamma}\ln r_p - \ln(1 + y)]}\,d\eta. \qquad (C5.11a)$$

The heat exchange area becomes:

$$\frac{U\,dA}{M_o C_p} = \frac{(1+y+y')\exp\Psi}{y}\,d\eta. \qquad (C5.11b)$$

The entropy balance simplifies to:

$$\frac{dS_{gen}}{M_o C_p} = \frac{y(1+y+y')\exp\Psi}{1+y}\,d\eta. \qquad (C5.11c)$$

A set of integral equations can now be obtained for the mass flow rate, heat exchange area and the entropy respectively as:

$$\int_{\eta_c}^{\eta} [\frac{y+y'}{[\beta - \ln(1+y)]} - \Psi']d\eta = constant. \qquad (C5.12a)$$

$$\frac{UA}{M_o C_p} = \int_{\eta_o}^{\eta} \frac{(1+y+y')\exp\Psi}{y}\,d\eta. \qquad (C5.12b)$$

$$\frac{S_{gen}}{M_o C_p} = \int_{\eta_o}^{\eta} \frac{y(1+y+y')\exp\Psi}{1+y}. \qquad (C5.12c)$$

where

$$\beta = \frac{1}{\alpha}\ln r_p$$

Optimal precooling for this model then requires minimizing the generated entropy subject to continuity of mass flow rate and a fixed total heat exchange area the heat exchange area constraint (Eq. C5.12b). This is a classical variational calculus problem.

Variational calculus formulation

To minimize

$$\frac{S_{gen}}{M_o C_p} = \int \frac{y(1+y+y')\exp\Psi}{1+y}\, d\eta. \qquad (C5.13)$$

subject to the two constraints: equations (C5.12a) and (C5.12b), we define the functional with

$$I = \int (F + \lambda_1 G_1 + \lambda_2 G_2)\, d\eta. \qquad (C5.14)$$

where

$$F = \frac{y(1+y+y')\exp\Psi}{1+y}. \qquad (C5.15a)$$

$$G_1 = \frac{(1+y+y')\exp\Psi}{1+y}. \qquad (C5.15b)$$

and

$$G_2 = \frac{y+y'}{[\beta - \ln(1+y)]} - \Psi'. \qquad (C5.15c)$$

Thus

$$I = \int H(\eta, y, y', \Psi, \Psi')\, d\eta. \qquad (C5.16)$$

The Euler equations for this functional with two dependent variables (y, Ψ) and one independent variable η are:

$$\frac{\partial H}{\partial y} = \frac{d}{d\eta}\left(\frac{\partial H}{\partial y'}\right); \tag{C5.17}$$

$$\frac{\partial H}{\partial \Psi} = \frac{d}{d\eta}\left(\frac{\partial H}{\partial \Psi'}\right). \tag{C5.18}$$

The components of the Euler equation are first evaluated

$$\frac{\partial H}{\partial \Psi} = (1 + y + y')\exp\Psi[\frac{y}{1+y} + \frac{\lambda_1}{y}]. \tag{C5.19}$$

$$\frac{\partial H}{\partial \Psi'} = -\lambda_2. \tag{C5.20}$$

$$\frac{d}{d\eta}\left(\frac{\partial H}{\partial \Psi'}\right) = 0. \tag{C5.21}$$

The equations describing the optimal performance of the model can now be obtained by direct substitution in the Euler equation:

$$\frac{\partial H}{\partial \Psi} = \frac{d}{d\eta}\left(\frac{\partial H}{\partial \Psi'}\right). \tag{C5.22}$$

giving

$$(1 + y + y')\exp\Psi[\frac{y}{1+y} + \frac{\lambda_1}{y}] = 0. \tag{C5.23}$$

Solution

The resulting equation (Eq. C5.24) has two solutions:

$$\frac{y}{1+y} + \frac{\lambda_1}{y} = 0. \qquad (C5.24)$$

$$1 + y + y' = 0. \qquad (C5.25)$$

since

$$\exp \Psi \neq 0. \qquad (C5.26)$$

Equation C5.26 thus gives the distribution of y over the precooling temperature range in the quadratic form:

$$y^2 + \lambda_1 y + \lambda_1 = 0. \qquad (C5.27)$$

with the simple solution

$$y = \frac{-\lambda_1 + \sqrt{\lambda_1^2 - 4\lambda_1}}{2}$$

$$= \text{constant} \qquad (C5.28)$$

The differential equation for y can be rearranged into:

$$\frac{dy}{d\eta} = -(1+y). \qquad (C5.29)$$

which can then be integrated by the method of seperation of variables to give:

$$\ln\left[\frac{1+y}{(1+y_o)}\right] = -\eta \qquad (C5.30)$$

In terms of the temperature ratio the equation becomes:

$$ln\left[\frac{(1+y)}{(1+y_o)}\right] = -ln\frac{T}{T_o} \qquad (C5.31)$$

which gives

$$1+y = (1+y_o)\frac{T_o}{T} \qquad (C5.32)$$

or, in terms of the physical variables

$$\frac{\Delta T}{T} = [1+(\Delta T/T)_o]\frac{T_o}{T} - 1 \qquad (C5.33)$$

Thus $\Delta T/T < 0$ for $T > (T+\Delta T)_o$. Since $\Delta T/T$ must be positive for all values of T, the solution for y given by the differential equation is inadmissible. Consequently, the optimal distribution of $\Delta T/T$ must be given by equation C5.28 i.e.,

$$\frac{\Delta T}{T} = \text{constant} \qquad (C5.34)$$

For a given constant value for $\Delta T/T$, the first law equation may be integrated directly to give

$$\Psi = \Phi\eta. \qquad (C5.35)$$

where

$$\Phi = \frac{y}{[\frac{1}{\alpha}\ln r_p - \ln(1+y)]}. \qquad (C5.36)$$

The initial conditions are $\Psi_o = 0$ and $\eta_o = 0$.

Subsequently, the heat exchange area and the generated entropy are also obtained by direct integration after substituting for y and Ψ in Eqs. C5.12b, C5.12c. Thus

$$\frac{AU}{M_o C_p} = \frac{1+y}{y}\int_{\eta_o}^{\eta} \exp\Phi\eta\, d\eta \qquad (C5.37a)$$

$$= \frac{(1+y)(\exp\Phi\eta - 1)}{\Phi y} \qquad (C5.37b)$$

and

$$\frac{S_{gen}}{M_o C_p} = y\int_{\eta_o}^{\eta} \exp\Phi\eta\, d\eta. \qquad (C5.38a)$$

$$= \frac{y}{\Phi}[\exp\Phi\eta - 1]. \qquad (C5.38b)$$

Substituting for the dimensionless variables gives the distribution of the heat exchange temperature difference ratio,the mass flow rate, the heat exchange area and the generated entropy in terms of temperature in that order as:

$$\frac{\Delta T}{T} = constant; \qquad (C5.39)$$

$$\frac{M}{M_o} = \left(\frac{T}{T_o}\right)^{\Phi}; \qquad (C5.40)$$

$$\frac{AU}{M_o C_p} = \Phi_1[\left(\frac{T}{T_o}\right)^{\Phi} - 1]; \qquad (C5.41)$$

$$\frac{S_{gen}}{M_o C_p} = \Phi_2[\left(\frac{T}{T_o}\right)^{\Phi} - 1, \qquad (C5.42)$$

where

$$\Phi_1 = \frac{(1+y)}{\Phi y}. \qquad (C5.43)$$

$$\Phi_2 = \frac{y}{\Phi}. \qquad (C5.44)$$

and Φ is given by Eq. C5.36. Thus as noted in Chapter 4, the optimal distribution of the performance parameters is independent of the expander arrangement. Only the scaling constants change to account for the difference in the thermal duty for the two models.

Appendix D

SAMPLE COMPUTER PROGRAM FOR PARAMETRIC OPTIMIZATION

The final stage of the design algorithm outlined in Chap. 4 involved choosing the cycle temperature levels by a parametric optimization technique. The program for solving this mathematical optimization problem (analyzing a particular configuration) may be grouped into three(major) classes: an input data file , a main (driver) program, and a set of sub-programs. The structure is demonstrated by the sample analysis for the configuration shown in Fig. D.

An annotated listing of the input file COLD1H DATA, the main program COLD1 and a partial list of the subprograms used are given. For a typical run, the appropriate input parameters are defined by changes in the input data file. The analysis is then initiated by the exec command COLD1H. This exec command loads all the files required for the analysis and generates an output file OUTPUT COLD1H. A listing of the exec file COLD1H EXEC is as follows:

GLOBAL VFORTLIB FORTVS FILEDEF 8 DISK COLD1H DATA A1 FILEDEF 6 DISK OUTPUT COLD1H(RECFM FB LRECL 132 BLOCK264 LOAD COLD1 XPAND WETXP OPTIM1 CAREA HELIUM (START

The subroutine HELIUM is the program for calculating the properties of helium. It is basically the NBS helium properties package with additional subroutines from the MIT Cryogenic Engineering Laboratory.

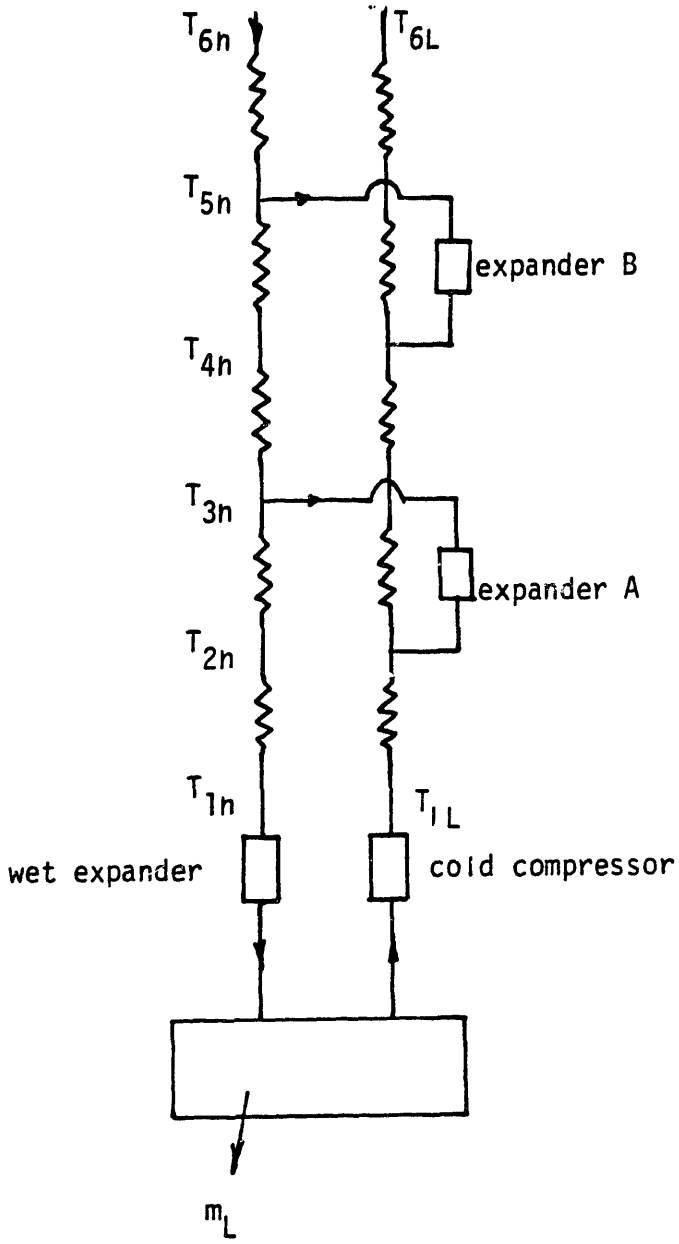


FIG. D COLD END CONFIGURATION OF AN SVC CYCLE.

```
39.784,39.891,39.905,39.932,39.955,39.980,40.0,4.0,27.0,65.0,
20.0,80.0,78.0,3,3,1.0,1.0,0.86,0.82,0.90,0.85,
9.711,30.13,8.287,3.454,6,1,5,0.01
```

EXPLANATORY NOTE.

THE DATA FILE CONTAINS THE FOLLOWING VALUES IN THE GIVEN ORDER:
PH(1), PH(2), PH(3), PH(4), PH(5), PH(6), PH(7), PL(1), TM1, TM2,
QL, TH(6), TL(6), ISV1, ISV2, DELTA1, DELTA2, ETA1, ETA2, ETAW, ETACC,
HF, HG, SG, SF, ITOTAL, JSTPIN,NHXS,PRATIO.

THE DEFINITION OF THESE VARIABLES ARE:

PH(I) = PRESSURE AT STATE POINT I IN HIGH PRESSURE CHANNEL.
PL(1) =PRESSURE IN COLD CHANNEL:THIS EQUALS PRESSURE AT STATE POINT 1
TM1 =STARTING VALUE FOR EXPANDER A INLET TEMP. THIS IS INCREMENTED
IN STEPS OF DELTA1 FOR ISV1 TIMES TO COMPUTE SETS OF VALUES
OF THE EXPANDER PARAMETERS IN SUBPROGRAM XPAND.
QL =MASS FLOW RATE OF LIQUID PRODUCED (G/S)
TH(I) =TEMP. AT STATE POINT I FOR HOT STREAM.
TL(I) =TEMP. AT STATE POINT I FOR COLD STREAM.
ETA1 =EXPANDER A ISENTROPIC EFFICIENCY.
ETA2 =EXPANDER B ISENTROPIC EFFICIENCY.
ETAW =WET EXPANDER ISENTROPIC EFFICIENCY.
ETACC =COLD COMPRESSOR ISENTROPIC EFFICIENCY.
HF =SATURATED LIQUID ENTHALPY AT LIQUID RESERVOIR PRESSURE.
HG =SATURATED VAPOR ENTHALPY AT LIQUID RESERVOIR PRESSURE.
SG =SATURATED VAPOR ENTROPY AT LIQUID RESERVOIR PRESSURE.
SF =SATURATED LIQUID ENTROPY AT LIQUID RESERVOIR PRESSURE.
ITOTAL=TOTAL NUMBER OF STATE POINTS FOR THE CYCLE.
JSTPTN=STATE POINT NUMBER FOR SET OF HEAT EXCHANGERS IN SERIES. THIS
IS REQUIRED IN SUBPROGRAM HTAREA.
NHXS =NUMBER OF HEAT EXCHANGERS IN SERIES (REQUIRED IN SUBPROGRAM HTAREA).
PRATIO=RATIO OF PRESSURE DROP TO TOTAL PRESSURE IN COLD CHANNEL FOR EACH
HEAT EXCHANGER.

```
C
C     MAIN(DRIVER) PROGRAM FOR COLD END CONFIGURATION C1.                    COL00010
C                                                                            COL00020
      COMMON PH,PL                                                           COL00030
      COMMON/OPTI/TH,TL,AMH,AML,HH,HL,QL                                     COL00040
      COMMON/ITER/T1H,AMV,T3H,H1H,H2H,H2L                                    COL00050
      COMMON/MASS/H3H,H4H,H4L,H5H,T5H,T4H,T4L,T2L,T2H                        COL00060
      COMMON/HXPROP/AREAL,AREAH,PDROPL,PDROPH,ANTUT,AFR,AL,TAFR,TAREA,       COL00070
     1TAREAM,TAREAC,CHX                                                      COL00080
      COMMON/LIQCON/HF,HG,SF,SG,ETAW,ETACC                                   COL00090
      DIMENSION HH(20),HL(20),TH(20),TL(20),AMH(20),AML(20),SH(20),SGENX     COL00100
     1 (20),DH(20),DL(20),SL(20),A(20,20),DELTA(20)                          COL00110
     1   ,H3H(20),H4H(20),H4L(20),T3H(20),T4H(20),T4L(20),H5H(20),           COL00120
     1 H2H(20),H2L(20),T2H(20),T2L(20),T5H(20),T1H(20),H1H(20),AMV(20),      COL00130
     1 CT1H(20),CH1H(20),T3L(20),T5L(20),PH(20),PL(20),PDROP(20)             COL00140
C                                                                            COL00150
C     INPUT DATA                                                             COL00160
C                                                                            COL00170
      WRITE(6,50)                                                            COL00180
50    FORMAT(1H1,10X,'**********  COLD END RESULTS **********')              COL00190
      READ(8,*)(PH(I),I=1,7),PLOW,TM1,TM2,QL,TH(6),TL(6),ISV1,ISV2,          COL00200
     1DELTA1,DELTA2,ETA1,ETA2,ETAW,ETACC,HF,HG,SG,SF,ITOTAL,JSTPIN,NHXS,     COL00210
     1PRATIO                                                                 COL00220
        DO 231 I=1,7                                                         COL00230
      PL(I)=(0.99**(I-1))*PLOW                                               COL00240
231   CONTINUE                                                               COL00250
C                                                                            COL00260
C     CALCULATE UNCHANGING VALUES:STATE POINTS 6 & 1L(COLD COMPRESSOR        COL00270
C     DISCHARGE CONDITION).                                                  COL00280
C                                                                            COL00290
      DH(6)=FINDD(PH(6),TH(6))                                               COL00300
      DL(6)=FINDD(PL(6),TL(6))                                               COL00310
      HH(6)=ENTHAL(DH(6),TH(6))                                              COL00320
      HL(6)=ENTHAL(DL(6),TL(6))                                              COL00330
      SL(6)=ENTROP(DL(6),TL(6))                                              COL00340
      SH(6)=ENTROP(DH(6),TH(6))                                              COL00350
      T=7.0                                                                  COL00360
      R=FINDD(PL(1),T)                                                       COL00370
      CALL CALCPS(PL(1),SG,R,T)                                              COL00380
      HS=ENTHAL(R,T)                                                         COL00390
      HL(1)=HG+(HS-HG)/ETACC                                                 COL00400
      CALL CALCHP(HL(1),PL(1),R,T)                                           COL00410
      TL(1)=T                                                                COL00420
C                                                                            COL00430
C     EXPANDER 1(BOTTOM EXP.) CALCULATION USING SUBROUTINE XPAND             COL00440
C     EXPANDER INLET TEMPERATURE TM1 IS INCREMENTED IN STEPS OF DELTA1       COL00450
C     ISV1 TIMES TO COMPUTE SETS OF VALUES OF EXPANDER EXIT CONDITIONS       COL00460
C     CORRESPONDING TO EACH INLET TEMP                                       COL00470
C                                                                            COL00480
      WRITE(6,121)                                                           COL00490
           (6,122)                                                           COL00500
      WRITE(6,123)                                                           COL00510
      WRITE(6,120)                                                           COL00520
121   FORMAT(/4X,'-------------------------------------------------')        COL00530
123   FORMAT(4X,'-------------------------------------------------')         COL00540
                                                                             COL00550
```

```
122   FORMAT(4X,'EXPANDER A PARAMETERS: RESULTS FROM SUBROUTINE XPAND') COL00560
120   FORMAT(/5X,'T3H',7X,'T2H',7X,'T2L',7X,'H3H',7X,'H2H',7X,'H2L')    COL00570
      CALL XPAND(3,2,TM1,ETA1,ISV1,DELTA1,A)                           COL00580
       DO 10 K=1,ISV1                                                  COL00590
      H3H(K)=A(K,4)                                                    COL00600
      H2H(K)=A(K,5)                                                    COL00610
      H2L(K)=A(K,6)                                                    COL00620
      T3H(K)=A(K,1)                                                    COL00630
      T2H(K)=A(K,2)                                                    COL00640
      T2L(K)=A(K,3)                                                    COL00650
10    CONTINUE                                                         COL00660
C                                                                      COL00670
C     EXPANDER 2(MIDDLE EXP.) CALCULATION USING SUBROUTINE XPAND       COL00680
C     EXPANDER INLET TEMPERATURE TM2 IS INCREMENTED IN STEPS OF DELTA2 COL00690
C     ISV2 TIMES TO COMPUTE SETS OF VALUES OF EXPANDER EXIT CONDITIONS COL00700
C     CORRESPONDING TO EACH INLET TEMP                                 COL00710
                                                                       COL00720
      WRITE(6,121)                                                     COL00730
      WRITE(6,221)                                                     COL00740
      WRITE(6,123)                                                     COL00750
      WRITE(6,110)                                                     COL00760
221   FORMAT(4X,'EXPANDER B PARAMETERS: RESULTS FROM SUBROUTINE XPAND') COL00770
110   FORMAT(/5X,'T5H',7X,'T4H',7X,'T4L',7X,'H5H',7X,'H4H',7X,'H4L')    COL00780
      CALL XPAND(5,4,TM2,ETA2,ISV2,DELTA2,A)                           COL00790
       DO 9 K=1,ISV2                                                   COL00800
     ,H5H(K)=A(K,4)                                                    COL00810
      H4H(K)=A(K,5)                                                    COL00820
      H4L(K)=A(K,6)                                                    COL00830
      T5H(K)=A(K,1)                                                    COL00840
      T4H(K)=A(K,2)                                                    COL00850
      T4L(K)=A(K,3)                                                    COL00860
9     CONTINUE                                                         COL00870
C                                                                      COL00880
C     CALCULATE WET EXPANDER-RESERVOIR-COLD COMPRESSOR UNIT PARAMETERS. COL00890
C     AMV IS MASS OF VAPOUR RETURNED TO LOW PRESSURE CHANNEL,CT1H IS A COL00900
C     CHECK VALUE FOR T1H.                                             COL00910
C                                                                      COL00920
      WRITE(6,131)                                                     COL00930
      WRITE(6,132)                                                     COL00940
      WRITE(6,133)                                                     COL00950
      WRITE(6,130)                                                     COL00960
131   FORMAT(/4X,'-------------------------------------------------COL00970
     1---------')                                                      COL00980
132   FORMAT(4X,'WET EXPANDER-RESERVOIR UNIT PARAMETERS:SUBROUTINE WETXPCOL00990
     1 RESULTS')                                                       COL01000
133   FORMAT(4X,'-------------------------------------------------COL01010
     1--------')                                                       COL01020
130   FORMAT(/7X,'AMV',9X,'T1H',9X,'CT1H')                             COL01030
      CALL WETXP(ISV1)                                                 COL01040
C                                                                      COL01050
C     CALCULATE MASS FLOW RATE VALUES FOR THE ARRANGEMENT OF COMPONENTS COL01060
C     AND PICK MINIMUM VALUE OF AM2H  AND CORRESPONDING STATE POINT    COL01070
C     CONDITIONS.                                                      COL01080
C                                                                      COL01090
      WRITE(6,230)                                                     COL01100
```

```
      WRITE(6,233)                                                      COL01110
      WRITE(6,232)                                                      COL01120
230   FORMAT(/4X,'_____________________________________________')       COL01130
232   FORMAT(4X,'_____________________________________________')       COL01140
233   FORMAT(4X,'MASS FLOW RATES:RESULTS FROM SUBROUTINE OPTIM1')       COL01150
      CALL OPTIM1(ISV2,ISV1)                                            COL01160
      WRITE(6,332)                                                      COL01170
      WRITE(6,886)                                                      COL01180
      WRITE(6,333)                                                      COL01190
332   FORMAT(/4X,'_____________________________________________')       COL01200
333   FORMAT(4X,'_____________________________________________')       COL01210
886   FORMAT(4X,'STATE POINT PARAMETERS AT OPTIMUM CONDITION.')         COL01220
      WRITE(6,887)                                                      COL01230
887   FORMAT(/4X,'THIGH',8X,'TLOW',7X,'HHIGH',8X,'HLOW',8X,'AMH',7X,'   COL01240
     1 AML')                                                            COL01250
      WRITE(6,1011)(TH(I),TL(I),HH(I),HL(I))                            COL01260
      WRITE(6,1010)(TH(I),TL(I),HH(I),HL(I),AMH(I),AML(I),I=2,ITOTAL)   COL01270
1010  FORMAT(/2P2E12.3,1P4E12.3)                                        COL01280
1011  FORMAT(/1P2E12.3,1P2E12.3)                                        COL01290
C                                                                       COL01300
C     CALCULATE HEAT EXCHANGER HEAT TRANSFER PROPERTIES FOR THE NHXS HEATCOL01310
C      EXCHANGERS STARTING FROM STATE POINT JSTPTN.                     COL01320
C                                                                       COL01330
      WRITE(6,108)                                                      COL01340
      WRITE(6,107)                                                      COL01350
      WRITE(6,109)                                                      COL01360
108   FORMAT(/4X,'_____________________________________________________COL01370
     1__________')                                                      COL01380
109   FORMAT(4X,'_____________________________________________________COL01390
     1_________')                                                       COL01400
107   FORMAT(/' HEAT EXCHANGER PARAMETERS CORRESPONDING TO OPTIMUM      COL01410
     1CONDITION')                                                       COL01420
      CALL HTAREA(JSTPTN,NHXS,PRATIO)                                   COL01430
      TAREAC=TAREA                                                      COL01440
      STOP                                                              COL01450
      END                                                               COL01460
```

```
      SUBROUTINE XPAND(I,M,TIH,ETA,N,PHI,A)                              XPA00010
C                                                                        XPA00020
C     THIS SUBROUTINE CALCULATES EXPANDER DISCHARGE CONDITION GIVEN      XPA00030
C     THE INLET TEMP.(TIH) AND THE ISENTROPIC EFFICIENCY(ETA). N SETS OF XPA00040
C     VALUES ARE COMPUTED WITH INCREMENTAL STEPS PHI ON TIH. I AND M     XPA00050
C     ARE THE STATE POINT NUMBERS AT THE INLET AND DISCHARGE RESP.       XPA00060
C     A IS THE OUTPUT MATRIX: N SETS OF VALUES FOR THE TEMPS. AND        XPA00070
C     ENTHALPIES.                                                        XPA00080
C                                                                        XPA00090
      COMMON PH,PL                                                       XPA00100
      DIMENSION A(20,8),PH(20),PL(20)                                    XPA00110
      TX=TIH-PHI                                                         XPA00120
      Y=PL(M)                                                            XPA00130
        DO 65 K=1,N                                                      XPA00140
      A(K,1)=TX+K*PHI                                                    XPA00150
      DIH=FINDD(PH(I),A(K,1))                                            XPA00160
      A(K,4)=ENTHAL(DIH,A(K,1))                                          XPA00170
      SIH=ENTROP(DIH,A(K,1))                                             XPA00180
      T=(A(K,1)-5)/2                                                     XPA00190
      R=FINDD(Y,T)                                                       XPA00200
      CALL CALCPS(Y,SIH,R,T)                                             XPA00210
      HDLS=ENTHAL(R,T)                                                   XPA00220
      A(K,6)=A(K,4)+ETA*(HDLS-A(K,4))                                    XPA00230
      CALL CALCHP(A(K,6),Y,R,T)                                          XPA00240
      A(K,3)=T                                                           XPA00250
C                                                                        XPA00260
C     THE HEAT EXCHANGER TEMP. DIFFERENCE IS COMPUTED FROM THE RATIO     XPA00270
C     TEMP. DIFFERENCE/HOT STREAM TEMP. = 1/40                           XPA00280
C                                                                        XPA00290
      A(K,2)=40*A(K,3)/39                                                XPA00300
      DDH=FINDD(PH(M),A(K,2))                                            XPA00310
      A(K,5)=ENTHAL(DDH,A(K,2))                                          XPA00320
      WRITE(6,11) (A(K,J),J=1,6)                                         XPA00330
11    FORMAT(/3F10.3,1P3E10.3)                                           XPA00340
65    CONTINUE                                                           XPA00350
      RETURN                                                             XPA00360
      END                                                                XPA00370
```

```
      SUBROUTINE WETXP(L)                                                WET00010
C                                                                        WET00020
C     THIS SUBPROGRAM CONTAINS A DO LOOP WHICH COMPUTES L SETS OF VALUESWET00030
C     OF THE WET EXPANDER INLET TEMPERATURE AND SATURATED VAPOR MASS     WET00040
C     FLOW RATE.                                                         WET00050
C                                                                        WET00060
      COMMON /ITER/T1H,AMV,T3H,H1H,H2H,H2L                               WET00070
      COMMON/LIQCON/HF,HG,SF,SG,ETAW,ETACC                               WET00080
      COMMON PH,PL                                                       WET00090
      COMMON/OPTI/TH,TL,AMH,AML,HH,HL,QL                                 WET00100
      DIMENSION H2H(20),H1H(20),CH1H(20),T1H(20),CT1H(20),H2L(20),AMV(20WET00110
     1 ),T3H(20),HL(20),HH(20),AMH(20),AML(20),TH(20),TL(20),T4H(20),PH(WET00120
     120),PL(20)                                                         WET00130
        DO 85 K=1,L                                                      WET00140
      T1H(K)=TITER(H2H(K),H2L(K),HL(1))                                  WET00150
      D=FIND'D(PH(1),T1H(K))                                             WET00160
      H1H(K)=ENTHAL(D,T1H(K))                                            WET00170
      S=ENTROP(D,T1H(K))                                                 WET00180
      X=(H1H(K)-HF)*(1-ETAW)/(HG-HF)+(S-SF)*ETAW/(SG-SF)                 WET00190
      AMV(K)=QL*X/(1-X)                                                  WET00200
      AML(2)=AMV(K)                                                      WET00210
      TH(1)=T1H(K)                                                       WET00220
      CH1H(K)=H2H(K)-AMV(K)*(H2L(K)-HL(1))/(QL+AMV(K))                   WET00230
      T=T1H(K)                                                           WET00240
      CALL CALCHP(CH1H(K),PH(1),D,T)                                     WET00250
      CT1H(K)=T                                                          WET00260
      WRITE(6,31)AMV(K),T1H(K),CT1H(K)                                   WET00270
31    FORMAT(/3F12.4)                                                    WET00280
85    CONTINUE                                                           WET00290
      RETURN                                                             WET00300
      END                                                                WET00310
                                                                         WET00320
                                                                         WET00330
                                                                         WET00340
      FUNCTION TITER(H6H,H6L,H7L)                                        WET00350
C     THIS SUBPROGRAM USES THE NEWTON RAPHSON ITERATION SCHEME TO        WET00360
C     COMPUTE THE WET EXPANDER INLET TEMPERATURE (T) AND THE MASS FLOW   WET00370
C     RATE OF SATURATED VAPOR (AMV) RETURNED FROM THE LIQUID RESERVOIR   WET00380
C     FOR GIVEN ENTHALPY VALUES AT THE 3 OTHER STATE POINTS OF THE J-T   WET00390
C     HEAT EXCHANGER.                                                    WET00400
C                                                                        WET00410
      COMMON/LIQCON/HF,HG,SF,SG,ETAW,ETACC                               WET00420
      COMMON PH,PL                                                       WET00430
      DIMENSION PH(20),PL(20)                                            WET00440
C      G'S ARE CONSTANTS                                                 WET00450
C                                                                        WET00460
      SFG=SG-SF                                                          WET00470
      HFG=HG-HF                                                          WET00480
      G1=(H6L-H7L)                                                       WET00490
      G2=1+(G1/HFG)*(1-ETAW)                                             WET00500
      G3=((1-ETAW)*HF/HFG+ETAW*SF/SFG)*G1+H6H                            WET00510
      G4=G1*ETAW/SFG                                                     WET00520
C                                                                        WET00530
C     FIND T,AMV (ITERATION USING NEWTON RAPHSON)                        WET00540
C                                                                        WET00550
```

```
C
C     USE N AS COUNTER FOR  # OF ITERATIONS
C
      N=1
      T=10.5
40    DH7=FINDD(PH(1),T)
      S7=ENTROP(DH7,T)
      H7H=ENTHAL(DH7,T)
      AM=CP(DH7,T)
      F=(H7H+G2)+(G4*S7)-G3
      FF=AM+(G2+G4/T)
      T7=T-F/FF
      IF(ABS(T7-T).LE. 0.00001   .OR. N .GT. 30) GO TO 50
      T=T7
      N=N+1
      GO TO 40
50    TITER=T7
      RETURN
      END
```

WET00560
WET00570
WET00580
WET00590
WET00600
WET00610
WET00620
WET00630
WET00640
WET00650
WET00660
WET00670
WET00680
WET00690
WET00700
WET00710
WET00720
WET00730
WET00740

```
      SUBROUTINE CAREA(AMH,AML,THIN,THOUT,TCIN,TCOUT,PRATIO,PH,PL)        CAR00010
      COMMON/HXPROP/AREAL,AREAH,PDROPL,PDROPH,ANTUT,AFR,AL,TAFR,TAREA,    CAR00020
     1TAREAM,TAREAC                                                       CAR00030
C                                                                         CAR00040
C     THIS SUBROUTINE CALCULATES HEAT TRANSFER PROPTS FOR COUNTERFLOW     CAR00050
C     HEAT EXCHANGER GIVEN THE MASS FLOW RATES (AMH,AML),AND THE TEMPS    CAR00060
C     WHEN THE MASS FLOW RATES, TEMPS. AND PRESSURES ARE SPECIFIED        CAR00070
C     PRATIO IS THE RATIO OF THE  PRESSURE DROP TO THE PRESSURE  IN THE   CAR00080
C     COLD CHANNEL.(HE GAS FLOWS THROUGH BOTH CHANNELS OF HEAT EXCH.).    CAR00090
C                                                                         CAR00100
      DIMENSION CPM(5),V(5),D(5)                                          CAR00110
C                                                                         CAR00120
C     CALCULATE FLUID PROPERTIES AT THE MEAN TEMPERATURE OF EACH STREAM.  CAR00130
C                                                                         CAR00140
        DO 10 K=1,2                                                       CAR00150
      IF(K.EQ.2) GO TO 8                                                  CAR00160
      T=(TCOUT+TCIN)/2                                                    CAR00170
      D(K)=FINDD(PL,T)                                                    CAR00180
      TK=THERM(D(K),T)                                                    CAR00190
      CPM(K)=CP(D(K),T)                                                   CAR00200
      V(K)=VISC(D(K),T)                                                   CAR00210
      PR=(CPM(K)*V(K)/TK)*1000.0                                          CAR00220
      GO TO 10                                                            CAR00230
8     T=(THOUT+THIN)/2                                                    CAR00240
      P=PH                                                                CAR00250
      D(K)=FINDD(P,T)                                                     CAR00260
      CPM(K)=CP(D(K),T)                                                   CAR00270
      V(K)=VISC(D(K),T)                                                   CAR00280
10    CONTINUE                                                            CAR00290
C                                                                         CAR00300
C     DETERMINE MINIMUN HEAT CAPACITY AND CALCULATE HEAT EXCHANGER HEAT   CAR00310
C     TRANSFER EFFECTIVENESS XHTE USING FORMULA BASED ON MINIMUM HEAT     CAR00320
C     CAPACITY.                                                           CAR00330
C                                                                         CAR00340
      CL=CPM(1)*AML                                                       CAR00350
      CH=CPM(2)*AMH                                                       CAR00360
      IF(CH.LT.CL)GO TO 20                                                CAR00370
      CMIN=CL                                                             CAR00380
      CMAX=CH                                                             CAR00390
      XHTE=(TCOUT-TCIN)/(THIN-TCIN)                                       CAR00400
      GO TO 30                                                            CAR00410
20    CMIN=CH                                                             CAR00420
      CMAX=CL                                                             CAR00430
      XHTE=(THIN-THOUT)/(THIN-TCIN)                                       CAR00440
C                                                                         CAR00450
C     CALCULATE CAPACITY RATIO AND HEAT EXCHANGER NUMBER OF TRANSFER      CAR00460
C     UNITS (ANTUT).                                                      CAR00470
C                                                                         CAR00480
30    CRR=CMIN/CMAX                                                       CAR00490
      ANTUT=(ALOG((1-XHTE)/(1-XHTE*CRR)))/(CRR-1)                         CAR00500
      AU=ANTUT*CMIN                                                       CAR00510
      DIA=0.341376                                                        CAR00520
      Y=.382                                                              CAR00530
      EX=0.226                                                            CAR00540
      CN=0.238                                                            CAR00550
```

```
      TETA=(1-Y)/Y                                                      CAR00560
      PLL=PL*1013250.0                                                  CAR00570
      PHH=PH*1013250.0                                                  CAR00580
C                                                                       CAR00590
C     COMPUTE VALUE OF AREA RATIO THAT OPTIMISES THE TOTAL HEAT TRANSFERCAR00600
C     AREA.                                                             CAR00610
C                                                                       CAR00620
      Z=0.5                                                             CAR00630
      GAMMA=AML*V(2)/(AMH*V(1))                                         CAR00640
      EPS=CL/CH                                                         CAR00650
      ARATIO=AREAR(GAMMA,EPS,Z)                                         CAR00660
C                                                                       CAR00670
C     CALCULATE PRESSURE DROP AND HEAT TRANSFER AREA.                   CAR00680
C                                                                       CAR00690
      BETA=ARATIO*GAMMA                                                 CAR00700
      FI1=(V(1)**2)/(2*D(1)*PLL*(DIA**2))                               CAR00710
      FI2=(V(2)**2)/(2*D(2)*PHH*(DIA**2))                               CAR00720
      PSI=BETA**TETA                                                    CAR00730
      PP1=PRATIO/FI1                                                    CAR00740
      PP2=PP1/PSI                                                       CAR00750
      TOTPRR=FI1*PP1+FI2*PP2                                            CAR00760
      PDROPL=PRATIO*PL                                                  CAR00770
      PDROPH=PP2*FI2*PH                                                 CAR00780
      GAM=(CL/CH)*(BETA**(EX-1))*(PSI**EX)                              CAR00790
      BW1=CN*(PP1**EX)/((1+GAM)*ANTUT*(PR**(2/3)))                      CAR00800
      Y=1/(1-EX)                                                        CAR00810
      W1=BW1**Y                                                         CAR00820
      W2=W1/BETA                                                        CAR00830
      AREAL=(AML*DIA)/(W1*V(1))                                         CAR00840
      AREAH=(AMH*DIA)/(W2*V(2))                                         CAR00850
C                                                                       CAR00860
C     COMPUTE HEAT EXCHANGER LENGTH (AL) AND FRONTAL AREA (AFR).        CAR00870
C                                                                       CAR00880
      AMMM=PP1*W1                                                       CAR00890
      AMM=AMMM**0.382                                                   CAR00900
      AL=CN*DIA*AMM/W1                                                  CAR00910
      AFR=(AREAL+AREAH)*12/(340.0*2.54*AL)                              CAR00920
      RETURN                                                            CAR00930
      END                                                               CAR00940
                                                                        CAR00950
                                                                        CAR00960
                                                                        CAR00970
      FUNCTION AREAR(GAM,EPS,Z)                                         CAR00980
C     THIS FUNCTION CALCULATES THE VALUE OF THE HEAT TRANSFER AREA RATIOCAR00990
C     THAT OPTIMISES THE TOTAL HEAT TRANSFER AREA USING NEWTON RAPHSON  CAR01000
C     ITERATION ON THE INITIAL GUESS Z OF THE AREA RATIO AREAH/AREAL.   CAR01010
C     GAM AND EPS ARE INPUT CONSTANTS DEFINED BY THE CALLING SUBPROGRAM CAR01020
C     (SUCH AS CAREA).                                                  CAR01030
C                                                                       CAR01040
      N=1                                                               CAR01050
20    ETA1=(GAM*Z)**(-0.408)                                            CAR01060
      ETA2=EPS*ETA1/Z                                                   CAR01070
      ETA3=1+EPS*ETA1                                                   CAR01080
      ETA4=ETA2*(ETA3**0.292)                                           CAR01090
      ETA5=ETA2**2                                                      CAR01100
```

```
      F=ETA3**1.292-0.527*ETA4*(1+Z)                                    CAR01110
      FF=-0.312*ETA4+0.742*ETA4/Z+0.06278*(1+Z)*ETA5                    CAR01120
      ZNEW=Z-F/FF                                                       CAR01130
      IF (ABS(ZNEW-Z).LE. 0.00005 .OR.  N .GT.20)GO TO 30               CAR01140
      Z=ZNEW                                                            CAR01150
      N=N+1                                                             CAR01160
C     WRITE(6,49)F,FF,N                                                 CAR01170
C49    FORMAT(/1P2E12.3,I4)                                             CAR01180
      GO TO 20                                                          CAR01190
30    AREAR=ZNEW                                                        CAR01200
C     WRITE(6,50)ZNEW,N                                                 CAR01210
50    FORMAT(/'ZNEW=',F10.6,4X,'N=',I4)                                 CAR01220
      RETURN                                                            CAR01230
      END                                                               CAR01240
                                                                        CAR01250
                                                                        CAR01260
      SUBROUTINE HTAREA(N,M,PRATIO)                                     CAR01270
C     THIS SUBPROGRAM CALCULATES HEAT TRANSFER PROPTS. FOR COUNTERFLOW  CAR01280
C     HEAT EXCHANGERS IN SERIES. M IS THE NUMBER OF HEAT EXCHANGERS,    CAR01290
C     N IS THE STATE POINT NUMBER AT THE COLD END (THE NUMBERING IS FROMCAR01300
C     THE COLD TO THE HOT END OF THE HEAT EXCHANGERS).  IT CALLS        CAR01310
C     SUBROUTINE CAREA M TIMES.                                         CAR01320
C                                                                       CAR01330
      COMMON/HXPROP/AREAL,AREAH,PDROPL,PDROPH,ANTUT,AFR,AL,TAFR,TAREA,  CAR01340
     1TAREAM,TAREAC,CHX                                                 CAR01350
      COMMON PH,PL                                                      CAR01360
      COMMON/OPTI/TH,TL,AMH,AML,HH,HL,QL                                CAR01370
      DIMENSION TH(20),TL(20),AMH(20),AML(20),HH(20),HL(20),PH(20),PL(20CAR01380
     1 ),SH(20),SL(20),DH(20),DL(20),SGENX(20),QLOAD(20)                CAR01390
      WRITE(6,219)                                                      CAR01400
219   FORMAT(1H1,'STAGE',4X,'AREAL',8X,'AREAH',7X,'AFR',8X,'PDROPL',7X,'CAR01410
     1PDROPH',7X,'NTUT',7X,'SGEN',7X,'QLOAD')                           CAR01420
      TAREA=0.0                                                         CAR01430
      TAFR=0.0                                                          CAR01440
      J=N+M-1                                                           CAR01450
      J2=J+1                                                            CAR01460
C                                                                       CAR01470
C     COMPUTE DENSITY AND ENTROPY FOR ALL STATE POINTS.                 CAR01480
C                                                                       CAR01490
        DO 998 I=N,J2                                                   CAR01500
      DH(I)=FINDD(PH(I),TH(I))                                          CAR01510
      DL(I)=FINDD(PL(I),TL(I))                                          CAR01520
      SH(I)=ENTROP(DH(I),TH(I))                                         CAR01530
      SL(I)=ENTROP(DL(I),TL(I))                                         CAR01540
998   CONTINUE                                                          CAR01550
C                                                                       CAR01560
C     THIS DO LOOP CALLS SUBROUTINE CAREA  TO COMPUTE THE PARAMETERS    CAR01570
C     CORRESPONDING TO THE HEAT EXCHANGERS DEFINED BY THE STATE POINTS. CAR01580
C                                                                       CAR01590
        DO 1001 K=N,J                                                   CAR01600
      PHIGH=PH(K+1)                                                     CAR01610
      PLOW=PL(K)                                                        CAR01620
      THOUT=TH(K)                                                       CAR01630
      THIN=TH(K+1)                                                      CAR01640
      TCOUT=TL(K+1)                                                     CAR01650
```

•••••••• COLD END RESULTS ••••••••

EXPANDER A PARAMETERS: RESULTS FROM SUBROUTINE XPAND

T3H	T2H	T2L	H3H	H2H	H2L
27.000	13.032	12.707	1.484E+02	6.535E+01	7.578E+01
28.000	13.538	13.200	1.543E+02	6.831E+01	7.860E+01
29.000	14.042	13.691	1.601E+02	7.129E+01	8.139E+01

EXPANDER B PARAMETERS: RESULTS FROM SUBROUTINE XPAND

T5H	T4H	T4L	H5H	H4H	H4L
65.000	33.639	32.798	3.589E+02	1.868E+02	1.844E+02
66.000	34.163	33.308	3.643E+02	1.898E+02	1.871E+02
67.000	34.686	33.819	3.696E+02	1.928E+02	1.898E+02

WET EXPANDER-RESERVOIR UNIT PARAMETERS: SUROUTINE WETXP RESULTS

AMV	T1H	CT1H
19.9385	10.0455	10.0455
21.5992	10.2183	10.2183
23.3111	10.3824	10.3824

MASS FLOW RATES: RESULTS FROM SUBROUTINE OPTIMI

T5H= 65.0000 T4L= 32.7981

T3H	AMA	AM4H	AM6H	T5L	T3L
27.0	3.822E+01	7.816E+01	1.1631E+02	59.482E+00	23.081E+00
28.0	3.608E+01	7.768E+01	1.1578E+02	59.465E+00	24.534E+00
29.0	3.409E+01	7.740E+01	1.1547E+02	59.454E+00	25.997E+00

T5H= 66.0000 T4L= 33.3085

T3H	AMA	AM4H	AM6H	T5L	T3L

27.0	3.932E+01	7.925E+01	1.1639E+02	60.725E+00	22.884E+00
28.0	3.713E+01	7.873E+01	1.1581E+02	60.707E+00	24.326E+00
29.0	3.510E+01	7.841E+01	1.1546E+02	60.696E+00	25.780E+00

T5H= 67.0000 T4L= 33.8186

T3H	AMA	AM4H	AM6H	T5L	T3L
27.0	4.042E+01	8.035E+01	1.1651E+02	62.000E+00	22.694E+00
28.0	3.818E+01	7.978E+01	1.1588E+02	62.000E+00	24.126E+00
29.0	3.610E+01	7.942E+01	1.1548E+02	62.000E+00	25.570E+00

STATE POINT PARAMETERS AT OPTIMUM CONDITION.

THIGH	TLOW	HHIGH	HLOW	AMH	AML
1.038E+01	7.646E+00	5.087E+01	4.345E+01		
14.042E+00	13.691E+00	7.129E+01	8.139E+01	4.331E+01	2.331E+01
29.000E+00	25.780E+00	1.601E+02	1.472E+02	4.331E+01	5.841E+01
34.163E+00	33.308E+00	1.898E+02	1.871E+02	7.841E+01	5.841E+01
66.000E+00	60.696E+00	3.643E+02	3.304E+02	7.841E+01	9.546E+01
80.000E+00	78.000E+00	4.388E+02	4.205E+02	1.155E+02	9.546E+01

HEAT EXCHANGER PARAMETERS CORRESPONDING TO OPTIMUM CONDITION.

STAGE	AREAL	AREAH	AFR	PDROPL	PDROPH	NTUT	SGEN	QLOAD
1	1.769E+04	6.014E+03	9.968E-01	4.000E-02	1.240E-01	5.254E+00	1.383E+01	8.844E+02
2	1.752E+05	7.540E+04	6.265E+00	3.960E-02	1.315E-02	1.195E+01	1.645E+01	3.847E+03
3	4.004E+04	1.491E+04	4.185E+00	3.920E-02	3.914E-02	4.222E+00	6.694E+00	2.328E+03
4	3.500E+05	1.563E+05	1.716E+01	3.881E-02	1.230E-02	1.294E+01	1.808E+01	1.368E+04
5	9.628E+04	3.914E+04	1.233E+01	3.842E-02	2.509E-02	5.110E+00	8.650E+00	8.602E+03

TOTAL AREA=9.708E+05 TOTAL FRONTAL AREA=7.716E+01 HX. COST=6.0785E+04

Appendix D2

Computer Program For Numerical Integration Encountered In Continuum Models

In numerical integration, a continuous integral is decomposed into a finite sum term and an error term as :

$$\int F(x)\,dx = \sum_i \alpha_i F(x_i) + R_n. \qquad (D2.1)$$

where x_i is the position of sampling point i

α_i is the weight for the function evaluation at position x_i.

R_n is the error term.

In the common integration schemes involving equally spaced sampling points such as the Simpson's rule or Newton Cotes formulae[106] (for larger numbers of sampling points), the position of the sampling points are fixed and the weights are determined to minimize the error term.

The Gauss quadrature is a numerical integration scheme which unlike the conventional methods, optimizes both the position of the sampling points and the weights. Thus, whereas n equally spaced points are used to integrate exactly a polynomial of order n-1, the same n points used in the Gauss quadrature evaluates a polynomial of order (2n-1) exactly. The Gauss scheme is therefore used in the numerical integration required in analyzing the continuum models.

The optimized sampling points r_i and the corresponding weights w_i for the Gauss integration from -1 to 1 have been published in the literature[107]. For integration from a to b, the corresponding sampling points and weights are given respectively by

$$x_i = \frac{a+b}{2} + \frac{(b-a)r_i}{2}; \qquad (D2.2)$$

$$\alpha_i = \frac{(b-a)w_i}{2}. \qquad (D2.3)$$

A six-sampling point scheme was used for evaluating all the numerical integrals in the analyses. The values of r_i and w_i are stored in the 2-dimensional matrix ID in the subprograms RGQIS,RGQACT,LGQIS,LGQACT,SGARGQ. The first column of ID gives the sampling points r_i and the second column gives the corresponding weights. The function of these subprograms are now described.

RGQIS: Gauss quadrature algorithm for integrating the mass flow rate for the reversible full pressure ratio model in the refrigeration mode.

RGQIS: Gauss quadrature algorithm for integrating the mass flow rate for the reversible full pressure ratio model in the refrigeration mode

LGQIS: Gauss quadrature algorithm for integrating the mass flow rate for the reversible full pressure ratio model in the liquefaction mode.

RMACT: Gauss quadrature algorithm for integrating the mass flow rate for the mass crossflow model with non-zero heat exchange temperature difference.

LMACT: Gauss quadrature algorithm for integrating the mass flow rate for the mass crossflow model with non-zero heat exchange temperature differece and a liquefaction mode.

SGARGQ: Gauss quadrature algorithm for integrating the heat exchange area and the generated entropy for the mass crossflow model with non-zero heat exchange ΔT.

Each of these integration subprograms are called several times by a driver program

which is essentially a do loop. The specific heat capacity and entropy values are computed by the function CP(T,PN). The data for these properties are stored in a two-dimensional matrix called M3DD in the file DATA4. The call arguments for CP are the temperature in degrees Kelvin and an integer which is the column of the matrix corresponding to the required pressure. There are 22 columns of the matrix representing entropy(odd-numbered columns) and specific heat capacity (even-numbered columns) for the following pressure (atm.) levels in that order: 0.1,0.5,1.0,2.0,3.0,4.0,5.0,10.0,20.0,30.0,40.0.

A listing of the computer programs now follow.

```
(D2) RMISOT(PLN, PHN, DT, TIN, VIN, NTIMES) :=

BLOCK(VAL : ZEROMATRIX(NTIMES, 2), VAL      : TIN, VAL      : VIN,
                                      1, 1           1, 2

FOR I FROM 2 THRU NTIMES DO (VAL      : VAL          + DT,
                               I, 1      I - 1, 1

VAL      : RGQIS(PLN, PHN, VAL     , VAL          , VAL          )))
   I, 2                    I, 1      I - 1, 1       I - 1, 2



(D3) RGQIS(PLN, PHN, ULT, LLT, LLM) :=

BLOCK(ID : MATRIX([- 0.93246952, 0.171324492], [- 0.66120939, 0.36076157],

[- 0.238619186, 0.467913933], [0.238619186, 0.467913933],

[0.66120939, 0.36076157], [0.93246952, 0.171324492]), SUM : 0.0,

                                        (ULT - LLT) ID
                           ULT + LLT                 I, 1
FOR I THRU 6 DO (ST(I) := --------- + ----------------,
                             2                2

                  CP(ST(I), PHN) - CP(ST(I), PLN)
SF(I) := ------------------------------------------------,
         ST(I) (CP(ST(I), PLN - 1) - CP(ST(I), PHN - 1))

                                    (ULT - LLT) SUM
SUM : SUM + SF(I) ID     ), NSUM : ---------------,
                     I, 2                  2

MDOT : EXP(LOG(LLM) + NSUM))

(C4)
```

```
(D6) LMISOT(PLN, PHN, TIN, DT, MIN, NTIMES) :=

BLOCK(LVAL    : ZEROMATRIX(NTIMES, 3), LVAL    : TIN, LVAL    : MIN,
       1, 1                                1, 1           1, 2

                MLIQ
EPS    : 1 + ----, FOR I THRU NTIMES DO LVAL    : EPS    ,
   1, 2       MIN                            I, 3      I, 2

FOR I FROM 2 THRU NTIMES DO (LVAL    : LVAL         + DT,
                              I, 1      I - 1, 1

LVAL    : LGQIS(PLN, PHN, LVAL    , LVAL        , EPS    , EPS        ,
    I, 2                  I, 1      I - 1, 1     I, 2     I - 1, 2

                                MLIQ
LVAL        ), EPS    : 1 + --------, LVAL    : EPS    ))
    I - 1, 2      I, 2       LVAL          I, 3      I, 2
                             I, 2
```

```
(D16) LGQIS(PLN, PHN, ULT, LLT, ULEPS, LLEPS, LLM) :=

BLOCK(ID : MATRIX([- 0.93246952, 0.171324492], [- 0.66120939, 0.36076157],

[- 0.238619186, 0.467913933], [0.238619186, 0.467913933],

[0.66120939, 0.36076157], [0.93246952, 0.171324492]), SUM : 0.0,

                                                  (ULT - LLT) ID
                                ULT + LLT                      I, 1
FOR I THRU 6 DO (ST(I) := ---------- + ------------------------,
                                  2                    2

                                (ULEPS - LLEPS) ID
                    ULEPS + LLEPS                    I, 1
EPS(I) := ------------- + ----------------------,
                 2                    2

                EPS(I) CP(ST(I), PHN) - CP(ST(I), PLN)
SF(I) := ------------------------------------------------,
         ST(I) (CP(ST(I), PLN - 1) - CP(ST(I), PHN - 1))

                                          (ULT - LLT) SUM
SUM : SUM + SF(I) ID    ), NSUM : ---------------,
                    I, 2                    2

MDOT : EXP(LOG(LLM) + NSUM))

(C17)
```

```
(D8) IMISOT(PLN, PHN, DT, TIN, MIN, NTIMES) :=

BLOCK(VAL : ZEROMATRIX(NTIMES, 2), VAL      : TIN, VAL      : MIN,
                                      1, 1           1, 2

FOR I FROM 2 THRU NTIMES DO (VAL      : VAL          + DT,
                               I, 1      I - 1, 1

VAL      : RGQIS(PLN, PHN, VAL     , VAL          , VAL          ),
   I, 2                      I, 1     I - 1, 1     I - 1, 2

                MLIQ
EPS      : 1 + -------))
   I, 2        VAL
                  I, 2

(C9)


(D10) RMACT(PLN, PHN, DT, TIN, MIN, Y, NTIMES) :=

BLOCK(VAL : ZEROMATRIX(NTIMES, 2), VAL      : TIN, VAL      : MIN,
                                      1, 1           1, 2

FOR I FROM 2 THRU NTIMES DO (VAL      : VAL          + DT,
                               I, 1      I - 1, 1

VAL      : RGQACT(PLN, PHN, Y, VAL     , VAL          , VAL          )))
   I, 2                         I, 1     I - 1, 1     I - 1, 2

(C11)
```

```
(D11) RGQACT(PLN, PHN, Y, ULT, LLT, LLM) :=
BLOCK(ID : MATRIX([- 0.93246952, 0.171324492], [- 0.66120939, 0.36076157],
[- 0.238619186, 0.467913933], [0.238619186, 0.467913933],
[0.66120939, 0.36076157], [0.93246952, 0.171324492]), SUM : 0.0,
                                                    (ULT - LLT) ID
                                ULT + LLT                        I, 1
FOR I THRU 6 DO (ST(I) := ---------- + ----------------------,
                                  2                  2

                                                CP(ST(I), PLN)
                                CP(ST(I), PHN) - --------------
                                                    1 + Y
SF(I) := ------------------------------------------------------,
         ST(I) (CP(ST(I), PLN - 1) - CP(ST(I), PHN - 1))

                                                (ULT - LLT) SUM
SUM : SUM + SF(I) ID     ), NSUM : ---------------,
                     I, 2                  2

MDOT : EXP(LOG(LLM) + NSUM))
(C12)
```

```
(D13) LMACT(PLN, PHN, MLIQ, Y, TIN, DT, MIN, NTIMES) :=
BLOCK(VAL : ZEROMATRIX(NTIMES, 3), VAL      : TIN, VAL      : MIN,
                                      1, 1           1, 2

              MLIQ
EPS      : 1 + ----, FOR I THRU NTIMES DO VAL      : EPS     ,
   1, 2       MIN                              1, 3      I, 2

FOR I FROM 2 THRU NTIMES DO (VAL      : VAL          + DT,
                                I, 1      I - 1, 1

VAL      : LGQACT(PLN, PHN, Y, VAL     , VAL          , VAL     , VAL          ,
   I, 2                           I, 1     I - 1, 1     I, 3     I - 1, 3

                                MLIQ
VAL          ), VAL      : 1 + -------, EPS      : VAL     ))
   I - 1, 2       I, 3         VAL           I, 2      I, 3
                               I, 2
(C14)
```

```
(D15) LGQACT(PLN, PHN, Y, ULT, LLT, ULEPS, LLEPS, LLM) :=
BLOCK(ID : MATRIX([- 0.93246952, 0.171324492], [- 0.66120939, 0.36076157],
[- 0.238619186, 0.467913933], [0.238619186, 0.467913933],
[0.66120939, 0.36076157], [0.93246952, 0.171324492]), SUM : 0.0,

                                                  (ULT - LLT) ID
                                 ULT + LLT                     I, 1
FOR I THRU 6 DO (ST(I) := ---------- + ------------------------,
                                    2                  2

                                                 (ULEPS - LLEPS) ID
                          ULEPS + LLEPS                         I, 1
EPS(I) := ------------- + ----------------------,
                 2                    2

                                                      CP(ST(I), PLN)
                    EPS(I) CP(ST(I), PHN) - --------------
                                                        1 + Y
SF(I) := ------------------------------------------------,
           ST(I) (CP(ST(I), PLN - 1) - CP(ST(I), PHN - 1))

                                                 (ULT - LLT) SUM
SUM : SUM + SF(I) ID     ), NSUM : ---------------,
                    I, 2                    2

MDOT : EXP(LOG(LLM) + NSUM))
```

```
(D17) IMACT(PLN, PHN, DT, TIN, MIN, Y, NTIMES) :=
BLOCK(VAL : ZEROMATRIX(NTIMES, 2), VAL      : TIN, VAL      : MIN,
                                      1, 1           1, 2

FOR I FROM 2 THRU NTIMES DO (VAL      : VAL          + DT,
                                I, 1      I - 1, 1

VAL      : RGQACT(PLN, PHN, Y, VAL     , VAL         , VAL         ),
   I, 2                          I, 1     I - 1, 1     I - 1, 2

                MLIQ
EPS      : 1 + -------))
   I, 2       VAL
                 I, 2

(C18)
```

```
(D21) SGAR(PLN, PHN, TIN) := BLOCK(SAR : ZEROMATRIX(15, 4), SAR      : TIN,
                                                                1, 1
FOR I THRU 3 DO SAR      : VAL                    , SAR      : VAL      ;
                  I, 2       37 - 5 (I - 1), 2       4, 2       22, 2

FOR I FROM 5 THRU 7 DO SAR      : VAL
                           I, 2       19 - 2 (I - 5), 2

FOR I FROM 8 THRU 10 DO SAR      : VAL
                            I, 2       14 - 2 (I - 8), 2

FOR I FROM 11 THRU 15 DO SAR      : VAL                    , SAR      : 0.0,
                             I, 2       9 - 2 (I - 11), 2       1, 3

SAR      : 0.0, FOR I FROM 2 THRU 15 DO (IF I <= 4 THEN DT : 5.0
  1, 4

 ELSE (IF I > 4 AND I <= 8 THEN DT : 10

 ELSE (IF I > 8 AND I <= 11 THEN DT : 20.0

 ELSE (IF I > 11 AND I <= 13 THEN DT : 40.0

 ELSE (IF I > 13 THEN DT : 50.0)))), SAR      : SAR          + DT,
                                          I, 1       I - 1, 1

SAR      : SGARGQ(PLN, PHN, SAR      , SAR          , SAR      , SAR          ,
  I, 3                          I, 1       I - 1, 1       I, 2       I - 1, 2

SAR          , SAR          ), SAR      : SGEN), SAVE([SAR4, MNT, DSK, MMMM], SAR).
  I - 1, 4       I - 1, 3       I, 4

(C22)
```

```
(D22) SGARGQ(PLN, PHN, ULT, LLT, ULM, LLM, ISGEN, IAREA) :=
BLOCK(ID : MATRIX([- 0.93246952, 0.171324492], [- 0.66120939, 0.36076157],
[- 0.238619186, 0.467913933], [0.238619186, 0.467913933],
[0.66120939, 0.36076157], [0.93246952, 0.171324492]), SSUM : 0.0, SUM : 0.0

                                                    (ULT - LLT) ID
                                  ULT + LLT                      I, 1
FOR I THRU 6 DO (ST(I) := ---------- + ----------------------------,
                                  2                    2

                                                (ULM - LLM) ID
                    ULM + LLM                             I, 1                MS(I) CP(ST(I), PLN)
MS(I) := ---------- + ----------------------------, SF(I) := ----------------------------,
                    2                    2                                    ST(I)

                                                                  Y (ULT - LLT) SUM
SUM : SUM + SF(I) ID        ), SGEN : ------------------------- + ISGEN,
                    I, 2                                2 (1 + Y)

                (ULT - LLT) SUM
AREA : ---------------------- + IAREA)
                    2 Y

(C23)
```

```
(D24) CP(T, P) := BLOCK(IF 2.5 <= T AND T < 5.0
 THEN FOR I WHILE 2 + 0.5 I <= T DO (N : I, Z1 : 0.5, Z2 : T - 2.0 - 0.5 I)
 ELSE (IF 5.0 <= T AND T < 6.0 THEN FOR I WHILE 4.9 + 0.1 I <= T
DO (N : I + 5, Z1 : 0.1, Z2 : T - 4.9 - 0.1 I)
 ELSE (IF 6.0 <= T AND T < 10.0 THEN FOR I WHILE 5.5 + 0.5 I <= T
DO (N : I + 15, Z1 : 0.5, Z2 : T - 5.5 - 0.5 I)
 ELSE (IF 10.0 <= T AND T < 26.0 THEN FOR I WHILE 9.0 + I <= T
DO (N : I + 23, Z1 : 1.0, Z2 : T - 9.0 - I)
 ELSE (IF 26.0 <= T AND T < 40.0 THEN FOR I WHILE 24.0 + 2 I <= T
DO (N : I + 39, Z1 : 2.0, Z2 : T - 24.0 - 2.0 I)
 ELSE (IF 40.0 <= T AND T < 80.0 THEN FOR I WHILE 35.0 + 5.0 I <= T
DO (N : I + 46, Z1 : 5.0, Z2 : T - 35.0 - 5.0 I)
 ELSE (IF 80.0 <= T AND T < 100.0 THEN FOR I WHILE 70.0 + 10.0 I <= T
DO (N : I + 54, Z1 : 10.0, Z2 : T - 70.0 - 10.0 I)
 ELSE (IF 100.0 <= T AND T < 300.0 THEN FOR I WHILE 75.0 + 25.0 I <= T
DO (N : I + 56, Z1 : 25.0, Z2 : T - 75.0 - 25.0 I)
 ELSE (IF 300.0 <= T AND T < 400.0 THEN FOR I WHILE 250.0 + 50.0 I <= T
DO (N : I + 64, Z1 : 50.0, Z2 : T - 250.0 - 50.0 I)))))))), C1 : M3DD     ,
                                                                    N, P
                                                (C2 - C1) Z2
C2 : M3DD          , CPV : C1 + ------------)
        N + 1, P                     Z1

(C25)
```

Appendix E1

INSTRUMENTATION

Two classes of instrumentation were provided on the device. One set of sensors provided information for diagnostic purposes. This included pressure sensors in the pneumatic circuit (used for tuning the circuit), and temperature sensors distributed along the cylinder length which provided conduction heat flow information along the cylinder. The other class of sensors had the dual role of providing information for diagnostic purposes as will as measurements for evaluating the performance of the engine. This latter class included a displacement transducer which gave the working volume-time relationship for the engine, and both pressure and temperature sensors at various locations in the process stream. The types of sensors used for the experiment are now presented together with some other peripheral equipment such as power sources and data acquisition system.

E1.1 Temperature Measurements

Four types of sensors are commonly used for cryogenic temperature measurements: thermocouples, semiconductors, resistance thermometers and gas thermometers. The unique characteristics associated with each of these sensors, generally determine the choice for a particular application. With the exception of the semiconductor type, all these sensors were employed in the experiment as explained below.

Thermocouples: Themocouples are easy to build, easy to use and inexpensive. However, the copper-constantan(type T) sensors commonly used are accurate over a limited range of temperatures and therefore cannot be used at liquid helium temperatures. These were employed primarily to monitor the cooldown process as well as the temperature distribution

along the cylinder length . Eight thermocouples were soft-soldered along the length of the cylinder and one each on the inlet, discharge and heater tanks. Also one thermocouple each was used to measure the temperature of the process gas inside the inlet, discharge and heater tanks (these are numbered 10, 11 and 12 respectively). The thermocouples were made of 0.012" wires TIG welded to form the cold junction. The other end of the wires were connected to the signal conditioning module of a data acquisition system with in-built ice-point compensation facilitating direct voltage readout. The data acquisition system had microprocessing capabilities which could convert the measured voltage to centrigrade degrees. A printed output was provided at desired time intervals.

Resistance Thermometers: Allen-Bradley (carbon composition) resistors were used to measure the temperature of the working fluid at three different locations in the flow process: at the inlet and the discharge to the engine and at the heater tank further downstream of the engine. The resistance-temperature characteristics of the Allen-Bradley resistors have been found [108] to closely fit the three-constant semi-empirical calibration curve of Clement and Quinnell[109]:

$$\frac{1}{T} = A \ln R + B + \frac{C}{\ln R} \qquad (E1.1)$$

where R is the resistance in ohms,and T is the temperature in degrees K. A, B, C are constants to be determined empirically. The resistors were calibrated from measurements at room temperature, liquid nitrogen temperature, and liquid helium temperature.

At very low temperatures, ohmic heating due to the exciting current may introduce errors in the measurement as the resistance increases. The choice of resistors without an inordinate increase in resistance at low temperatures and a low excitation current $1.0 \mu A$ minimized this error. Four 0.008" film insulated copper leads were soft-soldered to the two

"pigtails" on each resistor (two on either side of it). All three resistors were connected in series with a $10M\Omega$ resistor and a digital multimeter and then to a power source (a Lambda dual regulated power supply with a voltage range of 0-20V and a maximum rated current of 1.7A .) The digital multimeter was used to measure the current while the other pair of leads were connected to the signal conditioning module of the data acquisition system for the measurement of the voltage drop across each resistor. Typical calibration curves for the three resistors are shown in Fig E1.1 and E1.2.

Gas Thermometers: It is sometimes argued that Allen-Bradley resistors require calibration after each recooling to cryogenic temperatures although a number of researchers have shown otherwise.[110,111] Also, the resistance of Allen-Bradley resistors tend to drift. The resistance thermometers were to be located inside sealed tanks. Therefore they would not be easily accessible after installation and any malfunctioning could not be easily corrected. In particular it would be impractical to recalibrate them after each run of the experiment. Consequently gas thermometers were also installed as backup for the resistance thermometers.

The gas thermometer is based on the thermodynamic behaviour of a gas: the unique temperature-pressure relation of a pure fluid. It consists of two volumes: a warm volume at ambient temperature and a cold volume at the cryogenic temperature connected by a capillary tubing. It may be classified according to the phase behaviour at the cold end [112]. Thus depending on the initial charging pressure and volume ratio, the cold end behaviour may lie in one of four regions defined by Holten[112]. In two of the four regimes, the cold volume of the thermometer is partly filled with liquid and partly with vapor in equilibrium with liquid. In this mode of operation the temperature is determined from the saturated pressure-temperature relationship, and the sensor is then called a vapor pressure thermometer.

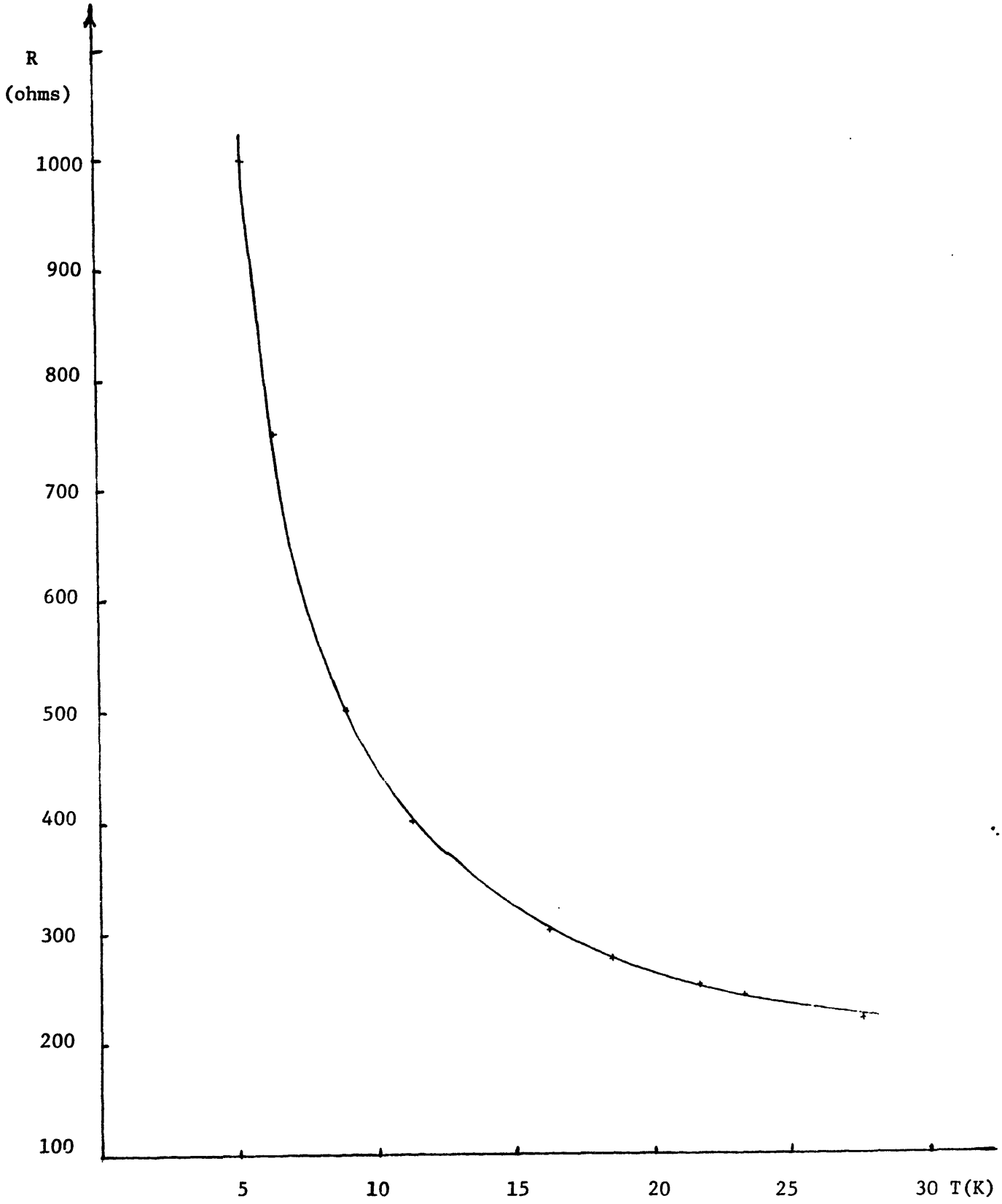


FIG. E1.1 COLD END CALIBRATION CURVE FOR ALLEN-BRABLEY RESISTOR LOCATED AT THE EXPANDER INLET. TABULATED VALUES ARE GIVEN ON TABLE E1.1

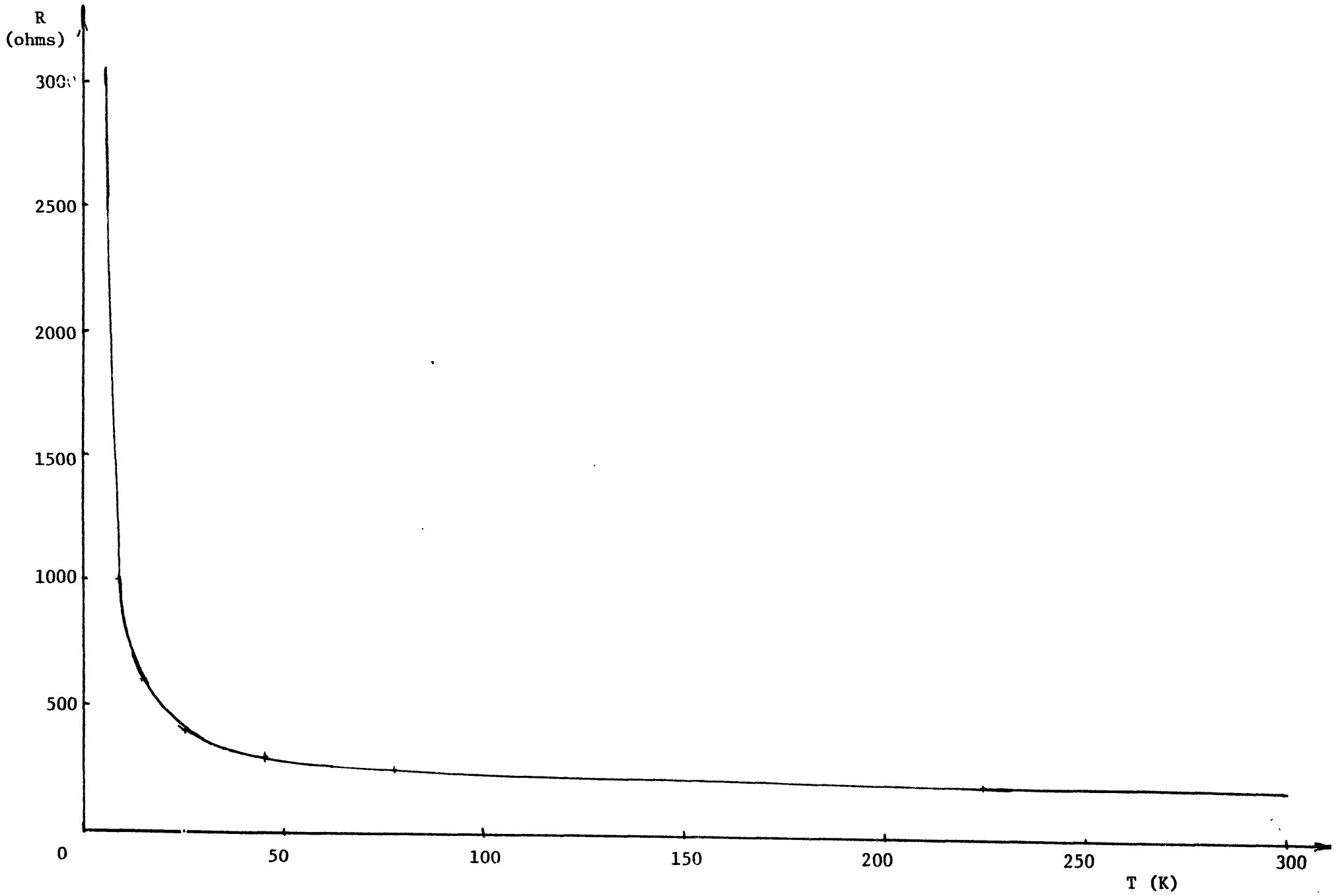


FIG. E1.2 FULL RANGE CALIBRATION CURVE FOR ALLEN-BRADLEY RESISTOR LOCATED AT THE HEATER TANK.

The volume ratio and the charging pressure essentially fix the performance of the sensor. These are chosen from considerations of response time, temperature errors and sensitivity as discussed by Holten[112]. There is an error due to warm-volume(ambient) temperature changes occurring during utilization of the thermometer. This cannot be accounted for a priori, for example by physical calibration. However an analytical correction curve may be provided for applications where the resulting error would be appreciable. (It has not been found necessary to provide such a correction curve for the sensors.) There is also an error due to the interconnecting capillary tubing. This error depends on the mass in the capillary tube and is minimized by reducing the transition volume. The response is determined by two factors:

1. The time lag for thermal conduction between the cold bulb and the enclosed fluid;
2. The time lag for mass transfer required to reestablish pressure equilibrium after a change in temperature.

Heat transfer in the cold-volume has been found experimentally to dictate the response time. Thus the capillary tubing can be made as small as possible to reduce the error due to the size of the capillary tubing without any significant loss in response time. Consequently 0.012"-ID capillary tubing was used to interconnect the warm and cold volumes. The cold bulb was made of copper because of its thermal characteristics. Also higher charging pressures improve the response time.

In general the charging pressure and the volume ratio are chosen to obtain maximum sensitivity over a desired limited temperature range. However, for this experimental engine, it was desired to monitor the cooldown process and also provide the flexibility of operating the engine at higher temperature levels (as a single phase expander.) Consequently, a charg-

ing pressure of about eleven atmospheres was used which, in combination with a volume ratio (warm to cold) of 37.5, enabled a wide range of temperature measurements with a single sensor. The calibration curve was obtained analytically from continuity of mass:

$$M_{total} = M_{warm} + M_{cold} \qquad (E1.2)$$

In terms of the cold and warm volumes,

$$\rho_o(V_w + V_c) = \rho_w V_w + \rho_c V_c \qquad (E1.3)$$

which gives

$$\rho_c(T, P) = (N + 1)\rho_o(T_w, P_o) + \rho_w(T_w, P) \qquad (E1.4)$$

The temperature-pressure relationship given by E1.4 (Fig. E1.4) was checked at liquid nitrogen and liquid helium temperatures. The volume ratio was also checked to ensure that in the two-phase operating regime, the cold volume would not be completely filled with liquid. This eliminates the possibility of creating a colder spot between the cold volume and the volume.

E1.2 Pressure Measurements

Two types of pressure tranducers were employed for the experiments . The expected temperature of the working space of the engine precluded the use of pressure transducers with built-in amplifiers: the electronic circuit limits the operating temperatures usually to about 77K. A miniature high impedance piezoelectric transducer from Kistler Instrument

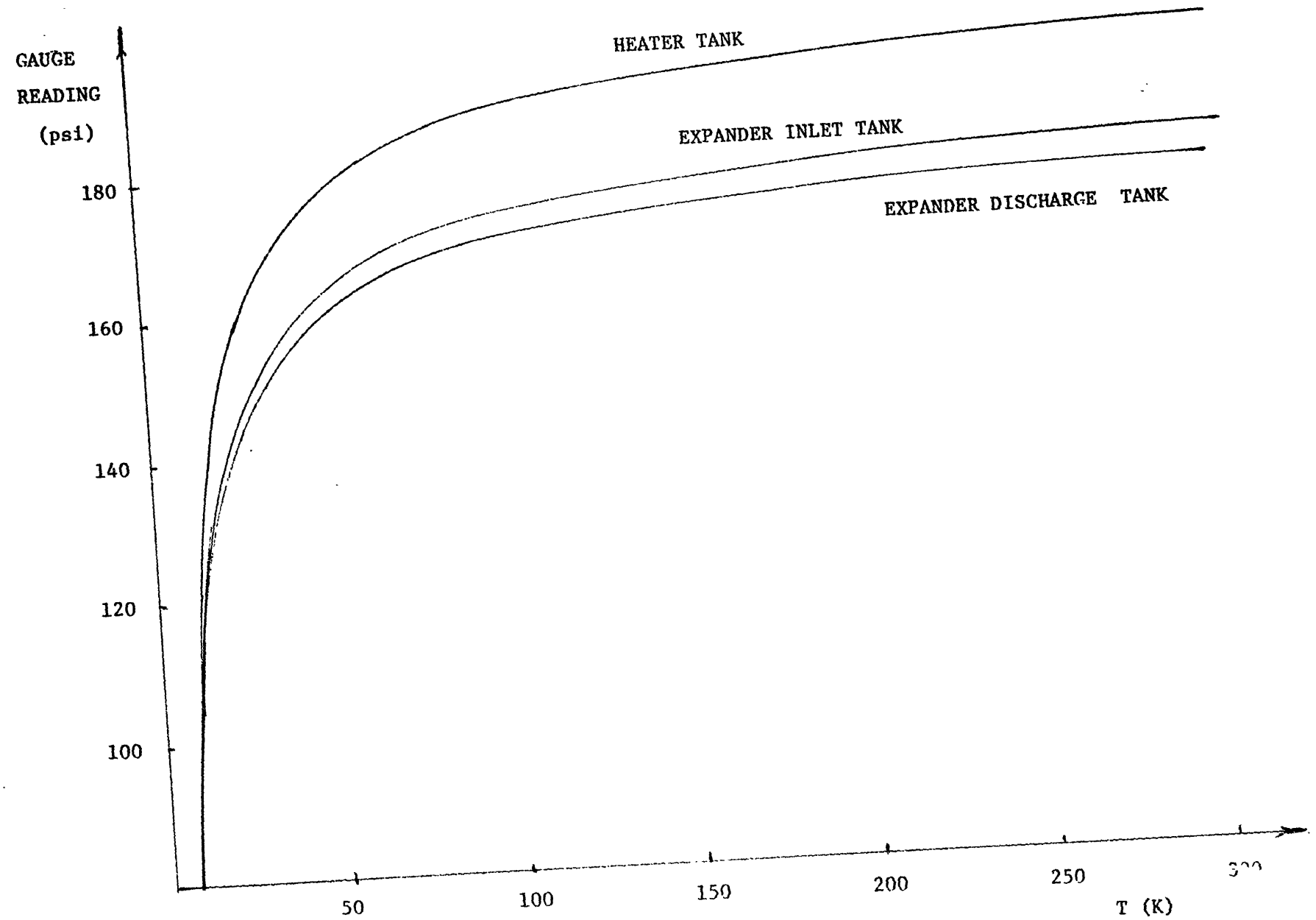


FIG. E1.4a CALIBRATION CURVES FOR VAPOR PRESSURE THERMOMETERS. TABULATED VALUES ARE SHOWN ON TABLE E1.2

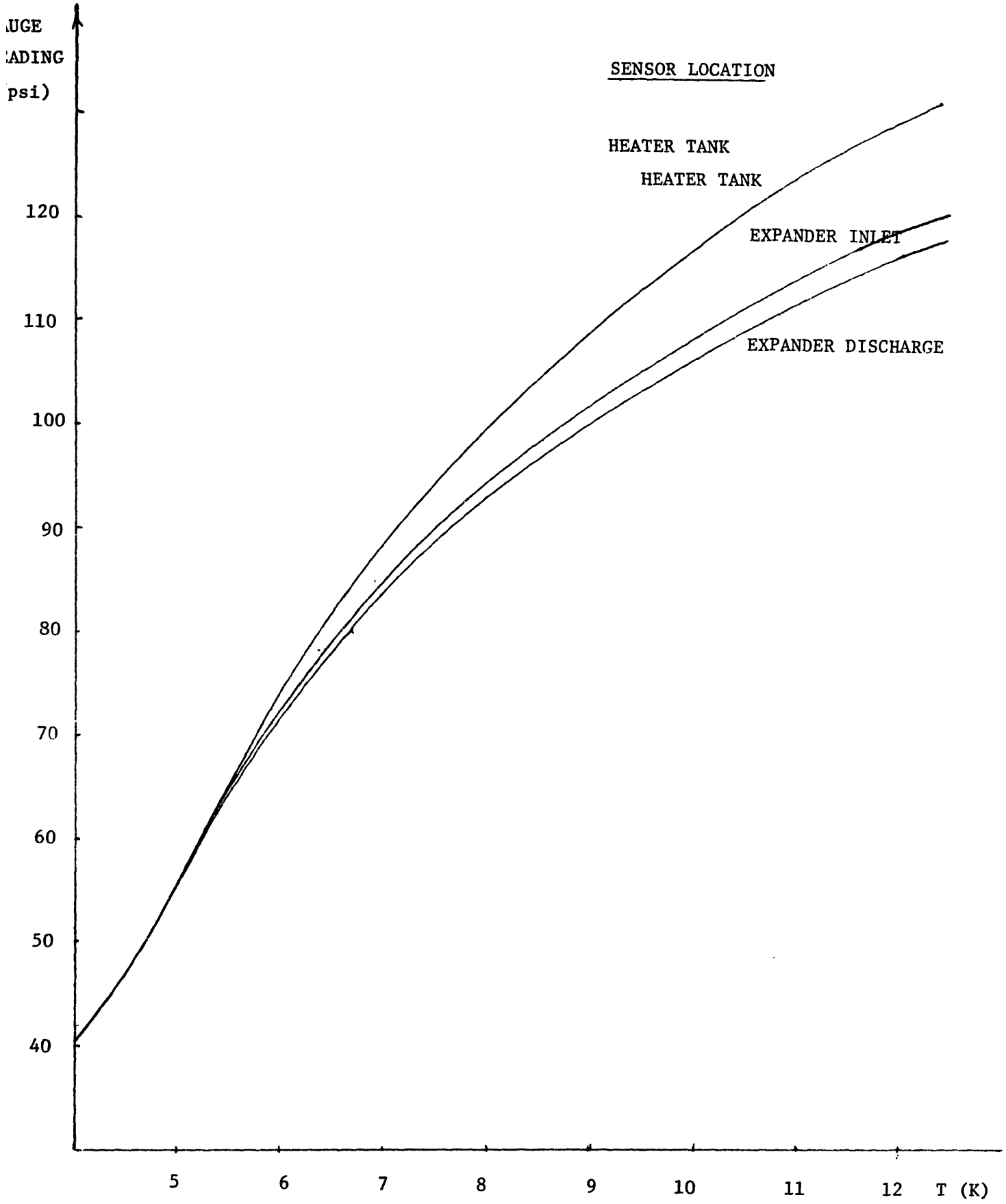


FIG. E1.4b COLD END CALIBRATION CURVES FOR VAPOR PRESSURE THERMOMETERS

Corporation (Model 603B3) having a sensing element made of crystalline quartz and a rated operating temperature range from 6K, was used to measure the pressure in the working space of the engine. The sensor threads into a mounting adaptor (Model 221A) which was TIG welded to one end of a short capillary tube. The other end of the tube was soft-soldered to the cylinder. The electrical charge output of the sensor is fed into a charge amplifier (Model 5004) which converts the charge signal to a proportional voltage signal. This voltage signal is then monitored on a digital oscilloscope.

CEC Type 4-312 variable-resistance -type pressure transducers were also used. The sensing element consists of an unbounded-strain-gauge winding connected in a four-arm bridge circuit. Pressure against the diaphragm produces a displacement of the sensing element changing the resistance of the active arms and causing an electrical output proportional to the applied pressure. The full-scale output was 20mV for an excitation voltage of 5.5VDC. Because of this low level of the output signal, these transducers were susceptible to spurious noise signals. However, the desired phase information was easily obtained from the resulting signals. Again these signals were monitored on a digital oscilloscope.

Typical pressure-time traces are shown in Chapter 5. One set of these sensors could measure pressure up to 125 psi and the other set had a range of 0-250 psi.

E1.3 Data Acquisition System

Two types of data acquisition system were used for the experiment: a microprocessor-controlled system (AUTODATA NINE) from the Acurex Autodata Company, and a digital oscilloscope with magnetic disk memory capability from Nicolet Instrument Corporation.

Autodata Nine: The Autodata Nine was used to measure the themocouple and resistance

thermometer signals. The sensor cables were connected to a signal conditioning module, in the data acquisition system, which converts the output from the sensor to a dc voltage for measurement by an integrating digital voltmeter. The signal conditioning module plugs into a reed multiplexer which switches the conditioned signal from the sensors to the voltmeter one at a time.

Nicolet Explorer II Digital Oscilloscope: The oscilloscope had a plug-in unit with two channels. This was therefore used to display the Pressure-Volume curve of the expansion engine. The P-V data was also stored on a magnetic disk and later transferred to a VAX PDP 11 computer for processing. The basic program for transferring the data was written by H. B. Faulkner [113] and was used with minimal modification. The data is transferred in the form of printable binary codes and is translated first to integers and then to floating point numbers using normalizing constants associated with the oscilloscope. Signals from the CEC pressure sensors were also displayed and processed with the digital oscilloscope.

E1.4 Liquid Level Gauge

The liquid level in the heater tank was monitored using a liquid level sensor from American Magnetics,Inc. The sensor element is a superconducting wire filament. A constant current of 70mA was maintained in the wire. This kept the portion of the wire in the gas normally conducting (resistive) while the section submerged in the liquid remained superconducting. Thus a linear relationship between the output voltage and the liquid level is obtained. The output voltage is measured across the superconducting wire to eliminate errors associated with the voltage drop across the current carrying leads. Thus a total of four leads connect the gauge. A Lambda dual regulated power supply was used to maintain the constant current measured on a Data Precision digital multimeter.

Appendix E2

ANALYSIS OF RESULTS

Two methods were used to measure the actual work extraction rate of the expander. The first involved measuring the mass flow rate while the other involved measuring the losses due to heat transfer. In both cases the state of the working fluid entering the expander and leaving the heater tank are required as indicated in Sec. 5.3. Typical values are as given presently.

- Expander inlet condition:

Pressure = 13.15 atm.

Temperature = 6.55 K

From a table of helium properties,[90]

Enthalpy h_1 = 23.973 J/g

Entropy S_1 = 4.377 J/(g-K)

Density ρ_c = 13.28 g/cm^3

- Expander discharge condition (saturated gas):

Pressure = 1.2 atm

Again from the table of helium properties:

Temperature = 4.424 K

Enthalpy h_3 = 29.94 J/g

Entropy S_3 = 7.993 J/(g-K)

Mass Flow Rate Method.

The mass flow rate is calculated from the cylinder volume, the fluid state at the cutoff point and the cycle rate. Thus

$$M = \frac{\pi d^2}{4} \frac{L_c \rho_c}{\tau}$$

where

d = cylinder bore

L_c = piston displacement at cutoff from BDC

=2.35 cm.

τ = cycle time

= 1.63 s

Substitution gives the mass flow rate

$\underline{M = 2.183 \text{ g/s}}$

The reversible expander power is then given by:

$$W_{rev} = M(h_1 - h_3) - T_3(S_1 - S_3)$$
$$= 21.8\text{W},$$

and the actual expander power is similarly given as:

$$W_{act} = M(h_1 - h_3) + Q_{act}$$
$$= 20.4\text{W}.$$

The ratio gives the expander efficiency as:

$$\eta = 94\%.$$

Heat loss method

The actual work is also obtained from the indicated work (area under the P-V diagram) as:

$$W_{act} = W_{ind} - Q_{losses}$$

The indicated power $= \frac{1}{\tau} \oint PdV$

$= 21.41$ W

The piston motion loss = 1.3 W (from the data of Table 5.2).

The total static heat loss is = 2.61 W (from the data of Table E2.1)

Table E2.1

Static Heat Leak Test Results

	Test 1	Test 2	Test 3
Temperature at expander inlet tank (K)	4.6	4.6	4.6
Temperature at heater tank (K)	5.347	5.495	6.16
Mass flow rate transducer reading (Volts)	4.73	4.665	4.398
Heat leak rate $M(\Delta h)$	2.44	2.58	2.82

The static heat loss associated with the engine is obtained by comparing the measured heat loss with the calculated static heat loss. The conduction heat losses are calculated

from Fourier's law using the integrated conductivity values for stainless steel and the room temperature value of the conductivity for micarta as explained in Sec. 5.2.3. From Table E2.2,

The expander heat loss = 1.63 W.

Therefore

$$Q_{losses} = 2.9W$$

These values now give the actual expander power as:

$$W_{act} = 18.5W$$

The expander efficiency is then given as:

$$\eta = 84.5\%$$

These values are reported in chapter 5.

Table E2.2

Estimates Of Conduction And Radiation Heat Losses

Source	Q_{cond} (W)
Engine Cylinder	0.208
Engine Displacer	0.124
Valve Sheath	0.129
Valve Rod	0.014
Heater Tank Support	0.26
	$Q_{rad.}$ (W)
Engine	0.0055
Heater Tank	0.011
Discharge Surge Tank	0.0076
Inlet Surge Tank	0.0076

REFERENCES

1. J. Wilkis, *The Properties Of Liquid And Solid Helium*, Clarendon Press, Oxford (1967)
2. W. H. Keesom, *Helium*, Elsevier Publishing Company, Amsterdam (1942)
3. K. Mendelsohn, *The Quest For Absolute Zero*, Taylor and Francis, London (1977)
4. R. W. Vance, *Cryogenic Technology*, John Wiley and Sons,Inc., New York(1963)
5. F. E. Hoare, L.C. Jackson and N. Kurti, *Experimental Cryophysics*, Butterworths, London (1961)
6. A. J. Croft, *Liquefiers And Refrigerators*, Advanced Cryogenics Plenum Press, N.Y.(1971)
7. H. Brody, *Superconductors:Finally Ready For Business*, High Technology 3:2 (1983)
8. R. F. Barron, *Cryogenic Systems*, McGraw-Hill, NY(1966)
9. R. B. Scott, *Cryogenic Engineering*, Van Nostrand, Princeton(1959)
10. S.C. Collins, R. L. Cannaday, *Expansion Machines For Low Temperature Processes*, Oxford Press, London (1958)
11. S. C. Collins, *Helium Liquefiers*, Science, 116:289(1958)
12. J. L. Smith, Jr., et al, *EPRI Final Report 92*, (1975)
13. J. L. Smith, Jr., et al, *Demonstration Of An Advanced Superconducting Generator*, Interim Report 1(1977)
14. A. D. Appleton, *Status Of Superconducting a.c. Generator In The UK*, AIM, Centrales Electriques Modernes, Liege(1981)
15. W.R. McCourn, J. S. Edmonds, *300mVA Superconducting Generator:Plan For Design, Testing And Long Term Operation*, CIGRE, Paris (1980)
16. M. Iwamoto et al, *A 6250 kWA Superconducting Generator*, IEEE, PES Winter Meeting NY (1979)
17. W. E. Keller, *Worldwide Cryogenics - U.S. Cryogenics At The Los Alamos Scientific Laboratory*, Cryogenics 20:10 (p 247)

18. D. Lambrecht, *Status And Development Of Superconducting a.c. Generator.* IEEE Trans Mag. 17:5 (1981)

19. E. B. Forsyth, G. A. Mulligan, J. W. Beck, J.A. Williams, *The Technical And Economic Feasibility Of Superconducting Power Tranmission*, A case study presented ot the 1974 IEEE Summer meeting.

20. R.W. Meyerhoff, *Cryogenics*, 11(2):191 (1971)

21. D. E. Daney , *Refrigeration For An 8K to 14K Supercritical Transmission Line*, NSBIR 74-375 (1974)

22. D. A. Haid, *ASME paper 74 - WA/PID - 18*, (1974)

23. H. Brody , *Superconductors : Finally Ready For Business*, High Technology , 3:2 (1982)

24f. Preprint, *Second International Seminar On Superconductive Magnetic Levitated Train*, Miyazaki, Japan, Nov 1982

25. J.E.C. Williams, *ICEC9-ICMC*, Kobe, Japan, May 1982

26. P. Berglung et al, *ICEC9-ICMC*, Kobe, Japan, May 1982

27. D. V. Byrne, *Future Application Of Resonant Stirling Cycle Cryocoolers*, CEC83, Colorado.

28. C. A. Hamilton, *Space Applications Of Superconductivity: Microwave And Infrared Detectors*, Cryogenics 20:5 (1980)

29. S. R. Stein, *Space Applications Of Superconductivity*, Cryogenics 20:7 (1980)

30. R.E. Harris, *Space Applications Of Superconductivity*, Cryogenics 20:4(1980)

31. S.J. Williams and L.Kaufman, *Application Of SQUID Detectors In Biomagnetism*, NBS 508 (1978)

32. J.C. Zimmerman , *Space Applications Of Superconductivity; Low Frequency Superconducting Sensors*, Cryogenics 20:1 (1980)

33. E. B. Qvale and J. L. Smith, Jr., *Mathematical Model For Steady Operation Of Stirling-type Engines*, Transactions Of ASME, Journal Of Engineering For Power, 90:A1 (1968)

34. P. A. Rios, E. B. Qvale, J.L. Smith, Jr., A*An Of The Stirling Cycle Refrigerator*, Advances In Cryogenic Engineering 14 (1969)

35. E. B. Qvale and J.L. Smith, Jr., *An Approximate Thermal Performance Of A Stirling-Engine Generator*, Transactions Of ASME, Journal Of Engineering For Power, 91:A2(1969)

36. P. A. Rios and J.L. Smith, Jr., *An Analytical And Experimental Evaluation Of The Pressure-drop Losses In The Stirling-Cycle*, Transactons Of ASME, Journal Of Engineering And Power 92:A2(1970)

37. J. L. Smith, Jr., *Some Aspects Of The Selection Of Regenerators*, Cryogenics 5:6 (1965)

38. S. N. Rea and J. L. Smith, Jr., *The Influence Of Pressure Cycling On Thermal Regenerators*, Trans. ASME, Journal Of Engineering For Industry 89:B3(1967)

40. W.S. Harris, P.A. Rios and J. L. Smith, Jr., *The Design Of Thermal Regenerators For Stirling-type Refrigerators*, Advances In Cryogenic Engieering 16(1971)

41. J. W. Colangelo, E. E. Fitzpatrick, S. N. Rea and J. L. Smith, Jr., *An Analysis Of The Performance Of The Pulse Tube Refrigerator*, Advances In Cryogenic Engineering, 13(1968)

42. J. L. Smith, Jr., *A Metal Bellows Expansion Engine*, Advances In Cryogenic Engineering, 12 (1967)

43. M. Minta and J. L. Smith, Jr., *Helium Liquefier Cycles With Saturated Vapor Compression*, Advances In Cryogenic Engineering, 27(1982)

44. R. H. Hubbell and W. M. Toscano, *The Thermodynamic Optimization Of Helium Liquefaction Cycles*, Advances In Cryogenic Engineering, 25(1980)

45. M. Minta, *Study Of Helium Liquefaction Cycles At Elevated Pressures*, MSME Thesis MIT(1981)

46. J. L. Smith, Jr., and E. G. Cravalho, *Engineering Thermodynamics*, Pitman,Boston (1983).

47. J.H. Keenan, *Thermodynamics*, MIT Press (1941)

48. J. L. Smith, Jr., Class notes for Course 2.649, *Low Temperature Refrigeration*, MIT (1983)

49. R. A. Smith , *The Physical Principles Of Thermodynamics*, Chapman and Hall, London (1952)

50. Ray Radebaugh, *Refrigeration Fundamentals: A View Toward New Refrigeration Systems*, NBS508 (1978)

51. P. Kittel, *Magnetic Refrigeration In Space -practical Considerations*, Journal Of Energy 4:266 (1980)

52. P. Kittel, *Temperature Stabilised Adiabatic Demagnetization Refrigerator For Space Applications*, Cryogenics 20:599 (1980)

53. R.D. Britt and P. L.Richards, *An Adiabatic Demagnetization Refrigerator For Bolometers*, Int. Journal Of Infrared And Millimeter Waves 2:1083 (1981)

54. W. A. Steyert, *Small Magnetic Refrigerators To Pump Heat From Helium Temperatures To Above 10K*, NBS 508 (1978)

55. H. J. Goldmid, *Thermoelectric Refrigeration*, Plenum Press, NY (1978)

56. W. S. Sims, *Army Requerements For Cryogenic Cooling Of Infrared Detectors*, AFFDL-TR-73-149 (1973)

57. G. Walker, *Stirling-cycle Machines*, Clarendon Press, Oxford (1973)

58. J. Ericsson, *Encylopaedia Americana*, 10:p547,NY(1972)

59. J. L. Smith, Jr., Class notes for Course 2.649, *Low Temperature Refrigeration*, MIT (1983)

60. G.F.C. Rogers and Y.R.Mayhew, *Engineering Thermodynamics, Work And Heat Transfer*, Longman, London (1980)

61. S. B. Horn, M.L. Lumpkin, B.T.Walters and T.T. Acord, *Miniature Cryogenic Cooler For Tow Night Sight*, AFFDL-TR-73-149 (1973)

62. J. S. Buller, *A miniature Self-regulating Rapid-cooling J-T Cryostat*, Advances In Cyogenic Engineering, 16 (1971)

63. W. A. Little, Scaling Of Miniature Crycoolers To Microminiature Size, NBS508, (1978).

64. R. F. Barron, *Liquefaction Cycles For Cryogens*, Advances In Cryogenic Engineering 17 (1972)

65. S. C. Collins, R. W. Stuart and M. H. Streeter, *Closed Cycle Refrigeration At 1.85k*, The Review Of Scientific Instruments, 38:11 (1967)

66. P. A. Rios, *An Analytical And Experimental Investigation Of The Stirling Cycle*, MIT Sc.D. Thesis (1969)

67. A. Daniels, M. Gasser and A. Sherman, *Magnetically suspended Stirling Cryogenic Space Refrigerator: Status Report*, Presented at the CEC83, Colorado (1983)

68. F. F. Chellis, *The Future Of The Stirling Cycle Refrigerator In Airborne I-R Applications*, AFFDL-TR-73-149 (1973)

69. D. V. Byrne, *Future Application Of Resonant Stirling Cycle Cryocoolers*, Presented ot the CEC83, Colorado (1983)

70. C. Balas, Jr., *An Acoustically Quiet , Low Power Minimum Vibration, Stirling Cycle Refrigerator*, AFFDL-TR-73-149 (1973)

71. D. A. Daney, *Cooling Capacity For Stirling Cryocoolers-The Split Cycle And Non-ideal Gas Effects*, Cryogenics 22:10 (1981)f

72. H. D. McMahon and W.E. Gifford, *A New Low Temperature Gas Expansion Cycle, Parts I and II*, Advances In Cryogenic Engineering 5 (1960)

73. W. E. Gifford, *The Gifford-McMahon Cycle*, Advances In Cryogenic Engineering, 11 (1965)

74. R. C. Longsworth, *A Modified Solvay-Cycle Cryogenic Refrigerator*, Advances In Cryogenic Engieneering, 16(1971)

75. W. S. Sims, *Army Requirements For Cryogenic Cooling Of Infrared Detectors*, AFFDL-TR-73-149 (1973)

76. *Lockheed Missiles and Space Company Report On Refrigerators A98458*, Section 3

77. F. N. Magee and R. D. Doering, *Vuillenmier Cycle Cryogenic Refrigerator Development*, Air Force AFF Flight Dynanmics Lab Report, WPAFB, Ohio (1968)

78. B. Shelpuk and M. Crouthamel, *VM Thermal Actuation And Bruner Investigation*, USAE Report Ft. Belvoir, Virginia (1972)

79. T. T. Rule and E.B. Qvale, *Steady-state Operation Of The Idealized VM Refrigerator.*

80. R. White and W.J. Uhl, Jr., *VM Heat Driven Cryogernic Refrigerator*, Air Force Flight Dynamics Laboratory Report WPAFB, Ohio (Jan.1967)

81. W. E. Gifford and R.C. Longsworth, *Pulse Tube Refrigeration*, ASME 63-WA-290

82. M. Thirumaleshwar, *Exergy Method Of Analysis And Its Application To A Helium Refrigerator*, Cryogenics 19:6 (1979)

83. S. C. Collins, R. W. Johnson and J. L. Smith, Jr., *Hydraulically Operated Two-phase Helium Expansion Engine*, Advances In Cryogenic Engineering 16 (1971)

84. D. P. Brown, A. P. Schlafke, K. C. Wu, and R. W. Moore, *Cycle Design For The Isabelle Helium Refrigerator*, Advances In Cryogenic Engineering 27(1982)

85. D. E. Daney,*Low Temperature Losses In Supercritical Helium Refrigerators*,Advances In Cryogenic Engineering 21 (1976)

86. T. R. Strobridge and R. O. Voth, *Refrigeration Technology For Superconductors*,IEEE Trans On Nuclear Science NS-24:3 (1971)

87. W. J. Olszewski,*Efficient Turbine Processes For The Liquefaction Of Cryogens*, Advances In Cryogenic Engineering 17 (1972)

88. J. L. Smith, Jr., *The Presentation Of Heat-Transfer And Friction-Factor Data For Heat Exchanger Design*, ASME, 66-WA/HT-59

89. A. Bejan, *Entropy Generation Throuth Heat And Fluid Flow*, Wiley Interscience, NY (1982)

90. R. D. McCarty, Thermophisical Properties Of Helium-4 From 2 To 1500 K With Pressures To 1000 Atmospheres, NBS 631(1972).

91. A. Khalil and G. E. McIntosh *Thermodynamic Optimization Study Of The Helium Multi-engine Claude Refrigeration Cycle*, Advances In Cryogenic Engineering 23 (1978)

92. M. A. Hilal, *Optimization Of Helium Refrigerators And Liquefiers For Large Superconducting*

Systems, Cryogenics ,19:(1979)

93. Y. Matsubara, M. Kameko, Y. Hiresaki, and K. Yasuteochi, *Exergetic Analysis Of Multistaged Claude Cycle Helium Refrigerators*, Cryogenic Processes And Equipment In Enerty Systems, ASME (1981)

94. W. M. Kays and A. L. London, *Compact Heat Exchangers*, McGraw Hill, NY (1964)

95. Gardner Cryogenics, *Expansion Engines In Cryogenic Processes* , Ref.RFQ 7125K-206668-7-27, General Dynamics Convair Division and Gardner Cryogenics

96. P. J. Kerney, and D. A. McWilliams,*A 50 Litre Per Hour Helium Liquefier For A Superconducting Magnetic Energy Storage System*, Addvances In Cryogenic Engineering , 25 (1978)

97. T. J. Peterson,*Fermilab's Satelite Refrigerator Expansion Engines*, Presented at CEC 83, Colorado (1983)

98. G. Y. Robinson,sl Large Scale Helium Refrigeration Systems In The 2 To 20 K Range, ICEC ,Kyoto, Japan (1967)

99. H. Sixsmith,*Miniature Cryogenic Expansion Turbines: A Review* , Presented at the CEC83, Colorado (1983)

100. H. Sixsmith and W. L. Swift, *A Pair Of Miniature Helium Expansion Turbines*, Advances In Cryogenic Engineering, 27 (1982)

101. R. W. Brekenbridge, Jr., *Development of A Miniature Reciprocating Cryogenic Refrigerator For Space Applications*, AFFDL-TR-67-149 (1967)

102. Metals and Ceramics Information Centre, Battlelle, *Handbook On Materials For Superconducting Machinery*, (Jan. 1977)

103. Kangpil Lee, J.L. Smith, Jr., and H. B. Faulkner, *Performance Loss Due To Transient Heat Transfer In The Cylinders Of Stirling Engines*, 15th, Intersociety Conversion Engineering Conference Proceedings 2(1980)

104. K. Lee, I. P. Krepchin and W. M. Toscano, *Thermodynamic Description Of An Adiabatic Second Order Analysis For Stirling Engines*, Report 819794

105. P. A. Rios, *An Approximate Solution To The Shuttle Heat-Transfer Losses In A*

Reciprocating Machine, Journal Of Engineering For Power, April(1971).

106. K. J. Bathe and E. L. Wilson, *Numerical Methods In Finite Element Analysis*, Prentice Hall, NJ (1976)

107. A. N. Loxan, N. Davids and A. Levenson, *Table Of Values Of The Legendre Polynomials Of Order 1-16 And The Weight Coefficients For Gauss Quadrature Formula*, Bulletin Of The American Mathematical Society 48(1942)

108. J. L. Smith, Jr. et al, *Demonstration Of An Advanced Superconducting Generator*, Interim Report IR4 (1978)

109. J. R. Clement, E. H. Quinnell, *The Low Temperature Characteristics of Carbon Composition Thermometers*, Review of Scientific Instruments, Vol. 23, (1952)

110. R. Guenther, H. Wenstock and R. W. Schleicher, *Carbon Resistors for Secondary Cryogenic Thermometry*, Cryogenic Technology(March/April 1970)

111. H. Weinstock and J. Parpia, *A survey Of Thermometric Characteristics Of Recently Produced Allen Bradley/Ohmite Resistors*, Temperature:Its Measurement and Control In Science and Industry, Instrument Society Of America, Pittsburgh,4:2(1970)

112. D. C. Holten, *Static and Dynamic Behaviour Of Helium-gas Thermometers Below 77K*, Advances In Cryogenic Engineering, 9(1964).

113. H. B. Faulkner, *An Investigation of Instantaneous Heat Transfer During Compression and Expansion In Reciprocating Gas Handling Equipment*, Ph.D. Thesis MIT (1983)

BIOGRAPHICAL SKETCH

The first grade teacher was convinced he was smarter than his age and decided to enrol him even though he was still under the legal school age. He had to be dragged to school each morning but very soon school was all fun. The teachers liked him because he was enthusiastic about studies; the students liked him because of his soccer prowess. Before the end of grade school everybody was predicting an academic career for him.

All hopes for the future seemed dashed when just before entering high school, his father died. However, with help from his mother and his big brother he managed to go through high school and finally college where he won a fellowship for the four years of college. After four years in college, he changed his mind about an academic career and went to work as an assistant publisher but soon realized he still loved school. He went back to his college, worked as a teaching assistant and finally entered MIT for graduate studies.

He has since contributed papers for the last two cryogenic engineering conferences and he has been elected to the MIT chapter of Sigma Xi. His publications include:

1. "An Optimum Cold End Configuration for Helium Liquefaction Cycles," Advances in Cryogenic Engineering, Vol. 29 (to be published).
2. "An Entropy Flow Optimization Technique for Helium Liquefaction Cycles," Advances in Cryogenic Engineering, Vol. 29 (to be published).
3. "Helium Liquefier Cycles with Saturated Vapor Compression," Advances in Cryogenic Engineering, Vol. 27